Fall 2011

Diesel particulate matter dispersion analysis in underground metal/nonmetal mines using computational fluid dynamics

Yi Zheng

Follow this and additional works at: https://scholarsmine.mst.edu/doctoral_dissertations

Part of the Mining Engineering Commons

Department: Mining and Nuclear Engineering

DIESEL PARTICULATE MATTER DISPERSION ANALYSIS IN UNDERGROUND

METAL/NONMETAL MINES USING COMPUTATIONAL FLUID DYNAMICS

by

YI ZHENG

A DISSERTATION

Presented to the Faculty of the Graduate School of the

MISSOURI UNIVERSITY OF SCIENCE AND TECHNOLOGY

In Partial Fulfillment of the Requirements for the Degree

DOCTOR OF PHILOSOPHY

in

MINING ENGINEERING

2011

Approved by

Jerry C. Tien, Advisor
R. Larry Grayson
Lee Saperstein
David Summers
Hai-Lung Tsai

ABSTRACT

Diesel Particulate Matter (DPM) is a natural by-product from operating diesel engines. Since diesel power is a major source of energy for mining operations today, the adverse health effects of DPM are of a great concern. To thoroughly resolve DPM problems, it is critical that DPM propagation characteristics be understood to arrive at a sensible and practical method for addressing DPM-related issues. To achieve this, a computational fluid dynamics (CFD) method is used to simulate DPM dispersion and to predict its concentration distribution.

Industrial field studies were reconstructed to evaluate the possibility of different CFD models. Experiments were also carried out in the Missouri University of Science and Technology (MISSOURI S&T) Experimental Mine to validate the selected CFD model. Based on the verified CFD model, the DPM dispersion pattern in both a straight entry and a dead-end entry were studied. The effect of variables (for example, different mining operations, inclination of dead-end entry, buoyancy effects, orientation of the tailpipe and a vehicle's motion) on DPM distribution were systematically simulated to reveal high DPM regions in similar real mining scenarios. Different main airflow speeds, diesel particulate filter (DPF), and local ventilation devices were evaluated for effectiveness in clearing the DPM plume.

This research can provide a means for identifying high DPM-level areas which can be used in miner health and safety training. It can also improve the understanding of the impacts of various control measures on DPM distribution which can result in an objective decision-making scheme for mining engineers to choose individual or a combination of control strategies to upgrade a miner's working environment.

ACKNOWLEDGMENTS

TABLE OF CONTENTS

LIST OF ILLUSTRATIONS

LIST OF TABLES

NOMENCLATURE

Abbreviation	Description
BTL	Biomass to Liquid
CFD	Computational Fluid Dynamics
cfm	Cubic feet per minute
CFR	U.S. Code of Federal Regulations
D2	Ultra Low Sulfur Diesel Fuel
DEEP	Diesel Emission Evaluation Program
DOC	Diesel Oxidation Catalyst
DOCCs	Diesel Oxidation Catalytic Converters
DPM	Diesel Particulate Matter
EC	Elemental Carbon
EPA	Environmental Protection Agency
ER	Emission Rate
GTL	Gas to Liquid
IMVC	International Mine Ventilation Congress
LHD	Load-Haul-Dump
M/NM	Metal/Nonmetal
MSHA	Mine Safety and Health Administration
S&T	Missouri University of Science and Technology
NIOSH	National Institute for Occupational Safety and Health
OC	Organic Carbon
PAHs	Polycyclic Aromatic Hydrocarbons
PAS	Photoelectric Aerosol Sensor
PI	Particulate Index
PIB	Program Information Bulletin
ppm	Part per million
RCD	Respirable Combustible Dust
SME	Society for Mining, Metallurgy & Exploration
SCR	Selective Catalytic Reduction

TC	Total Carbon
UGAS	Undiluted Gas Analysis System
VOF	Volume of Fluid

Symbols	Description
a	Number of the treatment levels for factor A
b	Number of the treatment levels for factor B
C_i	Net pollutant concentration in $\mu g/m^3$
D_t	Turbulent diffusivity
$F_{v-1,n-v,a}$	F distribution with v - 1 and n - v degrees of freedom with significance level α
G_b	Generation of turbulence kinetic energy due to buoyancy
G_k	Generation of turbulence kinetic energy due to mean velocity gradients
g_i	Component of the gravitational vector in the i th direction
Gr	Grashof number
$\vec{J}$	Mass diffusion in turbulent flows
k	Kinetic energy
l	Characteristic of length
msE	Mean square for error
msT	Mean square for treatment
$\sim N(0, \sigma^2)$	Denotes a normal distribution with mean 0 and variance σ^2
n	Total number of observations
Pr_t	Turbulent Prandtl number
r	Number of observations within a treatment
Ra	Rayleigh number
Re	Reynolds number
S	Modulus of the mean strain tensor
Sc_t	Turbulent Schmidt number
ssE	Sum of squares for error
ssT	Sum of squares for treatment

sstot	Total sum of squares
T	Temperature
T_0	Operating temperature
$\langle u_i \rangle$	Mean velocity components (i=1,2,3)
$u_i^{'}$	Fluctuating velocity components (i=1,2,3)
V_i	Ventilation rate in m^3/s
v	Number of treatments, velocity
V_c	Critical velocity
$\widehat{V}$	Velocity scale
Y_i	Mass fraction of each local species
Y_{it}	DPM concentration obtained on the tth observation of the ith treatment

Greek letters	Description
α	Significance level of the test, thermal diffusivity
β	Thermal expansion coefficient
Δ	The smallest difference among two of the treatments that are of interest
ε	Turbulence dispersion rate
ε_{it}	Error variable, representing all minor sources of nuisance variation
μ	Constant DPM level, dynamic viscosity
μ_t	Turbulent viscosity
$\pi(\Delta)$	The probability of rejecting H_0 when the effects of at least two of the treatments differ by Δ
ρ	Fluid mass density
σ^2	Error variance
σ_k	Turbulent Prandtl numbers for k
σ_ε	Turbulent Prandtl numbers for ε
τ_i	Deviation from the constant when the ith treatment is observed

ν Kinematic viscosity

ϕ Function of noncentrality parameter and number of treatment

$\langle\phi\rangle$ Mean scalar

$\phi^{'}$ Fluctuating scalar

ω Specific dispersion rate

1. INTRODUCTION

1.1. OVERVIEW

Diesel-powered equipment have been widely used in all U.S. underground mines, coal and metal/nonmetal (M/NM) alike. According to a survey by MSHA, between 1998 and 1999, 196 out of 264 underground M/NM mines used 3,998 pieces of diesel equipment (Anon., 2001a), and 145 out of 910 underground coal mines used 3,121 pieces of diesel engines (Anon., 2001b). If the existing restrictions on the use of diesel-powered equipment in Ohio, Pennsylvania, and West Virginia were relaxed, 339 more underground coal mines in these states are likely to begin using diesel fuel to power their mining equipment (Anon., 2001c).

Diesel engines are rugged, reliable and fuel efficient; they have lower maintenance costs due to a lack of sparking and spark wires and they are quite durable. It is not uncommon for diesel engines in heavy-duty trucks to have a life of 1,000,000 miles (Anon., 1999). Compared to electricity-powered equipment, they provide greater flexibility underground with greater maneuverability and efficiency. They also provide more power and eliminate time-consuming battery change-out time compared to on-board battery-powered equipment. Other hybrid electric or fuel-cell power sources are still not commercially available for use on large equipment. Therefore, it is assumed that the underground mining community's significant reliance on diesel power will continue (Anon., 2001a).

However, during the past two to three decades, the health effects caused by diesel emissions have also received attention worldwide. It is believed that long-term exposure to diesel exhaust can be carcinogenic (Anon., 1988; 2002). In addition, acute overexposure to diesel exhaust has also been linked to deleterious health effects such as eye and nose irritation, headaches, nausea, and asthma (Kahn and Orris, 1988; Rundell et al., 1996; Wade and Newman, 1993).

To protect miners, the U.S. Congress has passed laws to legislate DPM concentrations for all underground mines. Later, MSHA published final rules for coal mining in the Federal Register on January 19, 2001 (Part II – 30 CFR Part 72 – Diesel Particulate Matter Exposure of Underground Coal Mines), and with final corrections on May 21, 2001.

They became effective on July 19, 2002. There are also six Program Information Bulletins (PIB02-04, PIB02-07, PIB03-14, PIB03-15, PIB05-01 and PIB10-07) to assist with compliance in the field. For underground coal mines, diesel engines used underground are divided into three categories under MSHA regulations: "permissible", "nonpermissible heavy-duty equipment, generators, and compressors" and "nonpermissible light-duty equipment." Equipment under each category is required to emit no more than a certain amount of DPM per hour; otherwise, it will not be allowed to operate underground.

In its 2001 DPM rule for M/NM underground mines, MSHA established an interim concentration limit of 400 micrograms of total carbon (TC) per cubic meter of air (400_{TC} µg/m^3) and a final concentration limit of 160_{TC} µg/m^3 in the future. In 2005, MSHA issued a final rule converting the interim concentration limit from 400_{TC} µg/m^3 to 308 micrograms of elemental carbon (EC) per cubic meter of air (308_{EC} µg/m^3) based on a miner's personal exposure rather than as a concentration limit (The relationships of DPM concentration, TC concentration, and EC concentration are: DPM ≈ TC/ 0.8 and TC ≈ 1.3 × EC). In January 2007, the DPM limit was further lowered to 350_{TC} µg/m^3 and finally reached 160_{TC} µg/m^3 in May 2008.

For underground coal mines, DPM regulations are executed on diesel equipment instead of the underground environment or a miner's personal exposure to DPM. Coal mines did not face much difficulty in complying with these regulations. For underground M/NM mines, however, it was reported by MSHA that many mines still have difficulties in meeting the regulation limit.

In a 2001 risk assessment study by MSHA using NIOSH Analytical Method 5040, exposures based on 355 samples collected at 27 underground M/NM mines, showed that mean DPM concentrations in the production areas and haulage ways in those mines ranged from about 285 µg/m^3 to about 2,000 µg/m^3, with some individual measurements exceeding 3,500 µg/m^3. The overall mean DPM concentration was 808 µg/m^3. MSHA also collected 464 DPM samples at 31 underground M/NM mines in 2001 and 2002. Results based on 358 valid samples from 30 mines showed that the mean DPM concentration was 610 µg/m^3 for metal mines, 465 µg/m^3 for stone mines, 94 µg/m^3 for trona mines, and 359 µg/m^3 for others (Anon. 2005a).

MSHA's baseline sampling, collected between October 30, 2002 and October 29, 2003, had a total of 1,194 valid samples from 183 underground M/NM mines. The mean DPM concentration was 444 µg/m^3 for metal mines, 295 µg/m^3 for stone mines, 132 µg/m^3 for trona mines, and 243 µg/m^3 for others (Anon., 2005b). Between November 1, 2003 and January 31, 2006, 1,798 valid personal compliance samples were collected from all underground N/NM mines covered by the regulation. Of these, 1,151 samples (64 percent) exceeded the 160$_{TC}$ µg/m^3 final limit. These data show that miners are still being exposed to high levels of DPM (Anon., 2006a). It is clear that many of the underground M/NM mines will face difficulties in complying with the final DPM limit without further effort.

Therefore, DPM dispersion under different face layouts and operations in underground M/NM mines are the focus of this study. DPM dispersion patterns are similar for underground coal mines when the situation is comparable, although they are not regulated.

For underground M/NM mines to control DPM hazards, two types of strategies have been commonly used. One is DPM reduction and removal before it is released from the engine tailpipe, which includes proper diesel engine selection and maintenance, use of alternative fuels and exhaust gas treatment devices, e.g., diesel particulate filters (DPF).The other is through control measures after DPM is discharged into the environment – mine ventilation, an enclosed equipment cab with filtered breathing air, and administrative controls.

Experience shows that no single strategy can solve all DPM problems, and a combination of several measures needs to be implemented in the field to attain compliance. Since none of the strategies are cost free, an effective, efficient, and economical control scheme for operations under different mining conditions is essential in order for a mining company to provide a safe working environment and to meet regulatory criteria.

The focus of this research is to study DPM propagation behaviour and to develop viable CFD models to simulate DPM dispersion, which can potentially reduce the numerous DPM exposure problems encountered underground today. Through simulation, valuable information can be obtained for identifying areas with high DPM concentrations and it can be used to evaluate the effectiveness of different control measures under

various working layouts and operating conditions. This will facilitate proper decisions on lowering DPM exposure levels under different circumstances. The success of the simulation depends on the careful evaluation of available field studies and experiments, as well as the development of proper CFD models to predict the DPM levels in various layouts and operating conditions. If successful, the simulation results will potentially help mines to lower miners' DPM exposure levels in the most effective and efficient way. This research provides a significant step toward understanding DPM distribution behaviour as a basis for improving the working environment for underground miners.

1.2. STATEMENT OF THE PROBLEM

Diesel particulate matter is the by-product of incomplete combustion of diesel fuel in diesel engines and is defined as a sub-micron (< 1.0 micron) physical aerosol component of diesel exhaust made up of very small individual particles. These particles have a solid core consisting mainly of elemental carbon. They also have a very surface-rich morphology. This extensive surface adsorbs many other toxic substances that are transported with the particulates, and can penetrate deep into the lungs. More than 1,800 different organic compounds have been identified as adsorbed onto the elemental carbon core, such as organic chemicals (polycyclic aromatic hydrocarbons or PAHs), condensed liquid hydrocarbons, and inorganic compounds (sulphate compounds), as shown in Figure 1.1 (Anon., 2001d).
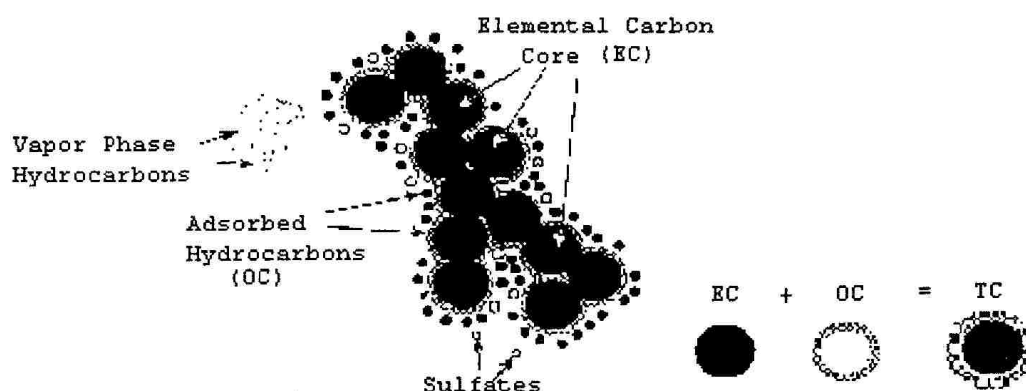
Figure 1.1 DPM Components.
Elemental Carbon (EC) + Organic Carbon (OC) = Total Carbon (TC)

Many underground mines, both coal and M/NM, utilize diesel-powered equipment in mining operations – transporting personnel and supplies; drilling, loading and hauling material; or powering various ancillary equipment. The use of diesel-powered equipment in confined spaces, such as underground mines, has caused concerns due to miners' exposure to diesel exhaust. Because of the confined areas in underground mines, miners in these areas can be exposed to DPM concentrations far more than workers in other industries.

Unlike other industrial environments where pollutant sources are localized and the ventilation system can be easily designed to isolate the contaminant source, all underground mine workings can contain air contaminants, such as DPM. For underground mines, the same passageways, in which air contaminants are generated or released, must be used for underground miners to breathe. Due to the small size of DPM, once it is airborne, it is likely to remain airborne throughout the entire entry. This means that DPM not only affects the workplace where it is produced, it also contaminates other areas of the workplaces, both downstream and immediately upstream.

This research proposed the use of CFD to characterize DPM propagation behavior in order to identify areas with high DPM concentrations, to validate the CFD study results by using field studies and experiments, and to develop better control strategies in underground working areas.

1.3. OBJECTIVES AND SCOPE OF THE STUDY

The primary objectives of this research were to characterize DPM propagation behavior through CFD modeling validated by field studies and experiments conducted at Missouri University of Science and Technology's (S&T) Experimental Mine, and to determine: (i) the relationship among incoming airflow, tailpipe emission patterns, and DPM concentration distribution in the immediate and surrounding areas; (ii) the worst operating condition in different mining operations; (iii) the DPM level in different areas (using both measurements and modeling); and (iv) good control strategies for different working conditions.

Due to the numerous operational features of diesel-powered equipment in different mining conditions, the current study was limited to commonly encountered exhaust

flow rates and DPM production for drilling, loading, or mucking. Several CFD simulation models, representing the worst working conditions in the face, were used to characterize the DPM distribution and evaluate the effectiveness of different control strategies.

Two of the most common working layouts: straight entry and dead-end entry were the focus of this research. Three types of mining equipment: a drill jumbo, a Load-Haul-Dump (LHD), and a truck that in different combinations of mining operations (drilling, loading, transporting, mucking) were simulated. Different mine ventilation devices were evaluated to identify high DPM areas, and control strategies discussed if the working environment exceeded the regulation limit.

1.4. RESEARCH METHODOLOGY

To achieve the set objectives, a detailed literature survey was conducted to identify current problems and existing techniques used to characterize DPM propagation simulation and experiments. Preliminary data on entry dimensions, local ventilation, and equipment emission rates were necessary for model construction. Since only limited information is available, two specially designed experiments were conducted in S&T's Experimental Mine and were used to validate CFD simulation results. The ultimate goal for this study was to build reliable CFD models to characterize DPM distribution patterns for effective ventilation planning and miner training.

The commercially available FLUENT program was used to model airflow and DPM propagation and to evaluate if the fluid flow, heat and mass transfer were accurately simulated in three dimensions. The simulation process included building the geometric face and entry model with mining equipment and ventilation control devices in a CAD design program, SolidWorks; a mesh model using CFD pre-processor software, GAMBIT; and then importing and converting the mesh file into FLUENT to simulate the DPM behaviour. The modeling task included models for different mine layouts and individual mining equipment in working faces in different mining operations, with or without fans and vent tubing in the entry, and proper mesh of the simulation domain with boundary conditions.

Due to the small size of DPM (< 1.0 micron), it was assumed that it would behave like a different type of gas, for instance CO_2. The species transport model in FLUENT

was used to simulate the DPM behaviour like that of a gas. In an industrial field study, DPM is considered as small particles. The discrete phase model in FUENT was used to characterize DPM behaviour in that simulation and compared the results with the species transport model. When properly utilized, both models were found to provide satisfactory results in DPM simulation. However, since the species transport model requires less computation time, all of the cases in this dissertation were simulated with that model.

1.5. STRUCTURE OF DISSERTATION

This section introduces background information about DPM problems in underground metal/non-metal mines and the objectives and methodology of this DPM study. Section 2 contains a comprehensive review of relevant literature on effective DPM control strategies, measurement, simulation in mining and other industries, and the rationale for this research. Section 3 presents theoretical formulation and governing equations used in this dissertation. Section 4 describes two industrial field studies on diesel exhaust collection and evaluation of diesel particulate filter (DPF). The mass fraction of DPM from a tailpipe (that is used in later sections) is calculated from research founding in a real mining environment. Due to lack of multiple DPM data from these industrial experiments to validate the species transport model, two experiments were executed in S&T's Experimental Mine. In the first experiment, DPM concentrations were collected in four locations; in the second experiment, 28 locations were sampled. The design and considerations of the experiment and a comparison between the simulation and experiment are illustrated in Section 5. Based on the information and experience gained from the above experiments, CFD was used to simulate the DPM problem in the face areas. In Section 6, the process and considerations of CFD simulation and detection of problematic locations are introduced. In Sections 7 and 8, DPM dispersion in a straight entry and a dead-end entry are studied to reveal the problem and evaluate the control strategies. Section 9 provides conclusions and recommendations for future work.

2. LITERATURE REVIEW

This section covers a comprehensive literature review on DPM and CFD simulation. The review covered current research work on DPM for the mining industry, simulation usage in mining, and simulation research on diesel emissions from other industries.

Until now, most of DPM research in the mining industry was focused on the evaluation of control strategies and DPM measurement. Studies on simulation of DPM propagation in underground mining environments were scant.

The reasons include: First, the health concern about DPM is a relatively new concept for mining that began in the late 1970s to early 1980s (Gamble et al., 1978; Anon., 1981; Ames et al., 1982; Reger et al., 1982). DPM regulations were developed in the early years of this century with the final rule addressing DPM exposure of underground coal and M/NM miners being announced on Jan. 19, 2001. The final version of DPM regulation for underground coal mines was effective July 19, 2002. The final concentration limit (160_{TC} $\mu g/m^3$) for underground M/NM mines was in effect on May 20, 2008. Most other major mining countries still do not have specific DPM regulations for underground mines.

Second, there has not been enough DPM study for simulation. All field studies conducted were to evaluate control strategies only. The available data, so far, have been incomplete and could not fulfill a satisfactory simulation (this gap will be addressed in Section 4).

Third, unlike methane and fire, the DPM problem is a health problem, which does not have an immediate effect, so it has not received very much attention.

Thus, this study can benefit the mining industry. Although CFD simulation in mining can be dated back to the early 1990s (Reed, 2005), when the DPM problem arose, it has not been used to study DPM dispersion. In this study, CFD simulation was used in a mining environment to capture high DPM level regions and to evaluate different control strategies. CFD simulation on DPM and diesel emissions is detailed in Section 2.

2.1. CURRENT DPM RESEARCH FOR THE MINING INDUSTRY

This section reviews the available DPM control technologies and their effects on the control of emissions from diesel-powered equipment used in underground coal and M/NM mines. It also includes DPM sampling methods and current research areas concerned with the DPM problems in the mining industry. Some of the field studies from this literature review have been reconstructed and simulated later in Section 4.

The strategies discussed include engine selection and maintenance, alternative fuels, exhaust gas treatment devices, mine ventilation, enclosed equipment cab with filtered breathing air, and administrative controls. The variety of DPM measurement methods includes the standard method for the U.S., Canada, and some European countries; it also includes some other commonly used instruments from the research reports.

2.1.1. Diesel Engine Selection and Maintenance. For underground mines, diesel engine selection needs to meet strict regulations for safety and health reasons. Engine maintenance is also an important issue under the same considerations.

2.1.1.1 Diesel inventory for underground mines. For diesel engines, diesel powered packages, and diesel equipment used in underground coal mines, MSHA has established standards in 30 CFR Part 7 (Testing by Applicant or Third Party) under subpart A (General Provisions), subpart E (Diesel Engines Intended for Use in Underground Coal Mines), and subpart F (Diesel Power Packages Intended for Use in Areas of Underground Coal Mines where Permissible Electric Equipment is Required), in 30 CFR Part 36 (Approval Requirements for Permissible Mobile Diesel-powered Transportation Equipment), and in 30 CFR Part 75 (Mandatory Safety Standards--Underground Coal Mines) under subpart T (Diesel-Powered Equipment).

For diesel engines used in underground M/NM mines, MSHA requires that a diesel engine needs to meet the standards in 30 CFR Part 7 (Testing by Applicant or Third Party) under subpart E (Diesel Engines Intended for Use in Underground Coal Mines), in 30 CFR Part 36 (Approval Requirements for Permissible Mobile Diesel-powered Transportation Equipment), or must meet or exceed the applicable particulate matter emission requirements of the Environmental Protection Agency (EPA). DPM emission control is required for the underground environment concerning DPM concentration in 30 CFR Part

57 (Safety and Health Standards – Underground Metal and Nonmetal Mines) under sub-part D (Air Quality, Radiation, Physical Agents, and Diesel Particulate Matter).

For manufacturers of diesel engines for underground mines, their diesel engines must meet the standards above and they must apply for certification from MSHA. All MSHA approved diesel engines, power packages, and equipment are listed on MSHA's website (Anon., 2010a).

To select a diesel product, a mine operator needs to consider the application's requirements, such as power, rated speed, physical size, etc.; then examine the MSHA approval list. For example, if one wants a permissible diesel equipment to be used in an underground coal mine, he/she should look at the 36C approved permissible diesel-powered equipment and upgraded Part 36 (Schedule 31) permissible diesel-powered equipment. If more than one machine meets the requirements, then check the diesel engines in these machines from the MSHA-approved diesel engines list for permissible and non-permissible equipment. From the engines lists, one should pick an engine with the lowest particulate index (PI, the amount of air needed to dilute the engine produced DPM to 1 mg/m^3) that closely matches the engine power and rated speed. Then, one can check the ventilation rate to see whether it is acceptable. Some engines require very high ventilation rates to dilute the pollutants produced.

To select diesel equipment for underground M/NM mines, the diesel engine of the equipment must also be listed on the MSHA-approved diesel engines for permissible and non-permissible equipment list. Then the PI and ventilation rate should be checked before selecting the equipment.

2.1.1.2 Engine maintenance. Although engine maintenance alone will not allow an operator to meet very low DPM specifications, it is still an essential step for limiting deleterious emissions. Unmaintained engines, over time, will deteriorate and increase their DPM output. It is important to realize that the very first step on the path to reducing worker exposures is to implement an effective diesel vehicle/engine maintenance protocol and apply it to every diesel unit that operates underground.

The early work in this area was performed by the U.S. Bureau of Mines (Waytulonis, 1992). The University of Minnesota's Center for Diesel Research (Spears, 1997) developed procedures for using tailpipe gas measurements as a diagnostic for engine

maintenance. A comprehensive study on the relationship between diesel engine maintenance and tailpipe emissions was completed by McGinn (2000) under a research effort by the Diesel Emission Evaluation Program (DEEP). McGinn developed a maintenance auditing procedure (McGinn, 2000) and guidelines (McGinn, 1999), which were implemented in a hardrock mine with demonstrable results. Also, Anyon (2008) in Queensland Australia, reported a 64 percent reduction in DPM by applying effective maintenance.

2.1.2. Fuels. Research on DPM reduction in fuels has identified the effects of alternative fuel such as biodiesel, biomass to liquid (BTL), or gas to liquid (GTL) diesel; fuel-water emulsions; ultra low sulfur fuel; and fuel additives compared to regular petroleum diesel fuel.

Howell and Weber (1997) reported using pure biodiesel compared to diesel fuel in both lab and field testing. The lab testing showed a 50 percent DPM reduction and the field test showed a time-weighted DPM reduction of 55 percent compared to diesel fuel. Watts et al. (1998) and Bagley et al. (1998) reported an approximately 20 percent DPM reduction in an isolated zone of an underground metal mine by using a blend of biodiesel with D2 fuel (an ultra low sulfur diesel fuel) compared to standard low-sulfur No. 2 diesel fuel. Schultz et al. (2006) reported a field study in two underground limestone mines. Compared to No. 2 diesel, recycled vegetable oil (consisting of different fuel mixtures and a virgin soy oil), was reported to have a 35-65 percent DPM reduction, and water-blended diesel fuel emulsion had a DPM reduction of 52 to 79 percent. Gangal et al. (2008) studied the blended biodiesel for application in underground coal mines and detected a 31 percent DPM reduction relative to the mining diesel fuel. Wang et al. (2000) reported a study in which nine heavy trucks were tested for diesel emission with B35 (35 percent biodiesel and 65 percent No. 2 diesel) and pure No. 2 diesel. The results showed that engines with B35 can reduce about 25 percent of DPM as compared to engines with pure No. 2 diesel engine results.

Fuel-water emulsions have been reported to reduce both NO_x and PM by 40 percent to 50 percent (Anon., 1998). Water emulsified fuel was reported by Noll et al. (2006) to have a 45-57 percent DPM reduction as compared to 35 percent biodiesel, and 71-85 percent as compared to diesel fuels in underground stone mines.

When burnt, sulfur in fuel can form sulfur dioxide (gas) and sulfates (solids at room temperature). Sulfates can attach to the DPM particles and increase DPM production. Sulfates can also poison catalysts. For these reasons, it is advisable to use fuel and crankcase oil with the lowest sulfur content in underground mines (Schnakenberg et al., 2002).

Metals, when added to diesel fuel in small concentrations, were found to be efficient at oxidizing the soot, thereby reducing visible smoke (Howard and Kausch, 1980). Test results also showed that fuel additives may decrease solid PM in raw exhaust by 15 percent to 25 percent (Lepperhoff et al., 1995; Mayer et al., 1999).

2.1.3. Exhaust Gas Treatment. After DPM is produced by an engine, further reductions in emissions can be obtained by removing pollutants from the exhaust gases in the engine exhaust system. Technologies and devices that have been developed to achieve this result include diesel oxidation catalyst (DOC), diesel oxidation catalytic converters (DOCCs), selective catalytic reduction (SCR), diesel particulate filters (DPFs), three-way catalysts, thermal reactors, lean-NO_x catalysts, lean-NO_x adsorption, plasma-assisted catalytic reduction, flameless thermal oxidation, etc (Schnakenberg and Bugarski, 2002; Heywood, 1988).

Bugarski et al. (2004a) reported field tests of an underground metal mine where LHD and trucks were tested with DPFs and DOCs. Results showed that three DPFs can significantly reduce the EC concentrations when compared to the DOC test, but all results still exceeded the final DPM exposure limit. Mayer et al. (2005) reported a 99 percent filtration rate for EC by deployed DPFs in over 6,000 construction machines (about 400 were deployed underground) in Switzerland. Gangal et al. (2006) discussed the laboratory test results of DPFs after a long-term field test. The results showed that the reduction of NO_2 varied from 38 percent to 67 percent; DPM reduction was greater than 85 percent on a mass basis and greater than 93 percent on a number basis based on the photoelectric aerosol sensor (PAS) measurement. In general, laboratory-tested DPF efficiencies were similar to, or a little lower than, those measured during the field trials. Manos (2010) and Noll et al. (2010) reported a combination of DPM control strategies, including DPF, to meet requirement of the USA DPM regulation in two different underground M/NM mines. Stachulak et al. (2010) reported successful DPF usage in a Canadian underground

metal mine. Gangal et al. (2010) reported a laboratory evaluation of three advanced DOCs that indicated that availability of advanced DOCs that could reduce DPM without increasing NO_2. DPM reduction varied from 9 percent to 20 percent.

      2.1.4. Mine Ventilation. Working in a confined underground space, ventilation is critical because once DPM is released into the atmosphere, it is the ventilating air that eventually carries the DPM out of the working area. For example, suppose only 1 g is released into an underground environment, this amount can ultimately pollute 6,250 m^3 of space to the final 160 $\mu g/m^3$ if no ventilation is available. It is common for an underground diesel engine to produce this amount of DPM. For example, the Cat® 3306 DITA engine (165 horsepower), which is widely used underground, can produce 8.97 g/hr of DPM during operation. Therefore, the first step in developing a working face is to ensure that there will be an adequate air flow in the area.

      To effectively dilute DPM, many efforts can be made to upgrade the mine ventilation system. These include maintenance of existing airflow distribution systems; installation of stoppings and/or curtains to direct more air to the working area; upgrading the capacity of existing fans or installing new fans to provide more air; use of auxiliary fans to improve local airflow distribution (Pomroy and Saseen, 2008); using new material and technology to lower leakage; incorporating greater flexibilities in the ventilation system through better mine design; etc.

      To estimate DPM concentration for an underground mine, MSHA's "Work Place Diesel Emission Control Estimator" can be used (Haney and Saseen, 2000). The Estimator assumes DPM will be mixed uniformly in the working area. It is presented in the form of a computer spreadsheet and can provide a method to estimate the DPM levels and to evaluate the impact of using different control technologies on DPM exposures.

      If, under current mining conditions, the results obtained by the Estimator exceed the regulation limit, control strategies such as increasing main airflow quantity, using auxiliary ventilation, installing PDF, etc. can be incorporated into the Estimator by inputting the efficiency of the control and letting the Estimator re-evaluate the DPM level. If different combinations of strategies satisfy requirement of the existing regulations, the best strategy (or strategies) can be determined based on an economic evaluation.

This Estimator can be a handy tool for estimating the DPM concentration, but, in some cases, it may be difficult to use. First, it is hard to measure the airflow in very low velocity areas (less than 0.25 m/s or 50 fpm), especially in many underground M/NM mines with large openings. If there are mining activities in those areas, the main airflow direction and quantity cannot be easily and accurately measured. Second, the MSHA model assumes that DPM will be mixed uniformly in the face area, which may not be correct as diesel emission tends to flow upward or recirculate in a face area. This detailed information on the DPM distribution pattern can be critical in evaluating and utilizing control strategies if the distribution is different from what is expected.

Similarly, MSHA also provides a particulate index (PI) for the approved diesel engines, which is defined as the airflow needed to dilute the total particulate emissions to 1,000 μg/m3. To dilute the DPM emission to the final limit of 160 μg/m3, the airflow needed has to be 6.25 (1,000/160 = 6.25) times the PI number. Again, this PI is calculated with the assumption that the DPM is mixed uniformly in the working area.

2.1.5. Environmental Cabs. An environmental cab is equipped with a pressurizing and filtration system. To keep the system effective, cab doors and windows must be closed and sealed. In addition, an environmental cab will only protect the miners inside the cab, and cannot provide any protection to miners outside of the cab.

Noll et al. (2008) reported that the environmental cab was over 90 percent effective in removing DPM, as long as the cab system was properly maintained and the doors and windows were closed.

2.1.6. Administrative Controls. Acceptable DPM administrative controls are those work practices that can be controlled by the mine management. Rotation of miners is prohibited as a means of compliance, because this would increase the number of persons exposed to a potential carcinogen and thereby increase the number of individuals at risk.

Some common acceptable DPM administrative controls include (1) minimizing diesel engine idling; (2) keeping fuel and lube oil clean to prevent contamination; (3) routing vehicle traffic away from areas where miners work outside cabs; (4) running haul trucks with environmental cabs in return air, especially when the haul trucks are loaded and are ascending ramps; (5) limiting engine horsepower in work areas based on

available ventilation air and air quality; (6) retiring older machines that would typically have higher exhaust emissions，or only using such machines on a limited basis; and (7) scheduling blasters to work on non-production shifts (Pomroy and Saseen, 2008).

Minimizing diesel engine idle time can reduce emissions that would have to be controlled by other methods. Keeping fuel and lube oil clean can reduce the DPM formation from additional sources of contamination. Hauling with an environmental cab in return air prevents the truck exhaust from going to the production face. In addition, if a haulage truck travels from the intake to the exhaust, it can generate a "piston" effect which can help the ventilation. Upwind of production equipment keeps the workers, who have to work outside a cab (like the drillers and blasters), from being exposed to emissions from the equipment. If no other control strategies are used in a working area, ventilation will be the only strategy to dilute and remove the DPM that is produced. Therefore, if the airflow quantities are limited or the intake air contains DPM already, then to comply with the DPM regulation, the engine horsepower has to be limited to reduce the production of DPM so that it can be handled by the available ventilation. Similarly, a high-emission machine has to be replaced by a low-emission machine, or only used occasionally, to reduce DPM production if raising the ventilation rate is prohibitive. Scheduling blasters to work on non-production shifts will prevent their exposure to DPM from production equipment, since blasters often work outside a cab.

2.1.7. DPM Measurement. There are several DPM measuring methods that are utilized to enforce the regulations and estimate the environmental DPM level. And the most popular ones are listed as follows.

2.1.7.1 Standard measuring methods for different countries. In the U.S., the determination of emission for underground coal mines is listed in 30 CFR Part 72.503. Unlike the regulations for underground M/NM mines, for which the ambient concentration limit is set for DPM in underground coal mines, the machine emission limit is specified for different categories of diesel equipment (permissible, nonpermissible heavy-duty, generator or compressor, and nonpermissible light-duty). The amount of DPM emitted by a particular engine, with or without an aftertreatment device, is sampled and measured by a laboratory test, as described in 30CFR Part 7.86 and Part 7.89 (Anon., 2010b).

In the U.S., for compliance determinations made in underground M/NM mines, the regulations require the use of a full-shift personal sampling train to collect the miner's exposure to DPM in the underground environment. The sampling train consists of a cyclone, an impactor, the filter cassette, a length of tubing, lapel clips, and a constant flow sampling pump. The purpose of inserting an impactor between the cyclone and the filter cassette is to remove the respirable dust particles that are larger than 0.9 micron in size. This prevents larger, non-diesel dust particles from being sampled and analyzed as diesel particulate. The flow rate required in this case is 1.7 L/min. After the sampling, DPM sample will be analyzed by the NIOSH Analytical Method 5040, which uses a thermal-optical method and can quantify OC/EC at low levels (Pomroy, 2002).

In Canada, the respirable combustible dust (RCD) method is required by most Canadian provincial regulations to set the personal exposure limit at 1.5 mg/m^3. The method includes sample collection and RCD analysis. The Canadian sampling train consists of a cyclone, the filter cassette, a length of tubing, lapel clips, and a constant flow sampling pump. The difference from the U.S. sampling train is that it does not include a submicrometer impactor between the cyclone and the filter cassette. The pre-separator is a 10-mm nylon cyclone which removes the coarse (non-respirable) portion of the airborne dust. It should be cleaned prior to each use and checked for obstructions or manufacturing defects. The pump flow is also set at 1.7 L/min. After the sample is collected from the underground environment, the filter is placed in a furnace at a temperature of 400°C. This requires that a silver membrane filter (25 mm in diameter, and 0.8 μm in pore size) be used for the sampling process. Silver acts as a catalyst, which enables the DPM to be burned at a lower temperature. Weighing of the filter before and after burning yields the mass of dust burned off in the process. This value is used as an estimate of the DPM mass collected on the filter. The concentration is calculated using this mass, the sampling flow rate and the total sampling time (Grenier et al., 1998).

In Germany, method ZH 1/120.44 (sometimes called the coulometric method) is the official method used for determination of EC content in diesel engine emission (TC, OC can also be determined by this method). This method, or a variation of it, is also being used for threshold limit compliance measurements in Austria and Switzerland (Birch et al., 1999). For personal measurements, a sampling device includes a cyclone head, a

filter, and a personal sampling pump. The cyclone head separates large particles out to obtain the respirable fraction. The cyclone is backed-up with specially treated glass-fiber filters of 3.7 cm in diameter and connected to a personal sampling pump with a flow rate of 2.0 L/min. In general, personal sampling is preferred, but in some cases, with difficult sampling conditions, stationary samplers can be applied as well. According to the general regulations of the German TRGS 402, the measurement has to be based on the eight-hour shift. After a sample is collected from an underground environment, the filter is transferred to a laboratory. In the laboratory, the coulometric analyzer will be used to determine the EC, OC content. (Dahmann et al., 1996; Dahmann and Bauer, 1997; Czerwinski et al., 2003).

  2.1.7.2 Other DPM measuring methods and instruments. Although not used for regulatory purposes, other types of instruments and methods can be used for maintenance, experiments, comparisons, or other purposes. These include a near-real-time monitoring instrument developed by NIOSH that uses an optical absorbance method (Janisko and Noll, 2008; Takiff and Aiken, 2010); a near-real-time gravimetric equivalent analysis instrument (Wu and Gillies, 2008); a high-volume sampling train developed by NIOSH; an instrument that measures the particle numbers and size distribution called the scanning mobility particle sizer (SMPS); a TEOM series 1400a ambient particulate monitor (Mischler et al., 2006); an Undiluted Gas Analysis System (UGAS) developed by Noranda Technology Centre (McGinn et al., 2000); etc.

2.2. SIMULATION OF AIRFLOW AND CONTAMINANT PROPAGATION

  2.2.1. Current Simulation of Mine Ventilation Planning. Mine ventilation network design is traditionally conducted using Hardy-Cross based numerical simulators. There are several computer packages available on the market including: VnetPC (US), VentSim (Australia), VentGraph (Poland), MIVENA (Japan) and VUMA (South Africa). In every case, the mine openings are represented by nodes and branches collectively called a ventilation network. In this network, an airway, drift or shaft, is characterized by a single parameter: the airway resistance. This resistance can be measured or calculated from Atkinson's equation. The fluid used with the simulator is air or a mixture of air and airborne contaminants. In most cases, this fluid is assumed to be incompressible and of

constant density. The energy source is represented by a fan curve. For a given mine ge-
ometry and working face with fixed flow requirements, a simulator is used to determine
the airflow/pressure distribution in the network. The results are then evaluated against the
flow requirements and other external factors such as minimum required air velocity, max-
imum allowable gas concentration, allowable fan pressure, etc. If requirements are not
met, the input parameters are modified and the simulator is executed repeatedly until all
the constraints are satisfied.

While those one-dimensional fluid flow simulators can effectively simulate the
airflow network for normal mine ventilation planning, they are not always best suited to
analyze DPM dispersion patterns in the face area where diesel engine exhaust gases are
discharged at high temperatures and tend to stratify at the crown of the entry. For this
situation, the use of three-dimensional, fluid-flow models can provide more useful quan-
titative design information regarding environmental conditions throughout the entire en-
try cross section and the length of entry segment of interest than can one-dimensional
models.

2.2.2. CFD Simulation. Computational Fluid Dynamics, CFD, is one of the
branches of fluid mechanics that uses numerical methods and algorithms to solve and an-
alyze problems that involve fluid flows. Computers are used to perform the millions of
calculations required to simulate the interaction of fluids and gases with the complex sur-
faces used in engineering. CFD has the capacity to perform 2-D and 3-D simulations and
to provide an illustrative presentation of the results, which allows designers to have an
increased understanding of the problem. A good understanding of the fluid-flow behavior
results in improving the accuracy and, consequently, safety of designs with minimum
cost of the investigation.

However, a comprehensive validation process of CFD modeling against actual
mining experiments is an important issue in the application of the CFD results in a DPM
propagation study. That is the reason industry field studies and specially designed ex-
periments were carried out to validate the simulation in this research.

The aim of this section is to see whether CFD can be used as a tool to tackle the
DPM problem for underground mines. If CFD simulation can be used to solve airflow,
dust, methane, fire problems for the underground environment, and air pollutants

problems (including diesel emissions for other industries), it should be able to solve the DPM problem for the mining industry. Then, the next step is to simulate the DPM distribution according to the mining operations and environment, simplify the model if necessary, validate the simulation model through field study and experiments, then study the most commonly met working faces, evaluate the ventilation and other control strategies, and give recommendations to improve the working face.

2.2.2.1 CFD simulation for underground mines. CFD simulation has been widely used in mining to study the airflow, dust, and methane problems. It has also been used to tackle the spontaneous heating and fire problems. Summarized below are the areas that have been studied by CFD in the mining industry.

2.2.2.1.1 <u>Simulation of airflow, dust, and methane distribution in mining industry.</u> Airflow studies with CFD simulation have been executed extensively in every section of underground mines. Dust and methane distribution studies have been mostly focused on the face areas. Heerden and Sullivan (1993) used CFD to evaluate dust suppression of continuous miners. This study calculated the airflow patterns with individual airflow velocity vectors that plotted the total airflow throughout the entry. Dust dispersion was determined qualitatively by assuming the dust particles would follow the individual airflow velocity vector, i.e., only trends in dust dispersion were considered. Srinivasa et al. (1993) studied air velocities and the effect of dust control techniques on dust concentrations at a typical longwall face. Wala et al. (1997) studied airflow patterns that showed the individual velocity vectors of airflow in underground mine openings and ventilation shafts. These patterns were also experimentally validated using pressure and velocity measurements.

Studies have been done by Bennett et al. (2003a; b), which showed that CFD has the ability to predict air contaminant concentrations in indoor occupational environments. Although not directly related to mining operations, these studies confirm that CFD can be used for gas and dust dispersion in underground mine openings. Wala et al. (2003) studied the flow patterns in a continuous miner working face with different cutting scenarios. Later, Wala et al. (2007) studied the methane distribution in an empty (containing no continuous miner) face area and found that to keep the methane level the same in the face, about five times higher air quantity was needed during the box cut than during the slab

cut. Wala et al. (2008) compared the methane distribution in the face area with or without a continuous miner. The simulation results also were compared with experiment data and were in general agreement with each other. Aminossadati and Hooman (2008) developed a two-dimensional CFD model to examine the effects of brattice length on fluid flow behavior in the crosscut regions at different main air stream velocities. Jade and Sastry (2008) studied the airflow behavior in two-way junctions and splits by CFD and experiments. It was observed that the results of the shock loss coefficient from CFD agreed well with an experiment in the flow domain with 20 percent to 80 percent for splits and junctions.

Zheng and Tien (2009a) studied the methane distribution at a longwall face. The CFD simulation revealed the airflow pattern and high methane concentration regions when the shearer was located at different locations and evaluated the effects of walkway curtain, upwind-pointing venturi water spray, and airflow introduced from the shearer drum on methane distribution. The methane emission used came from a NIOSH field study (Krog et al., 2006). Falk et al. (2010) used CFD to evaluate fan losses and to determine the most efficient configuration of system components. Hurtado et al. (2010) studied the shock losses at the intake and exhaust raises of block-caving production level drifts with CFD simulation. It was concluded that the use of simulation can help in designing more efficient mine ventilation schemes at strategic sites. Kollipara and Chugh (2010) studied the ventilation performance of several tail-gate entry supports. The simulation results showed that ATLAS and CAN supports could offer lower resistance to airflow than the conventional cribs could. Purushotham and Bandopadhyay (2010) simulated several air-crossing configurations to study the influence of shape on shock losses. It was believed, in this study, that the CFD simulations could successfully model the shock-loss phenomena of real air-crossing configurations. Stephens and Calizaya (2010) studied the leakage flow in underground coal mines. A laboratory model and a CFD model were built for this purpose. The results of both models indicated that the pressure drop and leakage across stoppings followed a decay function rather than a linear one; 50-60 percent of total leakage occurred in the first 40 percent of the mine workings.

2.2.2.1.2 <u>Simulation of spontaneous heating and fire in mining industry.</u>
Brunner et al. (1995) used CFD to evaluate the effects of varying the airflow rate in a

ventilated airway on the layering along the roof of smoke and hot gases due to a vehicle fire.

Hwang and Edwards (2005) investigated the critical ventilation velocity to prevent the formation of reversed fires for two tunnels of different size. The CFD simulation was verified by checking the computed velocity profile against experimental measurements. The computed critical ventilation velocity showed fair agreement with available experimental data taken from both horizontal and inclined fire tunnels.

Edwards and Hwang (2006) simulated fire spread along combustibles in a ventilated mine entry, where the fire propagation rate was evaluated for the ribs and roof of a coal mine entry, timber sets, and a conveyor belt. The CFD program predicted a flame spread rate of 0.0145 m/s for an actual coal mine fire in which the estimated flame spread rate was 0.0086 m/s. The difference was a possible consequence of the presence of inert materials in the mine entry's roof and ribs.

Friel et al. (2006) simulated two mine-fire experiments in the NIOSH Safety Research Coal Mine. The CFD results demonstrated that smoke from diesel-fuel fires in a return airway can develop into a roof layer that can migrate upwind, forming a counter flow to the primary airflow in a crosscut. Smoke can also penetrate into an intake airway and create a hazardous atmosphere in the intake airway, upwind from the fire. The simulation correctly represented the smoke movement.

Yuan and Smith (2008) studied the effects of ventilation and gob characteristics on spontaneous combustion fires with a bleeder ventilation system. This study discussed the relationship of pressure differential across the gob area with the temperature and induction time. Smith and Yuan (2008) also reported a CFD study to investigate the spontaneous heating in longwall gob areas using a bleederless ventilation system. The permeability and porosity profiles for the longwall gob were estimated using a geotechnical model and were used as inputs for the CFD modeling. The effects of gob permeability and resistance of the collapsed entries on the spontaneous heating were studied. The effectiveness of using nitrogen injection to prevent spontaneous heating in the gob was also examined.

Later, Smith and Yuan (2010) studied the effects of seal leakage on spontaneous heating for a single longwall panel using a Y-type bleederless ventilation system. The

simulation results demonstrated that the effect of seal leakage on the spontaneous heating process depends on both seal leakage rate and gob permeability.

Yuan and Smith (2009) used CFD to simulate spontaneous heating in a large-scale coal chamber with a forced ventilation system. The CFD model was validated by comparing simulation results with test results from U.S. Bureau of Mines experiments conducted in the coal chamber. The model predicted lower than actual temperatures in the early stage but agreed well on the induction time for spontaneous heating. The calibrated CFD model was found to be useful for predicting the induction time for spontaneous heating in underground coal mines.

Trevits et al. (2009) reported two deep-seated fire tests: one coal fire and one mixed fuel fire (coal and wood combined). The coal fire test information was then used to develop a CFD model of the fire. CFD results showed the maximum surface temperatures in the simulation were very close to those measured in the test.

2.2.2.2 CFD simulation on air pollutants in other industries. CFD simulation has been widely used for environmental engineering to tackle air pollutant problems. It has the capacity to study the complex fluid flow problems, including complex physical processes such as turbulence, chemical reactions, heat and mass transfer, and multiphase flows. The problems listed below show how it has been used.

CFD simulation has been used to study atmospheric contaminant plumes and their interaction with surrounding structures. Critical prevailing wind conditions were investigated to ensure that the plume would be adequately dispersed and not subject to unacceptable temperatures and contaminant levels promoted by surrounding structures. It can also be used to examine building ventilation system performance and to analyze the effectiveness of planned responses (Anon., 2010c).

CFD simulation can also be used to study the air quality in an urban environment. CFD can simulate the dispersion of urban pollutants, such as the emissions from vehicles, which are influenced by architectural structures, city planning, and traffic control measures. It can also examine the environmental impact of new construction to be considered in planning and licensing of the project (Balczó et al., 2005; Barna and Gimson, 2002; Huber, 2006).

For diesel emission simulation, some researchers (Gidhagen *et al,*. 2003; Uhrner et al., 2007; Desantes et al., 2006; Ström and Andersson, 2009) used particle models to study the behavior of the DPM in different scenarios, such as on the road, on the cell culture, in flow-through devices, and inside a road tunnel. Other researchers, like Ray et al. (2004) studied the distribution of nitrogen dioxide (NO_2) as an indicator of diesel emissions in a passenger railroad tunnel utilizing diesel locomotives. Both natural and mechanical ventilation systems were evaluated for a stopped passenger train operating in "hot mode" (diesel engine running to supply lights and air conditioning/heating to passenger cars).

2.2.3. Conclusions. In summary, CFD simulation has long been used in the mining industry to study airflow, along with dust, methane, and fire dispersion. The experience obtained from these research efforts enabled this study to deal with the underground environment and mining operations for DPM simulation. Current research on CFD control strategies, based on an experimental approach to the study of DPM problems, also provided the simulation with valuable information for test methodology, procedure, and data. Although simulation on DPM has rarely been used in the mining industry, it has been used to tackle this problem in other industries. It was the goal of this study to use CFD simulation to study the DPM problem in an underground mining environment and in specific mining operations. It also provided valuable insight into the DPM problem, which can be used for DPM control and evaluation by the mining society.

2.3. CHARACTERISTICS OF DPM

DPM is a complex substance with thousands of components in it. Each species can be formed differently; therefore, to describe the formation of all of them is too huge a task for this section. However, as most of the particulate material results from incomplete combustion of fuel hydrocarbons, which makes carbonaceous material (soot) the principal component, the DPM formation discussed below is focused on the formation of soot by the diesel engine.

Soot formation is a complex process. As shown in Figure 2.1, particles arise from the fuel molecules via their oxidation and/or pyrolysis products in the cylinder. The appearance of the first recognizable particles (often called nuclei) is the process called nucleation, which produces large numbers of very small particles (d < 2 nm).

These particles then develop through surface growth, coagulation, and aggregation. Surface growth involves the attachment of gas-phase species to the surface of particles and their incorporation into the particulate phase. Surface growth leads to an increase in the volume, but the number of particles remains unchanged. The opposite process is true for growth by coagulation, where the particles collide and coalesce, which decreases the number of particles while the volume remains constant. Once surface growth stops, continued aggregation of particles into chains and clusters can occur.

In the above particle-generation and growth process, oxidation can occur in the presence of oxidizing species to form gaseous products such as CO and CO_2. The eventual emission of soot from the diesel engine will depend on the balance between the formation and burnout processes.

The emitted soot is then subject to a further mass addition process as the exhaust gases cool and are diluted with air. Adsorption into the soot particle surface and condensation to form new particles of hydrocarbon species in the exhaust gases occurs in the exhaust pipe and in the atmosphere.

Figure 2.1 illustrates the processes in discrete form, which may overlap during processing, and may occur concurrently in a given region within the combustion chamber. At any given time, different processes are in progress in different regions or packets of fluid.
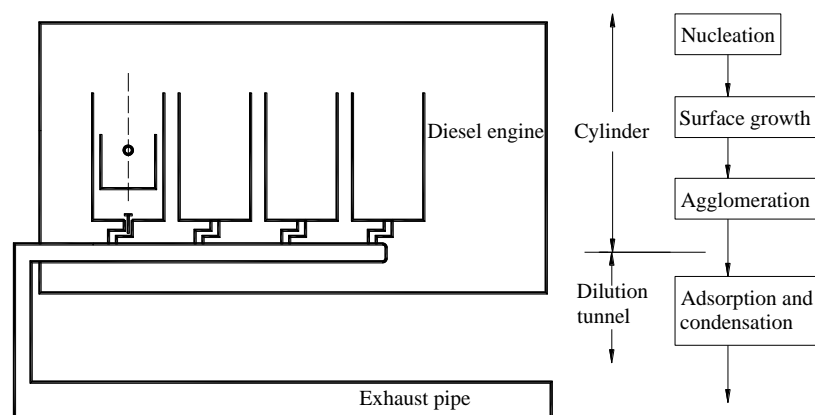
Figure 2.1. DPM Formation

By MSHA's definition, DPM is any material collected on a specified filter medium (fluorocarbon-coated glass fiber filters or fluorocarbon-based (membrane) filters (MSHA, 30 CFR Part 7.86)) after diluting exhaust gases with clean, filtered air at a temperature of $\leq 125\degree$F (52°C), as measured at a point immediately upstream of the primary filter. This material is primarily carbon, condensed HC, sulfates, and associated water. (MSHA, 30 CFR § 7.82).

The emissions from diesel engines are actually a complex mixture of compounds, containing gaseous and particulate fractions. The specific composition of the diesel exhaust will vary with the type of engine and its specific applications. Factors such as type of fuel, load cycle, engine maintenance, tuning, and exhaust treatment will all affect the composition of both the gaseous and particulate fractions of the exhaust. This complexity is compounded by the multitude of environmental settings in which diesel-powered equipment is operated. Nevertheless, there are a few basic facts about diesel emissions that are of general applicability.

The gaseous constituents of diesel exhaust include oxides of carbon, nitrogen and sulfur, alkanes and alkenes (e.g., butadiene), aldehydes (e.g., formaldehyde), monocyclic aromatics (e.g., benzene, toluene), and polycyclic aromatic hydrocarbons (e.g., phenanthrene, fluoranthene). The oxides of nitrogen (NO_X) merit particular mention because, in the atmosphere, they can precipitate onto particulate matter. Thus, reducing the emissions of NO_X is a way that engine manufacturers can indirectly control particulate production.

The particulate components of diesel exhaust gas include diesel soot and solid aerosols such as ash particulates, metallic abrasion particles, sulfates, and silicates. Most of these particulates are in the invisible sub-micron range of 100 nm.

The main particulate fraction of diesel exhaust is made up of very small individual particles. These particles have a solid core consisting mainly of elemental carbon. They also have a very surface-rich morphology. This extensive surface absorbs many other toxic substances that are transported with the particulates, and can penetrate deep into the lungs. More than 1,800 different organic compounds have been identified as absorbed onto the elemental carbon core. A portion of this hydrocarbon material results from incomplete combustion of fuel; however, most is derived from engine lubrication. In addition, the diesel particles contain a fraction of non-organic adsorbed materials.

Diesel particles released into the atmosphere can be in the form of individual particles or chain aggregates. In underground coal mines, more than 90 percent of these particles and chain aggregates are submicrometer in size, normally less than 1 micrometer (1 micron) in diameter. Dust generated by the mining and crushing of material is generally not submicrometer in size. Figure 2.2 shows a typical size distribution of the particles found in a mine environment (Cantrell and Rubow, 1992). The vertical axis represents relative DPM concentration, while the horizontal axis the particle aerodynamic diameter (μ m). As can be seen, the distribution is bimodal, with DPM generally less than 1 μm in size, and dust generated by the mining process larger than 1 μm.

As shown on Figure 2.3, diesel particulates also have a bimodal size distribution, which includes both small nuclei mode particles and a larger accumulation mode of particles. As also shown, most diesel particle mass is contained in the accumulation mode while most of the particle number can be found in the nuclei mode.

The particles in the nuclei mode (nanoparticles) were investigated because of their health hazard relevance. Interest in these particles was sparked by finding that newer ''low polluting'' engines emit higher numbers of small particles than the old engines do. Although the exact composition of diesel nanoparticles was not known, it was thought that they may be composed of condensates (hydrocarbons, water, sulfuric acid). The amount of these condensates and the number of nanoparticles depended very significantly on the particulate sampling conditions, such as dilution applied during the measurement.

Both the maximum particle concentration and the position of the nuclei and accumulation mode peaks, however, depended on which representation was chosen. In mass distributions, the majority of the particulates (i.e., the particulate mass) was found in the accumulation mode. The nuclei mode, depending on the engine technology and particle sampling technique, were as low as a few percent, sometimes even less than 1 percent. A different picture was presented when the number distribution representation was used. Generally, the number of particles in the nuclei mode contributed to more than 50 percent of the total particle count. However, sometimes the nuclei-mode particles represented as much as 99 percent of the total particulate number. The topic of DPM, with particular reference to very tiny particles known as nanoparticles, is discussed further below.
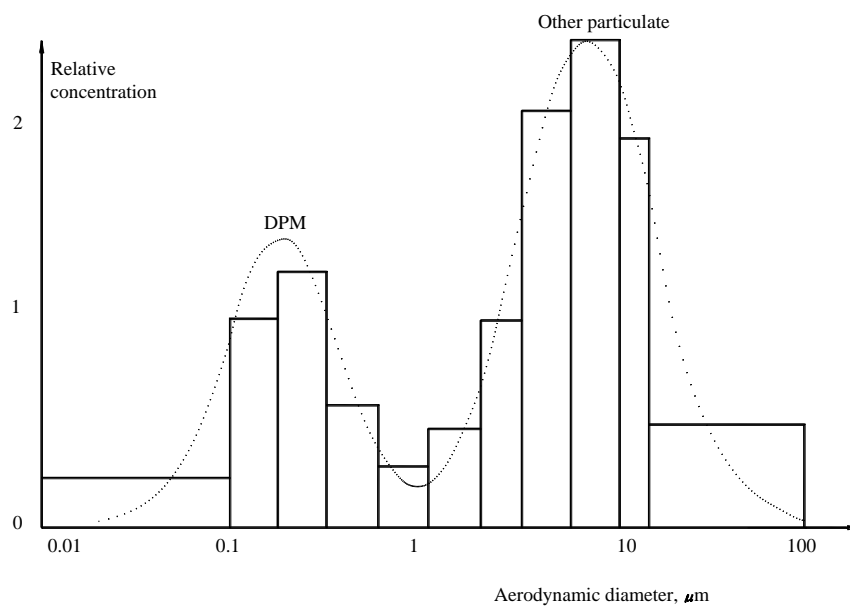
Figure 2.2 Typical Distribution of DPM Relative to Distribution of
Other Mining Particulates
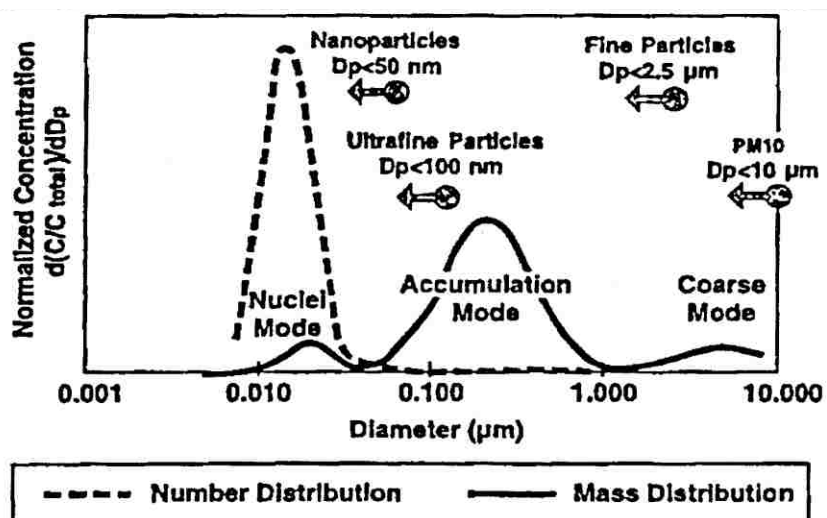
Figure 2.3. Diesel Particulate Size Distribution (Anon. 2001e)

The formation of particulates starts with particle nucleation, followed by subsequent agglomeration of the nuclei particles into an accumulation mode. Thus, as illustrated in Figure 2.3, the majority of the mass of DPM was found in the accumulation mode, where the particles were generally between 0.1 and 1 micron in diameter. However, when considering the number of particles emitted from the engine, more than half and sometimes almost all of the particles (by number) were in the nuclei mode.

2.4. DPM SAMPLING AND MEASURING METHOD FOR U/G M/NM MINES

For compliance determinations made in underground metal/nonmetal mines, the regulations require the use of a full-shift personal sampling to collect data on the miner's exposure to DPM in an underground environment, as shown in Figure 2.4. After the sampling, the DPM sample was analyzed by the NIOSH Analytical Method 5040. In the future, MSHA will adopt any methods of collection and analysis determined by NIOSH to provide equal or improved accuracy for the measurement of DPM.

For sampling, according to the MSHA final ruling for metal and non-metal mines, the sampling train consisted of a cyclone, an impactor, the filter cassette, a length of tubing, lapel clips, and a constant flow sampling pump (Figures 2.5 and 2.6). The purpose of inserting an impactor between the cyclone and the filter cassette was to remove the respirable dust particles that were larger than 0.9 micron in size. This prevented larger, non-diesel dust particles from being sampled and analyzed as diesel particulate. The flow rate required in this case was 1.7 L/min.

After a DPM sample was collected, it was sent to an accredited laboratory for analysis. In the U.S., for the purpose of enforcement, MSHA uses NIOSH Analytical Method 5040 to quantify the total carbon (TC), elemental carbon (EC), and organic carbon (OC) in the DPM to set the regulation limit. TC is defined as the sum of EC and OC. Both EC and OC are measured by NIOSH Analytical Method 5040, which is a thermal-optical method and can quantify OC/EC at low levels, typically down to 5 micrograms. Figure 2.7 shows the thermal-optical instrument used for the analysis, and Figure 2.8 reveals the thermogram of the analysis results.
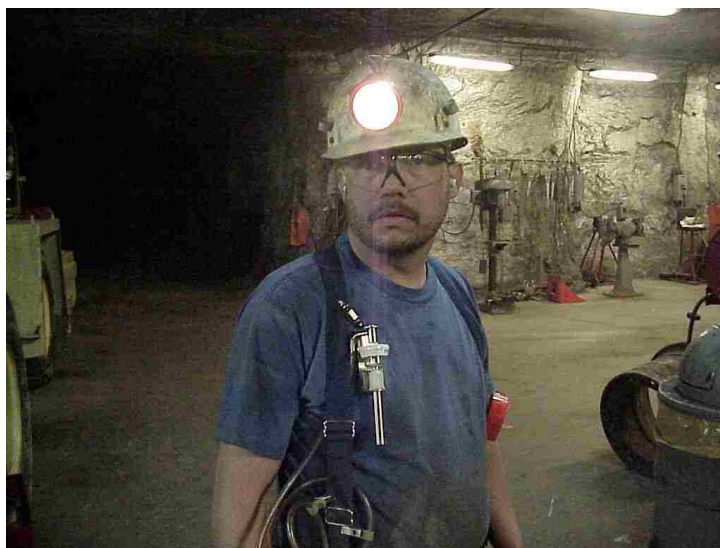
Figure 2.4 Personal Sampling of DPM in an Underground Environment
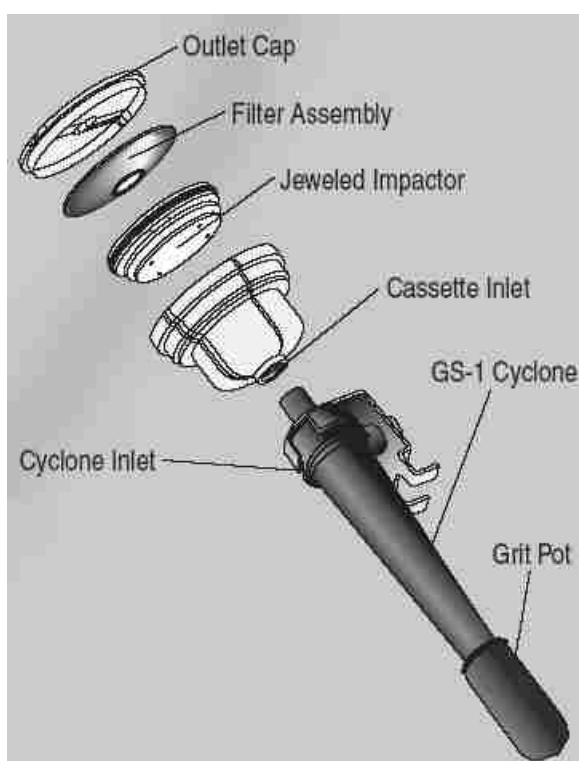
Figure 2.5 SKC DPM Sampler Includes DPM Cassette with Internal Impactor and GS-1 Cyclone (SKC Inc.)

Figure 2.6 DPM Sampling Train
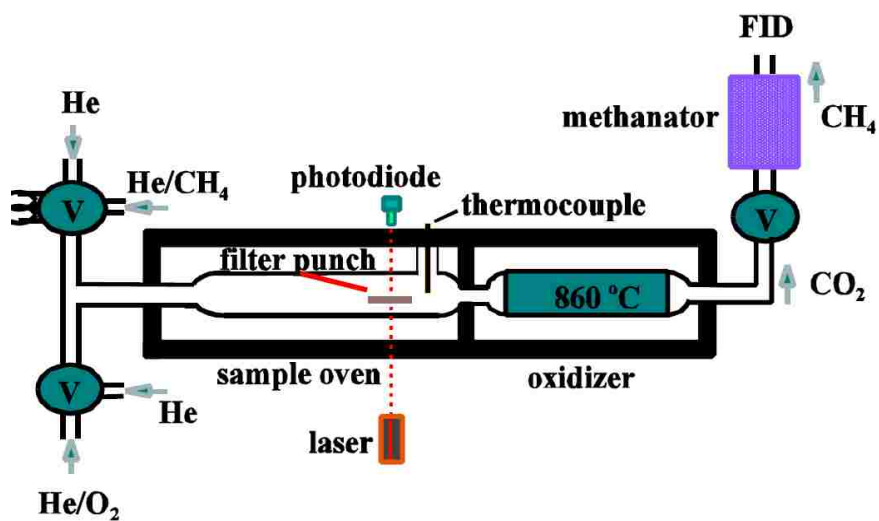
Figure 2.7. Thermal-Optical Instrument of NIOSH Analytical Method 5040 (V = valve)

In the lab, the sample cassette with the DPM filter was opened. A 1.5 cm^2 rectangular portion of the filter was extracted using metal punch. For the analysis, a homogenous filter deposit was assumed. The OC and EC are reported in terms of

microgram per cm^2 of the filter area. The total OC and EC on the filter were calculated by multiplying the reported values by the deposit area.

The filter punch was then loaded into the instrument (there was no need for the filter to be conditioned since any moisture on it would have no effect on the analysis). Laser light passed through the filter to continuously monitor the filter transmittance, which was used to separate the OC and EC content).

The thermal-optical analysis consisted of essentially two stages. In the process, the temperature and the analytical cell atmosphere were controlled to measure elemental carbon and organic carbon independently. The presence and quantity of carbonate (CC), as contained in some small particles of rock that deposited on the filter, were analyzed by a second filter punch.

In the first stage, pure helium (He) filled the atmosphere in a sample oven. As the temperature was stepped up to about 850°C, OC and CC (if present) evolved. The evolved carbon then catalytically oxidized to CO_2 in a bed of granular MnO_2 (oxidizer, as shown in Figure 2.7). When the CO_2 flowed through a nickel/firebrick methanator, it was reduced to methane (CH_4). The CH_4 was subsequently quantified by a flame ionization detector (FID). During the first stage, pyrolytically generated elemental carbon (PC) or "char" formed from materials like cigarette, wood smokes, pollen, etc. on the filter, which reduced the laser transmittance, as shown by the transmittance curve in Figure 2.8.

In the second stage, the oven temperature was lowered to about 500°C, an oxygen-helium mix was introduced, and the temperature was again stepped up to about 940°C. As the oxygen was present in the oven, the PC and original EC oxidized to CO_2. The CO_2 then was reduced to CH_4 and quantified by FID, as in the first stage. At the same time, the laser transmittance was increased by the evolvement of carbon on the filter. The point at which the laser transmittance reaches its initial value is defined as the "split" between OC and EC. Carbon that evolves prior to the split is considered OC (including carbonate), and carbon volatized after the split is considered EC. At the end of the second stage, a known quantity of CH_4 was introduced into the oven for calibration purposes.
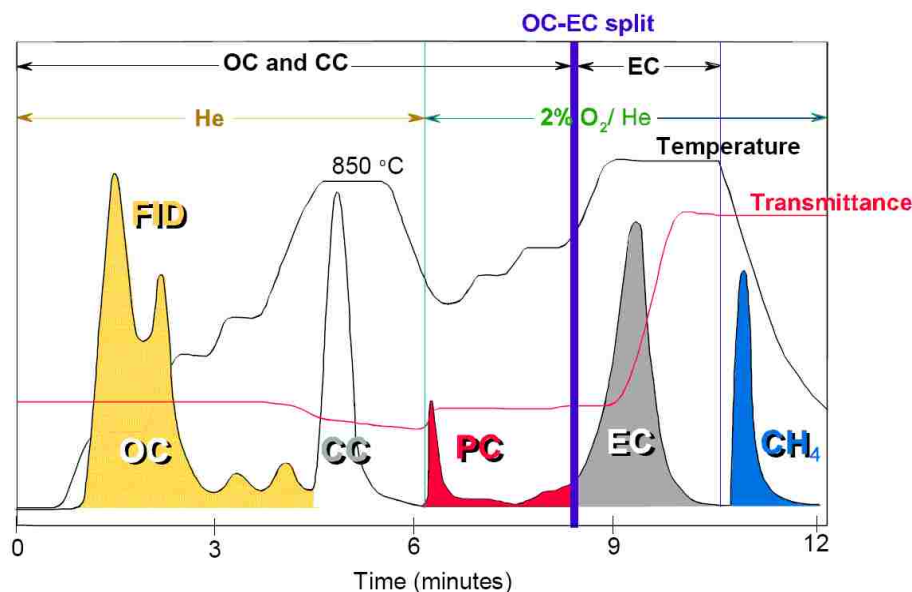
Figure 2.8. Thermogram for Filter Sample Containing Organic Carbon (OC),
Carbonate (CC), and Elemental Carbon (EC)

The presence of carbonate (from small rock particles) was removed by exposing a second filter punch to HCl vapour. The acidified sample was then analyzed by the same process, as described above. The difference between the TC results obtained from the two punches (before and after acidification) provided an estimate of carbonate-source carbon. The acidified sample results provide a better measure of the diesel-source OC and TC if a sample contains carbonates.

2.5. SPECIES TRANSPORT MODEL

Although DPM contains complicated materials, the current standard measuring method for U/G metal/nonmetal mines and the experiment done in S&T's Experimental Mine, did not differentiate between the materials. Also, DPM formation (before DPM release into the environment) was not considered, as well as any chemical reactions. DPM was only considered as a high density of gas-phase material in the simulation. The species transport model, without chemical reactions in FLUENT, was used to do the simulation work and was compared through field tests and experiment data. More detailed discussion of the species transport model is presented in Section 3.

3. THEORETICAL FORMULATION AND GOVERNING EQUATIONS

3.1. INTRODUCTION

Unlike an industrial environment where impurity sources are localized and the ventilation is designed to isolate the contaminant source, all underground mine workings contain the potential for release of air contaminants, including DPM. The same passageways in which the air contaminants are generated or released must be used to transport air for underground workers to breathe. In addition, the variety and quantity of the impurities generated underground add to the complexity of the situation.

Increasingly, in underground mining, environmental objectives require that a mining engineer condition the air to meet quality and temperature-humidity standards as well as quantity criteria. As these standards have been raised substantially in recent years, there has been increasing concern about standards for human comfort. The provision of a comfortable work environment is both cost-effective and humanitarian. Worker productivity and job satisfaction correlate closely with environmental quality. Further, excessive accident rates and workers' compensation rates are a consequence of unsatisfactory as well as unsafe environmental conditions. No mining company today can afford to be lax in its environmental and air-control practices.

Current mine ventilation planning programs like: VnetPC (US), VentSim (Australia), and VUMA (South Africa) use Hardy-Cross based numerical simulators to simulate one-dimensional fluid flow of air or a mixture of air and airborne contaminants. While those one-dimensional fluid flow simulators can effectively simulate the airflow network for normal mine ventilation planning, they are not always best suited to analyze DPM dispersion patterns in the face area where diesel engine exhaust gases are discharged at high temperatures and tend to stratify at the crown of the entry. For this situation, the use of three-dimensional fluid flow models can provide more useful quantitative design information regarding environmental conditions throughout the entire entry cross section and the length-of-entry segment of interest than can one-dimensional models.

Three-dimensional fluid flow models are the subject of fluid mechanics, especially fluid dynamics. Fluid mechanics can be mathematically complex and there are no general analytical schemes for solving nonlinear partial differential equations contained

in the governing equations for available fluid flow models. To resolve engineering problems, one approach is to simplify the governing equations and boundary conditions. Only limited cases can be solved, however, because too much simplification produces useless or unreliable results. Another approach is to use numerical methods and algorithms, with the help of a computer, to get the approximate solutions. This approach, called the computational fluid dynamics method, was used in this research to study DPM dispersion in working areas. A commercially available CFD program, FLUENT, was used to solve the governing equations of DPM dispersion.

3.2. ASSUMPTIONS

In this study, DPM was assumed as a different type of gas to simplify the simulation and save computation time. For the same purpose, diesel emissions, including DPM and air, were simplified as Newtonian, viscous, and multicomponent fluid. The diesel emissions flow within the mining environment was reduced to multi-component, incompressible, non-reacting and turbulent flow. The simplified assumptions were validated by the experiments introduced in Section 5.

Although DPM contains mostly particles or chains of particles, it can be assumed as gas for the following reasons: (1) DPM is very small in size; and (2) The quantity of DPM is comparatively low in air.

As shown in Figure 2.3, most DPM has a diameter less than 1 micron. In a NIOSH field study (Bugarski, et al., 2004), the geometric means of DPM range from 0.064 to 0.087 micron for vehicles without DPFs and from 0.035 to 0.045 micron if DPF is installed. In an experiment by DEEP (McGinn et al., 2004), particles emitted by vehicles with DPFs and DOCs have relatively high concentrations of DPM below 0.05 micron and 0.1 micron respectively. Particles at this size range are randomly drifting in the air (Brownian motion). The random movements of the particles are caused by the movements of gas molecules that nudge the particles first this way, then another way, resulting in a random series of movement that can be considered similar to the motion of fluid.

It can be calculated that, if the underground mining environment has a DPM concentration at the regulation limit (160 $\mu g/m^3$), the air (1.2041 kg/m^3) will contain about 0.13 part per million (ppm) of DPM. It has also been calculated in Section 4 that the mass

fraction of DPM in diesel emissions ranges from about 7 to 35 ppm without DPF and about 2 ppm if DPF is installed. With this quantity of DPM in the air, it was supposed in this study that the properties of DPM will not change the overall properties of air and air-flow. That is to say, the underground air with DPM still can be considered as Newtonian, viscous, and multicomponent fluid.

For the diesel emissions flow within the underground mining environment, it was assumed as multi-component, incompressible, non-reacting, and turbulent flow.

For the multicomponent nature of DPM flow, two components will be considered in the simulation, DPM and air, to reduce computation time of the study. For incompressibility, as mentioned by Hartman (1997), there are two circumstances in mine ventilation where compressibility effects have to be considered and corrections applied to quantity and head: (1) long ventilation-pipe installations in mines and tunnels where the pressure drop exceeds 5.0kPa (20 in. water); and (2) deep shafts or raises where the difference in elevation exceeds 427 m (1,400 ft.). In this study, none of these two has been reached, so incompressible flow will be assumed. For the non-reacting aspect, DPM dispersion is simulated after it is discharged from the outlet of tailpipe. From that point, the temperature of diesel emissions will drop quickly from several hundreds degrees Celsius to about the environment temperature. No chemical reactions were considered within this temperature range in this study.

To determine turbulent flow or laminar flow for underground ventilation, Reynolds number needs to be calculated. The Reynolds number is a measure of the ratio of the inertia force on an element of fluid to the viscous force on an element.

$$\mathrm{Re} = \frac{inertial\ force}{viscous\ force} = \frac{\rho u \dfrac{\partial u}{\partial x}}{\mu \dfrac{\partial^2 u}{\partial^2 y}} \sim \frac{\dfrac{\rho V^2}{L}}{\mu \dfrac{V}{l^2}} = \frac{\rho V l}{\mu} = \frac{V l}{\nu} \tag{3-1}$$

where:

ρ is fluid mass density,

ν is kinematic viscosity,

μ is dynamic viscosity,

l is characteristic of length, and

V is velocity.

When these two types of forces are important in a given problem, the Reynolds number will play an important role. However, if the Reynolds number is very small (Re<<1), this is an indication that the viscous forces are dominant in the problem, and it may be possible to ignore the inertial effects; that is, the density of the fluid will not be an important variable. Flows at very small Reynolds numbers are commonly referred to as "creeping flows". Conversely, for large Reynolds number flows, viscous effects are small relative to inertial effects and, for these cases, it may be possible to ignore the effect of viscosity and consider the problem as one involving a "non-viscous" fluid.

For air, $v = 14.8 \times 10^{-6}$ m^2/s at normal temperatures, its Reynolds number can be expressed as:

$$Re = 67,280 \, Vl \tag{3-2}$$

The fluid velocity corresponding to Re = 4,000, the lower boundary of turbulent flow for a conduit of given size, is called the critical velocity Vc. If the fluid velocity exceeds Vc, then the state of flow is always turbulent. The critical velocity can be found easily from the last relationship above, solving for Vc in m/s and setting Re=4,000:

$$Vc = \frac{Re}{67,280D} = \frac{4,000}{67,280D} = \frac{0.059}{D} \tag{3-3}$$

In mine openings, it is important that turbulent flow always prevails. This ensures satisfactory dispersion and removal of contaminants produced in the workplaces. Although the critical velocity to ensure turbulent flow varies with the size of the opening or duct, it is obvious from the above equation that turbulent flow will nearly always prevail in mine openings. A ventilation pipe or tubing that is less than 0.3 m in diameter is seldom used; thus, velocities over 0.2 m/s will always produce turbulent flow in vent tubing. Mine openings rarely have an equivalent diameter that is smaller than 1 m and, therefore, velocities exceeding 0.06 m/s will cause turbulent flow in mine headings, raises, and other openings. Exceptions where laminar flow may be encountered are in leakage through doors and stoppings in airways and in exhausts through caved or filled areas. In this study, no leakage was considered for mine-wide airflow simulation and all the cases were turbulent flow according to the calculation.

3.3. THEORY OF DPM DISPERSION MODEL

3.3.1. Modeling Turbulence. There are different ways to model turbulence. In this study, the widely recognized standard k-ε model is used for modeling the turbulence. The background information of turbulent flow, its modeling methods, and the standard k-ε model are introduced as follows.

3.3.1.1 Introduction. Turbulent flows are characterized by fluctuating velocity fields. These fluctuations mix transported quantities such as momentum, energy, and species concentration, and cause the transported quantities to fluctuate as well. Despite the complexity of the turbulent flow, the exact equations describing the turbulent motion have already been known (the Navier-Stokes equations), and numerical procedures are also available to solve these equations. However, they are too computationally expensive to simulate directly in practical engineering calculations. For the turbulent motion contains elements that are much smaller than the extent of the flow domain (typically on the order of 10^{-3} times smaller) to simulate the motion of these elements, the mesh size of the numerical grid would have to be even smaller, at least 10^9 grid points would be necessary to cover the flow domain in three dimensions.

Fortunately, for many practical problems, people are not interested in the details of the fluctuating motion and a complete time history over all spatial coordinates is not required. Instead, in turbulence modeling, a time-averaged Navier-Stokes equation is solved in such a way that small-scale turbulent fluctuations do not have to be simulated. The equations thus obtained are called Reynolds Averaged Navier-Stokes (RANS) equations.

Unfortunately, the process of averaging has created a new problem: now the equations no longer constitute a closed system since they have unknown terms representing the transport of mean momentum, heat, and mass by the turbulent motion. The system can be closed only with the aid of empirical input. Therefore, the calculation methods based on the averaged flow equations are semi-empirical.

Empirical information can be put into the system of equations by specification of the turbulent transport terms appearing in the equations. This specification is accomplished by a mathematical model of the turbulent transport processes which is called a "turbulence mode". Turbulence models are based on hypotheses about turbulent

processes and require empirical input in the form of constants or functions; they do not simulate the details of the turbulent motion but only the effect of turbulence on the mean-flow behavior. The classification of different turbulent models is briefly introduced below.

In Reynolds averaging, the solution variables in the instantaneous (exact) Navier-Stokes equations are decomposed into the mean (ensemble-averaged or time-averaged) and fluctuating components. For the velocity components:

$$u_i = \langle u_i \rangle + u_i^{'}$$ (3-4)

where $\langle u_i \rangle$ and $u_i^{'}$ are the mean and fluctuating velocity components (i=1,2,3).

Likewise, for pressure and other scalar quantities:

$$\phi = \langle \phi \rangle + \phi^{'}$$ (3-5)

where $\langle \phi \rangle$ and $\phi^{'}$ denote the mean and fluctuating scalar such as pressure, energy, or species concentration.

Substituting expressions of this form for the flow variables into the incompressible instantaneous continuity and momentum equations and taking a time (or ensemble) average yields the ensemble-averaged momentum equations. They can be written in Cartesian tensor form as:

$$\frac{\partial}{\partial x_i}(\rho \langle u_i \rangle) = 0$$ (3-6)

$$\frac{\partial}{\partial x_j}(\rho \langle u_i u_j \rangle) = -\frac{\partial \langle p \rangle}{\partial x_i} + \frac{\partial}{\partial x_i}\mu \left(\frac{\partial \langle u_i \rangle}{\partial x_j} + \frac{\partial \langle u_j \rangle}{\partial x_i} \right) + \frac{\partial}{\partial x_i}\left(-\rho \langle u_i^{'} u_j^{'} \rangle \right)$$ (3-7)

Equations 3-6 and 3-7 are the Reynolds-averaged Navier-Stokes (RANS) equations. They have the same general form as the instantaneous Navier-Stokes equations, with the velocities and other solution variables now representing ensemble-averaged (or time-averaged) values. Additional terms now appear that represent the effects of turbulence. These Reynolds stresses, $-\rho \langle u_i^{'} u_j^{'} \rangle$, are the unknown terms representing the transport of mean momentum.

A common method employs the Boussinesq hypothesis which assumes that, in analogy to the viscous stresses in laminar flows, the Reynolds (turbulent) stresses are

proportional to the mean velocity gradients. For general flow situations, this hypothesis may be expressed as

$$-\rho\langle u_i^{'} u_j^{'} \rangle = \mu_t (\frac{\partial u_i}{\partial x_j} + \frac{\partial u_j}{\partial x_i}) - \frac{2}{3}\rho k \delta_{ij} \tag{3-8}$$

μ_t is the turbulent viscosity (or eddy viscosity) which, in contrast to the molecular viscosity μ, is not a fluid property but depends strongly on the state of the turbulence. And k is the kinetic energy of the fluctuating motion:

$$k = \frac{1}{2}\langle u_i^{'} u_i^{'} \rangle \tag{3-9}$$

With the aid of (3-8), equation (3-7) can be transformed to:

$$\frac{\partial}{\partial x_j}(\rho\langle u_i u_j \rangle) = -\frac{\partial}{\partial x_i}(\langle p \rangle + \frac{2}{3}\rho k) + \frac{\partial}{\partial x_i}(\mu + \mu_t)\left(\frac{\partial\langle u_i \rangle}{\partial x_j} + \frac{\partial\langle u_j \rangle}{\partial x_i}\right) \tag{3-10}$$

This is the same as the Navier-Stokes equations, with $\langle u_i \rangle$ and $(\mu + \mu_t)$ in place of u_i and μ, and with $\langle p \rangle + \frac{2}{3}\rho k$ as the modified mean pressure. The appearance of k in equation (3-8) does not necessitate the determination of k, as it can be seen from equation (3-10) that k can be absorbed in the pressure term and replace the unknown static pressure with an unknown quantity by the pressure $\langle p \rangle + \frac{2}{3}\rho k$. The advantage of the Boussinesq hypothesis is the relatively low computational cost; the disadvantage of this approach, as presented, is that it assumes μ_t is an isotropic scalar quantity, which is not strictly true. In spite of the conceptual objection, the Boussinesq hypothesis has been found to work well in practice, simply because μ_t, as defined by equation (3-8), can be determined to a good approximation in many flow situations.

The problem of calculating Reynolds stresses now is shifted to determining the distribution of μ_t. To determine μ_t, turbulent viscosity was conceived by presuming an analogy between the molecular motion and the turbulent motion. The turbulent eddies were thought of as lumps of fluid, like molecules, that collide and exchange momentum. The molecular viscosity is proportional to the average velocity and mean free path of the

molecules; accordingly, the eddy viscosity is considered proportional to a velocity characterizing the fluctuating motion and to a typical length of this motion, which Prandtl called "mixing length", as shown below

$$\mu_t \propto \widehat{V}L \tag{3-11}$$

where $\widehat{V}$ is a velocity scale and L is a length scale.

Different turbulence models can be classified by the number of transport equations being employed. Some models use only a transport equation for the single velocity scale $\widehat{V}$, while others also use an equation for the length scale L; still more complex models solve equations for more than one velocity scale and/or length scale. For example, in the case of the Spalart-Allmaras model, only one additional transport equation is solved for the velocity scale and the length scale is assumed to be constant. In the case of the $k - \varepsilon$ and $k - \omega$ models, two additional transport equations (the turbulence kinetic energy, k, represents a velocity scale and either the turbulence dispersion rate, ε, or the specific dispersion rate, ω represent the length scale) are solved, and μ_t is computed as a function of k and ε or ω.

3.3.1.2 Standard $k - \varepsilon$ model. The Standard $k - \varepsilon$ model is probably the most widely used turbulence model. It is the simplest of all the "complete" turbulence models because it solves two separate transport equations, which allows the turbulent velocity and length scale to be determined independently.

Because of its robustness, economy, and reasonable accuracy for a wide range of turbulent flows, the standard $k - \varepsilon$ model is widely used in industrial flow and heat transfer simulations. In this research, the standard $k - \varepsilon$ model was used to simulate the underground turbulent flow.

The standard $k - \varepsilon$ model is a semi-empirical model based on model transport equations for the turbulence kinetic energy (k) and its dispersion rate (ε). The model transport equation for k is derived from the exact equation, while the model transport equation for ε was obtained using physical reasoning and bears little resemblance to its mathematically exact counterpart.

The governing equations of the standard $k - \varepsilon$ model for incompressible viscous turbulent flow are listed as below.

Turbulent Viscosity:

$$\mu_t = \rho C_\mu \frac{k^2}{\varepsilon} \tag{3-12}$$

Turbulence Kinetic Energy:

$$\frac{\partial}{\partial x_i}(\rho k \langle u_i \rangle) = \frac{\partial}{\partial x_j}[(\mu + \frac{\mu_t}{\sigma_k})\frac{\partial k}{\partial x_j}] + G_k + G_b - \rho\varepsilon \tag{3-13}$$

Dispersion Rate:

$$\frac{\partial}{\partial x_i}(\rho\varepsilon\langle u_i \rangle) = \frac{\partial}{\partial x_j}[(\mu + \frac{\mu_t}{\sigma_\varepsilon})\frac{\partial\varepsilon}{\partial x_j}] + C_{1\varepsilon}\frac{\varepsilon}{k}G_k - C_{2\varepsilon}\rho\frac{\varepsilon^2}{k} \tag{3-14}$$

In the above three equations, μ_t, k, ε are the unknown variables. After μ_t and k are determined by these closed equations, Reynolds stresses can be calculated by equation (3-8) and then Reynolds-averaged Navier-Stokes (RANS) equations can also be solved. The other variables and constants shown from equation (3-12) to (3-14) are determined as follows:

In these equations, G_k represents the generation of turbulence kinetic energy due to the mean velocity gradients, calculated as:

$$G_k = -\rho\langle u_i' u_j' \rangle \frac{\partial\langle u_j \rangle}{\partial x_i} \tag{3-15}$$

to evaluate G_k in a manner consistent with the Boussinesq hypothesis,

$$G_k = \mu_t S^2 \tag{3-16}$$

where S is the modulus of the mean strain tensor, defined as:

$$S \equiv \sqrt{2S_{ij}S_{ij}} \tag{3-17}$$

and mean strain rate is given by:

$$S_{ij} = \frac{1}{2}\left(\frac{\partial\langle u_i \rangle}{\partial x_j} + \frac{\partial\langle u_j \rangle}{\partial x_i}\right) \tag{3-18}$$

G_b is the generation of turbulence kinetic energy due to buoyancy, calculated as:

$$G_b = \beta g_i \frac{\mu_t}{Pr_t}\frac{\partial T}{\partial x_i} \tag{3-19}$$

where Pr_t is the turbulent Prandtl number for energy and g_i is the component of the gravitational vector in the i th direction. For the standard $k - \varepsilon$ models, the default value of Pr_t is 0.85. The coefficient of thermal expansion, β, is defined as:

$$\beta = -\frac{1}{\rho}(\frac{\partial \rho}{\partial T})_p \qquad (3\text{-}20)$$

C_μ, $C_{1\varepsilon}$, and $C_{2\varepsilon}$ are constants. σ_k and σ_ε are the turbulent Prandtl numbers for k and ε, respectively. They have the following default values:

$$C_\mu = 0.09, \ C_{1\varepsilon} = 1.44, \ C_{2\varepsilon} = 1.92, \ \sigma_k = 1.0, \ \sigma_\varepsilon = 1.3$$

These default values have been determined from experiments with air and water for fundamental turbulent shear flows, including homogeneous shear flows and decaying isotropic grid turbulence. They have been found to work fairly well for a wide range of wall-bounded and free shear flows.

3.3.2. Buoyancy-Driven Flows. When heat is added to a fluid and the fluid density varies with temperature, a flow can be induced due to the force of gravity acting on the density variations. Such buoyancy-driven flows are termed natural-convection (or mixed-convection) flows. In the case of DPM dispersion, the hot exhaust gases are discharged into the ambient atmosphere. This may also introduce buoyancy-driven flows.

The importance of buoyancy forces in a mixed convection flow can be measured by the ratio of the Grashof and Reynolds numbers:

$$\frac{Gr}{\mathrm{Re}^2} = \frac{g\beta\Delta TL}{v^2} \qquad (3\text{-}21)$$

When this number approaches or exceeds unity, you should expect strong buoyancy contributions to the flow. Conversely, if it is very small, buoyancy force may be ignored in your simulation. In pure natural convection, the strength of the buoyancy-induced flows measured by the Rayleigh number:

$$Ra = \frac{g\beta\Delta TL^3\rho}{\mu\alpha} \qquad (3\text{-}22)$$

where β is the thermal expansion coefficient:

$$\beta = -\frac{1}{\rho}(\frac{\partial\rho}{\partial T})_p \qquad (3\text{-}23)$$

and α is the thermal diffusivity:

$$\alpha = \frac{k}{\rho c_p} \qquad (3\text{-}24)$$

Rayleigh numbers less than 10^8 indicate a buoyancy-induced laminar flow, with transition to turbulence occurring over the range of $10^8 < Ra < 10^{10}$.

The Boussinesq assumption is used to model buoyancy.

The Boussinesq assumption treats density as a constant value in all solved equations, except for the buoyancy term in the momentum equation:

$$(\rho - \rho_0)g \approx -\rho_0\beta(T - T_0)g \qquad (3\text{-}25)$$

where ρ_0 is the (constant) density of the flow, T_0 is the operating temperature, and β is the thermal expansion coefficient. This approximation is accurate as long as changes in actual density are small; specifically, the Boussinesq approximation is valid when $\beta(T - T_0) \ll 1$.

3.3.3. Species Transport without Reactions. Species Transport Equations: when choose to solve conservation equations for chemical species, FLUENT predicts the local mass fraction of each species, Y_i, through the solution of a convection-diffusion equation for the i th species. This conservation equation takes the following general form:

$$\frac{\partial}{\partial t}(\rho Y_i) + \nabla\cdot(\rho\vec{v}Y_i) = -\nabla\cdot\vec{J}_i \qquad (3\text{-}26)$$

where $\vec{J}$ is the mass diffusion in turbulent flows. An equation of this form will be solved for N-1 species where N is the total number of fluid phase chemical species present in the system. Since the mass fraction of the species must sum to unity, the Nth mass fraction is determined as one minus the sum of the N-1 solved mass fractions.

Mass Diffusion in Turbulent Flows

In turbulent flows, FLUENT computes the mass diffusion in the following form.

$$\vec{J}_i = -(\rho D_{i,m} + \frac{\mu_t}{Sc_t})\nabla Y_i \tag{3-27}$$

where Sc_t is the turbulent Schmidt number ($\frac{\mu_t}{\rho D_t}$ where μ_t is the turbulent viscosity and

D_t is the turbulent diffusivity). The default Sc_t is 0.7. Note that turbulent diffusion gener-

ally overwhelms laminar diffusion, and the specification of detailed laminar diffusion

properties in turbulent flows is generally not warranted.

Treatment of Species Transport in the Energy Equation

For many multicomponent mixing flows, the transport of enthalpy due to species

diffusion $\nabla \cdot [\sum_{i=1}^{n} h_i \vec{J}_i]$ can have a significant effect on the enthalpy field and should not

be neglected. In particular, when the Lewis number

$$Le_i = \frac{k}{\rho c_p D_{i,m}} \tag{3-28}$$

for any species is far from unity, neglecting this term can lead to significant errors. FLU-

ENT will include this term by default. In Equation 3-28, k is the thermal conductivity.

4. CFD SIMULATION ON INDUSTRIAL STUDIES

To study DPM behaviour in an underground environment, the most convenient way is to perform research similar to well-known industrial field studies, reconstruct the tests into computer models, and then compare the simulation with experimental results. During the process of this research, the NIOSH field study (Zheng and Tien, 2009b) in Stillwater's Nye Mine and the DEEP field study in Brunswick Mine (Zheng et al., 2010) were simulated.

Both industrial studies provided detailed information about the mining environment of the test zone, diesel equipment used in the test, mining activities associated with the time period, sampling methodology, and instruments. This information was used to build the geometry of the CFD model. Most importantly, the sampling results helped to select CFD models that could satisfy DPM simulation. It also provided valuable experience that can be used to carry out future experiments needed for this research.

In this section, NIOSH and DEEP field studies are provided and simulated. Each study includes a description of the field study, the process of building the CFD model, CFD results, and discussion of CFD simulation and conclusions. At the end of the section is a summary of the simulation experience and the guidance provided for the experiment at S&T's Experimental Mine.

4.1. THE NIOSH FIELD STUDY

4.1.1. Isolated Zone Experiment Description. The experiment simulated in this study was performed by a consortium consisting of the National Institute of Occupational Safety and Health (NIOSH), the National Mining Association (NMA), the National Stone Sand and Gravel Association (NSSGA), the United Steel Workers of America (USWA), and the Methane Advisory Research Group (MARG) Diesel Coalition.

The experiment was conducted in an isolated zone in the Stillwater Nye Mine, Nye, Montana, as shown in Figure 4.1. The tested area was isolated from other parts of the mine where diesel-powered equipment is used. The tested vehicles were operated between the upstream and downstream load/dump points, which are approximately 300 m (984 ft) apart. The upstream sampling station was located approximately 90 m (295 ft)

upstream of the tested upstream load/dump point, while the downstream sampling station was about 140 m (459 ft) downstream of the downstream load/dump point. The average cross-sectional dimensions of the isolated zone entry were approximately 2.7 m (9 ft) wide by 3.6 m (12 ft) high.

The tested vehicles included haulage trucks and load-haul-dump (LHD) vehicles. In this NIOSH field study, only Caterpillar Elphinstone R1500 LHD was reconstructed. The duty cycle for LHDs is illustrated in Figure 4.1 with details described below (Bugarski et al., 2004):

"The LHDs started their cycles at the upstream load/dump point with the bucket loaded with ore. The operator would first take the vehicle into the upstream stope and unload the bucket, retreat for the length of the vehicle then advance forward and load the bucket again. The next step was to back the vehicle out of the stope and advance for two lengths of the vehicle up the ramp. At that location the operator would engage the hydraulics to simulate loading of an imaginary truck and then back the vehicle to the starting point. This loading operation would be repeated three times. After the third execution, the loaded LHD vehicle would tram up the ramp to the downstream load/dump point. The LHD would execute three load/dump tasks similar to that performed at the upstream location. At the end of the load/dump session at the downstream point the vehicle would tram loaded down the ramp to the upstream starting point to complete the cycle. It would then initiate a new cycle."

The duration of the LHDs' duty cycle averaged about 13 minutes and the lengths of the tests were dictated by the required time for the sampling instrument.

The actual ventilation rate in the test for the Caterpillar Elphinstone R1500 LHD was close to 23.60 m^3/s (50,000 ft^3/min); this rate was also used in the study to simplify the simulation cases. The adjusted contaminants' concentrations were listed in Table 4.1. In addition, all concentrations are net concentrations, which means, that the concentration of the pollutant in the upstream air had been subtracted from the downstream measurement.
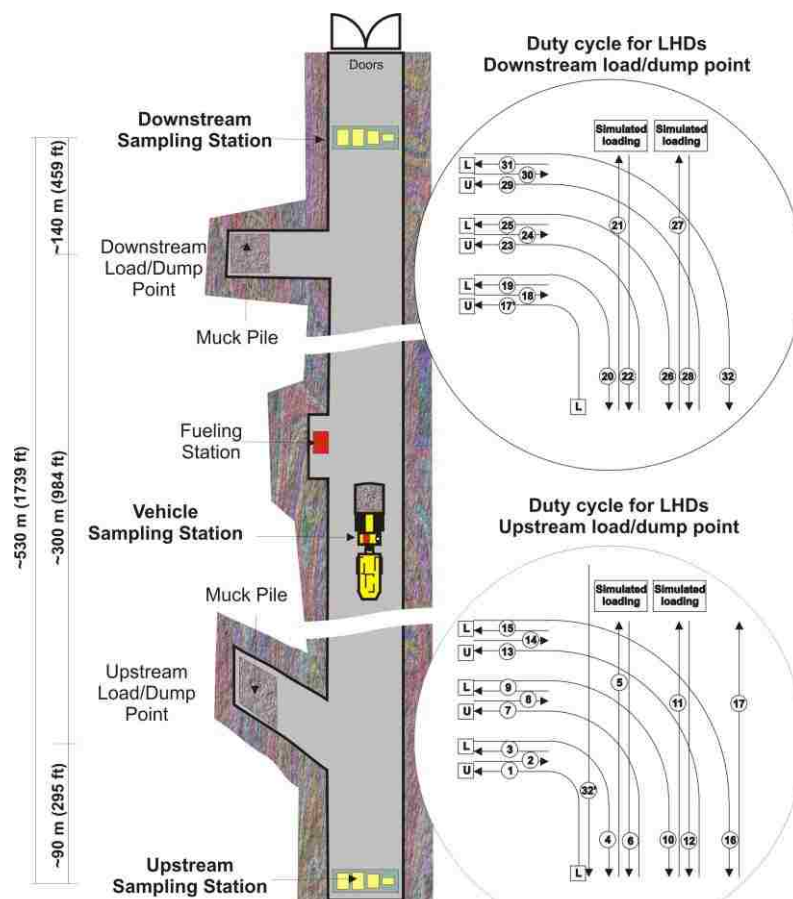
Figure 4.1. The Isolated Zone and Duty Cycle for the LHDs (Bugarski, et al., 2006)

Table 4.1. Adjusted Contaminants Concentrations

Caterpillar Elphinstone R1500 LHD, vent rate 23.60 m^3/s (50,000 ft^3/min)										
	CO [ppm]		CO_2 [ppm]		NO [ppm]		NO_2 [ppm]		EC	
	Max.	Ave.	Max.	Ave.	Max.	Ave.	Max.	Ave.	$\mu g/m^3$	CV (%)
No. 1 base-line	9.36	1.47	2,622	854.6	14.55	4.98	1.05	0.27	333.6	7.7
No. 2 base-line	8.04	1.35	2,708.4	858.4	14.04	5.01	0.9	0.24	366.6	4.0
DPF	0	0	2,596.8	813.8	12	3.63	1.71	0.63	44.7	2.6

Notes: EC means elemental carbon; CV is coefficients of variation; DPF represents diesel particulate filter; No. 1 and No. 2 baselines are the baseline test using two different diesel fuels.

In Table 4.2, the downstream EC concentration is less than 920 µg/m^3 because the standard DPM sampling method (NIOSH Analytical Method 5040) has a limit of quantification (LOQ). If the EC deposited on the sample was less than the LOQ, the downstream concentration was assigned the LOQ equivalent concentration. That is, this number is an uncertain number, and could not be used in the simulation. Therefore, in this study, only the upstream contaminants data were used for the emission production rate from the tailpipe. These data represent the baseline source emission rate and should be compared with the No.1 and No.2 baseline contaminants concentration listed in Table 4.1 to validate the CFD model.

Table 4.2. Testing of the Emission Rates at the Tailpipe

Caterpillar Elphinstone R1500 LHD, operating condition: TCS									
	CO [ppm]		CO_2 [%]		NO [ppm]		NO_2 [ppm]		EC[µg/m^3]	
	Ups.	Dns.	Ups.	Dns.	Ups.	Dns.	Ups.	Dns.	Ups.	Dns.
DPF	228.5	0	9.3	9.3	547.0	438.5	17.5	89.5	N/A	N/A
	215.0	0	9.1	9.1	607.0	523.0	10.0	45.0	16 417	< 920

Note: Ups and Dns. mean upstream and downstream measurements, respectively.

4.1.2. Development of CFD Model for the Isolated Zone Study. The analysis in this study used FLUENT to simulate diesel exhaust distribution, modeling different LHD locations operating in an isolated zone, as in the NIOSH experiment.

Figure 4.2 illustrates an overview of the CFD model where six CFD models were built to represent six different LHD positions: P1 is when the LHD is at the upstream load/dump point; P2 and P3 are when the LHD drives downstream (exhaust flow against the fresh airflow), with P2 and P3 close to the upstream and downstream load/dump point, respectively; P4 is at the downstream load/dump point; P5 and P6 are when the LHD drives upstream (exhaust flow is the same as fresh airflow), with P5 and P6 close to the downstream and upstream load/dump point, respectively.
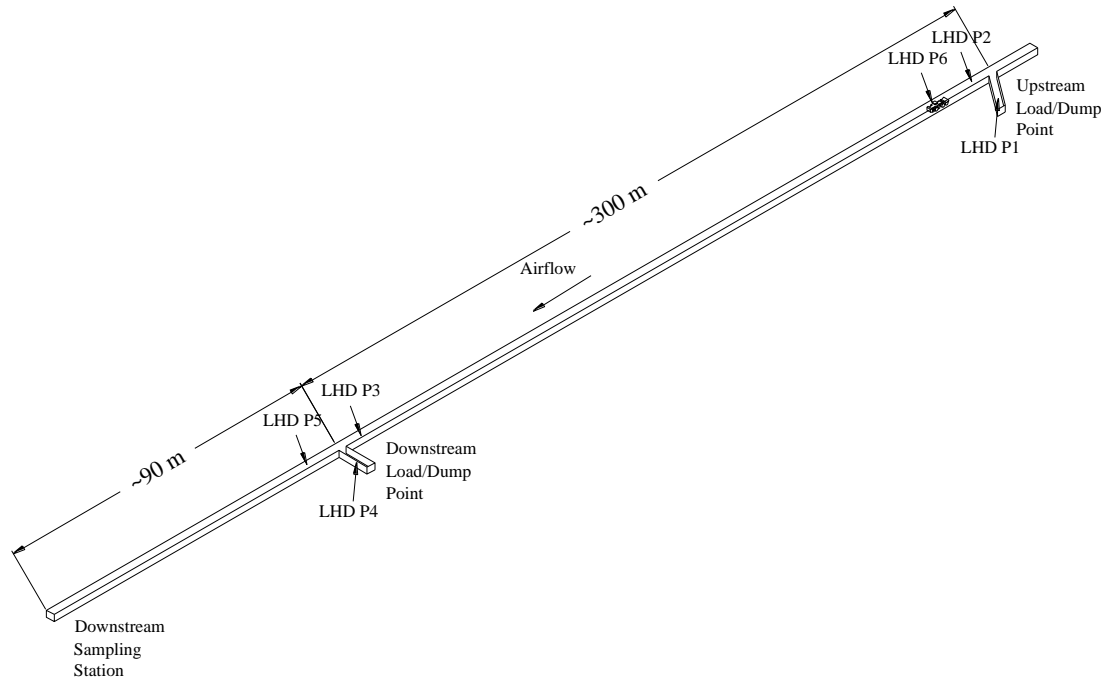
Figure 4.2. Overview of the Geometric Model and Six LHD Locations

All six models were imported as STEP files from the CAD program and then modified with the GAMBIT module of the CFD program to make them suitable for creating a proper CFD mesh. About 1.4 million tetrahedral cells were used for each CFD model (Figure 4.3).

The simulation of diesel emission distributions utilized the basic conservation equations, the k-epsilon turbulence model and the species transport model. The mass continuity and momentum equations were resolved with the SIMPLE algorithm.

In each model, six gas species were modeled from a total engine exhaust mixture of 0.89 m^3/s (1,886 cfm) on a mass fraction basis for the tailpipe setting: CO_2 (0.092), NO (0.000577), CO (0.000222), NO_2 (0.000014), DPM (0.000035) and air (remainder of the mixture). The mass fraction values for the first four gas species were calculated by averaging the two upstream numbers from Table 4.2. The value for DPM needs a little explanation. In this study, DPM was assumed to behave like air because the average geometric mean of DPM in the report (Bugarski et al., 2004) was 75.42 nm for No. 1 diesel

and 81.93 nm for No. 2 diesel. Since the exhaust temperature at the upstream port of the tailpipe was 500 ºC and the gauge pressure was 12 to 25 in. in the water gauge, the density of the air could be calculated (0.47 kg/m^3), as well as the mass fraction value of DPM at the tailpipe (0.000035).
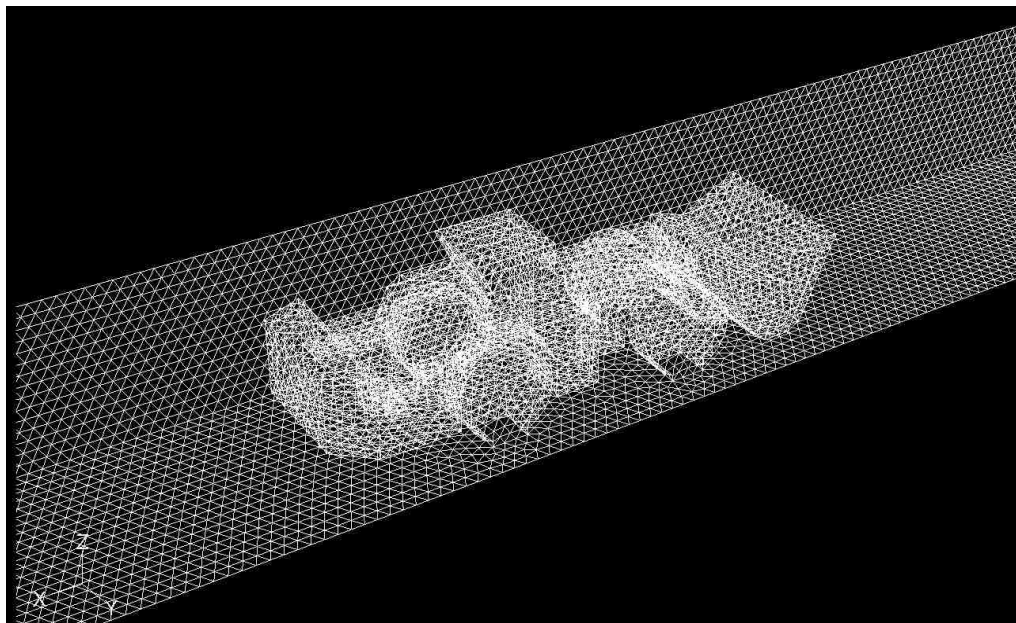
Figure 4.3. Mesh Generation near the LHD

4.1.3. CFD Results and Analysis. For the six models with the LHD in different positions, a steady state simulation was performed, with simulation results listed in Table 4.3. It can be seen from Table 4.3 that although the LHD locations in the entry were different, results at the downstream sampling station were consistent. The reason for that is quite clear: the entry was ventilated by a constant rate of fresh airflow and the engine emitted at a constant exhaust rate. After the diesel emissions were fully diluted by the fresh air, the concentrations stabilized.

Table 4.3 also compares the simulation with the NIOSH experiment results. Although data were in the same magnitude, differences remained for two main reasons. First, the tailpipe emission rates were measured in the main surface warehouse instead of being

collected during the test underground. On the surface, although the engine operated under different operating conditions, the LHD emissions were only collected in selected steady-state conditions, and the CFD simulation used the data only under high loading condition. Second, the exhaust flow rate from the tailpipe was set at 0.89 m^3/s (1,886 cfm). This number is calculated by reference to another LHD exhaust flow rate (McGinn et al., 2004), according to the different engines' displacements. Since that LHD had a more powerful engine size (247 kW, compared to 164 kW used in the S&T Experimental Mine), the number used in this simulation could be higher than the real exhaust flow rate. For the above two reasons, the simulation data were expected to be higher than the exper-imental results.

Table 4.3. Comparison of Simulation and Test Data at the Downstream Sampling Station

	LHD P1	LHD P2	LHD P3	LHD P4	LHD P5	LHD P6
CO_2 [ppm]	1237.67	1235.26	1234.56	1237.73	1236.55	1237.89
CO [ppm]	2.960	2.954	2.952	2.960	2.957	2.960
NO [ppm]	7.762	7.747	7.743	7.763	7.755	7.764
NO_2 [ppm]	0.188	0.188	0.188	0.188	0.188	0.188
DPM [$\mu g/m^3$]	551.54	553.13	552.78	554.23	553.63	554.13
	Average	Test	Diff. (%)			
CO_2 [ppm]	1236.61	856.48	44.38			
CO [ppm]	2.957	1.41	109.72			
NO [ppm]	7.756	4.995	55.28			
NO_2 [ppm]	0.188	0.255	-26.27			
DPM [$\mu g/m^3$]	553.24	350.1	58.02			

Most of the concentrations shown below were based on the current Threshold Limit Value-Time Weighted Average (TLV-TWA) and MSHA regulations: CO_2 5,000 ppm; CO 50 ppm; NO 25 ppm; NO_2 3 ppm; DPM 160 $\mu g/m^3$ (Anon., 2009).

For all six LHD positions, the distribution patterns of diesel emissions were quite similar when LHD was at P1 and P4 (at the upstream and downstream load/dump points),

P2 and P3 (exhaust flow against the fresh airflow), and P5 and P6 (exhaust flow the same as the fresh airflow).

When the LHD was at Locations P5 and P6, with the contaminants emitted from the tailpipe at high concentration, they then gradually spread to the full dimension of the entry's cross section and stabilized due to incoming fresh air (Figure 4.4). The emissions affected the operation downstream of the diesel engine, but the miners upstream or on the LHD were not affected because the CO, CO_2, NO and NO_2 concentrations were below the regulation requirements, only the miners operating adjacent to the downstream tail-pipe were affected by those which exceeded TLV-TWA (Figure 4.5). For DPM, the miners downstream of the LHD were out of compliance without personal protection (Figure 4.6).
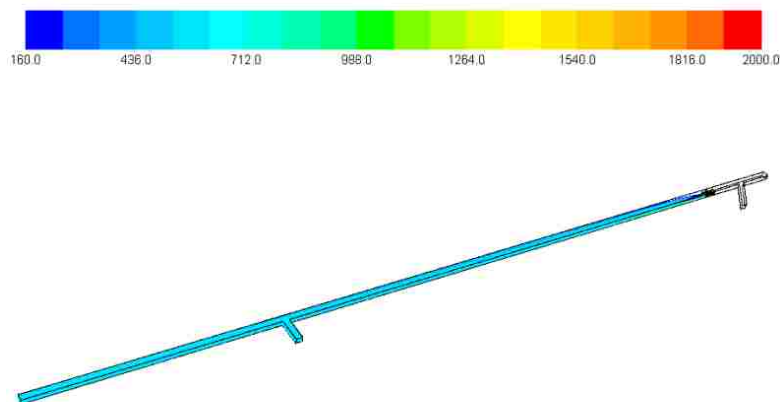
Figure 4.4. DPM Distribution at LHD P6

When the LHD was at Locations P2 and P3, since this was a well ventilated entry, contaminants were in compliance and did not affect the miners working upstream of the LHD; the distribution pattern was similar to the one at P5 and P6. The only difference was that the exhaust air affected the LHD operator when the cab was not well sealed. From the simulation, concentrations of DPM, NO, CO_2 (Figure 4.7) were above the TLV-TWA at the operator's position; the concentrations of NO_2 (Figure 4.8) and CO were not.
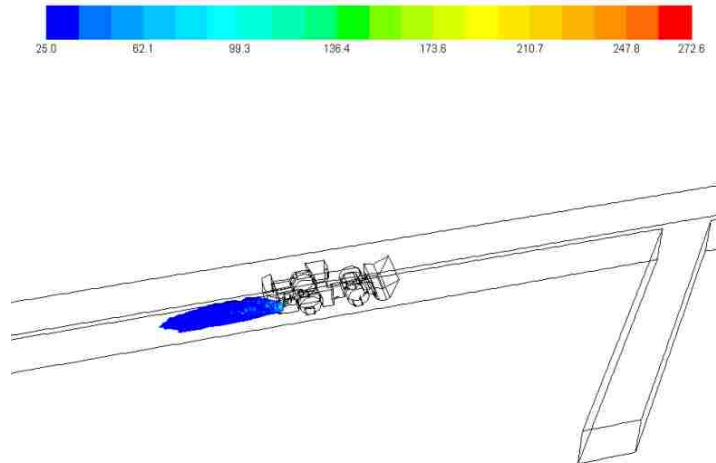
Figure 4.5. NO Distribution with Concentration above 25 ppm at LHD P6
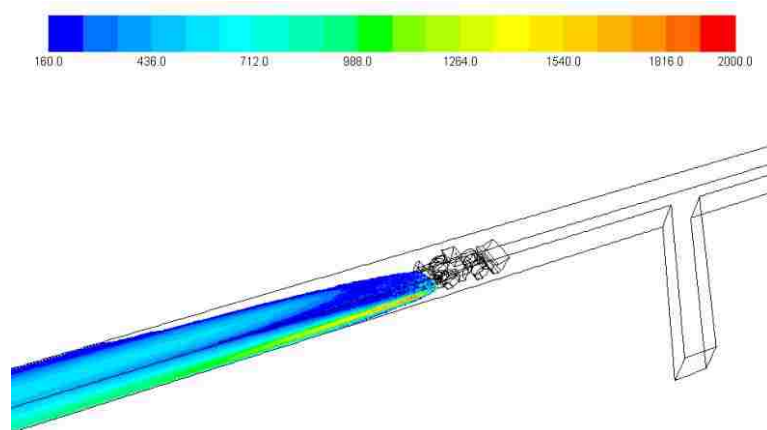
Figure 4.6. DPM Distribution with Concentration above 160 $\mu g/m^3$ at LHD P6

The worst condition happened when the LHD was near the load/dump point, because these areas were not well ventilated in these dead-end regions. In the simulation, the depth of the upstream and downstream load/dump point was about 20 m and 12 m, respectively. For the upstream load/dump point, all contaminants in the dead-end entry were above the TLV-TWA value (CO distribution shown in Figure 4.9). For the downstream load/dump point, most emissions were above the TLV-TWA value except for CO (Figure 4.10) and NO_2.
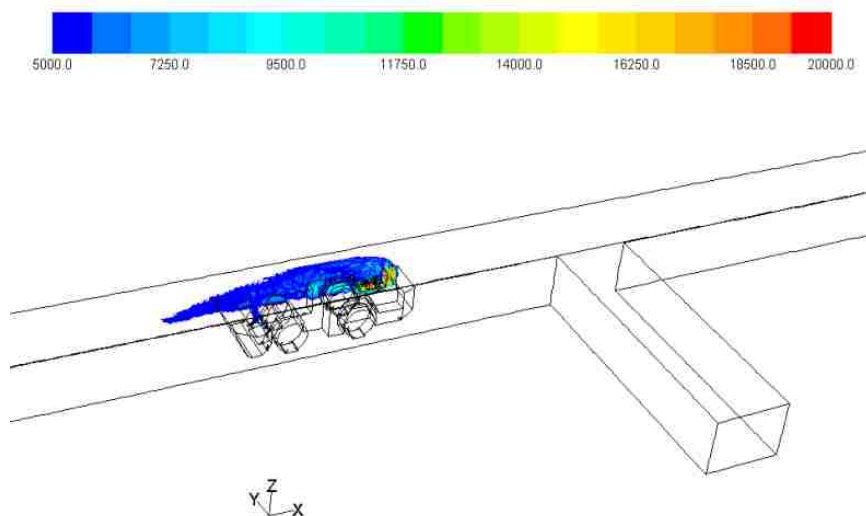
Figure 4.7. CO_2 Distribution with Concentration above 5,000 ppm at LHD P3
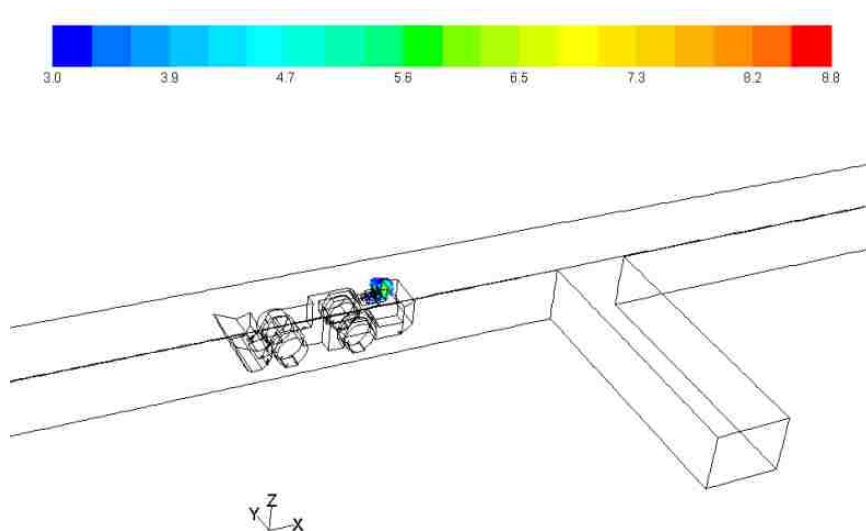
Figure 4.8. NO_2 Distribution with Concentration above 3 ppm at LHD P3

4.1.4. Conclusions from NIOSH Field Study. In this study, CFD models were reconstructed for an operating LHD in an isolated zone underground (based on a NIOSH field study) to simulate the diesel emissions distribution. High pollutant concentration

areas were identified when the diesel engine was operating in different locations. Good working practices and a proper selection of diesel emission reduction technologies can be made based on the simulation results.
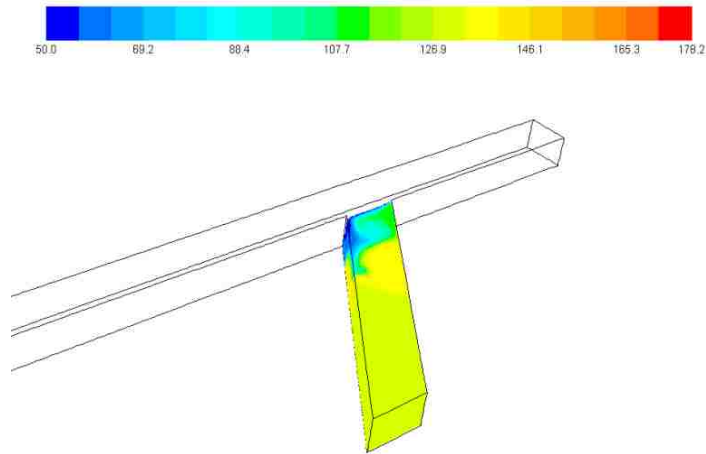
Figure 4.9. CO Distribution with Concentration above 50 ppm at LHD P1
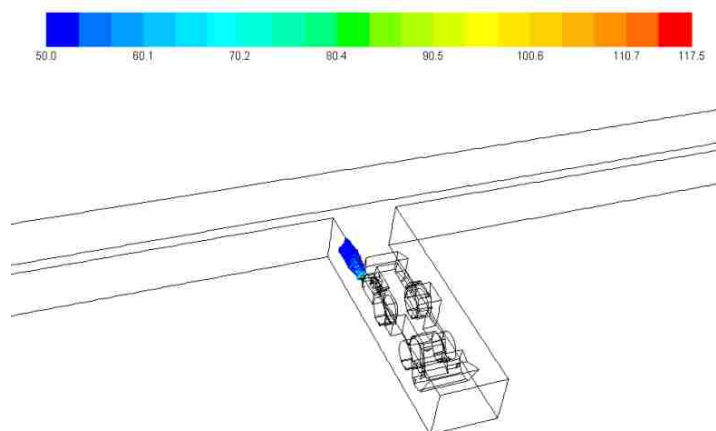
Figure 4.10. CO Distribution with Concentration above 50 ppm at LHD P4

The steady species transport CFD model showed that there was little variation in the contaminants' concentrations among the six LHD positions. Although the simulation results had some differences with the experiment data, the contaminants distribution pattern still appeared to be valid, according to other empirical studies.

In the NIOSH experiment, diesel emissions (including CO_2, CO, NO, NO_2, and DPM) were measured upstream and downstream of an isolated zone. The exhaust from the tailpipe (in the main surface warehouse) was measured also. The exhaust airflow quantity data was missed. In the study of the experiment, a LHD was simulated at six different positions. All of the simulation results of the diesel emissions gave very close numbers. Compared with the experiment data, there were some differences: CO_2 was 44.38 percent higher, CO was 109.72 percent higher, NO was 55.28 percent higher, NO_2 was 26.27 percent lower, DPM was 58.02 percent higher than the experiment. The main reason for the difference was the missed exhaust quantity used in the study. The exhaust quantity was referred to another experiment (McGinn et al., 2004) with a 51 percent higher power diesel engine. If the 51 percent higher power engine will use 51 percent more diesel, and produce 51 percent more exhaust flow rate, then the simulation results would be improved to the NIOSH experiment, except for NO_2: CO_2 was 6.62 percent lower, CO was 58.72 percent higher, NO was 4.28 percent higher, NO_2 was 77.27 percent lower, DPM was 7.02 percent higher than the experiment.

In the future, more accurate simulation results can be achieved by incorporating emission rates in different operating conditions, various lengths of operation, and exhaust flow rates at the tailpipe.

4.2. THE DEEP FIELD STUDY

4.2.1. Description of the DEEP Study. The simulated diesel activities were based on an isolated zone study performed at the Noranda Inc. Brunswick Mine. Brunswick, now part of Xstrata Zinc, is the world's largest underground zinc mine, producing 3.6 million tons of zinc, lead, copper, and silver ore per year (as shown in Figure 4.11). The section of the drift (entry) is about 400 m (~1,300 ft) long and ventilated with 14.16 m^3/s (~ 30,000 cfm) of fresh air.

Atlas Copco ST8-B Scooptrams® LHDs and Atlas Copco MT436-B haulage trucks were tested in this experiment. Each of the vehicles was operated inside the 400 m zone by repeating an 8-minute production cycle for 4 hours.

In the DEEP field study, three DPM sampling stations were established inside the zone: the fresh air sampling station (Station No. 1, at the right air intake side), the vehicle sampling station (Station No. 2, on the vehicles adjacent to the operator's compartment), and the exhaust sampling station (Station No. 3, at the left exhaust side of the zone), as shown in Figure 4.11, respectively.

Since Station No. 1 was in the fresh air current, DPM concentration was ignored. The total carbon (TC, a surrogate for DPM) concentrations were slightly higher at the exhaust sampling station than that near the vehicle operator. There were no actual data available at the vehicle sampling station from the DEEP report. In this study, the CFD simulation was based on the TC concentration collected at the exhaust sampling station only, as shown in Figure 4.11 (McGinn et al., 2004). In Figure 4.12, VH188, VH183, VH181 represent the haulage trucks equipped with a different DPF or diesel oxygen catalyst (DOC); VL254, VL244, VL247 are the LHDs with a different DPF or DOC. It can be seen from Figure 4.12, that three (VH188, VH183 and VL254) out of the six vehicles could still pollute the downstream sampling station above the current MSHA DPM regulatory limit (160 $\mu g/m^3$) for U.S. mines. Although the DEEP study was carried out in Canada, this situation was comparable to recent U.S. statistics. According to MSHA, 64 percent of the personal compliance samples exceeded the regulation limit in its survey from all of the available mines during the 2003-2006 periods (Anon., 2006a).
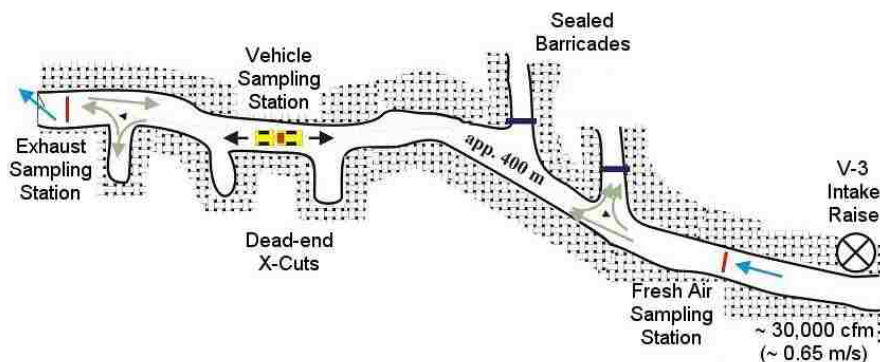
Figure 4.11. Isolated Zone Layouts in DEEP Field Study (McGinn et al., 2004)
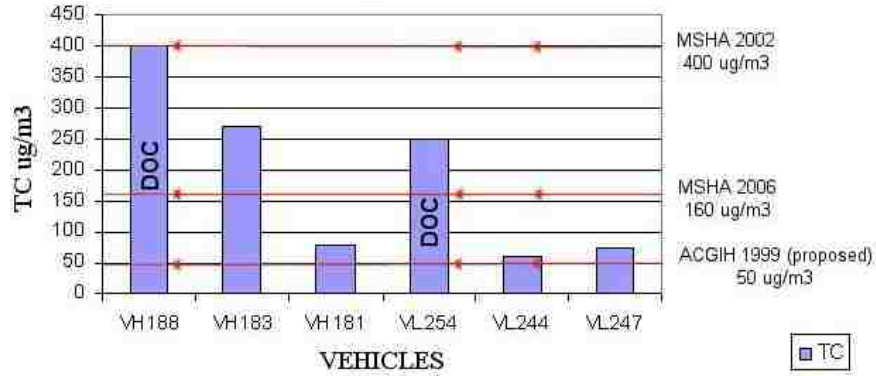
Figure 4.12. Total Carbon Levels at the Exhaust Sampling Station (McGinn et al., 2004)

In order to simulate the DPM concentration accurately, reliable input for the CFD model was required. Although DEEP supplied data for the tailpipe emission rate (ER), the data was obtained from a separate lab test. That is, the ER value was not measured from the on-site real-time test. Thus, the data from the lab test is probably different from the real emission rate when the vehicle is operating underground. The real ER had to be calculated by the exhaust sampling station data through the principle of mass conservation:

$$ER = C_i \times V_i \tag{4-1}$$

where,

C_i is the net pollutant concentration measured at exhaust sampling station, $\mu g/m^3$;

V_i is the ventilation rate where the pollutant was measured, m^3/s.

Since each vehicle was tested at a time in the isolated zone, its tailpipe emission was the only contaminant source, assuming that there was no leakage into or out of the sealed barricades (Figure 4.11). Therefore, from the TC concentration collected at the exhaust sampling station, the ER at the tailpipe could be calculated using Equation 4-1.

4.2.2. Development of the CFD Model. The analysis of DPM distribution in this study was performed by using FLUENT, one of the popular CFD simulation packages. In the DEEP experiment, two types of vehicles (LHD and truck), with six different operation settings, were constructed representing VL244, VL247, and VL254 for the LHDs and VH181, VH183, and VH188 for the trucks. Each of the six vehicles was set along the

airstream at two locations in the isolated zone using the same configurations that the DEEP study had.

Figure 4.13 is a schematic of the cases studied. For each vehicle, four different working scenarios were built with four different CFD models. In each model, a vehicle was located at a place denoted by codes from P1 to P4. P1 was where a vehicle was located close to the fresh air sampling station facing downstream. P2 and P3 were the cases where a vehicle was located in the middle of the fresh air and exhaust sampling station facing downstream and upstream, respectively. P4 was the same as P1, except that the vehicle faced upstream.

All four models for each vehicle were imported as STEP files from the CAD program and modified with the GAMBIT module in the CFD program to ensure that they were suitable for creating a proper CFD mesh (approximately 1.2 million tetrahedral cells were generated for each CFD model). Figures 4.14 and 4.15 show the mesh generated around the LHD and haulage truck, respectively.

The species transport model was used for modeling the DPM emission distribution. The steady state Navier-Stokes and continuity equations were solved, and the turbulence in the flow was modeled using the standard k-epsilon turbulence model with a buoyancy effect included in both kinetic energy and turbulence dispersion equations.
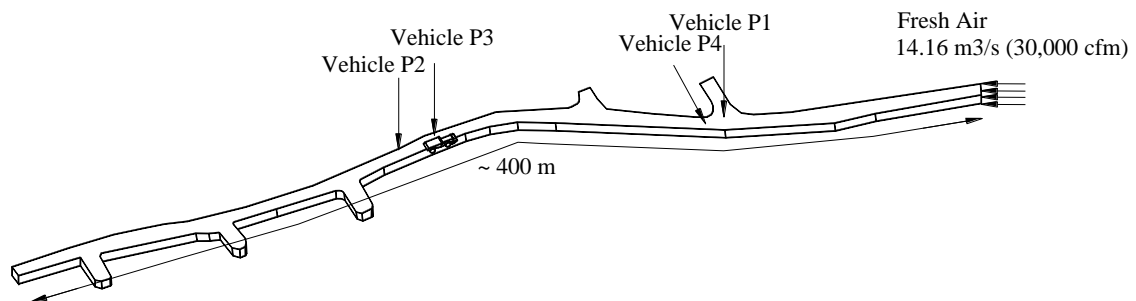
Figure 4.13. Overview of the Geometric Model and Four Vehicle Locations
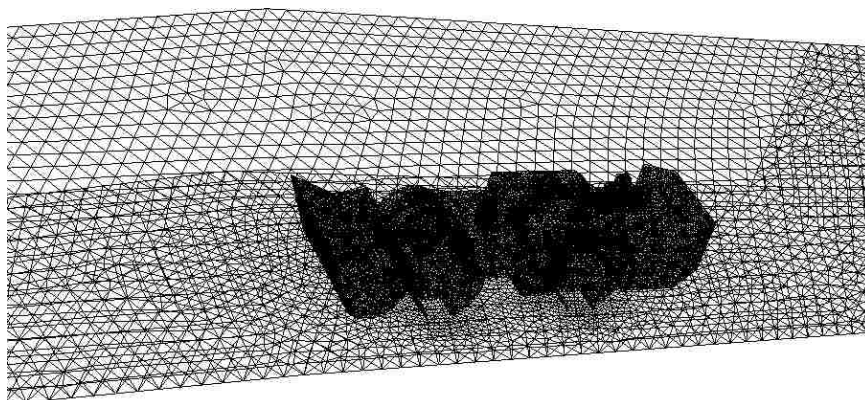
Figure 4.14. Mesh Generated around the LHD Model
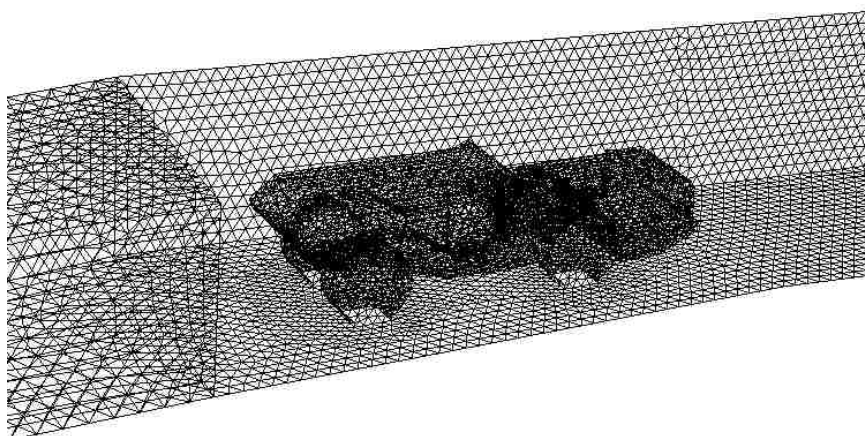
Figure 4.15. Mesh Generated around the Haulage Truck Model

In the species transport model, DPM was assumed to behave like air molecules because the size of DPM in the report is below 50 nm for VH183, VH181, VL 244 and VL247, and below 100 nm for VH 188 and VL254 from the DEEP report. For particles of this size, the air molecules' random motion controls their behaviour and result in Brownian motion of DPM. The movements of DPM were caused by the random movements of air molecules, thus DPM also moved randomly like air molecules.

To define tailpipe emissions in the CFD model, the exhaust was considered to contain two species: DPM and air. They left the tailpipe with a total engine exhaust mixture rate of 0.96 m^3/s (2,034 cfm) for the LHDs and 1.1 m^3/s (2,331 cfm) for the haulage

trucks. The temperature of the exhaust flows was 321°C (610°F) for the LHDs and 371°C (700°F) for the trucks from the DEEP report. Assuming that the mine was under standard pressure (1 atm or 101,325 Pa), then, density of the exhaust flow was 0.55 kg/m^3 for the trucks and 0.59 kg/m^3 for the LHDs. The DPM concentration can be read in Figure 4.12. Therefore, the mass fraction value of DPM in the exhaust could be calculated as 1.73 ppm for VL244, 2.07 ppm for VL247, 6.98 ppm for VL254, 10.13 ppm for VH188, 6.86 ppm for VH183, and 2.00 ppm for VH181. The mass fraction value of each vehicle was specified as boundary conditions at the outlet of the tailpipe.

In this study, the vehicles were built stationary in each model for the following reasons: (1) simplify the simulation to obtain meaningful results before the models became too complicated to manage; (2) compare with the speed of the exhaust flow (27.5 m/s or 5,413 ft/min for the trucks and 24 m/s, or 4,724 ft/min for the LHDs), the average speed of the vehicles was less than 2 m/s (400 ft/min) in the DEEP study. Therefore, after leaving the exhaust pipe, it appeared that DPM movement was only affected by the movement of the LHD when it was very close to the vehicle. The influence could be ignored after a short distance. The movement of the vehicle was considered in Section 7 which evaluates the effect of a vehicle's movement on DPM dispersion.

4.2.3. CFD Results and Analysis. For the four models of each vehicle, a steady-state simulation was performed with DPM concentration at the exhaust sampling station (outlet of the simulation domain), as listed in Table 4.4. It can be seen that although each vehicle's position in the models was different, results at the downstream sampling station were consistent for the same vehicle. The reason is quite clear, the entry was ventilated by a constant rate of fresh airflow and the engine emitted exhaust at a constant rate. After the DPM left the tailpipe, it was continually mixed by the surrounding fresh air. For a certain distance from the tailpipe, the DPM level was decreasing gradually by continuous dilution until it was fully diluted. DPM concentrations remained relatively constant beyond this point.

Table 4.4 also compares the average simulation results with the DEEP field data. Results show that the difference is quite small (≤ 0.36 percent), which means the DPM emission rate set at the tailpipe was quite close to the actual average DPM production rate underground. The simulated results were used to evaluate the DPM distribution pattern

and identify high concentration areas ($> 160_{TC}$ µg/m^3). Later, these data were used as input for the following sections to simulation DPM dissipation in commonly used straight entry and dead-end entry.

Table 4.4. Comparison of Simulation and DEEP Field Data at the
Downstream Sampling Stations

	DEEP Field Data (µg/m^3), TC	CFD Results (µg/m^3), TC					Difference (%)
		P1	P2	P3	P4	Average	
VL244	62.06	63.39	61.64	62.00	62.11	62.29	0.37
VL247	74.19	75.08	75.01	74.17	73.38	74.41	0.30
VL254	250	250.60	252.24	251.60	248.93	250.84	0.34
VH181	79.04	79.04	78.97	79.28	79.66	79.24	0.25
VH183	270.8	271.27	269.11	271.86	270.71	270.74	-0.023
VH188	400	399.50	401.49	399.95	398.45	399.85	-0.038

Note: Difference in the table is calculated as: (Average CFD Results – DEEP Field Data)/ DEEP Field Data × 100%

Results showed that the DPM distribution patterns for each vehicle in all four scenarios were quite similar when each individual vehicle was at P1 and P2 (vehicle was driving downstream toward the exhaust sampling station). A similar pattern was also observed at P3 and P4 (vehicle was driving upstream toward the fresh air sampling station). Therefore, the models with vehicles at P2 and P3 are discussed in this study.

Figure 4.16 is the general DPM distribution in the single entry. Fresh air entered from the right hand side and passed the vehicle half way between the intake and the exit on the left. The DPM concentration distribution is displayed with different colors, representing varying DPM levels. The figure indicates a high concentration in the immediate area after leaving the tailpipe and spread and filled the entire entry downstream from the tailpipe. Upstream of the vehicle, the airflow was free of DPM. A uniform color is shown

at the left end of the simulation domain, indicating that the DPM is fully diluted at the downstream sampling station. At this location, DPM level does not show much difference at different levels. This will be discussed in more detail later.
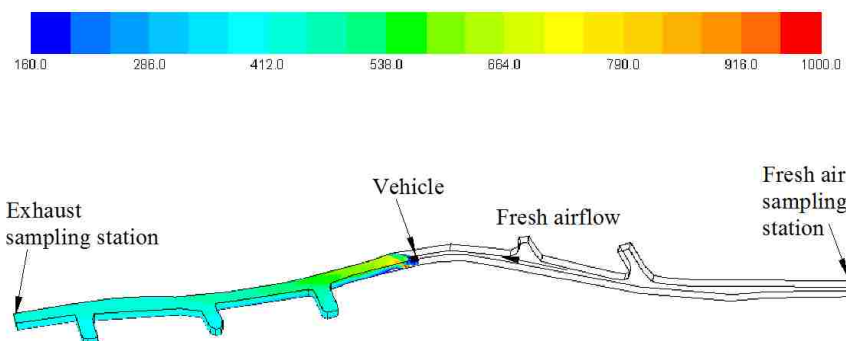
Figure 4.16. Overview of DPM Distributions in the Simulated Domain. From the legend bar, blue represents DPM concentration of 160μg/m^3 and red indicates DPM Level is no less than 1,000μg/m^3. The blank region in the domain means DPM is less than 160μg/m^3

A set of "sweep surfaces" was built to examine the DPM distribution. "Sweep surfaces" are the planes created to examine the grid, contours, or vectors on various sections of the domain without explicitly creating the corresponding surfaces. The set of "sweep surfaces" was built in the simulation domain approximately 60 m upstream from the tailpipe to the downstream sampling stations with 1-m intervals between adjacent planes to display the simulation values in each plane. Since the DPM distribution at P1 and P2 were similar, P3 was also similar to P4, therefore, planes were built when vehicles were only at P2 and P3, as shown in Figure 4.17. The DPM distribution data from the cells of these surfaces were obtained from the simulation results and were compared later in this study.

4.2.3.1 DPM dispersion of LHDs. Figures 4.18 to 4.21 show high DPM concentration regions (> 160 μg/m^3) for different LHDs (VL244, VL247, and VL254) at different positions (with the tailpipe at the back and pointing toward the back of the LHD). Fresh air flowed from the right of the entry to the left.

Among all of the LHDs in the DEEP report, VL254 produced the highest DPM level at the downstream sampling station, as shown in Figure 4.18, where different colors

represent different DPM levels. The exhaust is emitting against fresh airflow. High level DPM distribution is shown in Figure 4.19, as it was driven upstream with the exhaust flow in the same direction as the fresh airflow (P3).
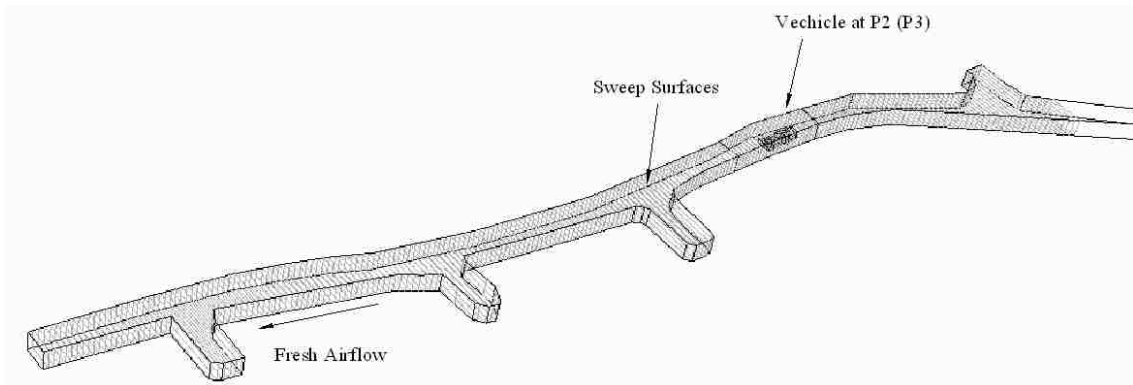
Figure 4.17. Cross Section Planes in the Simulation Domain
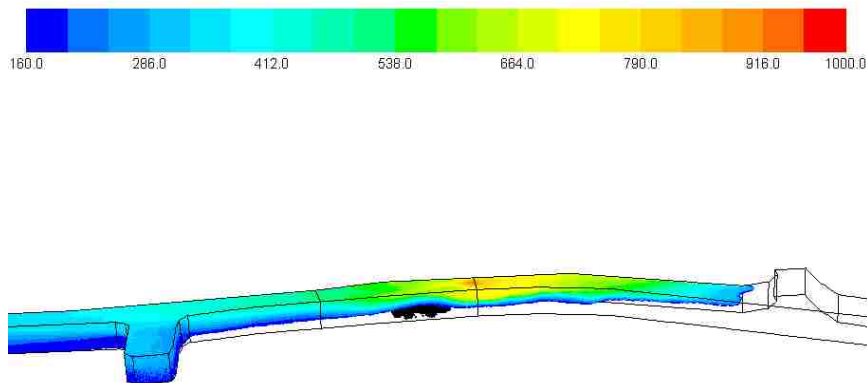
Figure 4.18. DPM Distribution for VL254 LHD with DPM above 160 µg/m^3 (P2)

Due to high DPM production from this vehicle, high DPM levels appeared immediately after they left the tailpipe and gradually occupied all of the cross section of the entry downstream. As shown in Figure 4.18, all miners downstream from the vehicle and the LHD operator were out of compliance and personal protection or an environmental

cab was needed in the affected area. In Figure 4.19, miners downstream of the VL254 were out of compliance as well, while the LHD operator was affected by the high level DPM.
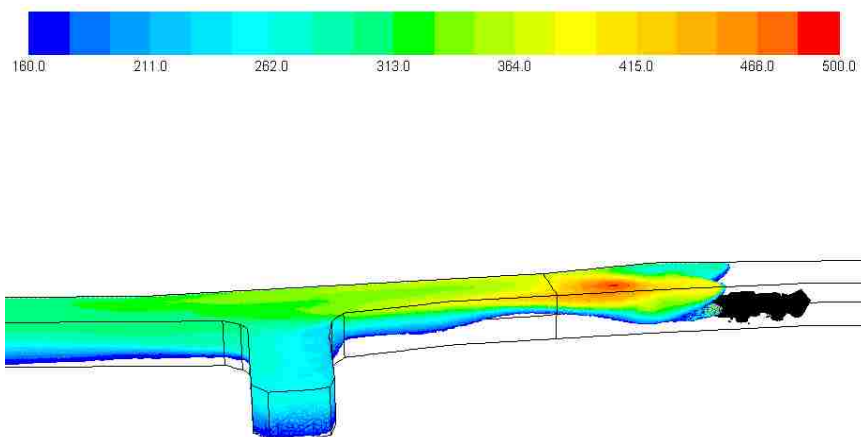
Figure 4.19. DPM Distribution for VL254 LHD with DPM above 160 µg/m^3 (P3)

Due to the buoyancy effect, the high-temperature exhaust from the tailpipe resulted in a lighter density in the upper half of the entry and tended to flow toward the back of the entry. As shown in Figure 4.18, the exhaust flow traveled against the fresh airflow (0.65 m/s or 128 ft/min) at a very high speed (24 m/s or 4,724 ft/min) from the tailpipe. DPM spread a long distance upstream against the ventilation flow to about 40 m from the tailpipe and then layered at the top. This was a very interesting phenomenon and should be verified in future experiments, since it can greatly affect local ventilation planning and the DPM control strategy for the immediate diesel engine area.

Both VL244 and VL247 were equipped with high-efficiency DPF. From Figures 4.20 and 4.21, it can be observed that the high DPM level areas were much reduced, as compared to that of VL254 (Figures 4.18 and 4.19). Only the miners who constantly work in the coloured region needed to take protective measures. Other than that, all miners, including the LHD operator, were working in compliance with the regulation.
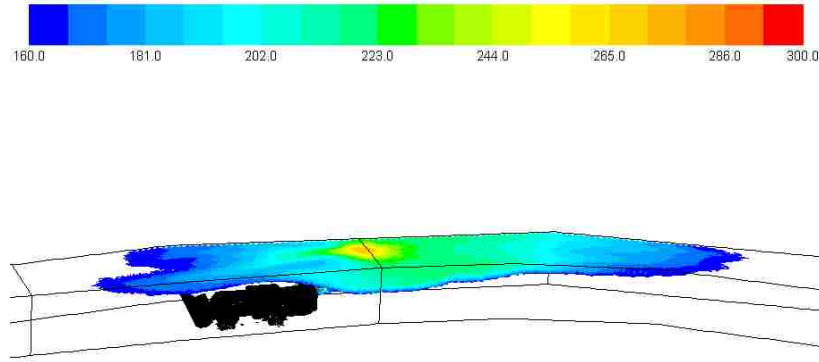
Figure 4.20. DPM Distribution for VL244 LHD with DPM above 160 μg/m^3 (P2)
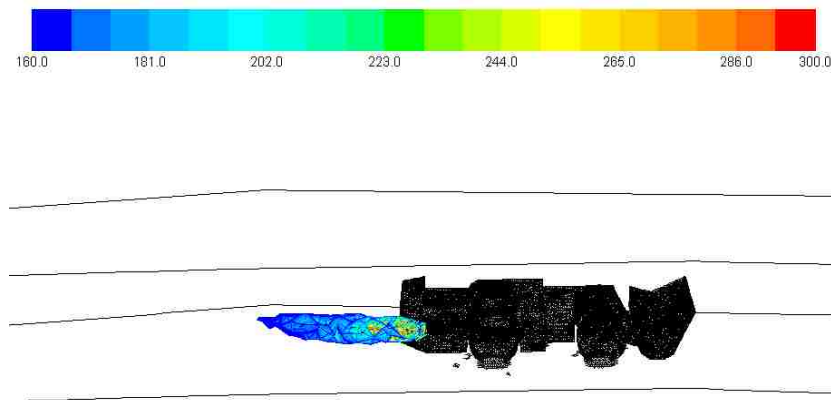
Figure 4.21. DPM Distribution for VL247 LHD with DPM above 160 μg/m^3 (P3)

Figures 4.22 and 4.23 show the minimum and maximum DPM concentrations in the different cross-sectional planes (sweep surfaces) when the LHDs were located at P2 and P3, respectively. The vertical axis shows the DPM concentration. The horizontal axis is the distance between the sweep surfaces and the tailpipe, with 0 being the location of the tailpipe opening. Minus values indicate the analysis plane was upstream from the tail-pipe opening and positive values were downstream of the tailpipe.

In areas immediately adjacent to the tailpipe, the maximum DPM concentration readings were as high as 1,000 μg/m^3 for VL244, 1,170 μg/m^3 for VL247 and about 4,000 μg/m^3 for VL254, while the minimum DPM readings were as low as zero. This

indicated that the DPM in this plane was not uniformly distributed, and high DPM exposure risks only existed for part of the sweep surface. As this front moved, it quickly mixed with the fresh air and the maximum concentration reading dropped sharply at 20 m downstream (of the tailpipe), then gradually dropped and stabilized to the average value in each case (Table 4.4). Meanwhile, the minimum DPM level gradually increased and came close to the maximum value at the same cross-sectional plane. When the minimum DPM value was above zero (> 1 μg/m^3), that was the place that the DPM distribution spread to the full dimension of the entry's cross section. At the downstream sampling station, the maximum and minimum DPM levels were very close, which means the DPM had been fully diluted at the location and beyond.
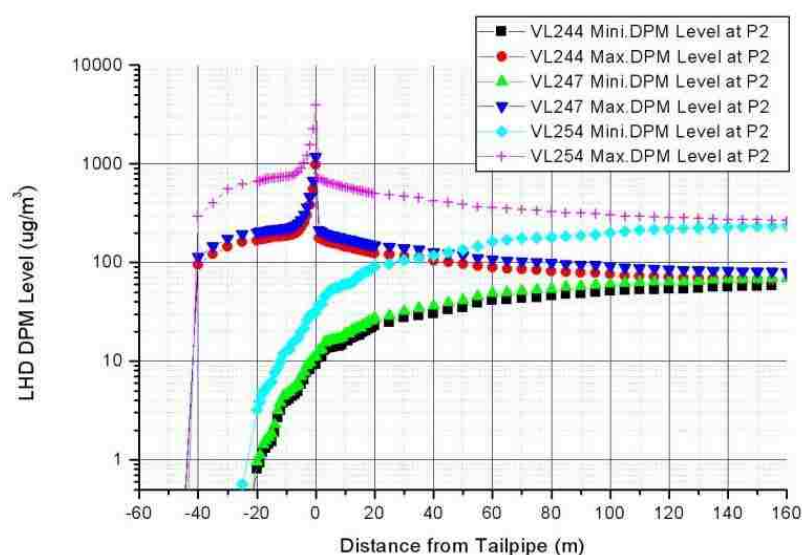
Figure 4.22. LHD DPM levels at Different Sweep Surfaces at P2

Table 4.5 highlights the DPM distribution characteristics for the LHDs. In the table, the column labeled maximum DPM level above zero (> 1 μg/m^3) means how far away DPM can affect the upstream entry and all the way downstream of the entry. For example, because of the buoyancy effect, at P2, DPM could reach about 44 m upstream

of the tailpipe. The maximum DPM level above 160 µg/m^3 indicates the position where at least part of the cross-sectional area was above the regulation limit. The minimum DPM level above zero (> 1 µg/m^3) shows where the exhaust spread to the full cross section of the entry. Finally, the minimum DPM level above 160 µg/m^3 was the place downstream at which all of the entry area was above regulation limit.
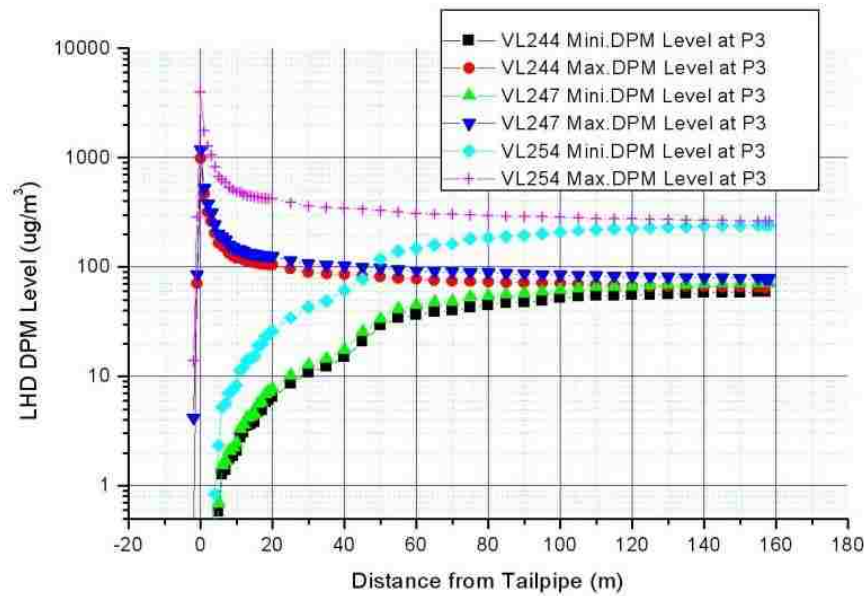
Figure 4.23. LHD DPM Levels at Different Sweep Surfaces at P3

From the table, it can be observed that high-emission diesel engines can pollute larger areas into unhealthy working places. For example, when driving downstream, VL254 could place the miners 43 m upstream of the tailpipe and all the downstream miners in working environments above the regulation limit. When driving upstream, it can affect the miners 2 m upstream and all the way downstream of the vehicle. Compared to VL254, VL244 will affect a much smaller area in both driving directions.

4.2.3.2 DPM dispersion of haulage trucks. High DPM level regions (exceeds 160 µg/m^3) with different haulage trucks (VH181, VH183, VH188) at different positions are shown in Figures 4.24 to 4.27. All truck tailpipes were pointing to the floor and all

LHD tailpipes were pointing to the rear of the vehicles. This generated different distribution patterns. In all cases (Figures 4.24 to 4.27), fresh air flowed from the right to the left of the entry at a constant flow rate of 14.16 m^3/s (~ 30,000 cfm).

Table 4.5. DPM Distribution for LHD from Different Sweep Surfaces

	LHD	Max. DPM > 1 µg/m^3	Max. DPM ≥ 160 µg/m^3	Mini. DPM > 1 µg/m^3	Mini. DPM > 160 µg/m^3
P2	VL254	~ -44 m	~ -43 to all downstream	~ 19 m	~ 60 m
	VL247	~ -44 m	~ -33 to ~ 15m	~ 20 m	N/A
	VL244	~ -44 m	~ -26 to ~ 5 m	~ 24 m	N/A
P3	VL254	~ -2 m	~ -2 to all downstream	~ 6 m	~ 26 m
	VL247	~ -2 m	~ -1 to ~8 m	~ 6 m	N/A
	VL244	~ -2 m	~ -1 to ~6 m	~ 5 m	N/A

Due to the large amount of DPM emitted from the tailpipes, the DPM concentrations exceeded the regulation limit (160_{TC} µg/m^3) downstream of both VH183 and VH188, and protective measures needed to be taken for miners working in these areas. Figures 4.24 and 4.25 show the high level DPM distribution for VH188, the worst of the three trucks, with concentrations at about $5,600_{TC}$ µg/m^3 close to the tailpipe.

High DPM level distributions downstream of VH181 are shown in Figures 4.26 and 4.27. Due to a high-efficiency DPF in this vehicle, the DPM level in the area was much improved. However, the regions in the immediate tailpipe area (colored region) were still above the regulation limit. This would be a concern for anyone who constantly works in these areas.
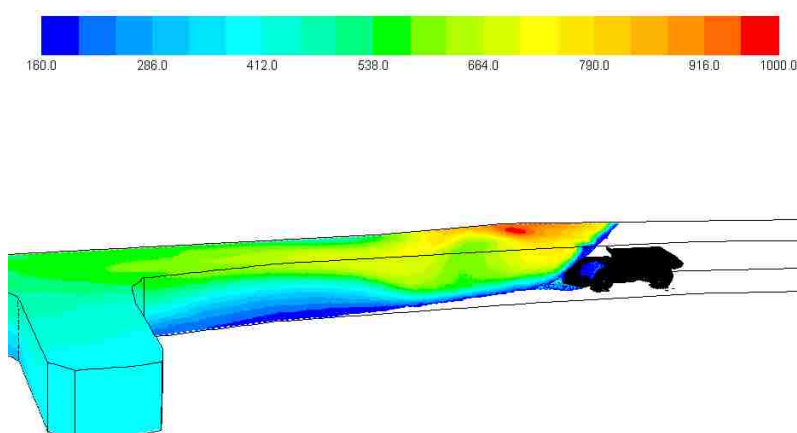
Figure 4.24. VH188 DPM Distribution with Concentration above 160 μg/m^3 (P2)

Both minimum and maximum DPM concentrations in the different cross-sectional planes when the trucks were located at P2 and P3 are shown in Figures 4.28 and 4.29.

Close to the tailpipe, the maximum DPM concentration readings reached about 1,100 μg/m^3 for VH181, about 3,800 μg/m^3 for VH183, and about 5,600 μg/m^3 for VH188; but at the same sweep surface, the minimum DPM level was still about zero. This meant that DPM in this plane was not uniformly distributed and the DPM could only affect part of the cross-sectional plane. When the DPM moved downstream, it mixed with fresh air rapidly and the maximum DPM concentration dropped sharply at about 10 m downstream of the tailpipe. It then gradually dropped and stabilized to the average value in each case (as shown in Table 4.4 DEEP field data). Meanwhile, the minimum DPM level gradually increased and came close to the maximum value at the same sweep sur-face. When the minimum DPM value was above zero (> 1 μg/m^3), that was the place where the DPM distribution spread to the full dimension of the entry's cross section. At the downstream sampling station, the maximum and minimum DPM levels were very close. This means the DPM had been fully diluted at the location and beyond. Table 4.6 highlighted the DPM distribution characteristics for the trucks. It has the same meaning as Table 4.5 and will not be discussed in detail.
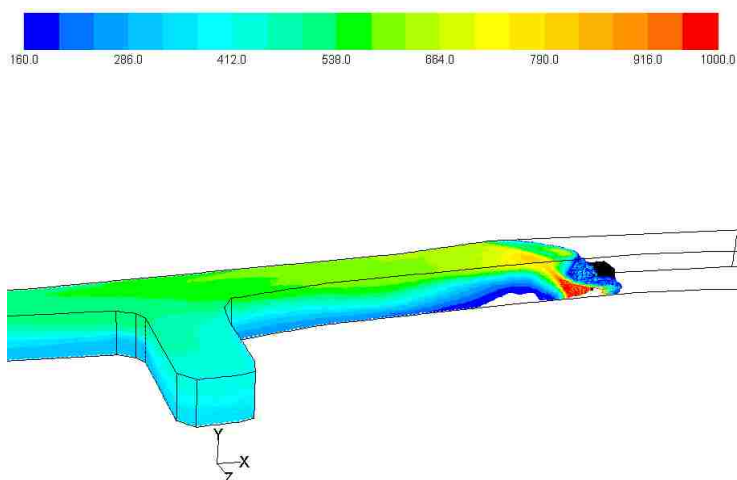
Figure 4.25. VH188 DPM Distribution with Concentration above 160 $\mu g/m^3$ (P3)
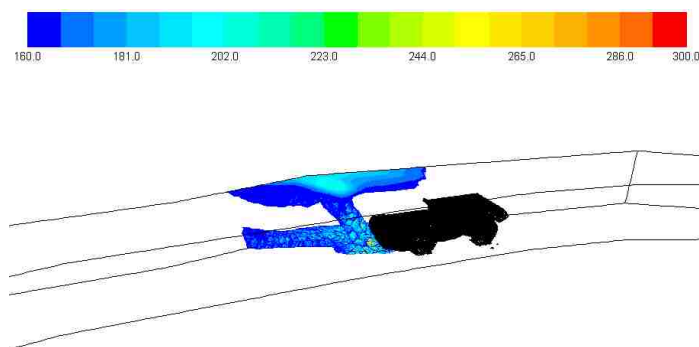
Figure 4.26. VH181 DPM Distribution with Concentration above 160 $\mu g/m^3$ (P2)
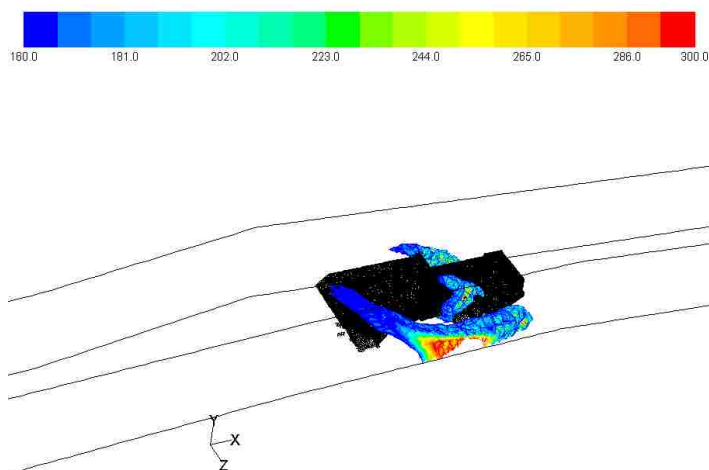
Figure 4.27. VH181 DPM Distribution with Concentration above 160 $\mu g/m^3$ (P3)
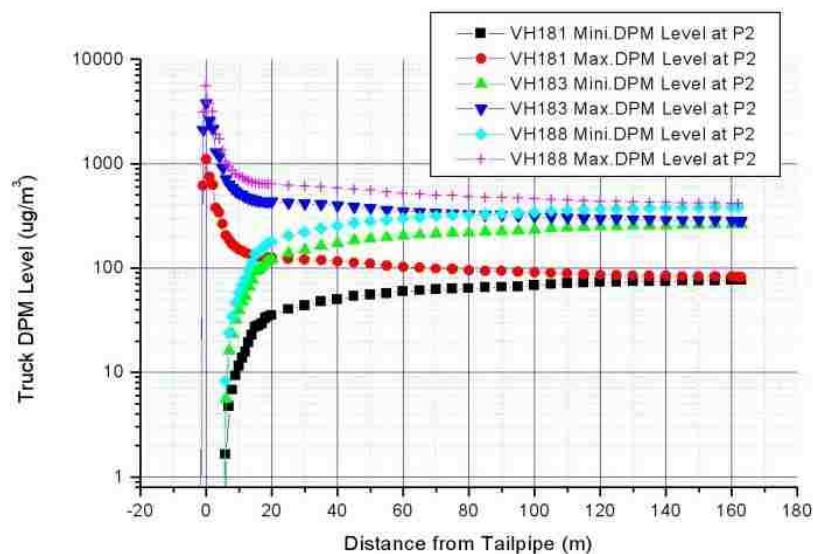
Figure 4.28. Truck DPM Levels at Different Sweep Surfaces at P2
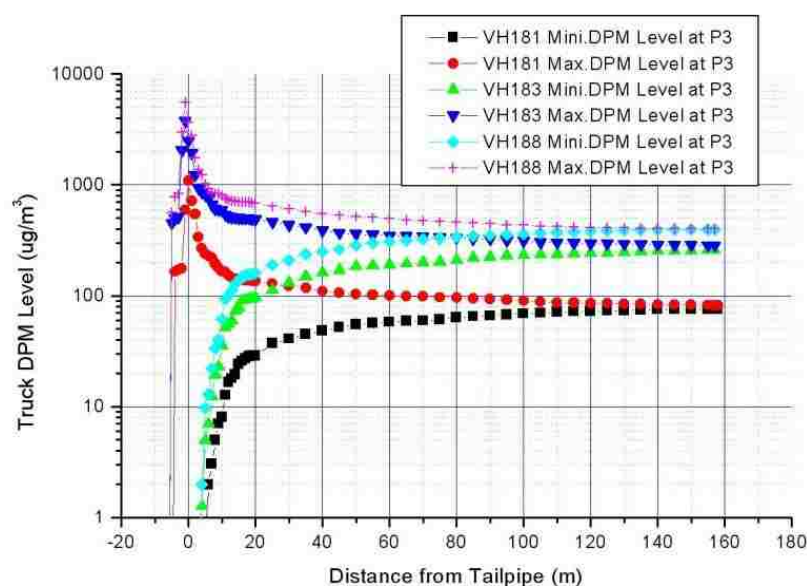
Figure 4.29. Truck DPM Levels at Different Sweep Surfaces at P3

4.2.4. Conclusions from the DEEP Field Study. This section covers CFD simu-lations that were performed to examine the DPM distribution with tailpipe emissions

from LHDs and haulage trucks in an isolated zone in an underground mine. All input parameters for the simulations were based on a DEEP field study. FLUENT was used as the CFD tool and the species transport model was selected to simulate the DPM diffusion pattern in the study zone. Diffusion patterns were examined and high DPM concentration areas identified with diesel engines operating in different locations.

Table 4.6. DPM Distribution for Trucks from Different Sweep Surfaces

	Truck	Max. DPM > 1 μg/m^3	Max. DPM ≥ 160 μg/m^3	Mini. DPM > 1 μg/m^3	Mini. DPM > 160 μg/m^3
P2	VH188	~ -2 m	~ -2 m to all downstream	~ 6 m	~ 18 m
	VH183	~ -2 m	~ -2 m to all downstream	~ 6 m	~ 34 m
	VH181	~ -2 m	~ -2 m to ~ 9 m	~ 6 m	N/A
P3	VH188	~ -5 m	~ -5 m to all downstream	~ 4 m	~ 22 m
	VH183	~ -5 m	~ -5 m to all downstream	~ 4 m	~ 41 m
	VH181	~ -5 m	~ -5 m to ~ 12 m	~ 4 m	N/A

Depending on the DPM emission rate from the tailpipe and the exhaust flow direction, high DPM level (above 160 μg/m^3) areas appeared to exist up to 40 m upstream and to all downstream airways from the tailpipe opening. The highest DPM level area was identified at the immediate tailpipe opening area and was continuously being diluted downstream of the tailpipe until it was fully diluted. The DPM level became relatively constant beyond that.

From the simulation, it was concluded that the DPM distribution pattern is mainly determined by the face layout, ventilation, exhaust flow direction, and buoyancy effect. For this field study with a single entry and a constant ventilation rate, the miners working downstream of the vehicle would be greatly affected by DPM emission rate and its closeness to the tailpipe. If the DPM emission rate is high (as in VL254, VH183, and VH188 cases), the miners working downstream of the vehicle would need protective measures. The LHD and truck operator would work in high DPM level areas if the vehicle was driven along the airflow and an environmental cab was needed. If the DPM emission rate was low (as in VL244, VL247, and VH181 cases), only the miners constantly behind the tailpipe would be out of compliance with the regulation limit, however, the effect would be offset with vehicle movement. The LHD and truck operator would be safely driving both upstream and downstream.

Like the NIOSH field study, the DEEP experiment did not provide enough input on boundary conditions of the tailpipe. To solve the problem, the diesel emission rate was calculated from the underground sampling data. This time, the simulation results were very close to the sampling data. However, this can only be considered as a calibration study, or verification study, which showed that the CFD program can calculate the concentration at a sampling station correctly. No other set of data was available for validation purposes. It is essential that an experiment be conducted for validation purposes with sufficient information for input to the simulation as well as more detailed information on DPM concentration close to the face areas. Then, more complicated face layouts can be simulated based on this additional study and different local ventilation designs can be evaluated and optimized to improve working conditions for miners.

4.3. SUMMARY

This section details NIOSH and DEEP field studies that were reconstructed with a 3-D CFD model. DPM and other air contaminants were simulated and compared with the sampling data collected from the industrial experiment.

Although these field studies provided detailed information for constructing a CFD model, one disadvantage of these studies is that the field tests did not have enough sampling results to validate the CFD model. Also, the sampling results were measured far

downstream from the mining activity where DPM were fully diluted by the ventilation airflow. DPM concentration around the diesel engine was not provided from the report, which could have been very useful for DPM control in the face area.

Nevertheless, CFD simulation of the field studies' data provided valuable information on simplifying the complicated mining process and primitive CFD model evaluation. In these studies, the species transport model of the FLUENT program was used to simulate DPM distribution, which considered DPM as air molecules. Through the simulation, it was illustrated that a CFD model had the potential to solve the DPM distribution problem for mining. Simulation based on these field studies also provided insight into the experimental design and data collection for S&T's Experimental Mine, which will be addressed in Section 5.

5. EXPERIMENTS

To further validate the CFD simulation of DPM distribution, two specially designed experiments were completed at the Experimental Mine of S&T. Unlike the industrial field studies mentioned in Section 4, where only one set of data per study was available for comparison, the experiments were designed to sample several locations to validate the model.

This section covers a comprehensive consideration of the experiment. It includes the experimental design, the methodology and procedures of the experiments, and the two experiments executed at S&T's Experimental Mine. In the first experiment, DPM was collected from four sampling points, while in the second experiment, 28 locations were sampled to compare the simulation results with the experimental data. The detailed validation studies are described in the following sections.

5.1. DESIGN OF STAGE I EXPERIMENT

The purpose of experimental design is to clarify the objectives of the experiment, identify variations, decide treatment factors and their levels, etc. Possibly the most important aim of the design is to calculate the number of observations needed for each sampling point. The checklist below details the various aspects of the design.

5.1.1. Defining the Objectives of the Experiment. The aim of the experiment was to measure the DPM concentration at different locations around a diesel engine. The data collected in the experiment was used to validate the simulation results, where the CFD method was used to predict the DPM concentration and propagation in the underground mining environment. This validation process helped to transfer the CFD expertise needed to analyze and design ventilation systems for mines that face difficulties in complying with DPM regulations.

5.1.2. Identifying All Sources of Variation. Several sources of variation were easy to identify in this experiment: different airflow rates, locations around the diesel engine, diesel engine type, operation mode, and diesel fuel type. Other possible sources of variation include: natural ventilation, leakage, temperature and humidity of the environment, other mining activity that may affect the experiment, etc.

However, due to the time and budget constraints, the experimental design needed to be as simple and clear as possible. Therefore, only one factor was considered: the locations around the diesel engine. Ventilation was set at one constant flow rate. One diesel engine was used that was operated in one fixed mode to further simplify the experiment and data analysis. The diesel fuel type was the same, only one type of fuel was used throughout the test.

Natural ventilation could not be controlled or predicted during the experiment since it can change at the beginning or during the conduct of the experiment. To compensate for part of this factor, the airflow rate during the experiment was measured several times and the mean airflow rate was used in the analysis.

Leakage was also deemed to be an uncontrollable factor. Changes may be caused by many sources, especially when a change in ventilation rate can cause a pressure difference (the higher the pressure difference, the higher the leakage rate). To eliminate this effect, the experiment provided that there was no stopping between the diesel engine and the sampling points.

The temperature and humidity were considered fixed for the experiment. Small fluctuations were not expected to be very significant.

Since the experiment was carried out in the Experimental Mine on campus, it was scheduled so there was no interference with other mining activities, and the airflow upstream of the experiment site was considered to be free of DPM.

- **Treatment factors and their levels.** There was only one treatment factor: location. The location factor has four levels: at the tailpipe outlet (level I), and theother three locations as specified by simulation results (level II, III, and IV).
- **Experimental units.** The experimental units were the DPM sampling cassettes that took the DPM samples.
- **Blocking factors, noise factors, and co-variates.** No blocking factors were considered in this experiment.

5.1.3. Choosing a Rule for Assigning the Experimental Units. A completely randomized design was selected and the DPM sampling cassettes were assigned at random to the four different treatments.

5.1.4. Specifying the Measurements. DPM sampling included two procedures: the collection of DPM and DPM exposure sample analysis. For the DPM collection, personal sampling was usually performed for measuring the exposure of individual workers and for assessing compliance with regulated exposure limits. For DPM exposure sample analysis, NIOSH Analytical Method 5040 was used. The DPM collected by the personal sampling followed the instruction for the equipment, and the DPM cassettes were then sent to a commercial laboratory to measure the DPM content.

Difficulties encountered included the selection of a testing area in the Experimental Mine and the sampling positions. Because the vehicle used in this experiment was a Bobcat skid-steer loader 753 with a 40 horsepower Kubota diesel engine, not much DPM was produced by this small diesel engine. If the sampling position had not been properly set within the DPM stream, the sampler might not have caught DPM. This would have given unreliable results that would have been hard to analyze and could not be used to validate the CFD simulation.

5.1.5. Runing a Pilot Experiment. A pilot experiment was not performed, but industrial field studies were referred to for this purpose.

5.1.6. Specifying the Model. There was one treatment factor in this experiment. The completely randomized design, with four treatments (four locations) model was (one-way analysis of variance model)

$$Y_{it} = \mu + \tau_i + + \varepsilon_{it} \qquad (5\text{-}1)$$

where,

$\varepsilon_{it} \sim N(0, \sigma^2)$

ε_{it}'s are mutually independent,

Y_{it} is the DPM concentration obtained on the tth observation of the ith treatment;

μ is a constant DPM level;

τ_i is deviation from the constant when the ith treatment is observed;

ε_{it} is the error variable, representing all minor sources of nuisance variation. It was assumed that the error variables were independent and that they had a normal distribution with zero mean and unknown variance σ^2.

5.1.7. Outlining the Analysis. The analysis was planned to compare differences in the DPM concentration affected by the four different locations. A one-way analysis of variance were computed at α =0.05 (the probability α was called the significant level of the test and was the probability of rejecting H_0 when, in fact, it was true (Type I error)) to test

$$H_0: \{ \tau_1 = \tau_2 = ... = \tau_v \}$$

versus

$$H_a: \{\text{the concentrations of at least two locations differ}\}.$$

For equal sample sizes, the computational formula for one-way analysis of variance are listed below.

Source of variation	Degrees of Freedom	Sum of Squares	Mean Square	Ratio
Treatments	v-1	ssT	ssT/(v-1)	msT/msE
Error	n-v	ssE	ssE/(n-v)	
Total	n-1	sstot		

where,

ssT is the sum of square for treatment;

ssE is the sum of square for error;

sstot is the total sum of squares;

msT is the mean square for treatment;

msE is the mean square for error.

$$n = vr \tag{5-2}$$

where,

n is the total number of observation;

v is the number of treatment;

r is the number of observation within a treatment.

For the first hypothesis at significance level, $\alpha = 0.05$, H_0 will be rejected if

$$\text{msT/msE} > F_{v-1,n-v,a} \tag{5-3}$$

where,

$F_{v-1,n-v,a}$ is F distribution with $v - 1$ and $n - v$ degrees of freedom with significance level α

5.1.8. Calculating the Number of Observations. The sample sizes were calculated by using the power of a test.

$$r = \frac{2v\sigma^2\phi^2}{\Delta^2}$$

$$\tag{5-4}$$

σ^2 is the error variance;

Δ is the smallest difference among two of the treatments that are of interest;

ϕ is a function of noncentrality parameter and number of treatment, which can be found in Power of the F-test Table (Dean and Voss, 1999).

In this research, v was 4. The experimenter deems it is important to be able to detect a difference in the DPM concentration of at least $\Delta = 31$ $\mu g / m^3$ among two different locations (the regulation limit for DPM is 160 $\mu g / m^3$ and the error factor for DPM sampling is 1.192 for TC. That is, a miner is not overexposed to DPM when TC on the personal sample is less than 191 $\mu g / m^3$. Therefore, it was decided that $\Delta = 31$ $\mu g / m^3$, which means that, when a point is measured to be 160 $\mu g / m^3$, if the other point is less than 191 $\mu g / m^3$, both of these two points are the same within regulation limit, if the other point is greater than 191 $\mu g / m^3$, then the first one is within limit but the second one is not, then they are different). Rejecting H_0 hypothesis had a probability 0.90 of correctly doing so, and a probability of 0.05 for a Type I error. This error variance σ^2 was estimated using data from another similar experiment conducted by NIOSH (Bugarski et al., 2004b), as shown in Table 5.1. From the experimental data below, the estimation of σ^2 was calculated.

Table 5.1. Results of Elemental Carbon from the Area Samples (Bugarski et al., 2004b)

Test	Sampling Location	EC [$\mu g / m^3$]	Test	Sampling Location	EC [$\mu g / m^3$]	Test	Sampling Location	EC [$\mu g / m^3$]
	300W	22		300W	33		300W	65
	300W	24		300W	36		300W	77
	300W	21		300W	32		300W	65
	3900W	226		3900W	228		3900W	291
2	3900W	240	3	3900W	198	4	3900W	279
	3900W	210		3900W	226		3900W	276
	6200W	400		6200W	360		6200W	763
	6200W	366		6200W	354		6200W	759
	6200W	394		6200W	360		6200W	696

The experiment listed above was a two treatment factors experiment. The control strategy factor had three levels (2, 3, 4), and the location factor also had three levels (300W, 3900W, and 6200W).

From statistics theory, an unbiased estimate of σ^2 (msE = ssE/(n-ab)) was made. By calculating using the above data: $\sigma^2 = 264.222$ ($\mu g / m^3$)^2. Compared to the NIOSH experiment, in which the diesel engine was operating in a complicated underground net-work and in different operation modes, this experiment was operating in a setting mode; thus, the error variance σ^2 should be smaller than the above number. It was estimated that $\sigma^2 = 100(\mu g / m^3$)^2

Therefore,

$$r = \frac{2v\sigma^2\varphi^2}{\Delta^2} = 0.83\varphi^2$$

Using a one-way analysis of variance model, for v = 4 treatments, with $\Delta = 31$, r = $0.83\,\phi^2$, and $v_2 = v(r - 1) = 4(r - 1)$, r was calculated as follows. Using power of the F-test, for $v_1 = v - 1 = 3$, $\alpha = 0.05$, and $\pi(\Delta) = 0.9$ ($\pi(\Delta)$ is the probability of rejecting H_0 when the effects of at least two of the treatments differ by Δ):

r	$v_2 = 4(r - 1)$	ϕ	r = $0.83\,\phi^2$	Action
	1000	2.00	3.32	Round up to r = 4
4	12	2.33	4.51	Round up to r = 5
5	16	2.33	4.51	Round up to r = 5

According to the calculation above, r = 5 samples needed to be taken on each location. Total samples number was 20.

5.1.9. Review. It was not very difficult to obtain five samples from each of the four locations and, therefore, the checklist did not need to be revised.

5.2. TEST METHODOLOGY & PROCEDURES FOR STAGE I EXPERIMENT

5.2.1. Test Area and Equipment. The objective of this study was to measure the DPM concentration in different locations around the diesel engine under different ventilation conditions.

To make it simple, only one diesel engine was used in the experiment. The engine was operated in a certain mode in a fixed position to offer a constant DPM stream. Since the basic character of the DPM dispersion in an underground tunnel is the objective of the most concern in this experiment, disturbances from other mining activities were eliminated from the measurement when possible. To meet these requirements, the Experimental

Mine of Missouri University of Science and Technology (S&T) was chosen for the field test.

Figure 5.1 shows the Experimental Mine of S&T. This mine is located on Bridge School Road in Rolla Missouri, about 1.5 miles from the S&T campus. It is an underground limestone mine using the room and pillar mining method. The elevation of the mine is 298 m (980 ft.) above sea level. The mine is ventilated from a single airshaft with a JOY series 1000 axivane fan, with the capacity to bring 17.93 m3/s (38,000 cfm) of fresh air from the surface. The shaded area in Figure 5.1 shows the location of the test zone in the mine. Due to the small size of the entry, a 40 horsepower Bobcat skid-steer loader 753 was used in the experiment. This diesel engine was operated at a fixed location in the test areas and was the single DPM source in the experiment. Figure 5.2 shows the Bobcat in the Experimental Mine of S&T in which regular diesel fuel was used during the experiment. Figure 5.3 shows the tank of the diesel fuel located in the mine.
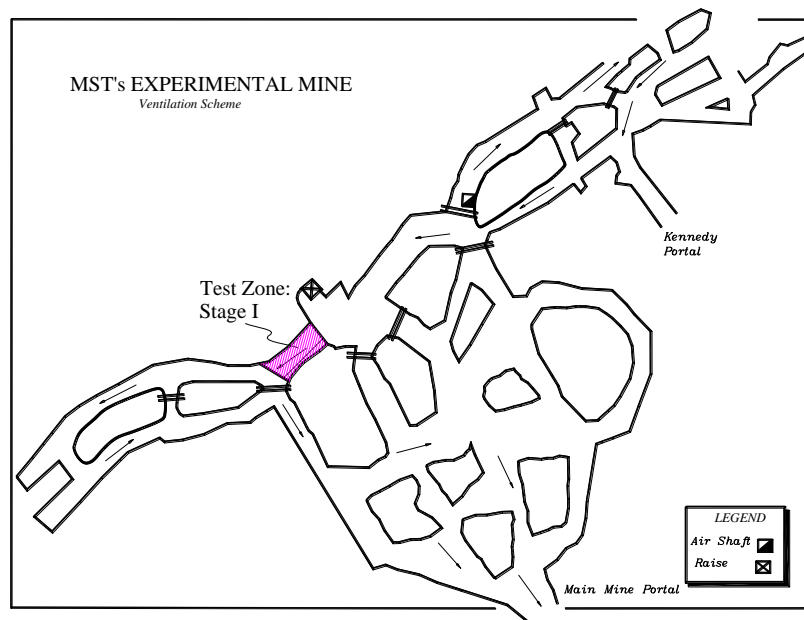
Figure 5.1. Test Zone of Stage I Test at S&T's Experimental Mine

Figure 5.2. Bobcat 753 at S&T's Experimental Mine

Figure 5.3. Diesel Fuel Tank at S&T's Experimental Mine

5.2.2. Sampling and Calibration Instrument. For DPM sampling, the standard DPM sampling method was used. The sampling train used for DPM collection was identical to the one used by MSHA for DPM compliance monitoring. It consists of a cyclone,

an impactor, the filter cassette, a length of tubing, lapel clips, and a constant flow sampling pump that are shown in Figures 2.5 and 2.6. The pump was calibrated at the mine at the beginning of the study. The flow rate was calibrated and recorded using a Gilibrator II bubble flow meter before the experiment, as shown in Figure 5.4.

5.2.3. Sampling Period. The standard sampling procedure requires a full shift (8 hours) to collect a DPM sample with sufficient material to obtain an accurate carbon analysis using the NIOSH Analytical Method 5040. This full shift time period was too long for the experiment to run without interfering with other activities in the mine. For the DEEP field test (McGinn et al., 2004), the DPM was collected during a 4-hour time period; for NIOSH field study (Bugarski et al., 2004a), a high-volume sampling train was used to accelerate the collection of DPM and shorten the sampling period. In this experiment, the flow rate of the sampling pump was raised to 3.4 L/min (standard flow rate is 1.7 L/min). To collect sufficient DPM, the sampling points were put close to the the exhaust flow stream of the diesel engine, as discussed previously. The sampling period was 2 hours for each of the five tests. During each test, four DPM samples were collected from four different sampling points.

Figure 5.4. Calibration of the Sampler Pump before the Experiment

5.2.4. Experimental Procedures. The DPM sampling experiment, run in S&T's Experimental Mine, included five 2-hour tests (Table 5.2). In each 2-hour test, four samplers (with SKC cassettes) were used to collect DPM. In total, 20 DPM samples were collected. Figures 5.5 to 5.7 show the experiment layout and the installation of DPM sampling trains. Before the experiment, the location of the sampling points was measured. It included measuring the distance of samplers from the tailpipe, cross section of the entry where the sampler hung, and the exact position of samplers in the cross section. The engine throttle was placed at a fixed position and marked to ensure that it would not change during the tests (for each test, the engine was started and allowed to run).

There was a 40-minute time period between tests. During the break time, the diesel engine was stopped and allowed to cool down; new DPM cassettes were then installed for each sampling train; the fan continued to ventilate the test zone to clear this area before the next test; and then the diesel engine was started 10 minutes before each test.

After all five tests were completed, the 20 sample cassettes were sent to a commercial laboratory for DPM analysis using the NIOSH Analytical Method 5040.

Figure 5.5. Layout of the Experiment: Bobcat loader Put in Fixed Position and Four SKC DPM Sampling Trains Located Downstream of the Exhaust Pipe
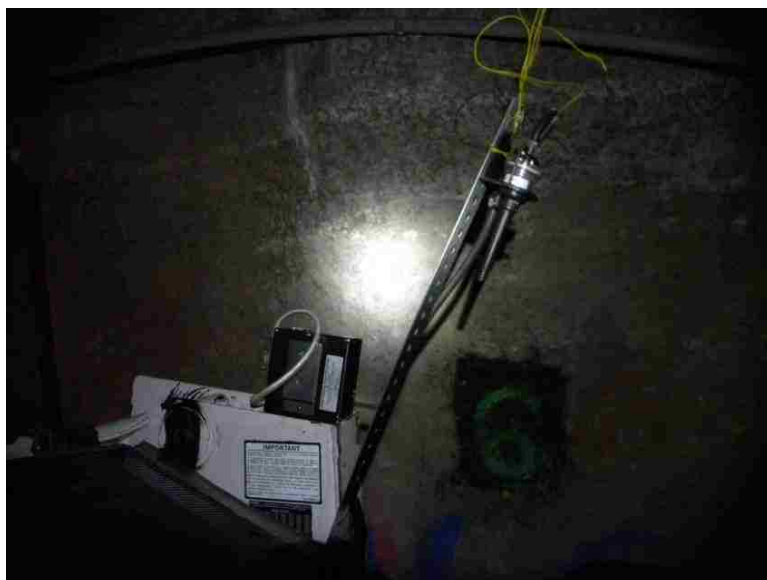
Figure 5.6. Installation of the Sampling Train Close to the Tailpipe
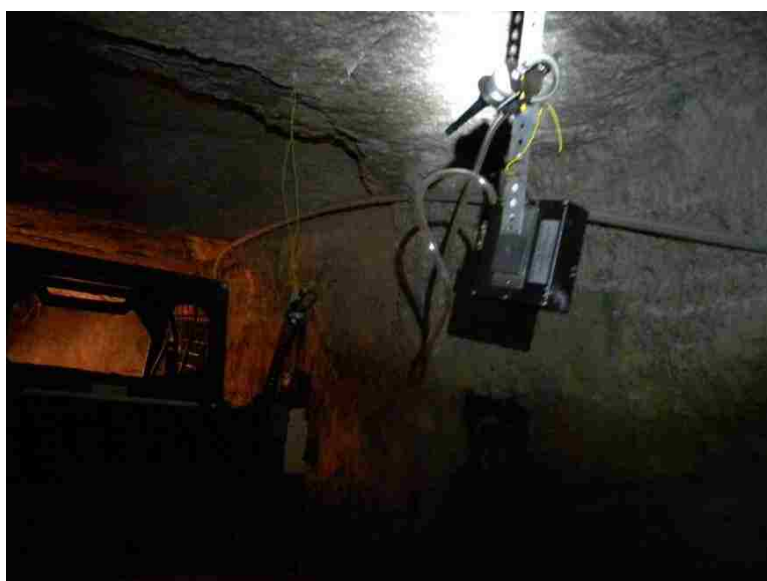
Figure 5.7. Installation of the Sampling Train at the Back of the Entry

Table 5.2. Time Schedule of the Experiment

	Day I		Day II
Test I	8:30-10:30	Test IV	8:30-10:30
	Break I (40 min)		Break III (40 min)
Test II	11:10 -13:10	Test V	11:10 -13:10
	Break II (40 min)		
Test III	13:50-15:50		

5.3. DATA ANALYSIS AND COMPARISONS IN STAGE I EXPERIMENT

5.3.1. Development of CFD Model. The portion of the test zone (shown in Fig-ure 5.1) was reconstructed for the present computational study (shown in Figure 5.8). Fresh air flowed from the right and swept through the Bobcat loader and sampling points (P1, P2, P3 and P4 in Figure 5.8). The air then flowed out of the domain at the left side of the entry as exhaust flow. The height and width were 2.33 m and 2.66 m, respectively, at the inlet and outlet of the entry, but the height was not constant in the sampling areas, ac-cording to the geometry measured in the mine. The sampler P1 was pointing toward the tailpipe and set as close (0.33 m) to it as possible to calibrate the DPM production rate from the exhaust flow. Other positions of samplers are listed in the table below (Table 5.3).

The computational domain was meshed using ANSYS FLUENT's preprocessor GAMBIT, as shown in Figure 5.9. In order to ensure the accuracy of the simulation, the mesh generation was made by ensuring high density near the Bobcat loader and in the sampling region where high gradients exist. Both hexahedral and tetrahedral meshes were generated inside the computational domain, as shown in Figure 5.9. During mesh genera-tion, the equal-size skewness was monitored and maintained at a value less than 0.8.

Table 5.3. Position of Sampling Points

	Distance Downstream of tailpipe (m)	Height from the floor (m)	Distance to the right rib (m)
Sampler P2	1.14	1.98	1.00
Sampler P3	3.05	1.66	1.25
Sampler P4	4.52	1.75	1.37
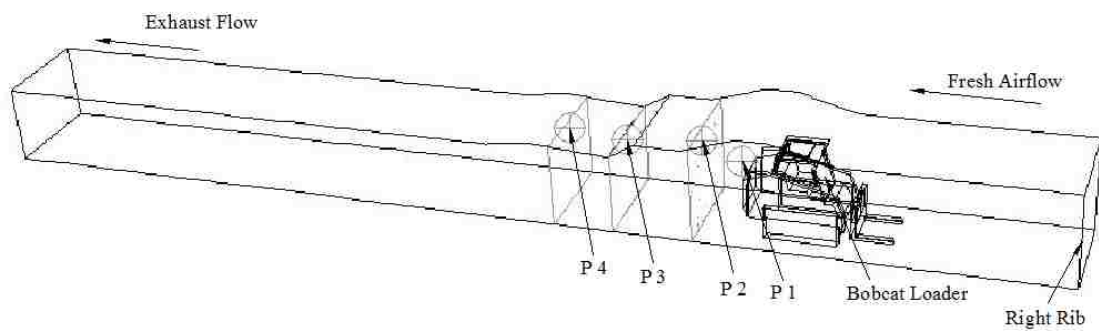
Figure 5.8. Schematic of the Test Zone
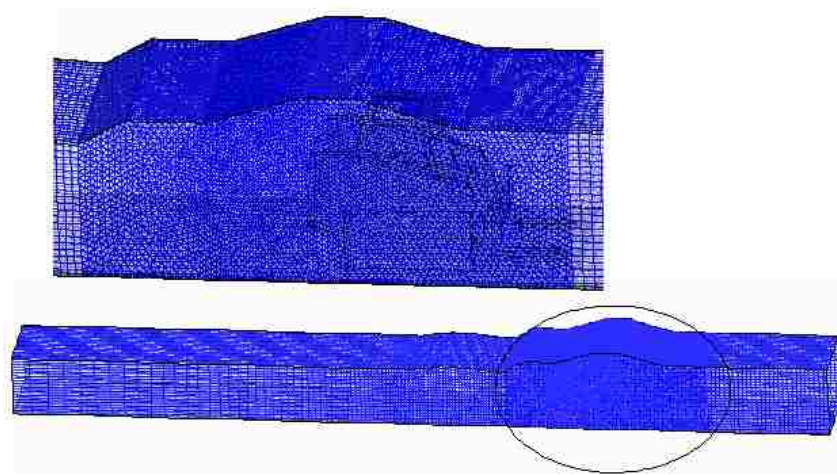
Figure 5.9. Mesh Generation for the Computational Domain

For this simulation, the physical properties of the fresh air flow were treated as constants and evaluated for an inlet temperature of $T_0 = 17°C$ (i.e., specific heat (C_p) was 1006 J/Kg·°C, dynamic viscosity (μ) was 1.789×10^{-5} kg/m·s, and thermal conductivity (k) equaled 0.0242W/m·°C). The density variation in the fluid, due to temperature gradients that existed between the air-intake temperature and the tailpipe emission temperature, were calculated using the incompressible ideal-gas model available in ANSYS FLUENT. In this model, the flow was assumed to be incompressible but the density change, due to the temperature, was calculated using ideal gas law. In the presence of gravity, this density gradient resulted in buoyancy flow. Numerical simulation of the DPM distribution inside the test zone was performed using the species transport model available in ANSYS FLUENT.

In the species transport model, DPM was treated as a gas (continuous phase) and the material that was selected as a representative for the DPM was n-octane vapor (C_8H_{18}) with density ($\rho = 4.84$ kg/m^3), specific heat ($C_p = 2467$ J/Kg·°C), thermal conductivity (k = 0.0178 W/m·°C) and dynamic viscosity ($\mu = 6.75 \times 10^{-5}$ kg/m·s). In the species transport model, the two species (air and DPM) diffused and formed a mixture. The mixture properties were derived using the incompressible ideal gas law for density and the mixing law for specific heat, thermal conductivity, and viscosity.

From the dimensions at the inlet, the hydraulic diameter ($D_h = 4A/P$), where 'A' is the inlet cross-sectional area and 'P' the perimeter, was calculated as $D_h = 2.48$ m. The Reynolds number calculation, based on this hydraulic diameter, was Re = 1.33×10^5 and the flow was turbulent at this Reynolds number. The turbulence in the flow was modeled using the standard k-ε turbulence model with standard wall functions for near wall treatment.

Other boundary conditions used in the simulation included: fresh airflow speed was 0.73 m/s, 0.76 m/s, 0.72 m/s, 0.84 m/s, and 0.78 m/s for tests 1 to 5 at the entry inlet, respectively, according to the measurement during each test; exit was set as outflow condition; wall was simulated as no-slip boundary; and adiabatic wall condition with airflow velocity on the walls was zero. For the tailpipe, the temperature was 127.0°C and the velocity was 14.4 m/s. The mass fraction for DPM was set at the tailpipe by iteration to make the simulated DPM concentration at P1 the same as the experimental data. This

way, the model was calibrated by the experimental data at P1 and validated by comparing DPM concentration at the other sampling points (P2, P3 and P4).

For the five 2-hour tests (Tests 1-5) in the mine, DPM concentration at P1 for Test 2 was far less than the others and was considered abnormal. Therefore, the data for Test 2 were abandoned.

Table 5.4 shows the experiment results at the four sampling locations. These data were obtained from a commercial lab with a certificate to analyze DPM using NIOSH Analytical Method 5040. Although every aspect was considered to be a constant during the tests, still, DPM concentration fluctuated at the same location for each test. To compensate for this, every test was simulated separately, instead of using the average.

Table 5.4. Experiment Results at Different Locations

	Test 1 ($\mu g/m^3$)	Test 3 ($\mu g/m^3$)	Test 4 ($\mu g/m^3$)	Test 5 ($\mu g/m^3$)
P1	2818.6	2161.8	2436.3	2161.8
P2	500.0	460.8	449.5	451.5
P3	323.0	222.1	216.2	223.5
P4	247.5	204.9	209.8	200.0

Numerical solutions of the governing equations and boundary conditions were performed by utilizing the commercial computational fluid dynamics (CFD) code ANSYS FLUENT 12.0. Other settings can be referred to Zheng, et al. (2011).

5.3.2. Comparison of the Experiment with Simulation. Steady simulations were carried out to predict DPM distribution in the test zone, using ANSYS FLUENT CFD code, as presented in Figure 5.8. At least 10,000 iterations were executed for each test simulation to make sure that the DPM dispersion was steady and well distributed.

Assuming DPM as a different gas (C_8H_{18}), the general flow features obtained in the test zone are shown in Figure 5.10. Contours of DPM are colored in the regions that are above the regulation limit (160_{TC} $\mu g/m^3$). The emissions from the tailpipe started

flowing toward the roof of the mine due to the buoyancy force caused by the density difference which, in turn, was caused by the temperature difference between the fresh intake air and tailpipe emissions. This formed a turbulent buoyant plume.
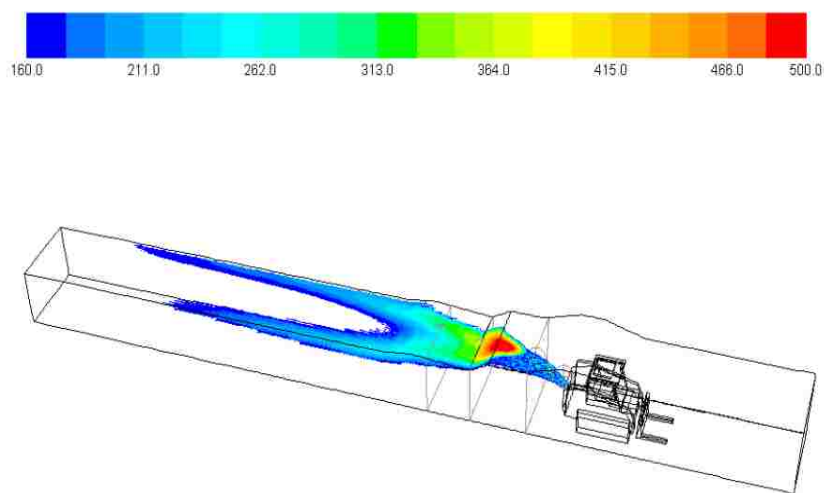
Figure 5.10. DPM Distributions above 160_{TC} µg/m^3 inside the Test Zone

The DPM concentrations at the four sampling points are shown in Table 5.5 by comparing the simulation data with the experimental data and displaying the difference The comparison of the experimental and simulation data at sampling point 1 (P1) was very accurate (less than ± 0.5 percent variation). That was because the DPM sampler at P1 was the closest one to the tailpipe and its location could be measured with reliable accuracy. Therefore, the experimental data at P1 was chosen to calibrate the CFD model. First, a random number of less than 10 ppm for the mass fraction of DPM was set at the tailpipe to start the simulation, based on previous studies (Zheng and Tien, 2009a and b). Then, the DPM concentration was compared at P1. By trial and error, the simulation changed the mass fraction of DPM at the tailpipe to make the DPM concentration at P1 as close to the experimental data as possible. The reason for using the complicated procedures above to derive the DPM condition at the tailpipe was that, the GS-1 cyclone (as

shown in Figure 2.5) in the sampling train was made of plastic material and might have been damaged if put too close to the high temperature outlet of the tailpipe. For the simulations, the mass fractions for DPM set at the tailpipe were: 7.201 ppm in Test 1, 5.538 ppm in Test 3, 6.284 ppm in Test 4, and 5.546 ppm in Test 5.

Table 5.5. Comparison of the Simulation with the Experiment at Sampling Points

	Test 1 ($\mu g/m^3$)			Test 3 ($\mu g/m^3$)		
	Exp. Data	Sim. Data	Dif. (%)	Exp. Data	Sim. Data	Dif. (%)
P1	2818.6	2815.2	-0.1	2161.8	2166.5	0.2
P2	500.0	782.7	56.5	460.8	609.0	32.2
P3	323.0	229.5	-28.9	222.1	174.7	-21.3
P4	247.5	199.4	-19.4	204.9	152.0	-25.8
	Test 4 ($\mu g/m^3$)			Test 5 ($\mu g/m^3$)		
	Exp. Data	Sim. Data	Dif. (%)	Exp. Data	Sim. Data	Dif. (%)
P1	2436.3	2424.6	-0.5	2161.8	2161.7	0.0
P2	449.5	525.4	16.9	451.5	550.4	21.9
P3	216.2	220.7	2.1	223.5	185.7	-16.9
P4	209.8	190.7	-9.1	200.0	160.6	-19.7

Note: Dif. is the difference between the simulation and the test. It is calculated as:

$$\frac{Simulation - Test}{Test} \times 100\%$$

At locations P2 to P4, it can be observed from Table 5.5 that a noticeable difference occurred between the experimental and simulation results. The differences were within 20 to 30 percent for most sampling points and could be as high as 56.5 percent.

To account for the differences, the experimental and simulation data need to be checked out first for possible errors. Therefore, the average value, average deviation, and relative average deviation of experimental and simulation results were calculated and listed in table 5.6.

For the experimental data, it can be observed from the table that the maximum average deviation occurred at P1 (232.83 $\mu g/m^3$). P1 was located 0.33 m away from and pointed toward the tailpipe. Compare to the ventilation flow speed (less than 1 m/s), the exhaust flow speed was high (14.4 m/s). At this closeness to the exhaust pipe, it was

unlikely that the deviation of DPM concentration was mainly affected by the ventilation. Instead, the fluctuation of DPM level at P1 should be due to the different DPM production rate from the diesel engine (although the engine was set to operate in a fixed operating point and sampled with the same time period). At other locations (P2 – P4), it can be observed that, the higher the DPM production rates from the exhaust pipe, the higher the DPM concentration at these downstream locations. That is, the average deviation and relative average deviation at P2 to P4 was mainly due to the different DPM production rate from the engine.

For the simulation results, DPM concentrations were calibrated using the experimental data at P1. Therefore, the average value, average deviation, and relative average deviation are close to the experiment values as shown in Table 5.6. The relative average deviation at P1 was about 10 percent. It can also be observed from the table that, at P2 to P4, the relative average deviations from the simulation are also about 10 percent. That is, the fluctuation of the data was mainly due to the different quantities of DPM produced during the operation. It can be observed from Figure 5.11 that, in general, the average DPM concentration from the simulation had the same trend as the test.
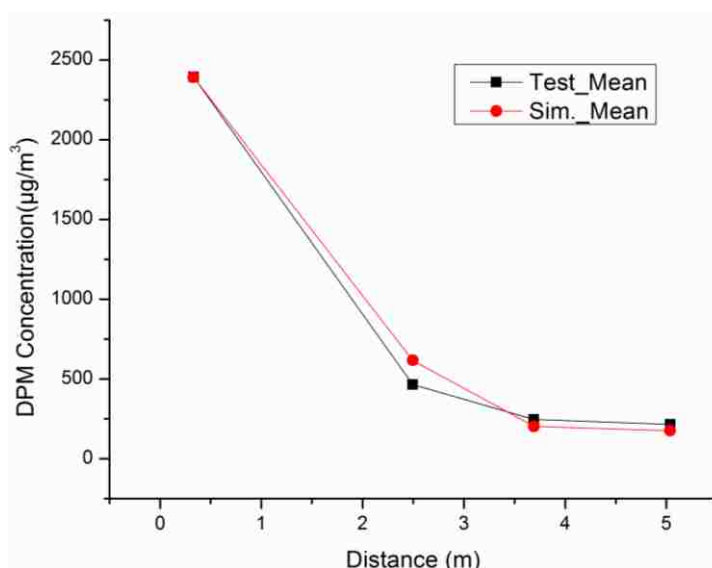
Figure 5.11. Comparison of Average DPM Concentration from
the Experiment and Simulation

Table 5.6. Deviation of Simulation and Experiment at Sampling Points

	Test 1 ($\mu g/m^3$)	Test 3 ($\mu g/m^3$)	Test 4 ($\mu g/m^3$)	Test 5 ($\mu g/m^3$)	Test_Mean ($\mu g/m^3$)	Ave. Dev. ($\mu g/m^3$)	Rel. Ave. Dev. (%)
P1	2818.6	2161.8	2436.3	2161.8	2394.6	232.8	9.7
P2	500.0	460.8	449.5	451.5	465.5	17.3	3.7
P3	323.0	222.1	216.2	223.5	246.2	38.4	15.6
P4	247.5	204.9	209.8	200.0	215.6	16.0	7.4
	Sim. 1 ($\mu g/m^3$)	Sim. 3 ($\mu g/m^3$)	Sim. 4 ($\mu g/m^3$)	Sim. 5 ($\mu g/m^3$)	Sim._Mean ($\mu g/m^3$)	Ave. Dev. ($\mu g/m^3$)	Rel. Ave. Dev. (%)
P1	2815.2	2166.5	2424.6	2161.7	2392.0	227.9	9.5
P2	782.7	609.0	525.4	550.4	616.9	82.9	13.4
P3	229.5	174.7	220.7	185.7	202.7	22.5	11.1
P4	199.4	152	190.7	160.6	175.68	19.4	11.0

Notes: Test_Mean and Sim._Mean are the average DPM concentration for the test and simulation results respectively at the four sampling points; Ave. Dev. means the average of the absolute deviations of DPM concentration from their mean, which is express as: $\frac{1}{n}\sum|x-\bar{x}|$; Rel. Ave. Dev. represents relative average deviation and is express as:

$$\frac{\frac{1}{n}\sum|x-\bar{x}|}{\bar{x}}\times 100\% \cdot$$

From the above error analysis, it can be seen that the fluctuation of the experimental results had a relative average deviation about 10 percent. This fluctuation was most probably caused by the different DPM production from the diesel engine for each test and could not be easily controlled. By calibration from the experimental data at P1, the simulation results resembled the DPM dispersion trend (as shown in Figure 5.11) and also had a relative average deviation of about 10 percent at P2 to P4. In general, the deviation of experimental and simulation results at P2 to P4 are reasonable if the deviation at P1 are accepted.

Although the experimental data and simulation results are reasonable by themselves, still, the two set of data are different at P2 to P4. The main reasons for this difference could be 1) High DPM concentration gradient at the sampling points; 2) The location of sampling points was hard to accurately locate in real mine conditions. Although great care was taken during the measurements, it was still possible that the precision was above 5 cm.

The previous reasoning provided a clue for looking at the results from another point of view. Instead of comparing the differences of DPM levels between the simulation and the experiment at the sampling points, the distance of the CFD-predicted concentration from the experimental data should be examined. Figures 5.12-14 show the cross sections of the entry that contained sampling points 2-4. For example, in Figure 5.12, the simulated DPM concentration at P2 is shown as 550.4 μg/m^3 (Test 5). P2 is located at the inner circle of the colored region. However, at P2, the experimental data was 451.5 μg/m^3, which in the simulation domain, this DPM level is located at the outer circle of the colored area. The average width of the colored ribbon was considered to be the precision of the simulation; the widths for all of the data are listed in Table 5.7. From the table, the maximum distance is 15 cm between the predicted and experiment data at the sampling point (average distance is 10.1 cm at sampling point 4, which was 4.52 m downstream of the tailpipe. Total average distance is 6.7 cm between the simulation results and the experimental data). That is, if the CFD simulation predicted the DPM plume to be located in a certain region, the actual DPM level would be ≤15 cm outside or inside the predicted plume. To be safe, 15 cm outside the predicted DPM plume above the regulation limit was considered for use in working practices and other controlling strategies for underground mining operations. CFD simulation at this precision was considered to be accurate for practical mining applications.

5.3.3. Summary for Stage I Experiment. In this section, the first experiment on DPM dispersion at S&T's Experimental Mine is introduced. CFD simulation was used to reconstruct the experiment to compare the simulation with the experiment. This validation process helped to transfer CFD expertise to analyze and design the ventilation systems for mines that faced difficulties in complying with the DPM regulation.

From the calculation of the experimental design, five samples were collected from each of four locations downstream of the exhaust flow (total of 20 samples). The first DPM sampler was located 0.33 m from the outlet of the tailpipe (with the same orientation as the tailpipe), while the other three were installed 1.14 m, 3.05 m, and 4.52 m, respectively, downstream from the engine. The simulation used the first sampling data to calibrate the simulation and adjust the mass fractions for DPM at the tailpipe so that the DPM concentration would be as close as possible to the measurement at the first point.
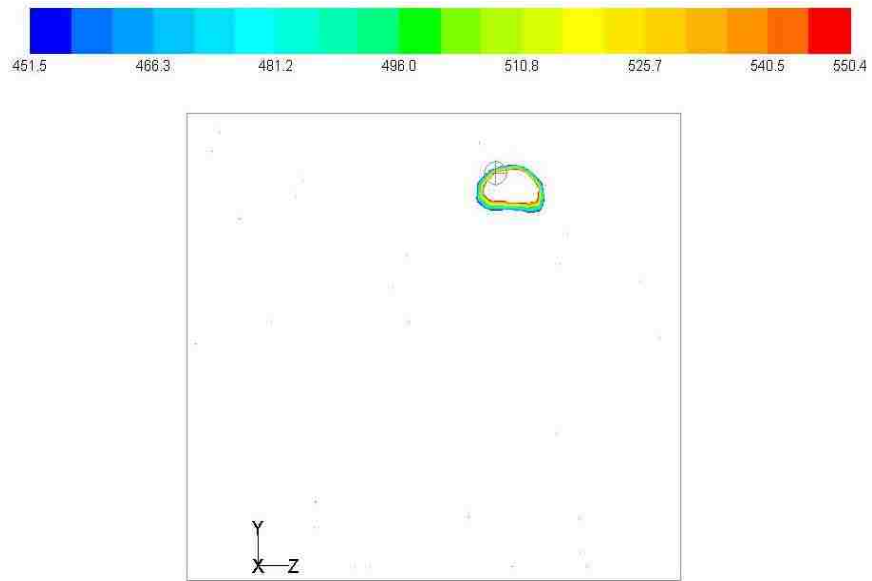
Figure 5.12. DPM Levels between Simulation and Experiment at the Cross Section of P2
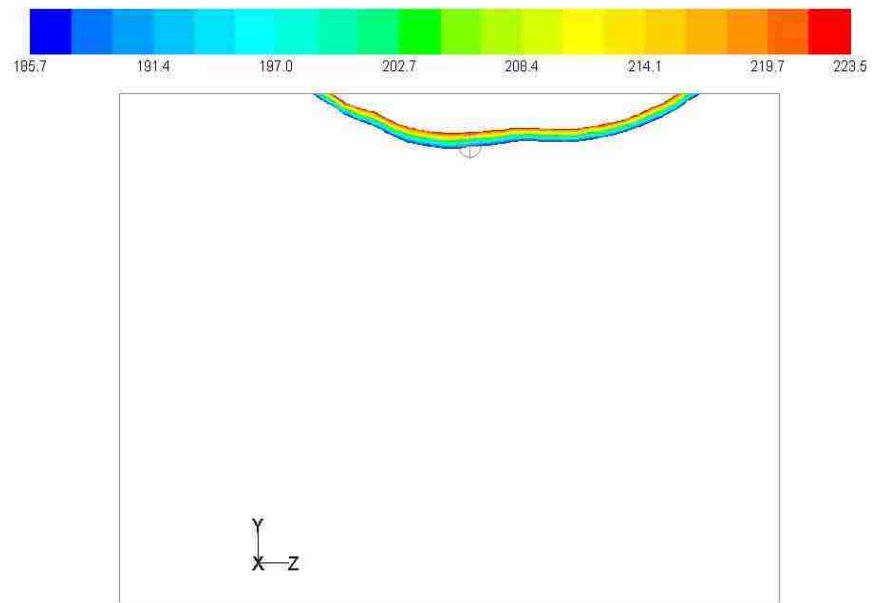
Figure 5.13. DPM Levels between Simulation and Experiment at the Cross Section of P3
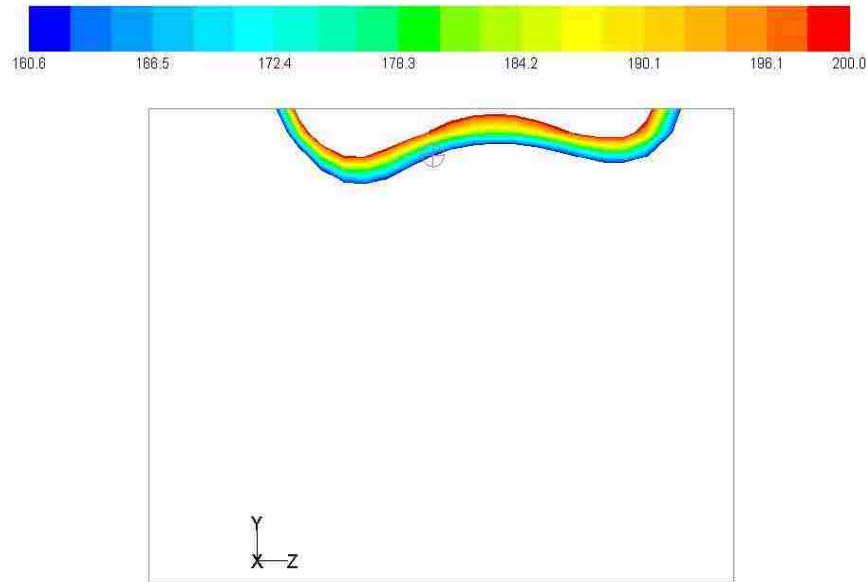
Figure 5.14. DPM Levels between Simulation and Experiment at the Cross Section of P4

Table 5.7. Average Distance of DPM Level between Simulation and Experiment

	Test 1 (cm)	Test 3 (cm)	Test 4 (cm)	Test 5 (cm)	Average (cm)	Total Average (cm)
Sampling P2	6.4	4.8	1.9	2.9	4.0	
Sampling P3	9.8	7.4	1.0	5.9	6.0	6.7
Sampling P4	9.6	15.0	5.1	10.6	10.1	

The comparison of simulation with experiment results at the other three locations showed that the CFD simulation had forecast the location of the DPM plume with practical accuracy. At 1.14 m downstream of the tailpipe, simulation results showed that it could locate the DPM plume with 6.4 cm accuracy; at 3.05 m downstream of the engine, the distance between the experiment DPM plume and the CFD simulated plume was within 9.8 cm; at 4.52 m downstream of the tailpipe, the difference between the experiment and the simulation was within 15.0 cm.

For this validation study, it was desirable to investigate the CFD model further by adding more sampling points at the same cross sectional area. Therefore, a second DPM experiment was executed at S&T's Experimental Mine, as described below.

5.4. EXPERIMENT ON DPM DISPERSION STUDY—STAGE II

5.4.1. DPM Dispersion study -- Experiment Stage II at S&T's Experimental Mine. The aim of the stage-II experiment was to measure the DPM concentration at multiple locations from the same cross-sectional areas downstream of the diesel engine. The data collected in the experiment were used to validate the simulation results and to outline the shape of the DPM plume.

Figure 5.15 shows the location of the second experiment at S&T's Experimental Mine. The reason for changing the location was because the roof of the new location was smoother, as compared to the segment of the previous experiment, which would facilitate the reconstruction of the CFD geometric model.
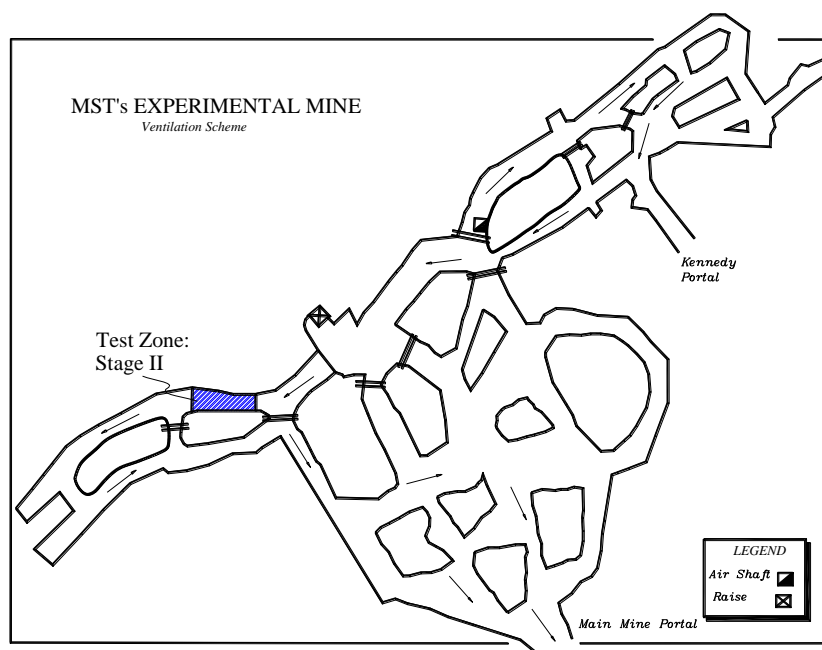
Figure 5.15. Test Zone of the Second Experiment at S&T's Experimental Mine

For the second experiment, the same diesel engine (Bobcat skid-steer loader 753) was used. This diesel engine was still operated at a fixed location and in a fixed operating condition in the test area, as shown in Figure 5.15; it was the single DPM source in the experiment. The four DPM samplers used for the previous experiment were still set at 3.4 L/min and were calibrated before the experiment with a Gilibrator II bubble flow meter. After sampling, SKC DPM cassettes were sent to the same commercial laboratory for DPM analysis using the NIOSH Analytical Method 5040.

The major differences between the two experiments were the location of the DPM sampling points, the sampling time periods, and the number of observations.

To shape the DPM plume, 27 points on three different cross-sectional planes downstream of the diesel engine were collected for the second experiment. In each plane, DPM samplers were installed at three levels: top level, medium level, and bottom level, with three locations in each level. Figure 5.16 shows the location of the samplers at the three cross-sectional planes for the second experiment. For the four DPM samplers available for the experiment, one was installed as close to the tailpipe as possible; the other three were put on the same level of the same cross-sectional plane during each sampling period. To sample all of the locations for one time, nine sampling periods were needed. The sequence for the sampling was as follows: 1) top level at the first cross-sectional plane (c1); 2) medium level at c1; 3) bottom level at c1; 4) top level at the second cross-sectional plane (c2); 5) medium level at c2; 6) bottom level at c2; 7) top level at the third cross-sectional plane (c3); 8) medium level at c3; and 9) bottom level at c3.

Before the first experiment began, there was considerable concern that not enough DPM could be collected during the short sampling time period. However, the experiment results showed that this was not a problem for even a small diesel loader. For the second experiment, the sampling period was further reduced to 40 minutes. The main reason for reducing the sampling period was to avoid disturbances from other mining activities listed on the schedule of activities for S&T's Experimental Mine. According to the schedule, the experiment had to be executed within a day or it would have to be split into several non-continuous days, which would pose a problem with the same ventilation and engine operation settings for DPM collection.

Figure 5.16. Layout and Sampling Locations of the Second Experiment

For the same reason, only three observations were performed at each location. Therefore, 27 sampling periods (40 minutes each) were used for the second experiment. Between two sampling periods, a 10-minute timeslot was used to change the location of the samplers and clear the region with fresh airflow. In total, about 23 hours were used for the second experiment.

5.4.2. Development of the CFD Model. The portion of the second experiment was reconstructed for CFD simulation, as shown in Figure 5.17. Fresh air flowed from the right and swept through the Bobcat loader and cross-sectional planes c1 through c3. It then flowed out of the domain at the left side of the entry as exhaust flow. The entry height and width were 2.05 m and 1.98 m, respectively.

Due to the irregularity of the surfaces, the relative distances of the sampling points from the center of the exhaust pipe were measured instead of referring to the right rib as was done in the previous study. The positions of the sampling points are listed in Table 5.8. The meanings of the x, y, and z values are shown in Figure 5.18.
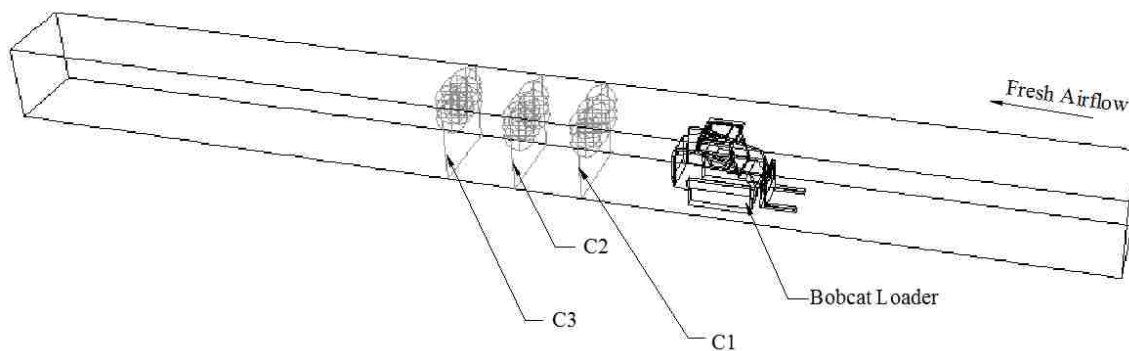
Figure 5.17. Geometric Model of the Second Experiment
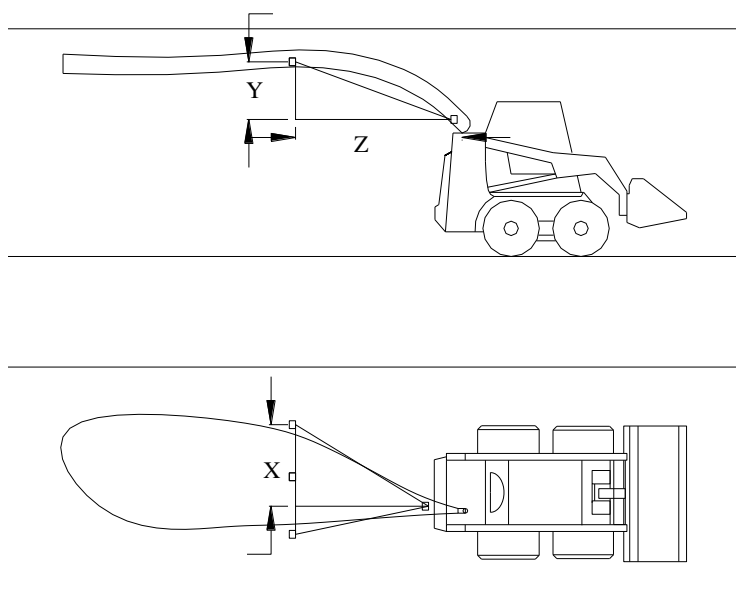
Figure 5.18. Relative location of sampling points

In Table 5.8, P0 indicates the DPM sampler that was installed the closest to the tailpipe (0.27 m pointing toward the exhaust outlet). In the table, C1, C2, and C3 are the cross-sectional planes; P means position; the letters T, M and B on the second-last position indicate top, medium, and bottom level; L, M, and R illustrate the left, middle, and

right locations of samplers at the same level (facing toward the fresh airflow). For example, C2PMM means that the sampler was located at the second cross-sectional plane at medium level in the middle position; C1PBR is the sampling point at the first cross-sectional plane at the bottom level in the right position. The negative value for Y in the table means that the sampling point was located below the exhaust pipe, while the negative value for X indicates the position was at the right of the tailpipe (facing against the fresh airflow).

Table 5.8. Relative Position of Sampling Points

Locations	X (cm)	Y (cm)	Z (cm)
P0		27	
C1PTL	106	65	280
C1PTM	33	65	280
C1PTR	-28	65	280
C1PML	106	36	280
C1PMM	33	36	280
C1PMR	-28	36	280
C1PBL	106	8	280
C1PBM	33	8	280
C1PBR	-28	8	280
C2PTL	94	52	476
C2PTM	27	52	476
C2PTR	-25	52	476
C2PML	94	24	476
C2PMM	27	24	476
C2PMR	-25	24	476
C2PBL	94	-6	476
C2PBM	27	-6	476
C2PBR	-25	-6	476
C3PTL	90	67	678
C3PTM	30	67	678

Table 5.8. Relative Position of Sampling Points (cont.)

Locations	X (cm)	Y (cm)	Z (cm)
C3PTR	-19	67	678
C3PML	90	45	678
C3PMM	30	45	678
C3PMR	-19	45	678
C3PBL	90	18	678
C3PBM	30	18	678
C3PBR	-19	18	678

The meshing procedure was the same as the previous experiment. For CFD simulation, the species transport model was used with ANSYS FLUENT. All of the detailed settings for the CFD model can be determined from the previous section, except for the boundary conditions at the inlet of the entry and the exhaust pipe. Fresh airflow speed was 0.88 m/s and the temperature was 13°C at the entry; the exhaust flow speed was measured at 17.3 m/s and the temperature was 137°C at the tailpipe.

5.4.3. Comparison of the Second Experiment with Simulation. Steady simulations were carried out to predict DPM distributions in the test zone, which are presented in Figure 5.17 using ANSYS FLUENT CFD code. At least 10,000 iterations were executed for the simulation to make certain that the DPM dispersion was steady and well distributed.

The general flow features in the test zone were obtained by assuming that DPM was a different gas (C_8H_{18}) and are shown in Figure 5.19 with colored using contours of DPM in the region that were above the regulation limit (160_{TC} µg/m^3). It can be observed from the figure that the DPM plume from the tailpipe started flowing towards the roof of the mine due to the buoyancy force caused by the density difference which, in turn, was caused by the temperature difference between the fresh intake air and tailpipe emissions. Then it was gradually diluted by the fresh air as it flowed downstream. Since the sampling time was shortened to 40 minutes for the second experiment, the diesel engine was operated at a more intensive level. And because the profile of this segment of entry was

lower than the location of the first experiment (2.05 m in height), it can be observed from the figure that the region where the DPM was above the regulation limit was larger than shown in Figure 5.10.
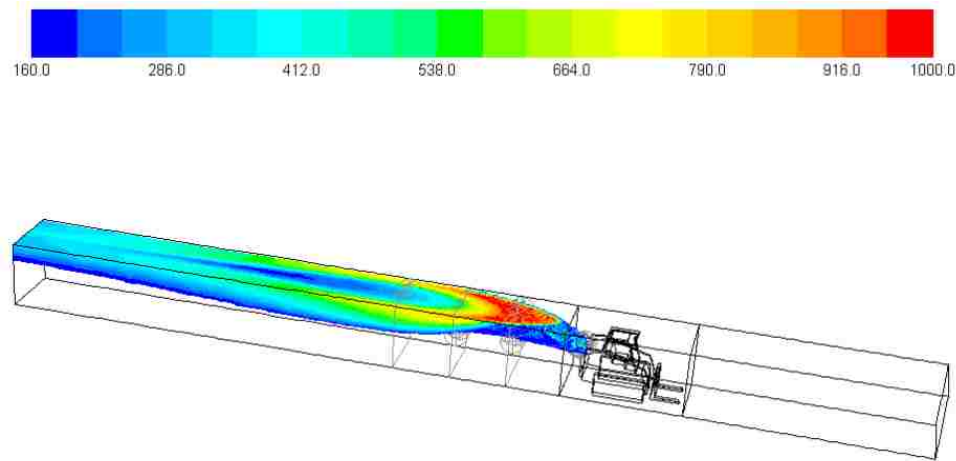
Figure 5.19. DPM distributions inside the test zone for the second experiment

Figures 5.20-5.25 illustrate the DPM concentrations and contours of speed in the cross-sectional planes (C1, C2, and C3) that contain the sampling points. It can be observed from Figure 5.20 that high DPM concentrations flowed at the top of the entry and gradually decreased towards the floor. The curved DPM region, as indicated in the figure, corresponds with the high-speed areas shown in Figure 5.21. In Figure 5.21, because the Bobcat loader blocked the lower center of the entry, fresh air had to enter the narrow spaces beside the vehicle, which increased the airflow speed at the lower two sides of the cross-sectional plane. The high airflow drug the DPM toward these two high-speed regions.

This trend can also be observed in Figures 5.22 to 5.25, in which a high DPM region at the top of the entry agreed with the high velocity areas at the same height.
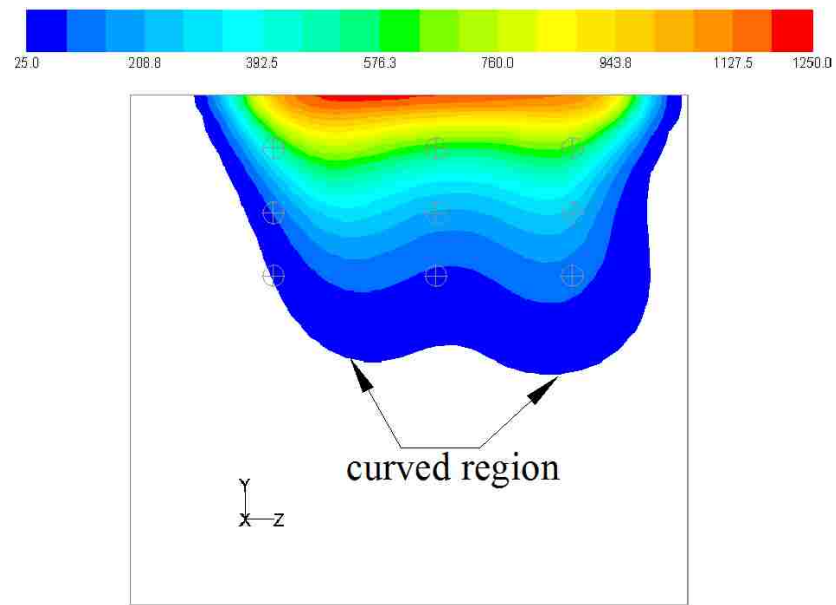
Figure 5.20. DPM Distributions in C1
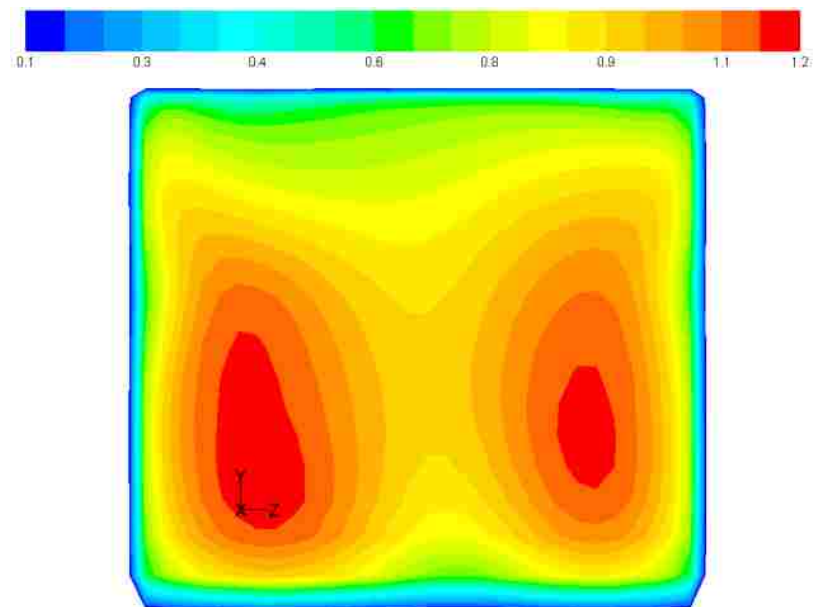
Figure 5.21. Contour of Speed in C1
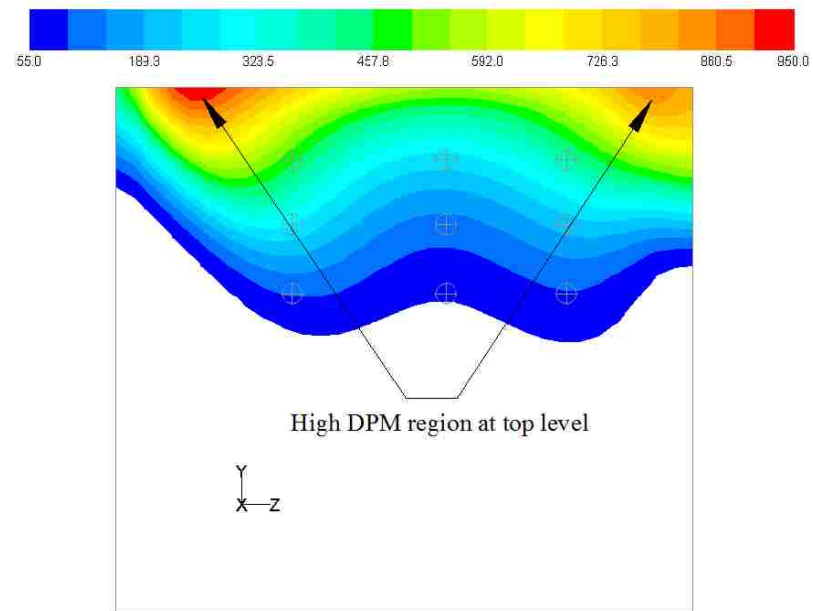
Figure 5.22. DPM Distributions in C2
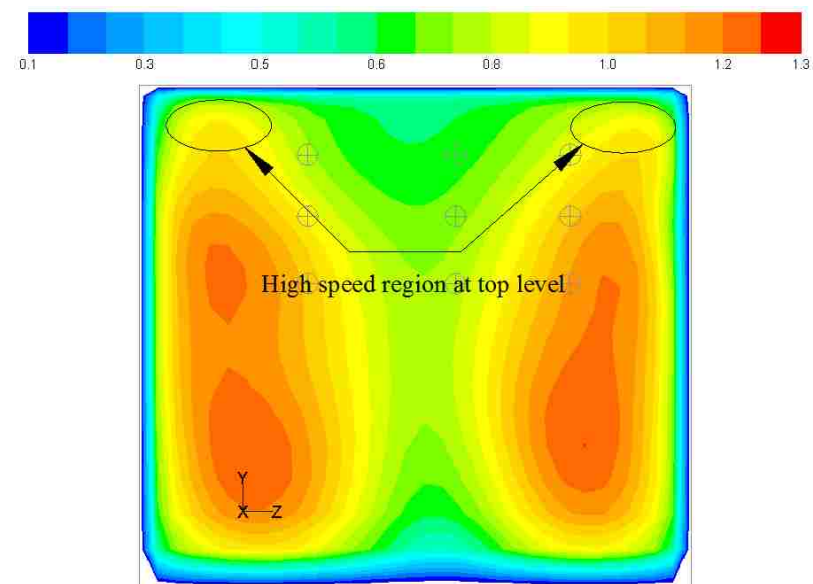
Figure 5.23. Contour of Speed in C2
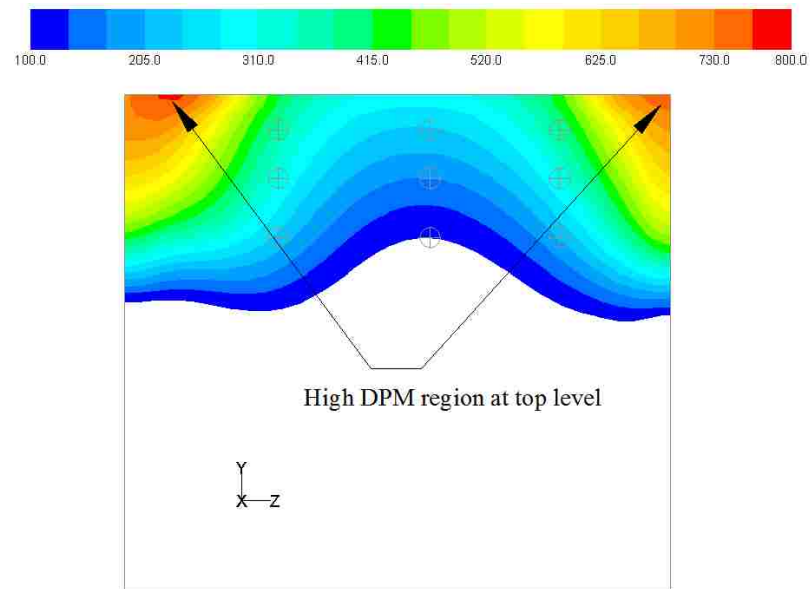
Figure 5.24. DPM Distributions in C3
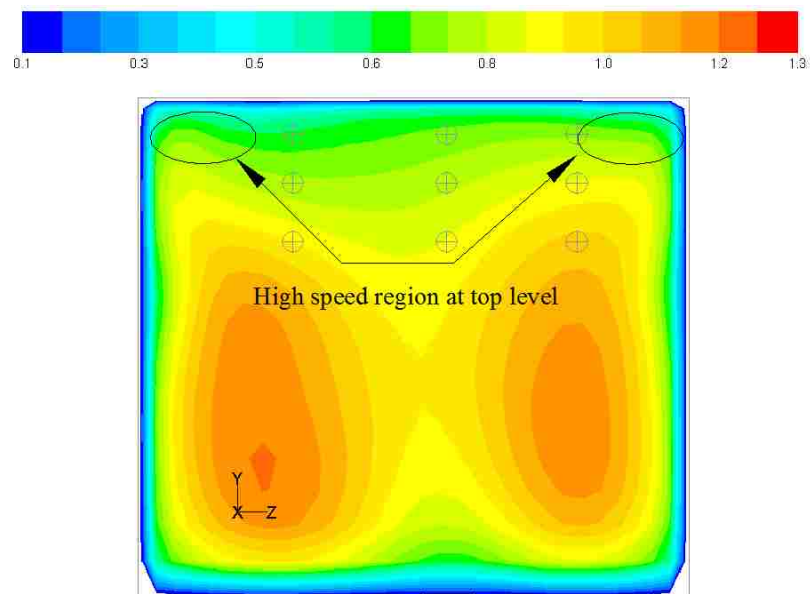
Figure 5.25. Contour of Speed in C3

During the experiment, it was found that the sampler that was located closest to the tailpipe was malfunctioning during the process. Due to its closeness to the tailpipe, moisture in the exhaust flow condensed into water and partially blocked the tube connected to the pump, making the flow rate deviate from the setting. The sampling data are questionable for that location. Therefore, the point was not used as a calibration data in the simulation.

The DPM concentrations at the 27 sampling points in the three cross-sectional planes (represented by C1, C2, and C3) downstream of the exhaust pipe are listed in Table 5.9. Groups 1-3 in the table indicate that each point was measured three times during the experiment. The top, medium, and bottom illustrate the height levels of samplers within each plane. Left, middle, and right are the relative locations of the sampling points when facing toward the Bobcat loader.

It can be observed from Table 5.9 that noticeable fluctuations of DPM concentration existed for the same point. The main reason for this difference in experiment results may have been due to the relatively short sampling time (40 minutes). Although the flow rate for the sampler's pump was doubled (3.4 L/min), it could be considered to have only been sampled 80 minutes in a normal operation setting (1.7 L/min for 480 minute). In this short period of time, the operating condition of the diesel engine, the ventilation flow rate (including natural ventilation), barometric pressure, and the temperature may have changed also and could not be controlled. Although the effect of each parameter was limited in the underground environment, the overall sequence was remarkable and hard to predict. As a result, DPM concentration from the experiment itself altered irregularly. For the second experiment, the average value of the three data at the same sampling point was used to compare with the simulation results.

The average DPM concentrations at the 27 sampling points are shown in Table 5.10 by comparing the simulation data with experimental data and the difference. Because the point closest to the tailpipe could not be used to calibrate the model, as in the first experiment, the sampling point at the first cross-sectional plane (C1) top level and middle position was used in the simulation to calibrate the CFD model. By trial and error, the simulation changed the mass fraction of DPM at the tailpipe to make the DPM

concentration at this point as close to the experimental data as possible. Table 5.10 shows that the difference between the simulation and experiment is 0.5 percent at this calibration point.

Table 5.9. Experiment Results at 27 Sampling Points

	Group 1 (µg/m³)			Group 2 (µg/m³)			Group 3 (µg/m³)		
	Left	Middle	Right	Left	Middle	Right	Left	Middle	Right
C1top	389.4	562.2	680.3	458.1	554.6	411.5	404.7	630.6	461.9
C1medium	107.5	306.5	232.9	92.4	243.6	217.6	136.1	247.8	171.8
C1bottom	109.9	94.1	127.4	92.1	90.7	87.8	79.7	100.8	74.9
C2top	537.5	264.7	311.5	377.9	183.2	487.9	394.7	244.3	288.6
C2medium	336.7	150.8	240.5	350.5	103.1	208.4	295.5	82.1	235.2
C2bottom	117.6	76.4	109.6	152.3	80.2	133.6	128.3	85.9	120.3
C3top	366.5	208.4	256.5	412.3	223.3	372.6	236.7	233.3	305.4
C3medium	335.9	282.6	366.5	374.1	217.6	236.7	297.8	167.7	290.1
C3bottom	305.4	111.3	274.9	268.8	136.1	268.8	268.8	111.3	226.0

Table 5.10. Comparison of Simulation with Experiment at 27 Sampling Points

	Experiment average (µg/m³)			Simulation results(µg/m³)			Difference (%)		
	Left	Middle	Right	Left	Middle	Right	Left	Middle	Right
C1top	417.4	582.4	517.9	447.0	585.4	611.3	7.1	0.5	18.0
C1medium	112.0	266.0	207.4	88.1	198.2	241.0	-21.3	-25.5	16.2
C1bottom	93.9	95.2	96.7	26.5	75.7	113.2	-71.8	-20.5	17.0
C2top	436.7	230.7	362.7	470.1	258.6	391.5	7.6	12.1	8.0
C2medium	327.5	112.0	228.0	279.3	128.1	209.9	-14.7	14.4	-7.9
C2bottom	132.7	80.8	121.1	102.7	59.7	94.9	-22.6	-26.1	-21.7
C3top	338.5	221.7	311.5	372.6	235.9	381.8	10.1	6.4	22.6
C3medium	335.9	222.6	297.8	316.3	169.4	308.0	-5.8	-23.9	3.4
C3bottom	281.0	119.6	256.5	231.0	100.8	207.0	-17.8	-15.7	-19.3

Note: Difference is calculated as: $\dfrac{Simulation - Test}{Test} \times 100\%$

Besides the calibration point, it can be observed in Table 5.10 that simulation showed noticeable differences from the experiment data. The differences were within 20 to 30 percent for most sampling points and could be as high as -71.8 percent.

To account for the differences, the experimental data need to be checked out first for possible errors. Therefore, the average value, average deviation, and relative average deviation (they have the same meaning and equations as shown in Table 5.6) of experimental results were calculated and listed in table 5.11. For the second experiment at S&T's Experimental Mine, simulation results were compared with the average experimental data. Since only one set of data was simulated, therefore, there were no average value, average deviation, and relative average deviation of the simulation data.

For the second experiment, the point closest to the tailpipe could not be used to calibrate the model as in the first experiment. Therefore, it was difficult to detect the sources of errors by the data available. However, since the methodology and procedures of the second experiment were the same as the first one, it was still possible that the fluctuation of experimental data was mainly due to the different DPM production rate from the diesel engine. Compare to the first experiment, the average deviation and relative average deviation of the second experiment were larger (most sampling points are within 20 percent). This might be due to the relative shorter sampling period of the second experiment, which introduced more random errors that were hard to differentiate during the process.

Figure 5.26 is the regression analysis result for the second experiment, whose vertical axis is the DPM concentration of the simulated value; the abscissa is the DPM concentration of the test value. The value of Pearson Correlation Score (R) for the simulated DPM concentration is 0.889, which prove that the correlation between the simulated and test value is good.

Although the correlation between the simulated and test value is good, there still exist noticeable differences between the experimental and simulation results at the 27 downstream sampling points. By considering all the possibilities, the main reasons for the differences include: 1) Simplification of simulation, in which only a constant value of the parameters (ventilation, height and width of the entry, temperature of the environment and tailpipe, exhaust flow from the diesel engine) were used. 2) High DPM gradient at

the sampling points that were located close to the diesel engine. 3) Position of the sampling point was hard to locate, although the measurement was improved by tracking the relative positions of the sampling points to the tailpipe for the second experiment.

Table 5.11. Deviation of Experimental Data at Sampling Points

	Group1 ($\mu g/m^3$)	Group 2 ($\mu g/m^3$)	Group 3 ($\mu g/m^3$)	Test_Mean ($\mu g/m^3$)	Ave. Dev. ($\mu g/m^3$)	Rel. ave. Dev. (%)
C1PTL	389.4	458.1	404.7	417.4	27.1	6.5
C1PTM	562.2	554.6	630.6	582.5	32.1	5.5
C1PTR	680.3	411.5	461.9	517.9	108.3	20.9
C1PML	107.5	92.4	136.1	112.0	16.1	14.3
C1PMM	306.5	243.6	247.8	266.0	27.0	10.2
C1PMR	232.9	217.6	171.8	207.4	23.8	11.5
C1PBL	109.9	92.1	79.7	93.9	10.7	11.4
C1PBM	94.1	90.7	100.8	95.2	3.7	3.9
C1PBR	127.4	87.8	74.9	96.7	20.5	21.2
C2PTL	537.5	377.9	394.7	436.7	67.2	15.4
C2PTM	264.7	183.2	244.3	230.7	31.7	13.7
C2PTR	311.5	487.9	288.6	362.7	83.5	23.0
C2PML	336.7	350.5	295.5	327.6	21.4	6.5
C2PMM	150.8	103.1	82.1	112.0	25.9	23.1
C2PMR	240.5	208.4	235.2	228.0	13.1	5.7
C2PBL	117.6	152.3	128.3	132.7	13.0	9.8
C2PBM	76.4	80.2	85.9	80.8	3.4	4.2
C2PBR	109.6	133.6	120.3	121.2	8.3	6.8
C3PTL	366.5	412.3	236.7	338.5	67.9	20.0
C3PTM	208.4	223.3	233.3	221.7	8.8	4.0
C3PTR	256.5	372.6	305.4	311.5	40.7	13.1
C3PML	335.9	374.1	297.8	335.9	25.4	7.6
C3PMM	282.6	217.6	167.7	222.6	40.0	18.0
C3PMR	366.5	236.7	290.1	297.8	45.8	15.4
C3PBL	305.4	268.8	268.8	281.0	16.3	5.8
C3PBM	111.3	136.1	111.3	119.6	11.0	9.2
C3PBR	274.9	268.8	226.0	256.6	20.4	7.9
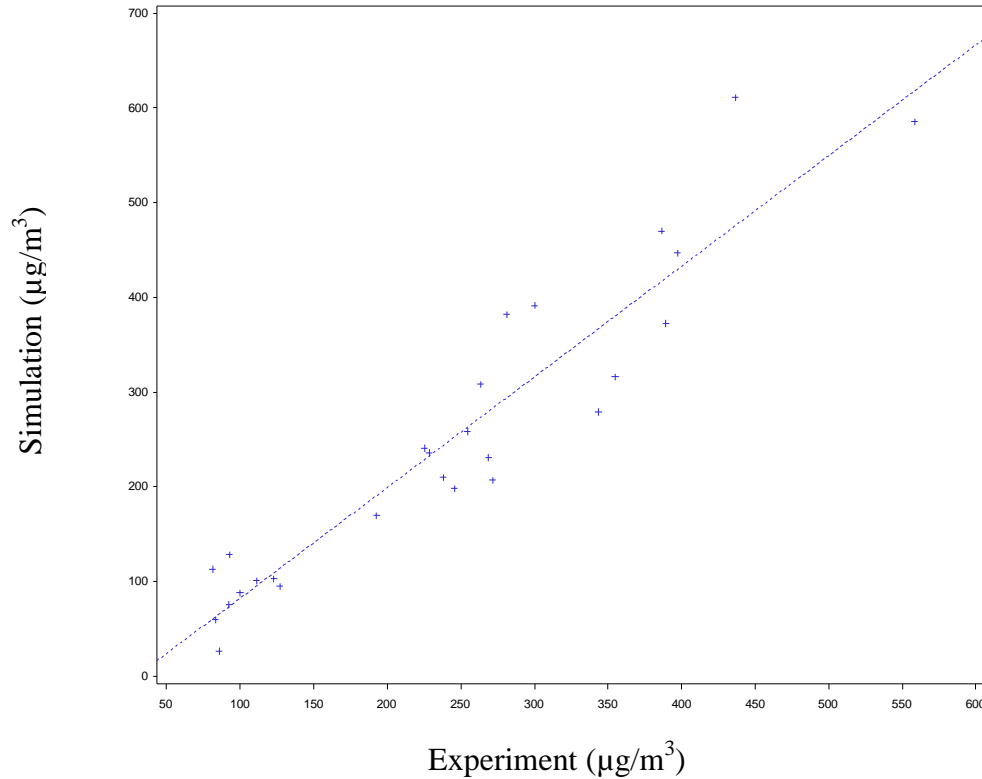
Figure 5.26. Regression Analysis Result for the Second Experiment

Although the correlation between the simulated and test value is good, there still exist noticeable differences between the experimental and simulation results at the 27 downstream sampling points. By considering all the possibilities, the main reasons for the differences include: 1) Simplification of simulation, in which only a constant value of the parameters (ventilation, height and width of the entry, temperature of the environment and tailpipe, exhaust flow from the diesel engine) were used. 2) High DPM gradient at the sampling points that were located close to the diesel engine. 3) Position of the sampling point was hard to locate, although the measurement was improved by tracking the relative positions of the sampling points to the tailpipe for the second experiment.

The distance of the simulation-predicted concentration from the experimental data, similar to the comparison of the first experiment, is shown in Table 5.12. In Table 5.12, the concept of the shortest distance between simulation and experiment was used. The meaning of the concept is shown in Figure 5.27. The colored area in the figure

reveals the DPM level between the simulation value and experimental data at the same sampling point. For the sampling point that is located in the first cross-sectional plane (C1), bottom level and left position, the DPM concentration from the experiment was 93.9 (μg/m^3), (shown in red in Figure 5.27). For the same sampling point, the simulation calculated DPM level was 26.5 (μg/m^3), as shown in blue in Figure 5.27. Also shown in the figure is the shortest distance that was measured from the sampling point in the simulation domain to the closest point where the experiment data were indicated by the simulation results. It can be observed in Figure 5.27 that the shortest route should be drawn from the sampling point perpendicular toward the red line which indicates the experiment data for the same sampling point. The shortest distance was the closest range of CFD simulation from the experiment results.
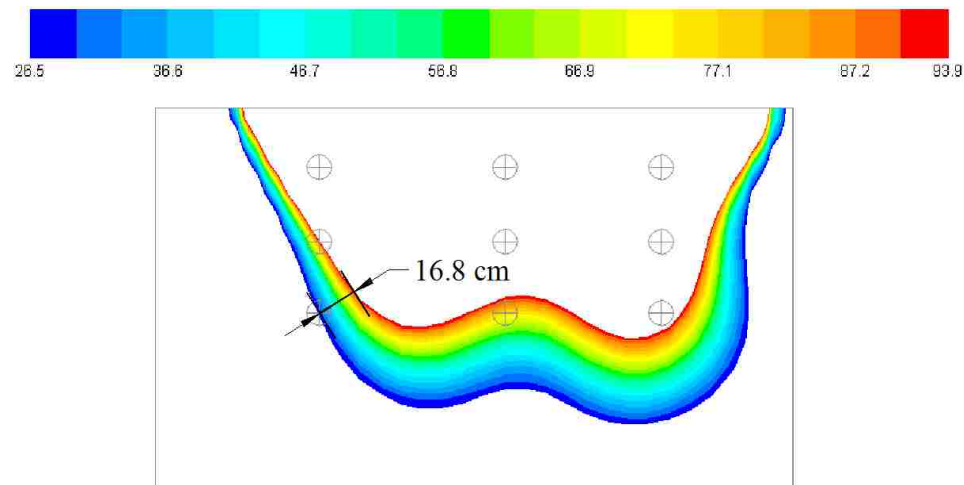
Figure 5.27. The Shortest Distance between Simulation and Experiment Data for Sampling Point Located at C1PBL (C1 Plane, Bottom Level and Left Position)

Table 5.12 illustrates the shortest distance between the simulation of DPM concentrations and the experiment. It can be observed from the table that the distance ranged from 1.2 cm for the calibration point (C1, top level and middle position) to 18.0 cm at the third cross-sectional (C3, medium level, and middle position). Although the highest DPM

concentration difference indicated in Table 5.10 was -71.8 percent, the shortest distance for that point is 16.8 cm as shown in Figure 5.27 and Table 5.12. The biggest difference revealed in Table 5.12 was located in the third cross-sectional plane (C3, medium level, and middle position): 18.0 cm between simulation and experiment results, as shown in Figure 5.28.
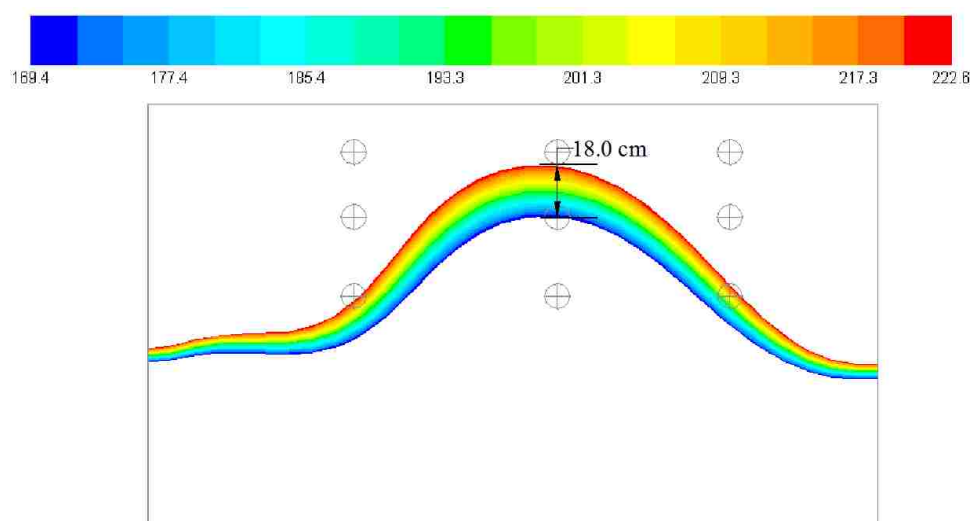
Figure 5.28. The Shortest Distance between Simulation and Experiment Data for the Sampling Point Located at C3PMM (C3, Medium Level and Middle Position)

It can be observed from Figure 5.28 that the simulation result was 169.4 ($\mu g/m^3$) for DPM at the sampling point (located at C3, medium level and middle position). This DPM level is shown in Figure 5.28 as the blue color on the down side of the colored ribbon. At the same point, the experimental data was 222.6 ($\mu g/m^3$), which is shown in red in the simulation plane (C3). The shortest distance between the two DPM levels is shown in Figure 5.28 as 18.0 cm. This large distance may have been due to the high fluctuation of the DPM level in this location, as revealed in the experiment results. Overall, the total average distance between the simulation and experiment for all of the 27 sampling points is 8.2 cm as shown in Table 5.12.

Table 5.12. Shortest Distance of DPM Level between Simulation and Experiment at 27 Sampling Points for the Second Experiment

	Distance (cm)			Average (cm)	Total average (cm)
	Left	Middle	Right		
C1top	2.6	1.2	7.5	3.8	
C1medium	6.5	6.7	4.3	5.8	
C1bottom	16.8	11.2	10.4	12.8	
C2top	4.5	6.1	4.6	5.1	
C2medium	7.2	7.1	3.5	5.9	8.2
C2bottom	10.6	12.3	10.3	11.1	
C3top	6.5	5.1	11.3	7.6	
C3medium	5.6	18.0	4.5	9.4	
C3bottom	12.3	11.7	12.8	12.3	

5.4.4. Summary of Stage II Experiment. In this section, the second experiment on DPM dispersion at S&T's Experimental Mine is introduced. CFD simulation was used to reconstruct the experiment to compare the simulation with the experiment.

For the second experiment, DPM were collected from 27 points on three different cross-sectional planes (C1, C2, and C3) downstream from the diesel engine with an extra sampler located 0.27 m from the outlet of the tailpipe. For the 27 sampling points, nine points were positioned on each of the three planes with three out of the nine points located at the top, medium, and bottom levels. C1, C2, and C3 were stationed 2.80 m, 4.76 m, and 6.78 m, respectively, downstream from the engine. DPM was collected three times for a period of 40 minutes, from each of the 27 sampling points. Due to the malfunction of the sampler installed closest to the tailpipe (0.27 m) and lack of a backup sampler to substitute the broken one, the sampling DPM concentration at C1PTM (C1, top level and middle position) was used to calibrate the simulation model.

Because of the short sampling time and changing of other uncontrollable parameters (engine operation point, natural ventilation, barometric pressure, environment temperature, etc.), fluctuations of the DPM concentration were observed in results of the experiment. In the second experiment, the average experimental data was used to compare with the simulation.

At the 27 sampling points, noticeable differences in DPM concentrations were observed between the experimental and simulation results. However, by comparing the

distance between the experimental and simulation data, the length was within practical precision (maximum 18.0 cm at 6.78 m downstream of the diesel engine between the experiment and simulation-predicted location).

At this point, it was concluded that the species transport model in FLUENT could be reasonably used to study DPM dispersion, with practical accuracy, for the mining industry. Thus, the simulation of the industrial commonly used face area was simulated with this model and described in the following sections.

5.5. SUMMARY

This section describes two experiments that were executed at S&T's Experimental Mine to validate the species transport model in FLUENT, which was used to study DPM dispersion in the face areas of underground metal/nonmetal mines.

Through these studies, it was found that, although many uncontrollable factors exist in a real mining environment, it was still possible to predict the DPM level around a diesel engine with practical accuracy. The researcher has no doubt that more ideal lab conditions would further increase the accuracy of the experiment data and improve the comparison results. However, an ideal condition for an experiment does not exist in a real mine, and the more accurate results may still be different from data collected in a real mining environment. For understanding DPM dispersion patterns, comparing and selecting different DPM control strategies, the species transport model will be sufficient to fulfill these purposes.

Therefore, the species transport model was used to simulate DPM dispersion in commonly used straight entry and dead-end entry in different mining operations and under different control strategies, as described in the following sections.

6. SIMULATION OF DPM DISPERSION IN COMMONLY USED WORKING AREAS

This section provides a comprehensive review of simulation programs, procedures, the capacity of CFD simulation for mine-wide airflow distributions, DPM dispersion in common face areas, evaluation of different face ventilation facilities, and a discussion of selection of DPM control strategies. The main purposes of this part are to reveal the consideration of CFD simulation in this research and to develop ready-to-use research results for the mining industry.

6.1. SIMULATION PROGRAMS AND PROCEDURES

In this study, the diesel emission and DPM dispersion analysis were performed by using FLUENT, a general-purpose CFD program. It is capable of simulating fluid flow and heat and mass transfer in two and three dimensions. The FLUENT solver has the capacity to model the turbulent, incompressible, multicomponent, or multiphase flow.

The structure of FLUENT is shown in Figure 6.1. It included GAMBIT, the preprocessor for geometry modeling and mesh generation; TGrid, an additional preprocessor that can generate volume meshes from existing boundary meshes; and FLUENT, the solver. Once the mesh was read into FLUENT, from GAMBIT, TGRID, or other CAD/CAE packages, all remaining operations were performed within FLUENT. These included setting boundary conditions, defining fluid properties, executing the solution, refining the mesh, and viewing and postprocessing the results.

The major procedures for DPM CFD simulation are listed below.

(i)   Building geometric model
(ii) Generating good mesh   } Pre-processing

(iii) Selecting correct governing equations
(iv) Assigning boundary conditions
(v) Choosing proper solution methods   } Solving
(vi) Obtaining converged solutions

(vii) Analysis/visualization of simulation data
(viii) Recommendations for DPM control   } Post-processing
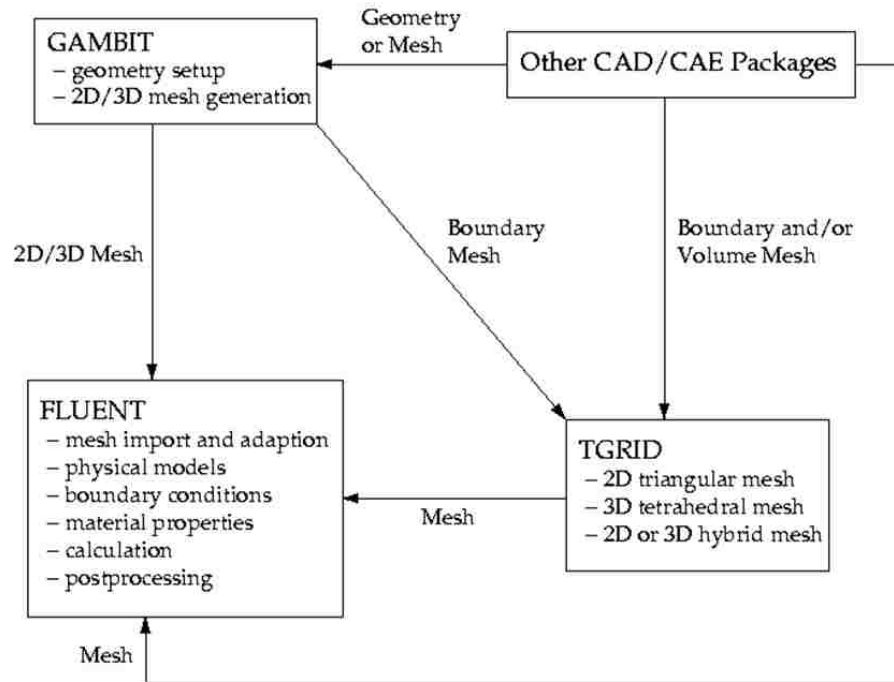
Figure 6.1. FLUENT Program Structure (Anon., 2006b)

In Section 6.2, the brief discussion on each CFD simulation step is explained, including geometry modeling and mesh generation (Pre-processing), CFD simulation (Solving Process) and analysis (Post Processing).

6.2. DPM SIMULATION STEPS

6.2.1. Geometry Modeling and Mesh Generation (Pre-processing). The geometry to closely resemble the actual mining operation was modeled using Mechanical desktop, and the generated CAD model was imported into GAMBIT. The geometry was repaired according to the need for mesh generation. The mesh generation was made by ensuring high density near the vehicles and in the bounding wall regions where high gradients existed in order to ensure the accuracy of the simulation. Hexahedral, tetrahedral, pyramidal, and wedge-shaped elements were generated inside the computational domain. The mesh generation around the vehicle's region was difficult due to the complicated shape of the vehicles. Hence, tetrahedral mesh was used to generate unstructured mesh around these regions. During the mesh generation, the equi-size skew was monitored and

maintained at a lower value that was suitable for each mesh element type. After the meshing operation was completed, boundary types (e.g., walls, inlet, fan, etc.) were assigned for each surface zone in the computational domain and the fluid/solid zone was assigned for all volume zones in the computational domain. After successful completion of the above steps, the mesh file was generated.

6.2.2. CFD Simulation (Solving Process). The mesh file was imported and the CFD simulation was carried out using FLUENT. Before started the CFD simulation, the solver type must be chosen. There are two types of solver available in Fluent: (i) pressure based and (ii) density based. The air flow inside the underground mine was incompressible and the pressure based solver, suitable for these types of flow conditions, was used for the DPM distribution calculation. The transient simulation option was selected to determine time-dependent results. The next step was to select governing equations and assign boundary conditions. The accuracy of the CFD simulation depended on the proper selection of governing equations and boundary conditions.

6.2.2.1 Governing equations.

- Since the simulation involved fluid flow (air) inside the computational domain, the 3D Navier-stokes equation, along with a continuity equation, was selected.

- Since the problem involved heat transfer due to the exchange of heat between high temperature tail-pipe exhaust and low-temperature ventilation air, an energy equation was selected.

- Since the fluid flow inside the computational domain was turbulent due to high velocity and large size of the computational domain, suitable turbulence model equations were selected.

- For DPM calculation, DPM governing equations were species transport model equations, as shown in Section 3.

6.2.2.2 Boundary conditions. The following boundary conditions were used to determine the DPM distributions inside an underground mine with a single straight entry and a single dead-end entry.

6.2.2.2.1 <u>Main ventilation.</u>

- Main Air Inlet:

Assign incoming air velocity (V);

Assign incoming air temperature (T); and

Assign DPM Mass fraction = 0.

- Exit:

Fully developed boundary conditions.

6.2.2.2.2 <u>Diesel equipments.</u>

- Tail pipe:

Assign diesel exhaust velocity (V) and temperature (T).

DPM is a gas. Assign DPM Mass fraction in species transport model.

6.2.2.2.3 <u>Walls.</u>

- Momentum:

No slip boundary conditions (i.e., the velocities in the x, y, and z directions on the walls were zero).

- Thermal:

Adiabatic walls (Heat flux = 0).

- DPM:

Zero diffusive flux (if DPM is a gas).

Reflect boundary condition (if DPM is a particle).

6.2.2.2.4 <u>Auxiliary ventilation (if any).</u> Provide fan pressure jump conditions.

6.2.2.3 Turbulence modeling. The turbulence in the flow was modeled using the **Standard *k*-epsilon** turbulence model for both particle tracking and species transport model. Near wall treatment was achieved using standard wall functions. This model was selected over many other turbulence models (***k*-omega, Reynolds Stress, Large Eddy Simulation** etc.) available in the FLUENT package due to

- The model is robust;
- Widely used for industrial applications;
- Reasonably accurate for wide ranging flow conditions; and
- Numerically less intensive and stable.

6.2.2.4 Dynamic modeling. The dynamic mesh method algorithm was selected if the diesel equipment inside the computational domain was moving rather than being stationary. In the dynamic mesh panel, a suitable dynamic mesh update method was chosen. In the present work, the dynamic layering method was chosen to update the mesh in the

deforming region. The motion was imparted to the vehicles using separately generated user defined functions and compiling it in FLUENT and hooking it to the dynamic mesh zones.

6.2.2.5 Solution methods. In FLUENT, governing equations and boundary conditions were solved using a numerical technique called Finite Volume Method. This method consisted of following steps.

- The computational domain was divided into discrete control volumes. The grid generated in pre processor GAMBIT became the control volume in FLUENT.

- The governing equations were then integrated over each control volume of the computational domain.

- The integrated equations were then discretized using a variety of discretization schemes available in FLUENT as listed below. After this process, all the integral equations were converted into algebraic equations.

    i) The pressure correction equation obtained from the continuity equation was discretized using the **Second Order** method. This technique was used because it was second order accurate. The other methods available in FLUENT are **Standard, First Order, PRESTO and Body force Weighted.**

    ii) The gradients in the governing equations were discretized using **Least Squares Cell Based** technique. This method was preferred over other methods (**Green Gauss Cell Based** and **Green Gauss Node Based**) because of the presence of a mixture of cells in the domain (hexahedral, tetrahedral etc) and for solution stability.

    iii) The convection terms in the governing equations (momentum, turbulence, species, and energy) were discretized using the **Second Order Upwind** scheme. This technique was used because it was second order accurate. The other methods available in FLUENT are **First Order Upwind, Power law and Quick.**

    iv) The **First Order Implicit** method was used for time discretization. The other method was **Second Order Implicit.** The second order implicit scheme was not required since it was needlessly time consuming for the same accuracy.

- The final step was the solution of the algebraic equations using an iterative method. The pressure and velocities in the momentum algebraic equations were coupled and this coupling was achieved using the **SIMPLE** (Semi-Implict Method for Pressure-Linked Equations) algorithm. This was the commonly used algorithm to solve all the discretized governing equations sequentially in an iterative approach to arrive at the final converged solution. The other coupling schemes available are **SIMPLEC and PISO. PISO** scheme could also be used for the present simulation. The integration of the governing equations, discretization of the integrated equations, and solution of the discretized algebraic equations were carried out using FLUENT's pressure-based solver. For the solution process, the following steps were undertaken.

    i)   Suitable under-relaxation factors were set for all of the governing equations for convergence purposes.

    ii) The unsteady flow calculations were made using time step ($\Delta t = 0.01$ s) for particle tracking model and using a time step ($\Delta t = 0.1$ s) for species transport model.

    iii) The convergence criterion required that the scaled residuals be smaller than 10^{-4} for the mass, momentum, scalar turbulence, species transport equations and smaller than 10^{-9} for the energy equation.

    iv) Calculations were performed on NIC CLUSTER using between 6-20 processors and the CPU time for a converged solution varied depending on the number of parallel processors used. In general, however, the CPU time required for the particle tracking method was more than twice that of the species transport model if a single piece of mining equipment was used in the face area. The situation became worse when multiple mining machines were involved. This was because of the large storage space required for storing the particle data for each vehicle.

6.2.3. Analysis (Post Processing). As explained before, analysis and visualization of the CFD simulation data obtained from Step II was carried out at this stage using FLUENT post processing tools or Tecplot 360 software to obtain useful results. In the post processing stage, the following results were obtained:

- Colored contours showing DPM, temperature, pressure, velocity distributions, etc. in the face area;

- Velocity vectors colored by suitable flow variables showing the fluid flow pattern;

- Streamlines (generated from the velocity vectors) to visualize more vividly the flow pattern and recirculation regions;

- Animation of the fluid flow, mesh motion, velocity vectors and DPM distribution patterns;

- Generating *x-y* plots to determine pressure temperature, DPM variations. etc. anywhere inside the flow domain; and

- Discussion of the generated results to arrive at meaningful conclusions and recommend DPM distribution control methods inside the underground mine.

6.3. MINE-WIDE AIRFLOW SIMULATION

CFD simulation has the capacity to simulate mine-wide airflow patterns to identify poorly ventilated areas. However, it must be realized that mines vary widely in their entry dimensions and mine layouts, depending on ore deposit, geological constraints, mining systems, etc. It would be an impossible and unnecessary task to show a "common" mine-wide airflow distribution and expect that it could provide guidance to the mining industry. What is shown here is only one possible mine layout to illustrate the CFD simulation capacity for a mine-wide airflow study and mine ventilation design.

As an example, Figure 6.2 shows a geometric model of the south section of an underground metal mine. It is a highly mechanized room-and-pillar mining operation in a relatively flat-lying bed. The primary design of room widths are typically 9.8 m (32 ft), with pillar sizes at 8.5 by 8.5 m (28 by 28 ft). Thick ore zones are mined first using an initial pillar pass followed by a varied combination of back, bottom, undercut, and overcut passes, resulting in pillar heights ranging from 4 to 37 m (13 ft to 121 ft). In the study, the height was modeled with a typical value of 6.7 m (22 ft). The length of the south section was about 3.1 km (1.9 mi), and the average width was about 0.9 km (0.6 mi). As the operation went on, some pillars with high-grade ore were extracted and, when it was economical, backfill was placed to allow for the extraction of additional pillars.
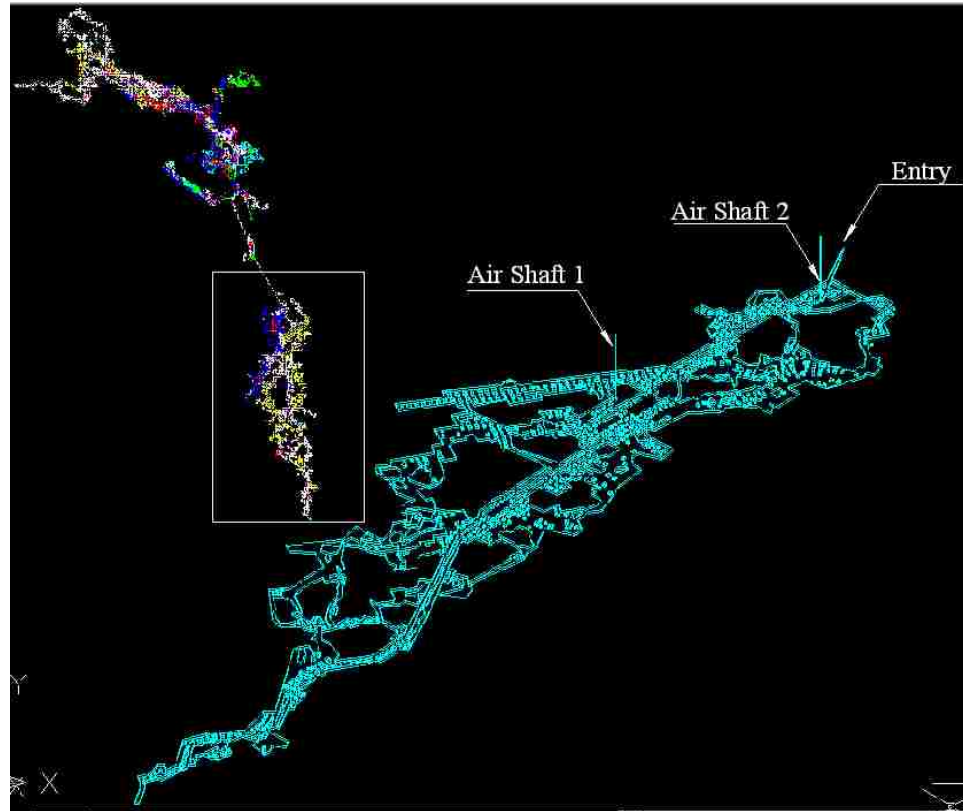
Figure 6.2. South Section of an Underground Metal Mine

6.3.1. Main Airflow Simulation without Stoppings. As shown in Figure 6.2, there were two air shafts (1 and 2) in the south section of the mine, which were connected to the north by a single entry. Airshaft 2 was a return airshaft and had a fan with 25.5 m^3/s (54, 000 cfm); Airshaft 1 was equipped with an intake fan providing 124.3 m^3/s (263,300 cfm) of intake air for the mine. The single entry connecting the two sections had an airflow of 98.8 m^3/s (209,300 cfm), traveling from south to north. Since more reserve had been found which extended the operation further south, the previously designed airshafts could not provide adequate ventilation to remote face areas. This situation can be seen in Figure 6.3, where a 3D model of the south section was constructed. Simulation showed that only the entries between the two air shafts can be ventilated by the main ventilation. Different colored lines in Figure 6.3 represent the airflow traveling path in the underground space.
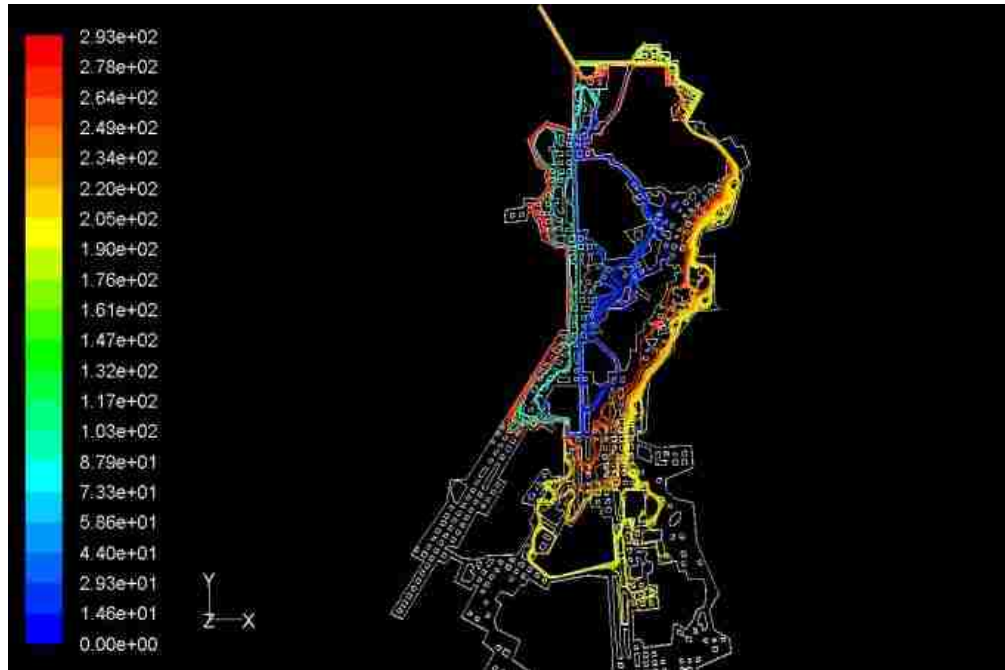
Figure 6.3. Path of Small Particles without Stoppings

Figure 6.4 shows locations of concrete block toppings;   No leakage was considered for the stoppings. Results are shown in Figures 6.5 and 6.6.

6.3.2. Main Airflow Simulation with Stoppings. Different colored lines in Figure 6.5 represent the traveling path of small (air) particles released from Airshaft 1, simulating airflow paths; entries that have color lines were ventilated by fresh air from Airshaft 1 and DPM produced in the area could be carried away by the main airflow. Simulation shows that most entries could be adequately ventilated using the fresh air from Airshaft 1 if effective stoppings were present as shown in Figure 6.5.

Although conditions were much improved by the addition of stoppings, three types of areas still remained poorly ventilated, as identified in Figure 6.6. Type I was a typical dead-end heading; Type II was a cross cut; although there was evidence of airflow at both of its ends, the cross cut itself was not ventilated. Type III were places downstream of the backfill block; these were places that were inadequately ventilated if the main airflow could not be guided by surrounding pillars or stoppings.
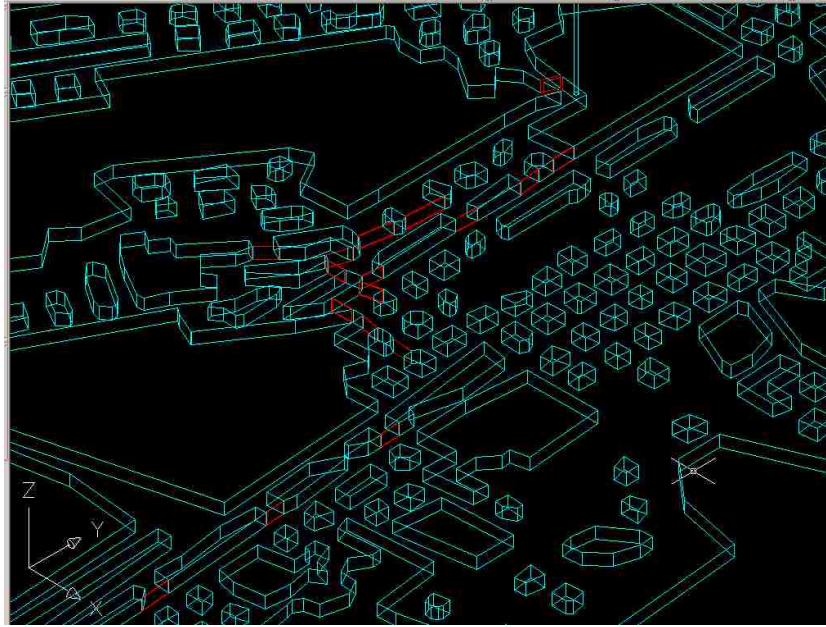
Figure 6.4. Stoppings to Guide the Air

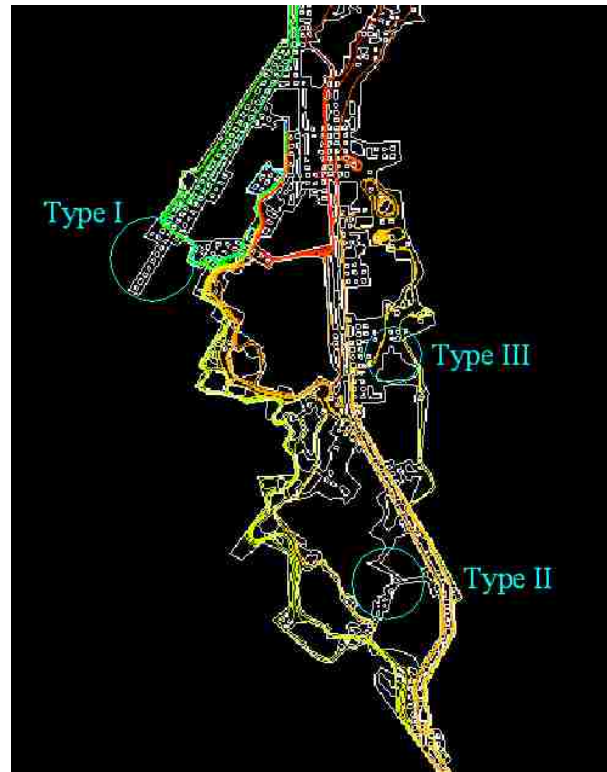Figure 6.5. Path of Small Particles with Stoppings

Figure 6.6. Three Types of Working Face with Ventilation Problems
Type I is a Typical Dead-end; Type II is a Cross Cut; Type III is a Backfilled Areas

To solve or reduce the DPM problem in the above three types of areas required both adequate airflow in the main entry and auxiliary ventilation devices to further deliver the air. The former required effective and continuous stopping lines to deliver needed air quantity to the entrance of the long dead heading, while the latter required proper placement of the auxiliary fan and tubing. For detailed information on mine-wide airflow simulation and stopping design evaluation, please refer to Zheng and Tien (2008b).

6.4. SIMULATION OF COMMONLY USED WORKING FACES

The layouts of every mine were unique, but there were some common characteristic on the face layout. The face area is the place where DPM is of most concern, for this is where most of the miners and diesel equipment are located. Therefore, simulation of

the commonly used face areas could provide more meaningful results for the mining industry.

The aim of this part was to develop ready-to-use research results for the industry. The more the simulation can resemble the real face area, then the better the results can be. Considerations in the simulation included face layout, diesel vehicle, mining operation, and local ventilation facilities. Through CFD simulation, it was expected that the DPM dispersion and high DPM areas can be identified under different face layout and mining operations, local ventilation facilities could be evaluated and compared. Other DPM control strategies, like the DPF or environmental cab, will be discussed, and the best working practices for different cases will be recommended based on the simulation results.

6.4.1. Main Considerations for Face Simulation. Main considerations for simulation include: face layout, diesel vehicle, mining operation, and local ventilation facilities. They are described below.

Two types of face areas that are commonly used are considered here: single dead-end entry and single straight entry. To decide the reasonable entry dimensions for a U.S. metal/non-metal underground mine, experts from MSHA were consulted. The final dimensions for the cross section of the entry were 6 m in width and 5 m in height.

The face simulation included three types of diesel vehicles: truck, drill jumbo, and LHD. To make the diesel vehicles consistent for all of the simulation cases, they were built as individual blocks and later merged into the face areas (Figure 6.7).

For different vehicles, two types of diesel emission rates were considered: low emission and high emission. Low emission represented the vehicle installed DPF, while high emission meant there was no DPF used in the tailpipe. For trucks, the low emission rate was 2.0 ppm from the tailpipe; the high emission rate was 7.0 ppm. For LHDs, the low emission was 1.7 ppm and the high emission was 7.0 ppm. For drill jumbos, the low emission was 2.0 ppm and 7.0 ppm for the high emission. These low and high emission rates for trucks and LHDs were calculated from the DEEP field study (Zheng, et al., 2010). For actual conditions, these numbers can be different, but they were used in the following simulation to compare the difference and show the possibly affected regions.

6.4.2. Other Considerations. This study was expected to include a comparison of the results from the species transport model and the discrete phase model in FLUENT.

The first model considered that DPM moved like an air molecule and the second model simulated DPM as really small particles. According to NIOSH and DEEP field studies (Zheng and Tien 2009b; Zheng, et al., 2010), the species transport model has been used and can provide very promising results. Still, the discrete phase model was tried to see whether it could provide more accurate DPM dispersion. It was discovered later that, when properly utilized, both models provided satisfactory results in DPM simulation. But since the species transport model required less computation time, all of the cases in this study were simulated with the species transport model.
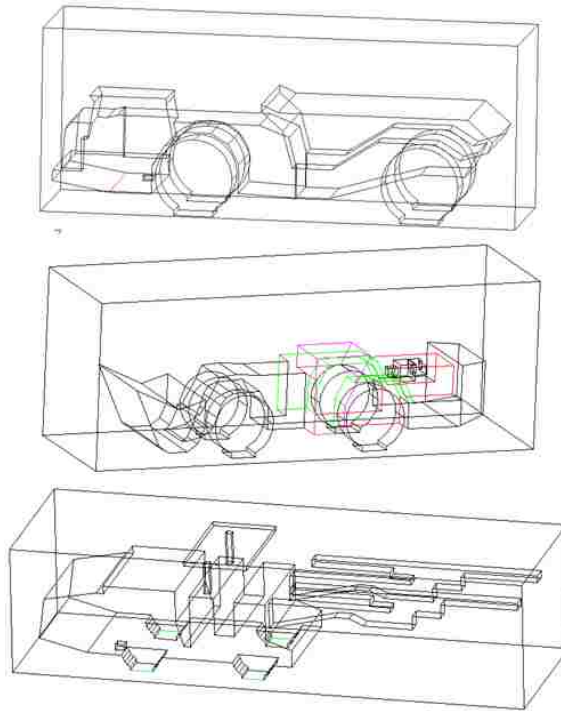

Figure 6.7. Block Models of Truck, Drill Jumbo and LHD

At the same time, the dynamic mesh technique was also incorporated into this study. Most of the simulation works in this study assumed that the vehicles were stationary in the mine. Although this provided the worst condition for mining operations, it could not reveal the actual DPM dispersion, as the vehicles moved around.

Normally, the mesh produced was fixed with the vehicles and the vehicles could not move in these fixed meshes, because they would be damaged. FLUENT provided dynamic mesh technology to permit the motion of some components in the fluid domain, while the other parts remained stationary. In the next section, dynamic mesh will be used in a straight entry to reveal the motion effect on DPM dispersion.

7. SIMULATION RESULTS AND ANALYSIS FOR SINGLE STRAIGHT ENTRY

This section presents a comprehensive review of the simulation cases of DPM dispersion regions in common face areas, an evaluation of different face ventilation facilities, and a discussion of the selection of DPM control strategies. The main purposes of this section were to develop ready-to-use research results for the mining industry and to reveal how to interpret these simulation results for application to the specific scenarios that the industry faces each day.

7.1. SIMULATION CONDITIONS

7.1.1. Considerations for Study of the Face Areas. Considerations for DPM dispersion in confined working areas included face layout, diesel vehicle, mining operations, main airflow rate, local ventilation facilities, vehicles' motion, entry inclination, and different cross-sectional areas.

Two types of commonly-used face areas were considered: single dead-end entry and single straight entry. Dimensions for the cross section of the entry were 6 m in width and 5 m in height for these two types of face. This size is common in underground metal/non-metal mines in the U.S., according to an expert consulted at MSHA.

Either one, two, or three diesel vehicles (a truck, a drill jumbo, and a LHD) were involved in the simulation according to the requirements of mining operations. For different vehicles, two types of diesel emission rates were considered: low emission and high emission as detailed in Section 6.4.1.

The geometry of the simulation included eight mining operations in a single straight entry and four mining activities in a single dead-end entry. For the straight entry working face, the eight mining operations included drilling operation with a drill jumbo working alone; LHD mucking operation with only an LHD in the face; LHD tramming operation with the LHD driving up and down the entry; truck hauling operation with a truck heading with and against the fresh airflow; LHD and truck loading operation in the face; and LHD and truck in the loading operation with a drill jumbo in the drilling operation at the adjacent face. For the dead-end entry working face, the four mining activities included single drilling operation at the face area; single LHD mucking operation in the

face; LHD and truck loading operation; and LHD and truck in the loading operation with a drill jumbo in the drilling operation at the adjacent face.

The main fresh air flow for the single straight entry had two settings: 0.65 m/s and 1.3 m/s. The low airflow speed (0.65 m/s) came from the DEEP field study, and the high speed was designed to investigate and determine the effect of main airflow speed on DPM dispersion. No local ventilation facilities were considered for the straight entry. In the dead-end entry, blower fan and tubing, exhaust fan and tubing, the push-pull system, and the jet-fan were compared.

For the vehicle's motion, some mining operations could be considered stationary, like drilling and LHD mucking operations. The loading operation was seen as stationary in this study even although the LHD moved from the face to the nearby stationary truck three or four times, dumping rocks or minerals. LHD tramming and truck hauling involve the vehicle's motion. In straight entry cases, the LHD tramming operation was considered with different driving speeds against the fresh airflow.

Entry inclination could cause difficulty for ventilation that might result in diesel fume accumulation in the area closest to the face, when diesel vehicles were operating. In this study, an upward and a downward inclined dead-end entry will be compared for DPM control.

Although most cases studied in this study were built 6 m in width and 5 m in height, the actual cross-sectional size of a mine may be different. For metal mines (gold, silver, platinum, lead-zinc, copper, etc.), main haulage drifts are usually around 4 m to 6 m wide by approximately 4 m to 6 m high. For some high roof mines (stone, lead, salt, etc.), the size can be 12 m to 15 m wide by 5 m to 10 m high. The simulation results in this study were calculated with different entry dimensions in mind. Eleven different cross-sectional sizes were compared in order to help interpret their use in various scenarios. This will be discussed in detail later in this section.

7.1.2. Comparisons of the Simulation Results. The mining scenarios above have been discretized with GAMBIT using approximately 500,000 (as in single straight entry with only one diesel engine) to 1,500,000 (as in single dead-end entry with more than two diesel engines) hexahedral and tetrahedral control volumes (cells), as shown in Figures 7.1 and 7.2. In order to ensure the accuracy of the simulation, the mesh

generation was made by ensuring high density near the diesel engine where high gradients existed. During mesh generation, for the tetrahedral cells, the equal-size skewness was monitored and maintained at a value less than 0.8. For the hexahedral cells, the equal-size skewness was controlled at a value less than 0.1 to make sure the calculation would converge.

All of the mesh models were then imported into FLUENT for CFD simulation. In FLUENT, the species transport model was used to study DPM dispersion behavior. In the species transport model, DPM was treated as gas (continuous phase) and the material that was selected as a representative for the DPM was n-octane vapor (C_8H_{18}). The properties of the mixture were derived from the experiments conducted at S&T's Experimental Mine and are described in detail in Section 5. The chemical reaction between the species was not considered in this study.
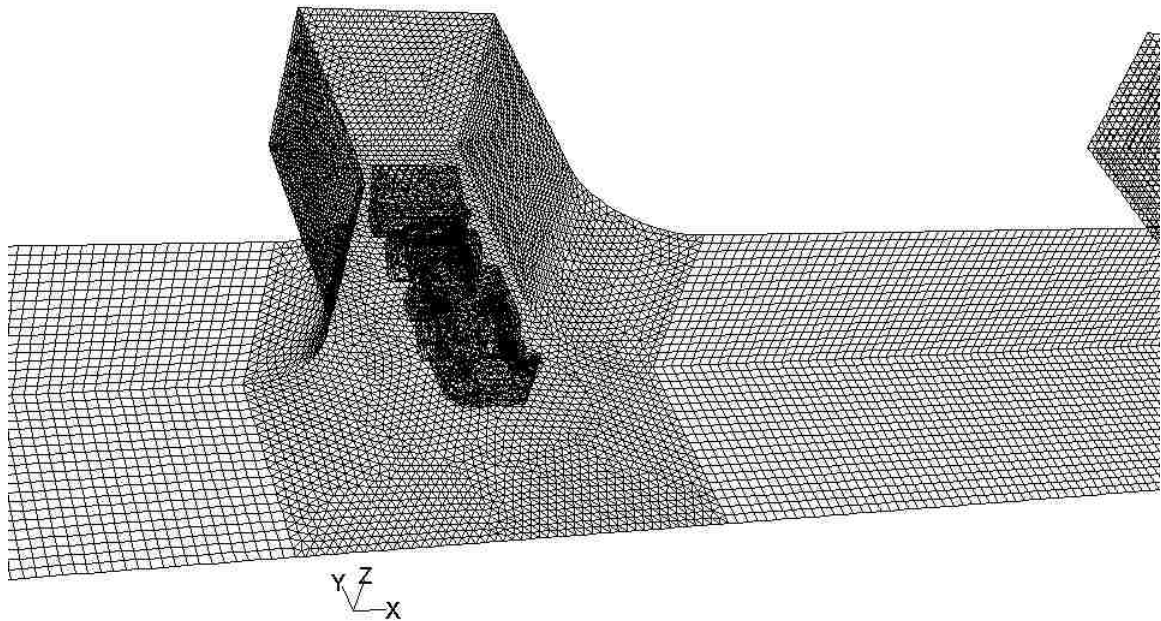

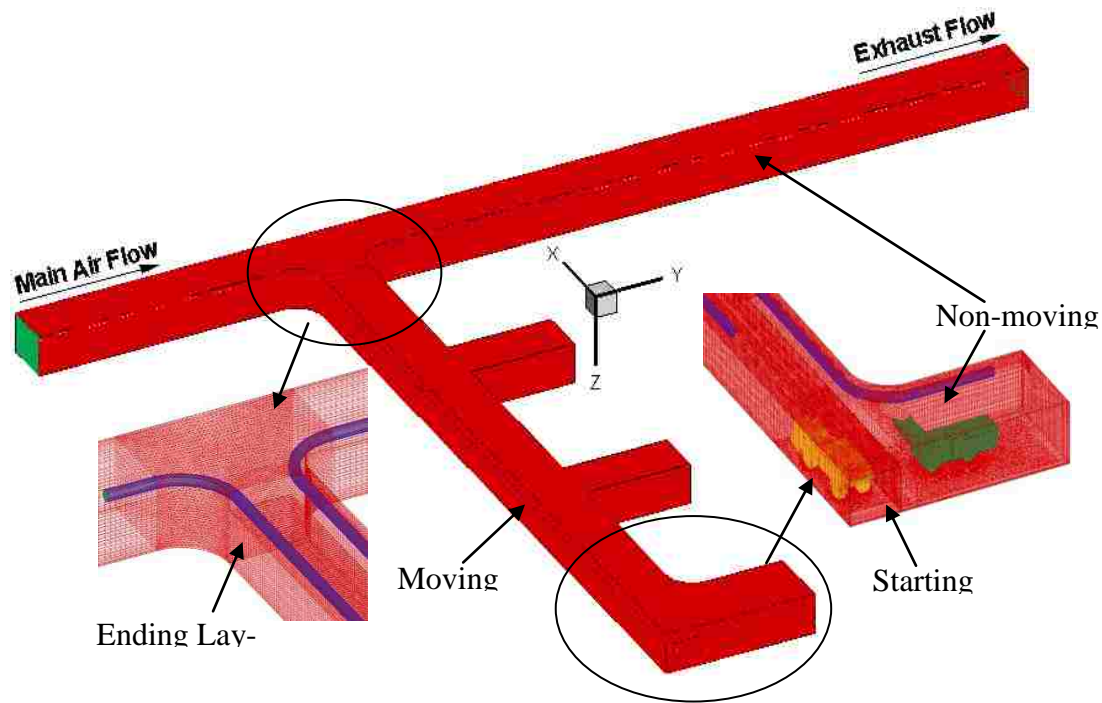Figure 7.1. Mesh Generation for a Straight Entry with a LHD Mucking Operation

Figure 7.2. Mesh Generation for a Dead-end Entry with a Loading Operation

In this study, more than 70 cases have been simulated with different considerations in the straight entry and dead-end entry face areas. For easy understanding and usage, DPM dispersion results are discussed in the following categories for the straight entry: baseline DPM simulation with low ventilation and high DPM emission, DPM dispersion with high ventilation and high DPM emission (to study the effects of increasing main airflow), DPM dispersion with low ventilation and low emission (to evaluate the effects of DPF installation), DPM dispersion with high ventilation and low DPM emission (to study the effects of high main airflow and DPF), the effects of vehicle's motion, and the effects of various cross-sectional areas.

For DPM dispersion with low ventilation and high DPM emission, eight mining operations were discussed in a single straight entry. The changing parameter for the discussion was the mining operation, while the fresh airflow rate and DPM emissions were constant. In this section, the fresh airflow rate has been set at 0.65 m/s in the straight entry. This airflow speed came from the DEEP field study (McGinn, et al., 2004). The

emission rates of truck, LHD and drill were 7.0 ppm from their tailpipes. The emission rates for the truck and the LHD were calculated from the DEEP field study (Zheng, et al., 2010), representing commonly used diesel engines without DPF. The emission rate from the drill was a devised number from that of the truck and LHD since no experimental data were available.

For DPM dispersion with high ventilation and high DPM emission, the main air flow rate in a single straight entry was doubled (1.3 m/s) to reveal the improvement in the different mining operations. In these cases, the DPM emission rate from the diesel engines was 7.0 ppm to show the effects of different mining operations on DPM distribution.

For DPM dispersion with low ventilation and low DPM emission, the emission rate was 2.0 ppm for the truck and drill jumbo, and 1.7 ppm for the LHD. The emission rates for truck and LHD were calculated from the DEEP field study (Zheng, et al., 2010), representing emission rates from the diesel engines after installing DPF. The emission rate for the drill jumbo was a devised number comparable to that of the truck and LHD.

For DPM dispersion with high ventilation and low DPM emission, the main air flow rate in a single straight entry was 1.3 m/s and the emission rate was 2.0 ppm for the truck and drill jumbo, and 1.7 ppm for the LHD.

For effects of a vehicle's motion, the LHD driving against fresh airflow with speeds of 1m/s, 2m/s, 3m/s, 5m/s and 10 m/s was simulated in single straight entry. The emission rates from the diesel engine resembled the vehicles without DPF.

All of the above cases were primarily simulated with an entry size of 6 m in width and 5 m in height (6m w × 5m h). According to MSHA experts, these are reasonable entry dimensions for U.S. metal/non-metal underground mines. To reveal the tendency of DPM dispersion on other commonly used entry sizes, LHD driving against the fresh airflow in straight entry was simulated under 4m w × 4m h; 4m w × 5m h; 4m w × 6m h; 5m w × 4m h; 5m w × 5m h; 5m w × 6m h; 6m w × 4m h; 6m w × 5m h; 6m w × 6m h; 5m w × 12m h; and 12m w × 5m h.

7.1.3. Fundamental Calculation for CFD Simulation. From the DEEP report (McGinn et al., 2004), the necessary parameters for the LHD and truck are cited as below. They were used in this research as the input.

LHD: Exhaust flow at rated speed was 57.8 m^3/min (0.96 m^3/s, or 2,034 cfm);

Exhaust temperature at rated speed 321 ºC or 610 ºF (594 K);

Truck: Exhaust flow at rated speed was 66 m^3/min (1.1 m^3/s, or 2,330 cfm);

Exhaust temperature at rated speed 371 ºC or 700 ºF (644 K).

According to the ideal gas law (used for this simulation study):

$$\rho = P/(R \times T),$$

where P is air pressure in Pa; R is the specific gas constant (for dry air, it is 287.058 J/(kg·K)); and T is absolute temperature.

Assuming that the mine was under standard pressure (1 atm = 101,325 Pa), the density of exhaust air from the tailpipe was 0.55 kg/m^3 for the truck and 0.59 kg/m^3 for the LHD. According to the DEEP experiment, the mass fraction value for LHD was 1.7 ppm for low emission and 7.0 ppm for high emission, and for the truck it was 2.0 ppm for low emission and 7.0 ppm for high emission. This means the DPM production rate from the LHD was 963 µg/s (0.59 kg/m^3 × 0.96 m^3/s × 1.7 × 10^{-6}) at low emission and 3,965 µg/s (0.59 kg/m^3 × 0.96 m^3/s × 7 × 10^{-6}) at high emission. The DPM production rate from the truck was 1,210 µg/s (0.55 kg/m^3 × 1.1 m^3/s × 2 × 10^{-6}) at low emission and 4,270 µg/s (0.55 kg/m^3 × 1.1 m^3/s × 7 × 10^{-6}) at high emission.

Similarly, the drill jumbo assumed the following parameters:

Drill: Exhaust flow at rated speed was 29.4 m^3/min (0.49 m^3/s, or 1,038 cfm);

Exhaust temperature at rated speed at 327 ºC or 620 ºF (600 K).

Therefore, the density of exhaust air from the drill jumbo was 0.59 kg/m^3. Emission rate for the drill was designed as 2 ppm for low emission and 7 ppm for high emission. For the drill jumbo, DPM production rate from the tailpipe was 578 µg/s (0.59 kg/m^3 × 0.49 m^3/s × 2 × 10^{-6}) for low emission and 2,023 µg/s (0.59 kg/m^3 × 0.49 m^3/s × 7 × 10^{-6}) for high emission.

In the straight entry, the fresh air flow was 19.5 m^3/s (0.65 m/s × 5 m × 6 m) at low main flow rate and 39 m^3/s (1.3 m/s × 5 m × 6 m) at the high main flow rate. If it mixed uniformly with DPM, as assumed by MSHA's "Work Place Diesel Emission Control Estimator", DPM concentration downstream of the face area could be calculated. For example, at a low main flow rate (19.5 m^3/s), DPM level downstream of LHD was 49.38 µg/m^3 (963 µg/s / 19.5 m^3/s) at low emission and 203.33 µg/m^3 (3,965 µg/s / 19.5 m^3/s)

at high emission. Similarly, all of the other DPM concentrations downstream of the diesel engine were computed and are listed in Table 7.1. These numbers will be discussed in the following sections.

Table 7.1. Uniform DPM Concentrations Downstream of Diesel Engine

	Downstream of LHD (µg/m^3)		Downstream of truck (µg/m^3)		Downstream of drill jumbo (µg/m^3)	
	Low emission	High emission	Low emission	High emission	Low emission	High emission
Low main flow rate (19.5 m^3/s)	49.38	203.33	62.05	218.97	29.64	103.74
High main flow rate (39 m^3/s)	24.69	101.67	31.03	109.49	14.82	51.87

From the CFD simulation below, it can be observed that DPM cannot be immediately mixed with fresh air to make a uniform exhaust flow. There were regions downstream of the engine where miners could work above the regulation limit, even though the uniformed downstream DPM concentration was below the regulation limit.

7.2. DPM BASELINE SIMULATION WITH LOW VENTILATION AND HIGH DPM EMISSION

For underground metal/non-metal mines, self-propelled diesel equipment that does not require electricity or water is preferred because working faces usually cover extensive areas where these facilities are not available. In the working face, diesel equipment can normally perform one or more mining operations. The commonly used equipment and operation include: drill jumbos for drilling operations, charging equipment to charge the drill holes, LHD or low-profile front-end loaders for mucking and loading, trucks for hauling, mechanical scalers for scaling, bolting machines for roof bolting, etc.

For underground metal/non-metal mines, the operations involved in extending the length of the drift or face are listed in the order in which they were done. These

operations include: drilling, blasting, mucking, loading and hauling, scaling, and reinforcing. Drilling was by drill jumbos that drilled a pattern of parallel blast holes. Next, explosives were placed (blown or pumped) in the blast holes with charging equipment and fired in a certain order to break the rock. The rock was then removed by a LHD or front end loader (mucking) and then dumped into a truck to be hauled to the surface as in shallow mines. In deeper mines, the ore was dumped down an ore pass (a vertical or near vertical excavation) where it fell to a collection level. The ore was then moved by conveyor belts, trucks, or even trains to be hoisted to the surface and dumped into bins beneath the surface headframe for transport to the mill. After the broken rock was removed (and sometimes even during the loading process), the roof, walls, and face were cleaned of loose rock. This process is called scaling. In small openings, scaling is normally done by hand with a special steel or aluminum tool resembling a long crowbar being used to "bar down" loose material. In larger openings and mechanized mines, a special machine with an impact hammer or scaling claw mounted on a boom is used. Depending on the ground conditions and the permanence of the openings, various means of rock reinforcement may be employed to keep the rock in place. The most common practice is to insert bolts into holes drilled around the opening.

As mentioned earlier, three diesel engines (drill, LHD, and truck) and their associated mining operations were considered in this report because of the time constraint and availability of information. Figure 7.3 shows some of the diesel equipment: top left is a drill jumbo, top right is a haulage truck, bottom left is a front-end loader and a truck loading, bottom right is a LHD mucking.

Eight mining cases with a single straight entry were considered: single drilling operation; single LHD mucking; LHD tramming 1and 2, which represents a LHD driving against, or in the same direction as, the fresh airflow, respectively; truck hauling 1 and 2, representing a truck heading against, or in the same direction as, the fresh airflow, respectively; LHD and truck loading; LHD and a truck in loading operation with a drill jumbo in drilling operation at adjacent faces.

In this section, the fresh airflow rate was set at 0.65 m/s flowing from left to right across the entry. In the cross section of the entry, the length of the simulation domain was about 200 m. The single straight entry measured 6 m in width, 5 m in height and about

200 m in length, with a short stub or face for facilitating traffic and loading on one side of the entry every 30 m (98 ft). The Reynolds number for this entry dimension and velocity was 2.39×10^5, therefore, it was considered turbulent flow.

Figure7.3. Common Mining Equipment and Its Operation

The emission rates of the truck, LHD, and drill were 7.0 ppm from their tailpipes. The airflow velocity and temperature for the truck were 27.5 m/s and 644 K (371 ℃ or 700 ℉); for the LHD, 24 m/s and 594 K (321 ℃ or 610 ℉); and for the drill, 15 m/s and 600 K (327 ℃ or 620 ℉).

For all the simulations below, unsteady flow calculations were made using time step $\Delta t = 0.1$ s. Results for different mining operations were compared at time 300 s (5 minutes) with contours of DPM concentration above the regulation limit (160 μg/m^3).

7.2.1. Drilling Operation (Case 1). For the drilling operation, the drill jumbo can work in one face for hours, according to the blasting requirements. For this reason, steady

flow simulation was also calculated for 12,000 iterations to achieve a steady state. By comparing the steady and unsteady flow results, it was found that, after three minutes, both simulations had similar flow patterns for the areas that could affect miners working in the same area. Therefore, to be consistent with other mining operations, an unsteady flow at 300 second was used to reveal the DPM dispersion pattern.

Using the high emission rate (7 ppm) calculated in 7.1.3, DPM production from the tailpipe was 2,023 µg/s. When provided with 19.5 m^3/s (41,300 cfm) fresh air, as in this case, the uniform DPM concentration was 103.74 µg/m^3 (2,023 µg/s / 19.5 m^3/s). This was under the current regulation limit of 160 µg/m^3. However, since DPM cannot be instantly diluted by incoming fresh air, high DPM level regions still existed. For the drill model, the tailpipe was located at the rear part of the vehicle (passenger side) and DPM was discharged toward the floor.

From Figure 7.4, it can be observed that, after DPM left the exhaust pipe (the exhaust discharged toward the floor), due to the buoyancy effect, a DPM plume rose toward the roof of the entry. After the plume touched the roof, it remained in the top area and was gradually dragged and diluted by the fresh airflow flowing downstream. As DPM was continuously provided, the colored region (representing high DPM level area above regulation limit 160 µg/m^3) stretched far downstream from the diesel engine.

A closer look at the diesel engine area (as shown in Figure 7.5) indicated that the drill jumbo operator in the driver's position would not be affected by the DPM plume. However, the miners immediately downstream of the exhaust could be affected. This affected region was as far as 30 m downstream, as shown in Figure 7.5, where the DPM cloud was dragged down toward the floor by the turbulent flow near the next face or stub downstream. Since the roof of the entry was 5 m in height, miners on the ground level might not be affected by the high DPM region 30 m downstream of the engine. However, the miners involved in scaling operations on a high platform could still be working in the colored region downstream.

7.2.2. LHD Mucking (Case 2). In the mucking operation, a LHD needed to remove the broken rock from blasting. The rock was then dumped into a truck or hauled away by an LHD to an ore pass to be dumped into a collection level. Either way, mucking needed several minutes in which to gather the rock, pack it, and load it in the bucket.

This was a continuous process. However, to simplify the simulation, the mucking operation was reduced to a LHD in one position as shown in Figure 7.6.

Using the high emission rate (7 ppm) calculated in 7.1.3, DPM production from the tailpipe was 3,965 μg/s. When provided with 19.5 m^3/s (41,300 cfm) of fresh air, the uniform DPM concentration was 203.33 μg/m^3 (3,965 μg/s / 19.5 m^3/s). This was higher than the current regulation limit of 160 μg/m^3. For the LHD model, the tailpipe was located at the rear part of the vehicle on the passenger side and DPM was discharged horizontally backward.
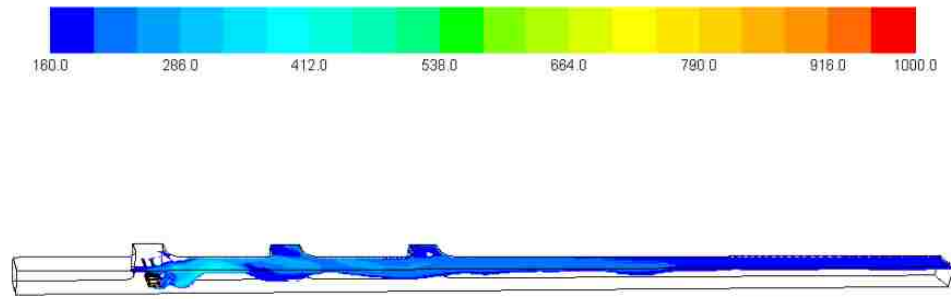
Figure 7.4. Overview of DPM Dispersion for Drilling Operation at 300 s with DPM above 160 μg/m^3
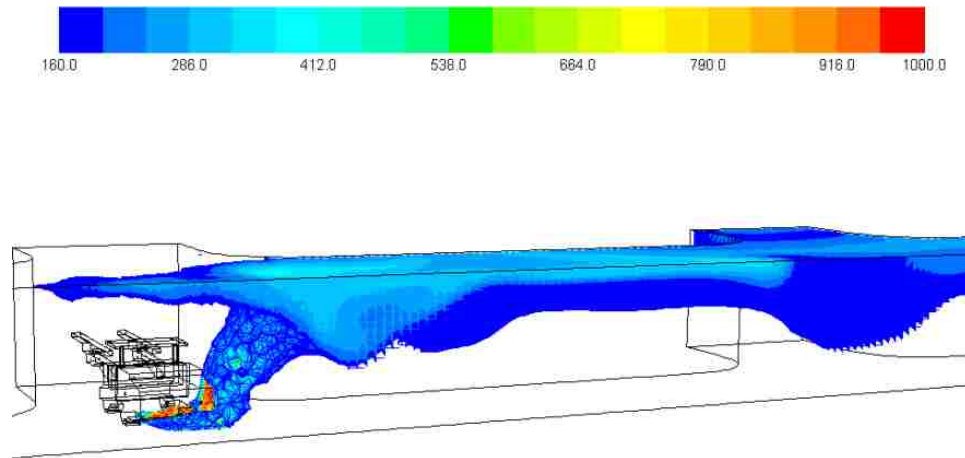

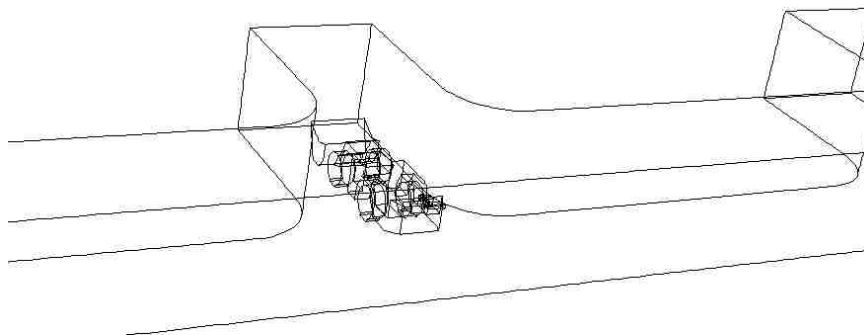Figure 7.5. Detailed View of DPM Dispersion for Drilling Operation at 300 s

Figure 7.6. LHD Mucking Position

Figures 7.7 and 7.8 show DPM dispersion for the mucking operation at time 200 s. DPM dispersion patterns were similar to those observed in the drilling operation. However, in the mucking operation, the exhaust flow left the tailpipe horizontally and hit the rib. Following that, the DPM flowed toward the roof. It can be seen that miners located within 30 m downstream of the diesel engine could be affected by the colored high DPM region. The LHD operator, miners more than 30 m downstream, and miners upstream would not be working above the regulation limit.

Yet, this was not the case. The above observation and conclusion could only be valid if the diesel engine stopped at that time period. Since the LHD was continuously moving in the face area in different orientations, and would work for hours in the region, all of the miners downstream of LHD and the LHD operator would be working above the regulation limit. This is illustrated in Figure 7.9. The steady flow simulation revealed that, when the LHD was continuously working in the face area, all of the regions downstream of the engine would become high DPM level areas. It can also be observed from the figure that part of the DPM plume also flowed upstream of the face area. However, it seems that the plume would not affect the miners working upstream from the diesel engine. Another important phenomenon revealed by the steady flow study was that, although all the entries downstream of the engine were filled with high DPM plume, DPM concentration was higher in the roof and the up level region, as revealed in Figure 7.9. When the vehicle was moving, this trend could be totally reversed as described in a later section.
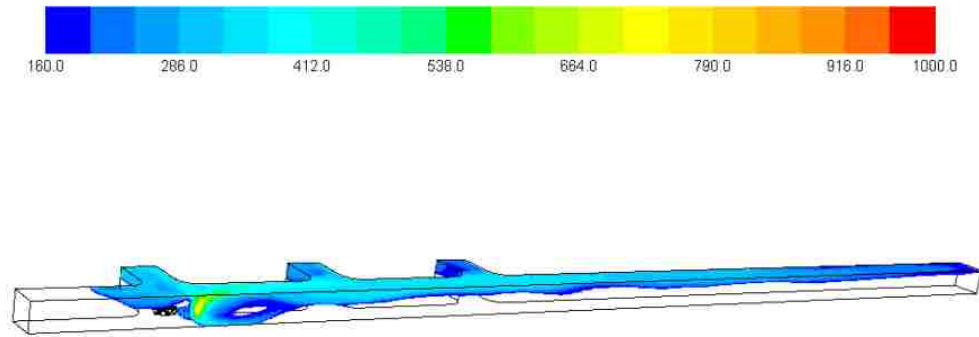
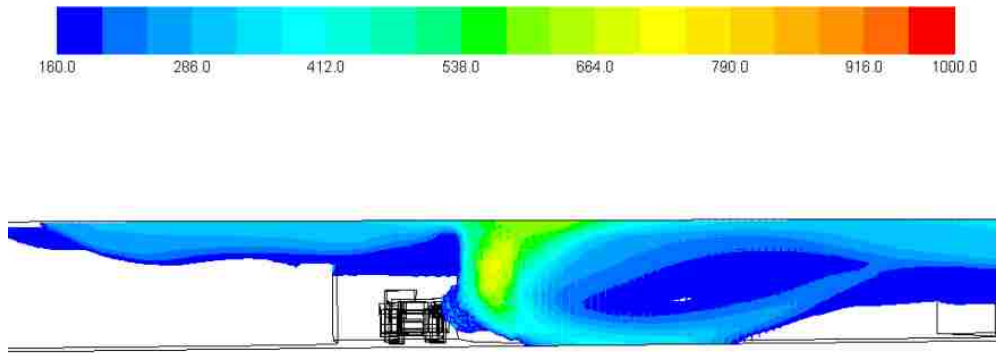Figure 7.7. Overview of DPM Dispersion for LHD Mucking in Straight Entry at 300 s

Figure 7.8. Detailed View of DPM Dispersion for LHD Mucking at 300 s

7.2.3. LHD Hauling Upstream and Downstream (Cases 3 and 4). After the mucking operation, LHD will drive either against, or in the same direction as, the fresh main airflow to load the truck or dump to an ore pass.

Figures 7.10 and 7.11 show DPM dispersion when LHD was driving against fresh airflow at 300 s; and Figure 7.12 and 7.13 reveal the vehicle heading in the opposite direction at 300 s, while the fresh airflow was constantly flowing from left to right.
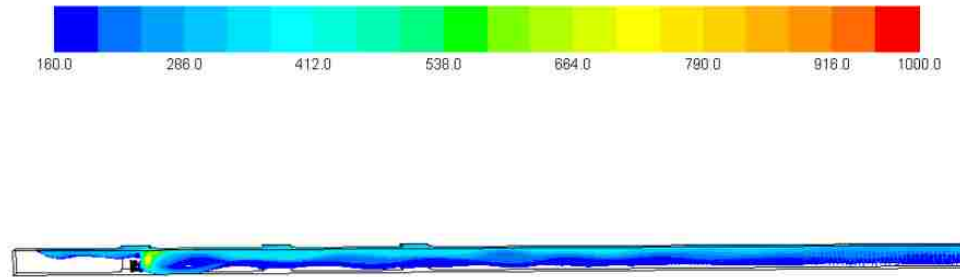
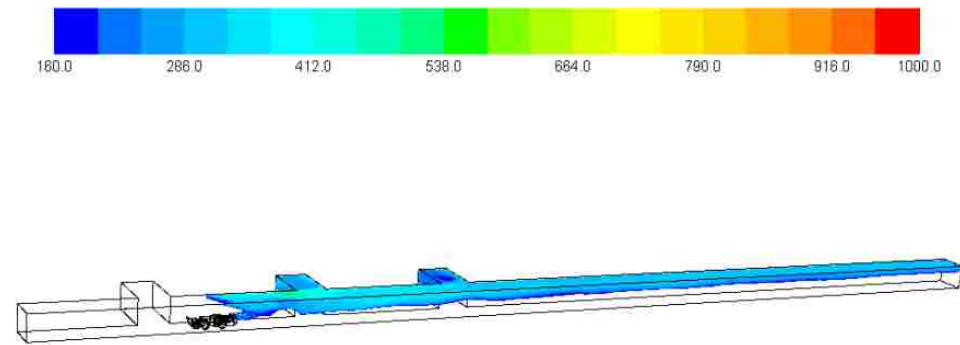Figure 7.9. DPM Dispersion for LHD Mucking with Steady Flow Simulation

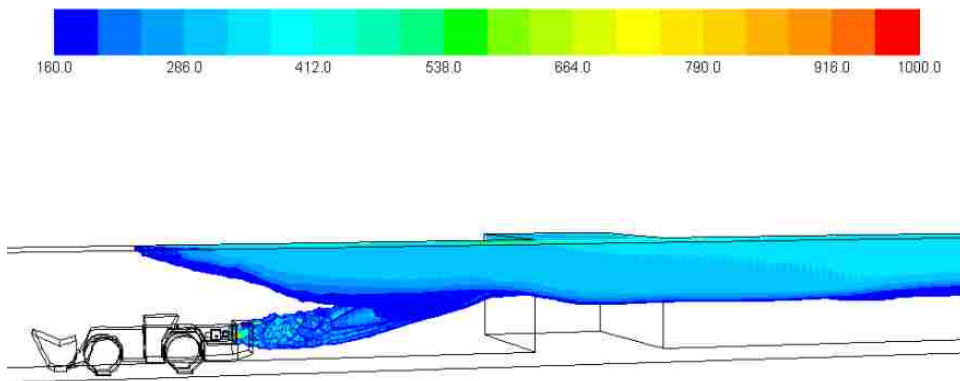Figure 7.10. Overview of DPM Dispersion for LHD Driving against Fresh Air at 300 s

Figure 7.11. Detailed View of DPM Dispersion for LHD Driving against
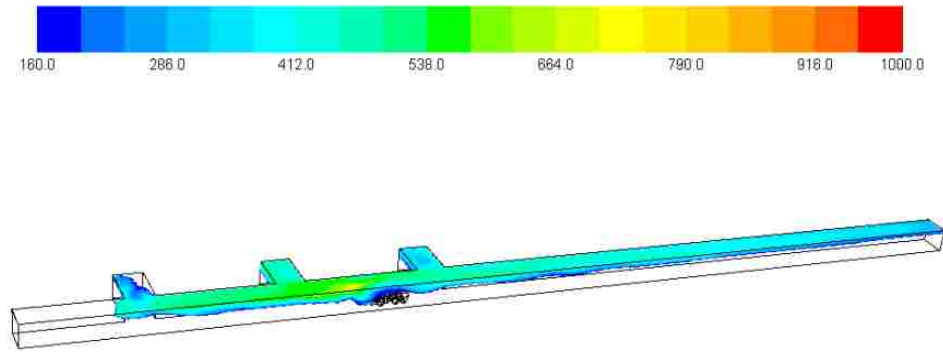Fresh Airflow at 300 s

Figure 7.12. Overview of DPM Dispersion for LHD Driving the same
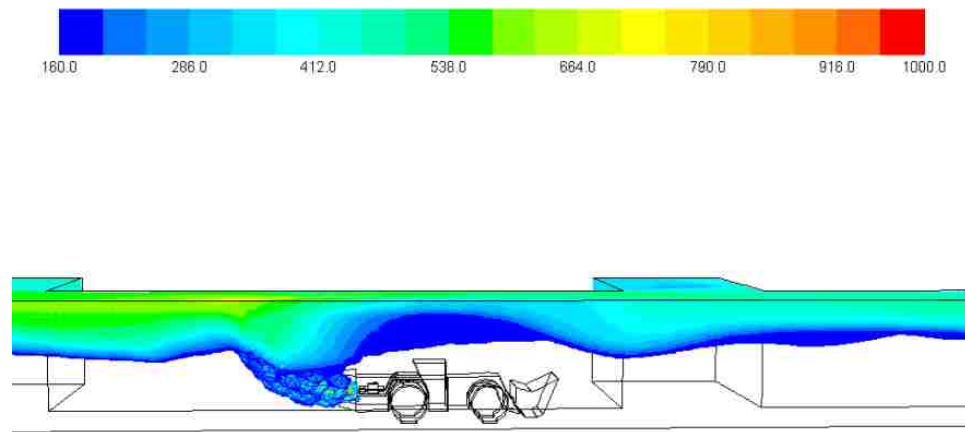Direction as Fresh Airflow at 300 s

Figure 7.13. Detailed View of DPM Dispersion for LHD Driving the
same Direction as Fresh Airflow at 300 s

From these figures, it can be seen that the DPM plume will not affect the LHD
operator (Figures 7.11 and 7.13). Unless miners are constantly chasing the tailpipe at
close range (about 8 m downstream from the diesel exhaust), all of the miners upstream
and downstream of the diesel engine worked in compliance with the regulation within the
300-second simulation period. Again, this is also a very time-dependent phenomenon. If
the LHD stayed in the face area for a longer period of time, more regions would be
polluted to a higher DPM level, as revealed in Figure 7.14, where steady flow was

simulated. In Figure 7.14, it can be observed that most of the downstream regions were out of compliance with the regulation limit.

Another very interesting feature revealed by those figures, especially in Figures 7.12-7.13, is that the exhaust flow migrated far upstream (about 45 m) in a short time (300 second) when the LHD stayed stationary and layered at the roof as it flowed upstream.
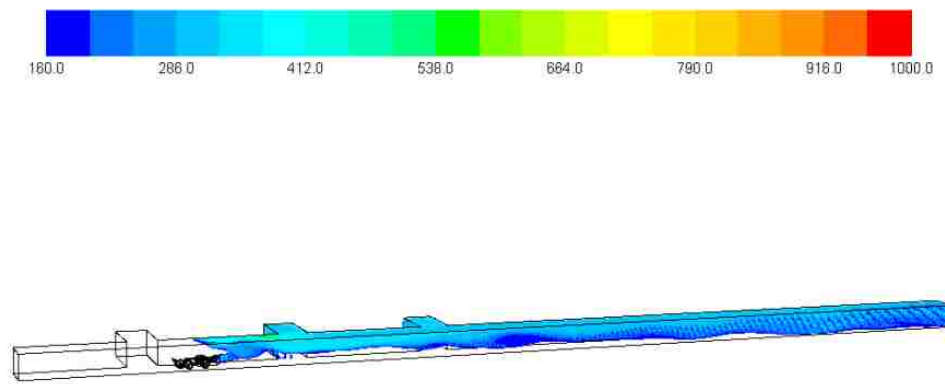

Figure 7.14. DPM Dispersion for LHD Driving against Airflow with Steady Flow Simulation

7.2.4. Truck Hauling Upstream and Downstream (Cases 5 and 6). In this study, a truck was used to transport the material out of the face area. Before and after the loading operation, the truck was driven in the main drift. Two driving directions were simulated to evaluate their effect on DPM dispersion for the truck driver and miners in the face area.

Figures 7.15 and 7.16 show DPM dispersion when the truck was driven against fresh airflow at 300 s; and Figure 7.17 and 7.18 reveal the vehicle heading in the same direction as the fresh airflow at 300 s. In both cases, the ventilation provided fresh air that was constantly flowing from left to right of the main entry.

Using the high emission rate (7 ppm) calculated in 7.1.3, DPM production from the tailpipe of the truck was 4,270 μg/s. When provided with 19.5 m^3/s (41,300 cfm) of

fresh air, the uniform DPM concentration was 218.97 µg/m^3 (4,270 µg/s / 19.5 m^3/s). This was higher than the current regulation limit of 160 µg/m^3. For the truck model, the tailpipe was located in the front part of the vehicle on the passenger side and DPM was discharged toward the floor.
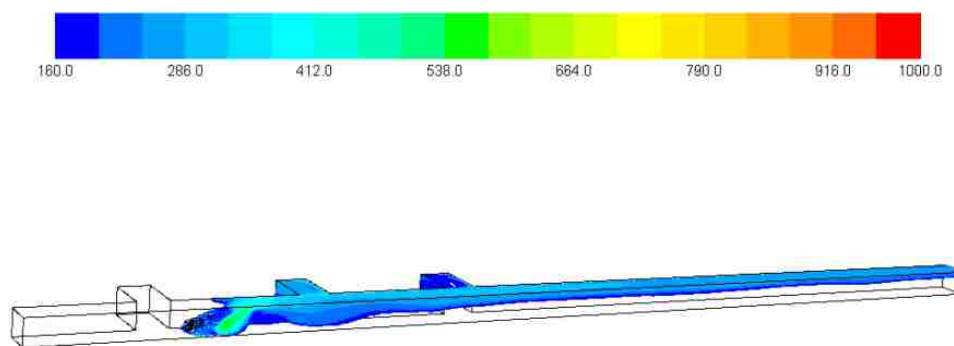

Figure 7.15. Overview of DPM Dispersion for Truck Driving against Fresh Airflow at 300 s

From the simulation results, it could be seen that, after the exhaust flow hit the floor, high DPM regions quickly dissipated into the surrounding areas. By comparing high DPM patterns with the LHD results, it was observed that when the exhaust pipe was in this location and orientation, more of the surrounding regions near the discharge outlet were affected. That is, after the exhaust flow hit the floor, DPM was more easily mixed with the surrounding fresh airflow. This is revealed in Figures 7.15 and 7.17. Approximately 20 m to 30 m downstream of the tailpipe, the miners working at ground level were surrounded by the DPM plume, while the miners who were more than 30 m away downstream were not affected. This was due to the buoyancy effect. After 30 m downstream, the plume rose toward the roof. From Figure 7.16, it can be seen that, when the truck is heading against the fresh airflow, the driver was inside the high DPM region. However, when the truck was heading in the opposite direction, as shown in Figure 7.18, the truck driver was not affected.
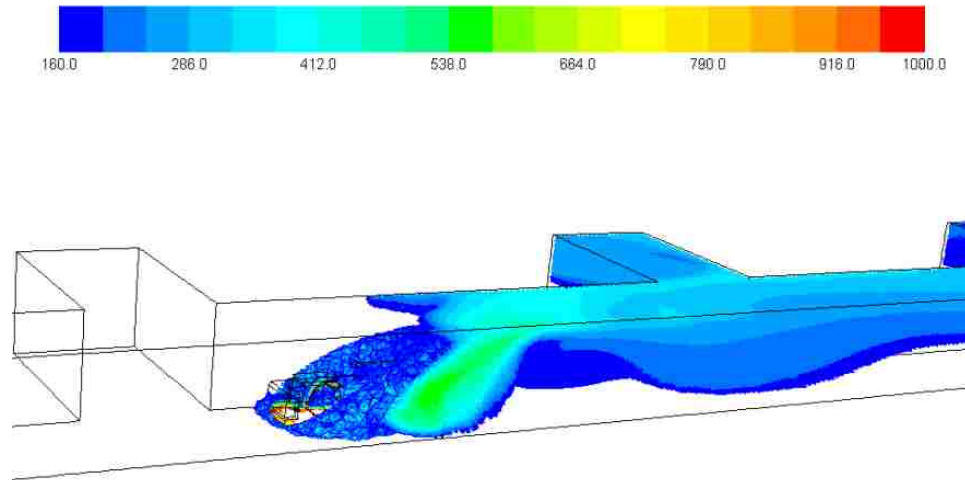
Figure 7.16. Detailed View of DPM Dispersion for Truck Driving against
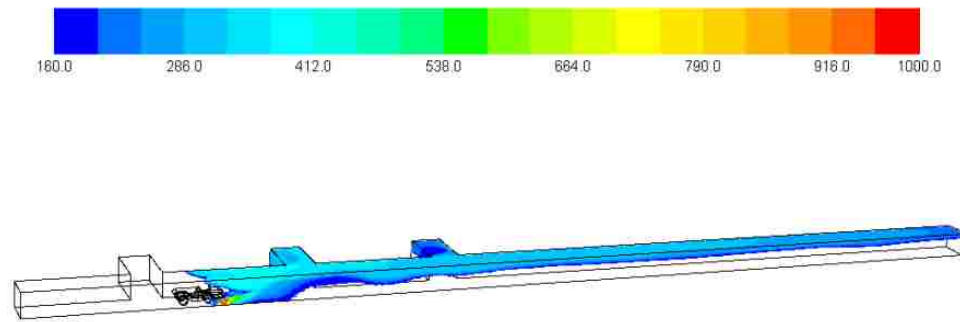Fresh Airflow at 300 s

Figure 7.17. Overview of DPM Dispersion for Truck Driving the
same Direction as Fresh Airflow at 300s

Again, this was also a very time-dependent phenomenon. When the truck stayed in the face area for a longer time, more regions were polluted and reached a higher DPM level, as revealed in Figure 7.19, where steady flow was simulated. In Figure 7.19, it can be observed that all of the downstream regions were not in compliance with the regulation limit.

7.2.5. Loading Operation (Case 7). For the loading operation, it was supposed that, in the simulation, both vehicles would still produce DPM at a constant rate, which represented the worst condition for the loading operation.
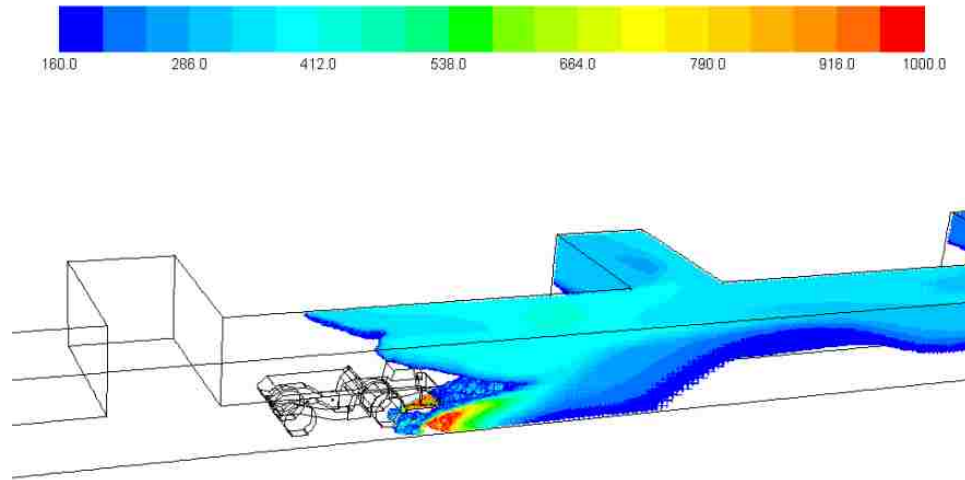
Figure 7.18. Detailed View of DPM Dispersion for Truck Driving the same Direction as Fresh Airflow at 300 s
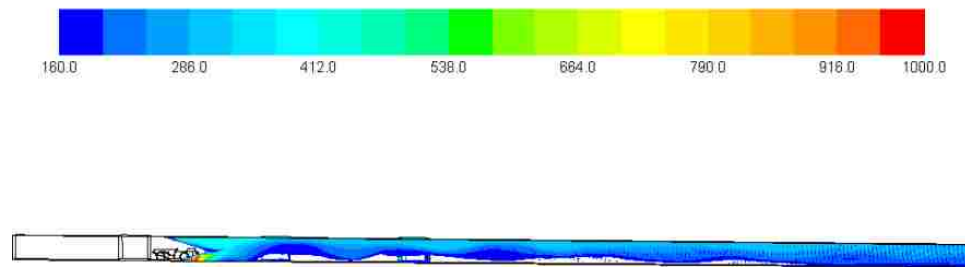

Figure 7.19. DPM Dispersion for Truck Hauling with Steady Flow Simulation

Using the high emission rate (7 ppm) calculated in 7.1.3, DPM production from the tailpipes of the LHD and truck was 3,965 μg/s and 4,270 μg/s, respectively. When provided with 19.5 m^3/s (41,300 cfm) of fresh air, the uniform DPM concentration was 422.31 μg/m^3 ((3,965 + 4,270) μg/s / 19.5 m^3/s), which was above the current regulation limit of 160 μg/m^3.

In this study, the loading operation took place in the first face area, counting from the left of the straight entry, as shown in Figure 7.20. The LHD was facing a truck with a raised bucket outside the face area. The truck was facing the fresh airflow as it blew from

the left to the right of the entry. The tailpipe of the LHD was pointing the exhaust flow against the face, making for a high DPM level (colored region) that occupied all of the space within the face (Figures 7.21 and 7.22). Both divers of the LHD and the truck were involved in the high DPM region. It was also observed that, after 300 seconds of DPM emission, within 50 m downstream of the loading face, all miners working at ground level were in compliance with the regulation limit.

Although there was no diesel exhaust that directly shot against the fresh airflow (as shown in Figures 7.11 and 7.12), it was still observed that high DPM emissions, which came out of the face area, resulted in layering on the roof. Most of the emissions came downstream by the fresh airflow, but part of it would gradually migrate upstream. This phenomenon will be discussed in detail later.

7.2.6. Loading + Drilling Operations (Case 8). For the loading + drilling operations, all vehicles in the simulation were supposed to produce DPM at a constant rate, which represented the worst condition of all of the cases.

In this study, the loading operation took place in the second face area, while the drilling operation was in the third face, counting from the left of the straight entry (as shown in Figure 7.23). For the loading operation, the LHD was facing a truck with a raised bucket outside the face area. The truck was facing the fresh airflow as it blew from the left to the right of the entry.
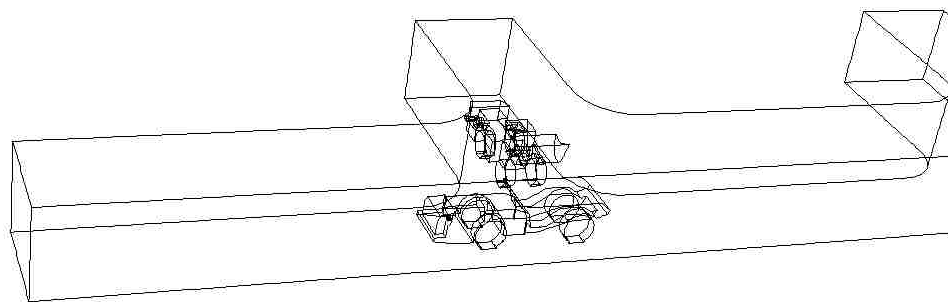

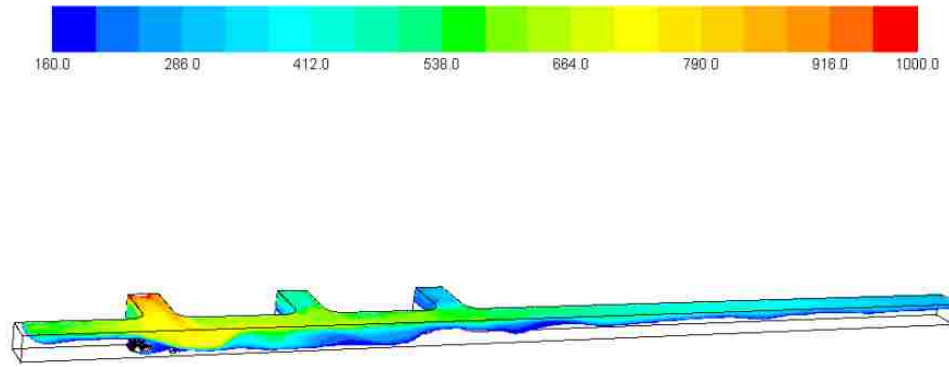Figure 7.20. Location of Loading Operation

Figure 7.21. Overview of DPM Dispersion for Loading at 300 s
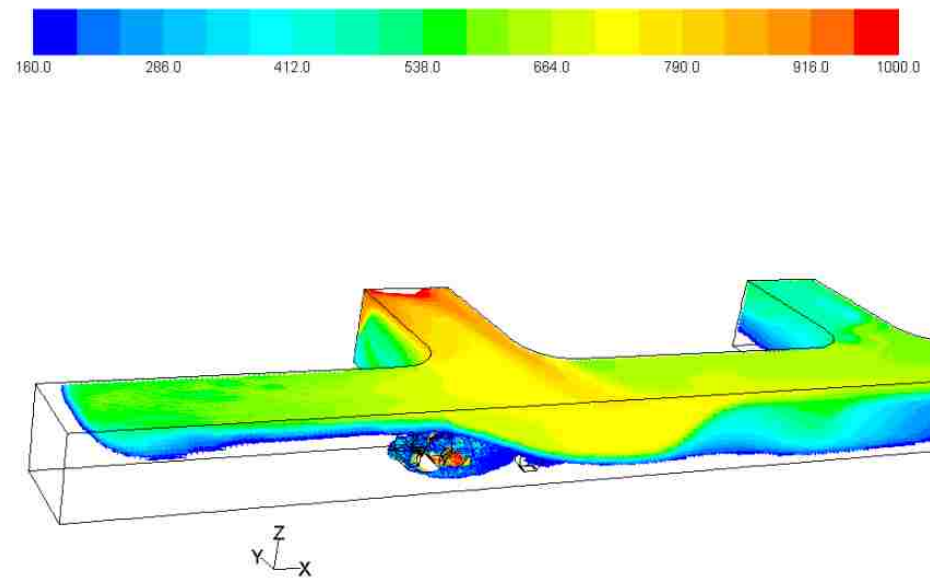

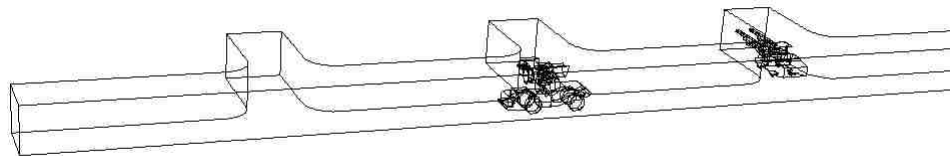Figure 7.22. Detailed View of DPM Dispersion for Loading at 300 s

Figure 7.23. Location of Loading and Drilling Operations

Using the high emission rate (7 ppm) calculated in 7.1.3, DPM production from the tailpipes of the drill, LHD, and truck was 2,023 µg/s, 3,965 µg/s, and 4,270 µg/s, respectively. When provided with 19.5 m^3/s (41,300 cfm) of fresh air, the uniform DPM concentration was 526.05 µg/m^3 ((2,023 + 3,965 + 4,270) µg/s / 19.5 m^3/s), which was above the current regulation limit of 160 µg/m^3.

As revealed in Figures 7.24 and 7.25, DPM dispersion in the loading face resembled that revealed previously, with high DPM levels (colored region) occupying all of the space within the loading face. Both drivers of the LHD and truck were working in high DPM regions. Part of the DPM plume gradually migrated upstream after it left the face area.

Previously, in Case 1, a clear drilling face was observed that was due to the low emission rate from the tailpipe. Only some areas downstream of the drill jumbo had high DPM levels. In this case, when the drill face was located downstream from the loading face, the upcoming ventilation was no longer fresh air. As a result, both the face area and the area downstream from the drilling face were filled with high DPM plume. It definitely affected the operator of the machine and miners working downstream.
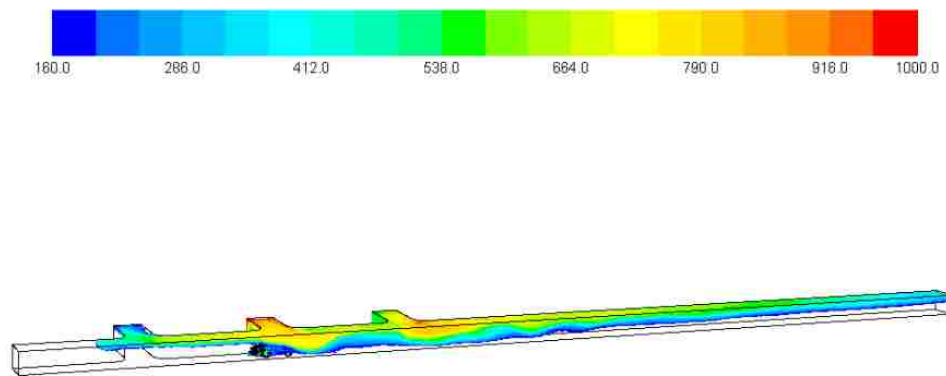

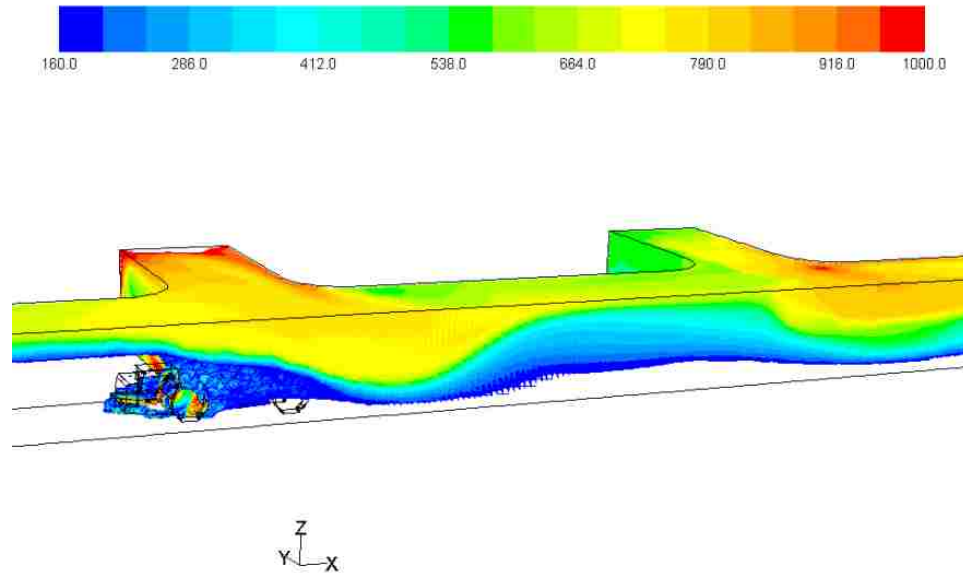Figure 7.24. Overview of DPM Dispersion for Loading + Drilling at 300 s

Figure 7.25. Detailed View of DPM Dispersion for Loading + Drilling at 300s

7.3. DPM DISPERSION WITH HIGH VENTILATION AND HIGH DPM EMIS-SION

It is readily concluded from the previous section that, when the DPM production rate o the diesel engine (or engines) in the face areas, divided by the fresh area, exceeded the regulation limit, and the engine (or engines) were designated to work for long periods of time, then the working face and all downstream locations would be affected. Miners in the face and downstream were working in conditions above the regulation limit. Personal protection or an environmental cab would be needed for the miners and vehicle operators. Although CFD simulation can revealed this phenomenon, no other corrective measures could be taken and there was no need to compare areas where DPM was higher.

Most of the working conditions were definitely not acceptable (except for the drilling operation alone) in the above section. How could this be improved? In this section, a higher main airflow was provided to the straight entry face to see the effect of upgrading on the mine ventilation system. The fresh airflow from the left of the entry was doubled to 39 m^3/s (82,600 cfm). With the same entry cross-sectional area, the airflow speed was 1.3 m/s. All of the other parameters were the same (as in the previous section)

with a high DPM emission rate (7 ppm) from the tailpipe of the drill jumbo, LHD, and truck. All operating locations were the same for the various cases.

From the simulations performed under the above conditions, it was observed that, with a higher main airflow velocity, the DPM dispersion pattern was stabilized before 200 seconds (although 300 second length movies were made of all of the cases). Therefore, no steady flow simulation was needed for a discussion of results. The improvement in the results is revealed as follows:

7.3.1. Drilling Operation (Case 1). Using the high emission rate (7 ppm) calculated in 7.1.3, DPM production from the tailpipe was 2,023 μg/s. When provided with 39 m^3/s (82,600 cfm) of fresh air, the uniform DPM concentration was 51.87 μg/m^3 (2,023 μg/s / 39 m^3/s), which was under the current regulation limit of 160 μg/m^3. Since DPM could not be instantly diluted by the incoming fresh air, high DPM level regions still existed near the tailpipe.

It can be observed from Figures 7.26 and 7.27, that high DPM regions were only located on the rear side and within 8 m downstream of the tailpipe. Because of the high fresh flow velocity, the DPM plume was only slightly curved toward the roof of the entry, and before it touched the ceiling, it had already been diluted to below the regulation limit. Only the miners who were constantly within the colored region needed personal protection. Other miners, including the drill jumbo operator, were not affected.
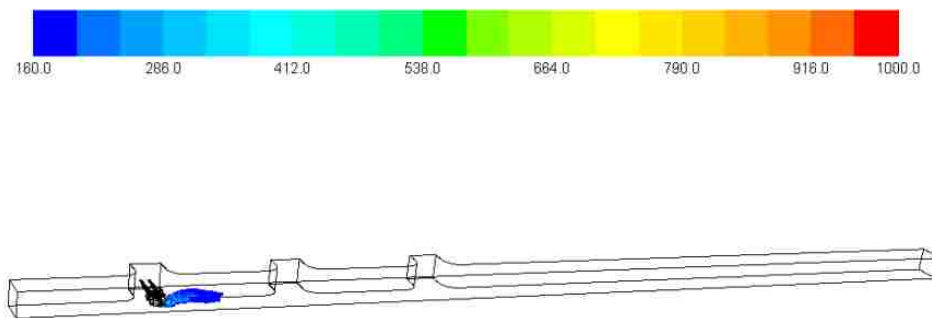

Figure 7.26. Overview of DPM Dispersion for Drilling with High Main Airflow
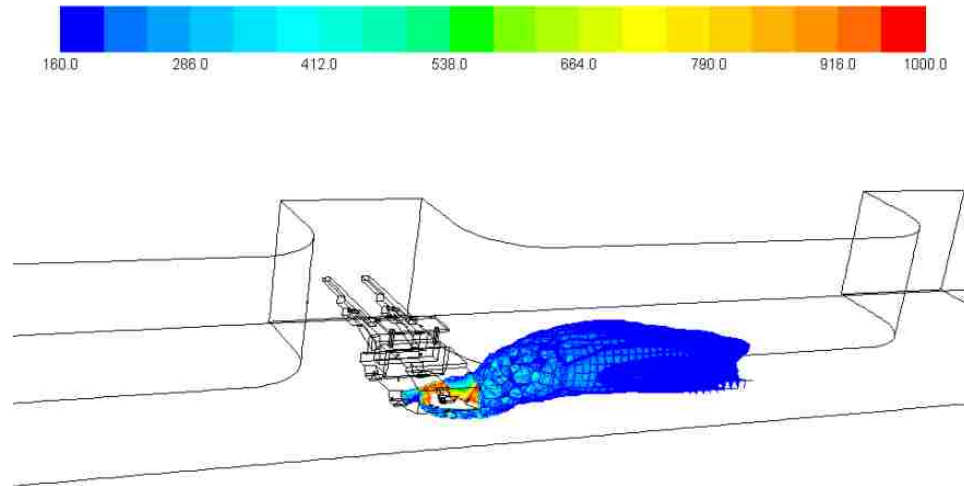
Figure 7.27. Detailed View of DPM Dispersion for Drilling with High Main Airflow

7.3.2. LHD Mucking and Tramming Operations (Cases 2, 3 and 4). Using the high emission rate (7 ppm) calculated in 7.1.3, DPM production from the tailpipe was 3,965 μg/s. When provided with 39 m^3/s (82,600 cfm) of fresh air, the uniform DPM concentration was 101.67 μg/m^3 (3,965 μg/s / 39 m^3/s), which was lower than the current regulation limit of 160 μg/m^3.

Under high main airflow conditions, LHD mucking and tramming operations were combined together. They represented a LHD working continuously in the face area with exhaust emission discharged in different horizontal directions. For the LHD mucking operation, DPM was released perpendicular to the main ventilation flow, while in the LHD tramming operation, DPM is emitted against, or in the same direction as, the fresh flow.

Figure 7.28 shows the DPM dispersion pattern in the LHD mucking operation in the face area. It was revealed that the DPM plume first hit the rib of the main entry after it was discharged at high speed (24 m/s) from the tailpipe. Then, due to the collision and high temperature of the exhaust flow (594 K or 321 °C or 610 °F), DPM tended to flow toward the roof. At the same time, the high ventilation fresh flow was mixed rapidly with the diesel exhaust flow. It was observed that the high DPM region extended to the next face 30 m downstream of the mucking face.
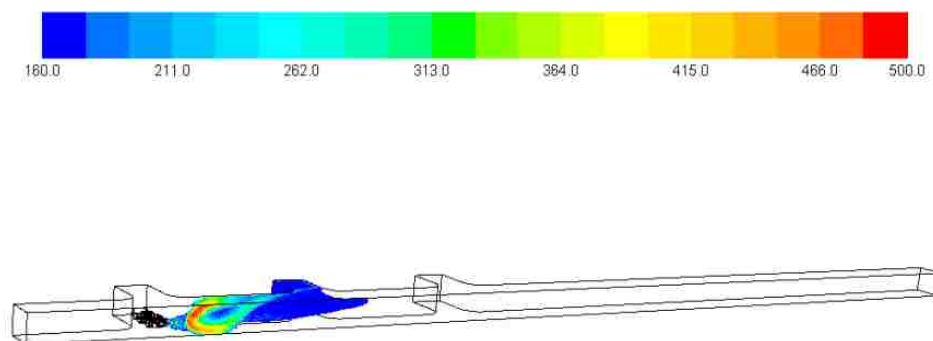
Figure 7.28. DPM Dispersion for LHD Mucking with High Main Airflow

Figure 7.29 reveals different DPM levels within the entry, with LHD as the only diesel machine that discharged DPM in the same direction as the ventilation flow. It can be seen that the DPM plume gradually flowed toward the roof and stuck there. Miners at ground level were not affected by the colored DPM plume about 20 m downstream from the diesel engine. The LHD operator and other miners outside the colored space were not affected.

Figure 7.30 illustrates DPM distribution when diesel exhaust was emitted against the fresh airflow. It can be observed that this was probably the worst condition with only a LHD in the face. Upstream of the tailpipe (up to 4 m to 6m), the LHD operator and possibly miners about 30 m downstream of the diesel engine were affected by the colored DPM plume, which represented DPM level above the regulation limit. Further downstream, only miners working close to the roof were affected.

7.3.3. Truck Hauling Operation (Cases 5 and 6). Using the high emission rate (7 ppm) calculated in 7.1.3, DPM production from the tailpipe of the truck was 4,270 µg/s. When provided with 39 m^3/s (82,600 cfm) of fresh air, the uniform DPM concentration was 109.49 µg/m^3 (4,270 µg/s / 39 m^3/s), which was lower than the current regulation limit of 160 µg/m^3.

The colored region in Figures 7.31 and 7.32 revealed the space with DPM levels above the regulation limit. As observed in Figure 7.31, the colored region only surrounded the truck. The truck driver would be affected by this DPM distribution when

driving against the fresh air. All of the other areas were below the regulation limit. In Figure 7.32, the truck was driving downstream of the entry. It can be seen that the DPM plume hit the floor and then rose toward the roof. Only the miners within 10 m in front of the vehicle were working in conditions out of compliance with DPM regulations. The truck driver and other miners were not affected by DPM problems.
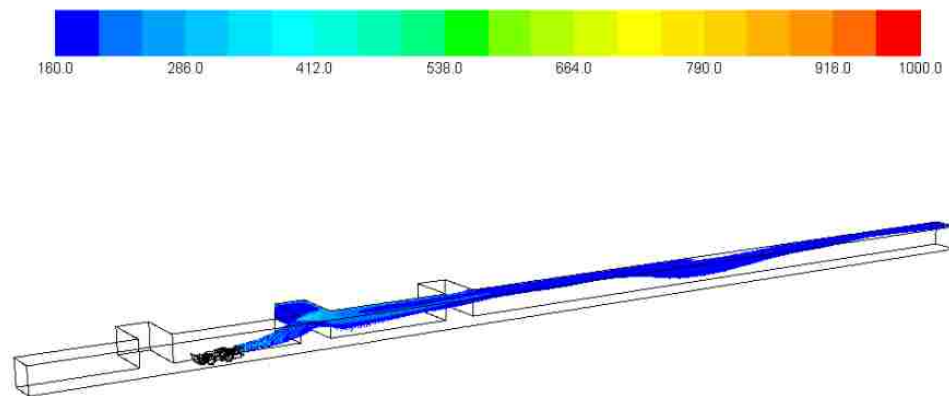
Figure 7.29. DPM Dispersion for LHD Driving against Fresh Air with High Main Airflow
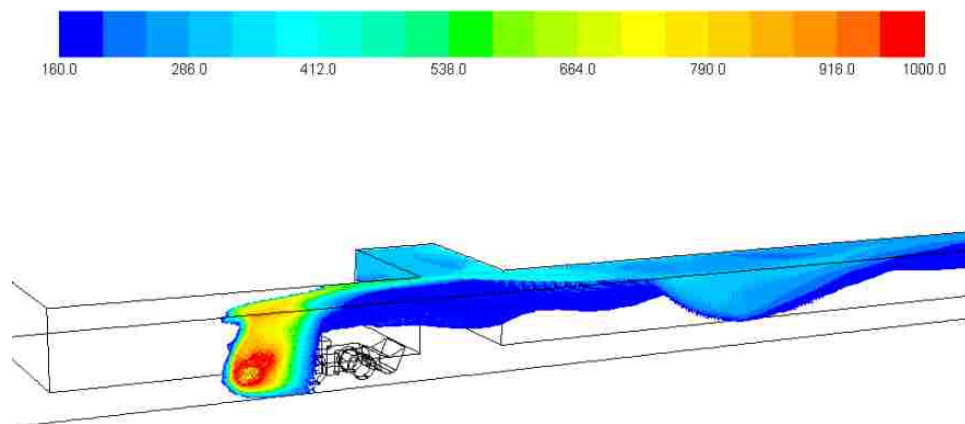
Figure 7.30. DPM Dispersion for LHD Driving the same Direction as Fresh Air with High Main Airflow
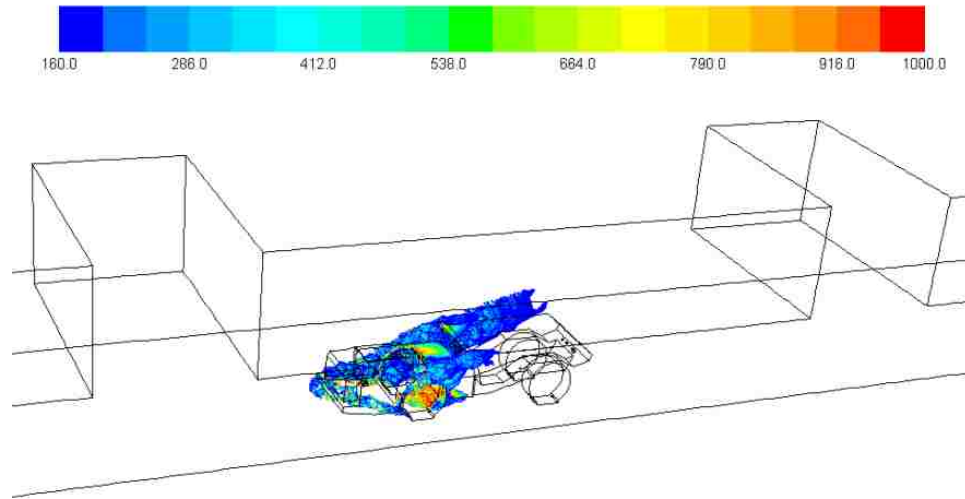
Figure 7.31. DPM Dispersion for Truck Driving against Fresh Air with High Main Airflow
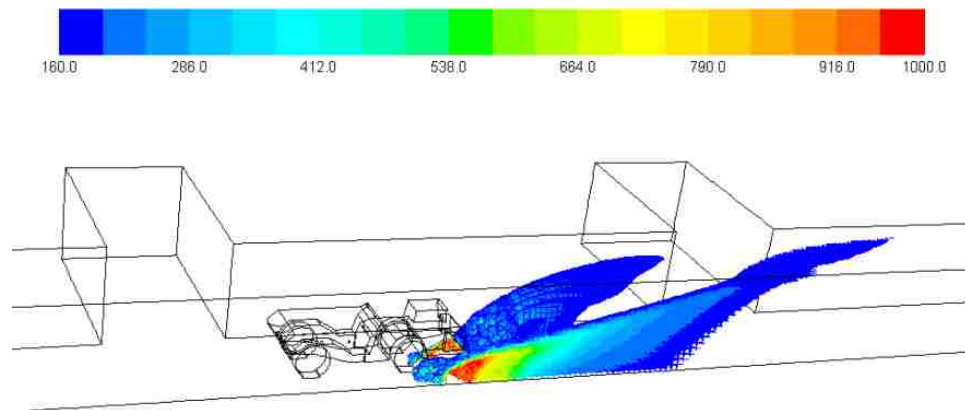
Figure 7.32. DPM Dispersion for Truck Driving the same Direction as Fresh Air with High Main Airflow

7.3.4. Loading Operation (Case 7). Using the high emission rate (7 ppm) calculated in 7.1.3, DPM production from the tailpipes of the LHD and truck was 3,965 μg/s and 4,270 μg/s, respectively. When provided with 39 m^3/s (82,600 cfm) of fresh air, the uniform DPM concentration was 211.15 μg/m^3 ((3,965 + 4,270) μg/s / 39 m^3/s), which was above the current regulation limit of 160 μg/m^3.

Figure 7.33 shows a loading operation in a high DPM level region with high fresh main airflow. In the entire working face and downstream of the loading region, miners were working in conditions above the DPM regulation limit. The main difference of DPM dispersion from the low main airflow scenario was that there was no DPM plume flowing upstream from the loading face. Miners working upstream of the loading face were not affected by high DPM levels.
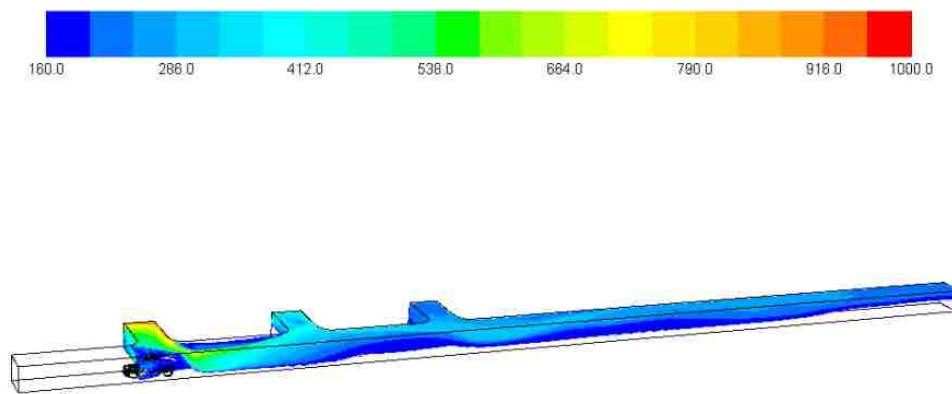
Figure 7.33. DPM Dispersion for Loading with High Main Airflow

7.3.5. Loading + Drilling Operations (Case 8). Using the high emission rate (7 ppm) calculated in 7.1.3, DPM production from the tailpipes of the drill, LHD, and truck was 2,023 µg/s, 3,965 µg/s, and 4,270 µg/s, respectively. When provided with 39 m^3/s (82,600 cfm) of fresh air, the uniform DPM concentration was 263.03 µg/m^3 ((2,023 + 3,965 + 4,270) µg/s / 39 m^3/s), which was above the current regulation limit of 160 µg/m^3.

It can be observed from the simulation results shown in Figure 7.34 that the loading face and downstream drilling face were filled with high DPM emissions. In the main entry downstream from the loading face, miners were working above the regulation limit. However, miners upstream of the loading region were not affected.
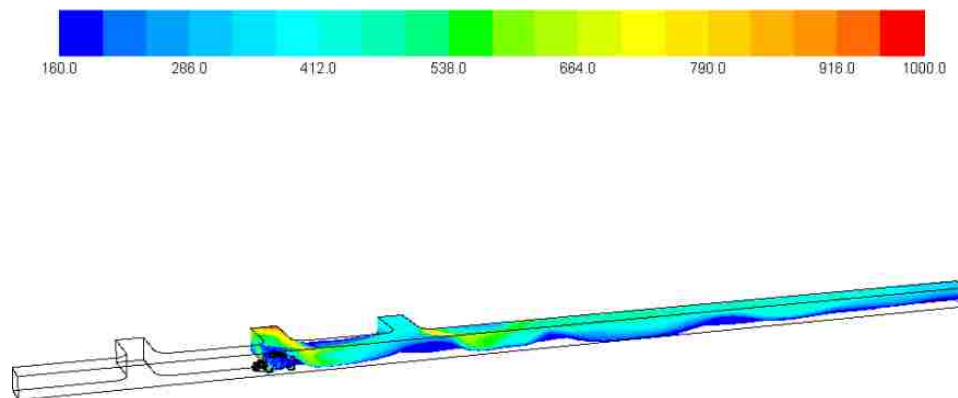
Figure 7.34. DPM Dispersion for Loading + Drilling with High Main Airflow

7.4. DPM DISPERSION WITH LOW VENTILATION AND LOW DPM EMIS-SION

In the previous section, main ventilation capacity was doubled from 19.5 m^3/s (41,300 cfm) to 39 m^3/s (82,600 cfm) to solve the DPM problem in the straight entry. By comparison of the simulation results before and after the ventilation upgrade, it can be observed that it greatly improved the working environment for a single-engine working face. However, for multi-engine scenarios, the DPM problem still exists. At the same time, for some underground metal/non-metal mines, this enhancement of the ventilation system may not be economically feasible, especially in some metal mines where different working faces can be several miles away.

Another very important and effective DPM control strategy is to install diesel particulate filters (DPF). In the simulation described below, a low DPM emission rate was applied to the tailpipes of the drill, LHD, and truck. This represented DPF being installed in the vehicles. For the drill and truck, a low emission rate of 2 ppm was applied at the outlet of the tailpipe. For the LHD, the low emission number was 1.7 ppm.

7.4.1. Drilling Operation (Case 1). Using the low emission rate (2 ppm) calculated in 7.1.3, DPM production from the tailpipe of the drill jumbo was 578 μg/s. When provided with 19.5 m^3/s (41,300 cfm) of fresh air, the uniform DPM concentration was 29.64 μg/m^3 (578 μg/s / 19.5 m^3/s), which was under the current regulation limit of 160

µg/m^3. But since DPM could not be instantly diluted by the incoming fresh air, high DPM level regions still existed close to the machine.

It can be observed in Figure 7.35 that, after leaving the tailpipe, a high DPM plume hit the floor and then rose toward the roof. Before it reached the ceiling, it had been diluted to less than the regulation limit by the fresh airflow from the entry, left to right. Only miners working in the colored regions were affected.
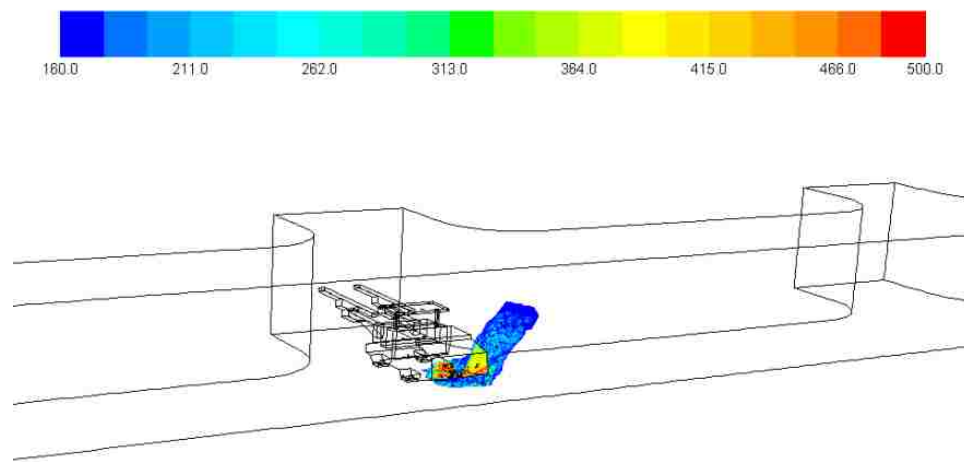
Figure 7.35. DPM Dispersion for Drilling with DPF

7.4.2. LHD Mucking and Tramming Operations (Cases 2, 3 and 4). Using the high emission rate (1.7 ppm) calculated in 7.1.3, DPM production from the tailpipe of the LHD was 963 µg/s. When provided with 19.5 m^3/s (41,300 cfm) of fresh air, the uniform DPM concentration was 49.38 µg/m^3 (963 µg/s / 19.5 m^3/s), which was lower than the current regulation limit of 160 µg/m^3.

LHD mucking and tramming operations were combined to represent a LHD moving continuously in the face area with exhaust emission discharge in different horizontal directions. For the LHD mucking operation, DPM was released perpendicular to the main ventilation flow, while in the LHD tramming operation, DPM was emitted against or in the same direction as the fresh flow.

It can be observed in Figures 7.36-7.38 that, under current conditions, only very limited regions near the tailpipe were above the regulation limit. These regions are shown as colored spaces in the figures.

7.4.3. Truck Hauling Operation (Cases 5 and 6). Using the high emission rate (2 ppm) calculated in 7.1.3, DPM production from the tailpipe of the truck was 1,210 μg/s. When provided with 19.5 m^3/s (41,300 cfm) of fresh air, the uniform DPM concentration was 62.05 μg/m^3 (1,210 μg/s / 19.5 m^3/s), which was lower than the current regulation limit of 160 μg/m^3.

High DPM-level spaces were revealed as colored regions in Figures 7.39 and 7.40. When the truck was driving against the fresh airflow, only the areas close to the vehicle and driver were affected by a high DPM plume. Other areas were clear of DPM pollution, as shown in Figure 7.39. When the truck was driving downstream, as shown in Figure 7.40, the only place above the DPM regulation limit was located about 3-4 meters in front of the vehicle, where miners are rarely located.

7.4.4. Loading Operation (Case 7). Using the high emission rate calculated in 7.1.3, DPM production from the tailpipes of the LHD and truck was 963 μg/s and 1,210 μg/s, respectively. When provided with 19.5 m^3/s (41,300 cfm) of fresh air, the uniform DPM concentration was 111.44 μg/m^3 ((963 + 1,210) μg/s / 19.5 m^3/s), which was below the current regulation limit of 160 μg/m^3.
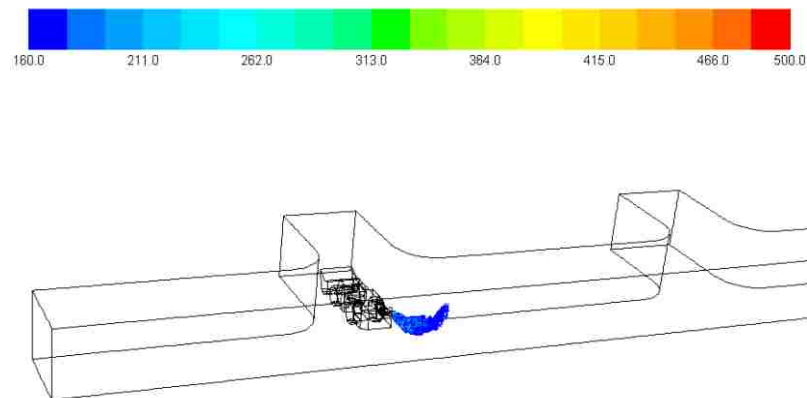
Figure 7.36. DPM Dispersion for LHD Mucking with DPF
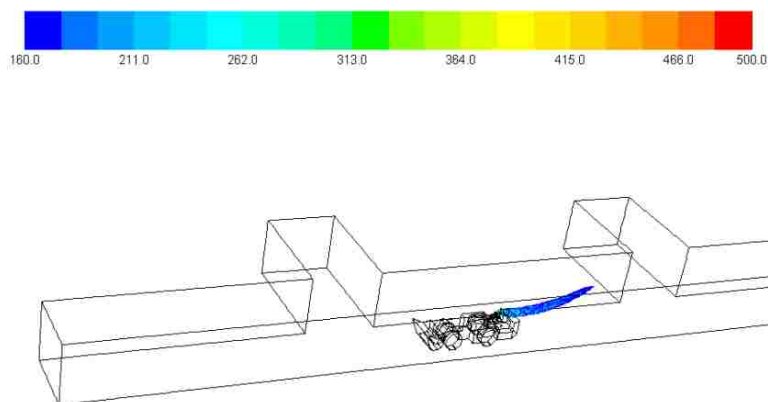
Figure 7.37. DPM Dispersion for LHD Driving against Fresh Air with DPF
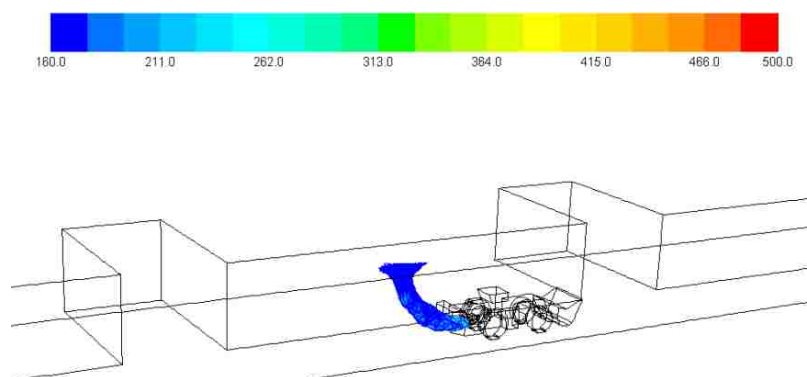
Figure 7.38. DPM Dispersion for LHD Driving the same Direction as
Fresh Air with DPF
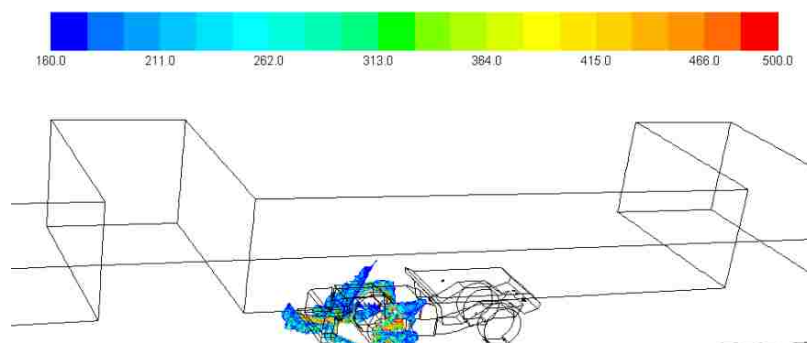
Figure 7.39. DPM Dispersion for Truck Driving against Fresh Air with DPF
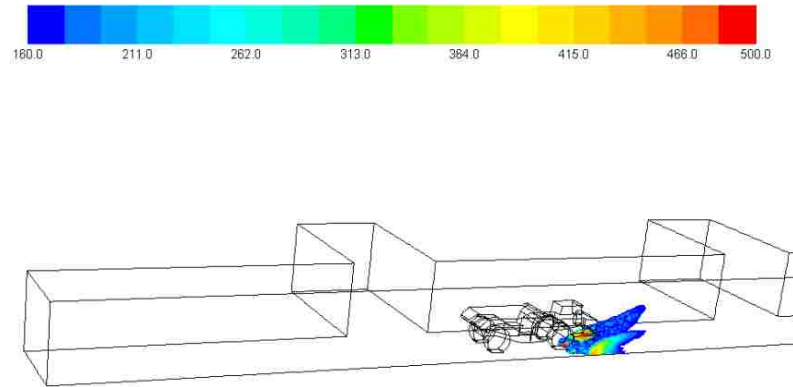
Figure 7.40. DPM Dispersion for Truck Driving the same Direction as
Fresh Air with DPF

It can be observed in Figure 7.41 that, the total DPM emission did not pollute the
ventilation air quantity above the regulation limit. Still, in the loading face area and about
10 m downstream of the face, miners worked in conditions above the regulation limit,
while the truck driver worked without a DPM problem.
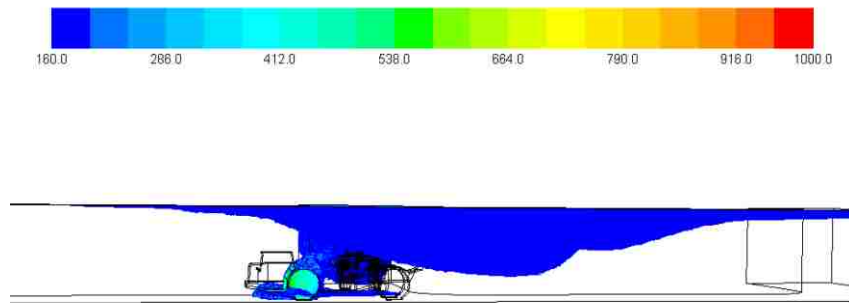
Figure 7.41. DPM Dispersion for Loading with DPF

7.4.5. Loading + Drilling Operations (Case 8). Using the high emission rate
calculated in 7.1.3, DPM production from the tailpipes of the drill, LHD, and truck was
578 μg/s, 963 μg/s, and 1,210 μg/s, respectively. When provided with 19.5 m^3/s (41,300

cfm) of fresh air, the uniform DPM concentration was 141.08 μg/m^3 ((578 + 963 + 1,210) μg/s / 19.5 m^3/s), which was below the current regulation limit of 160 μg/m^3.

It is revealed in Figure 7.42 that, in the loading face area, about 10 m downstream from the loading face and the region close to the tailpipe of the drill jumbo, miners were working in conditions above the regulation limit. Outside the colored regions, there was no DPM problem for miners, including the truck driver and drill jumbo operator.
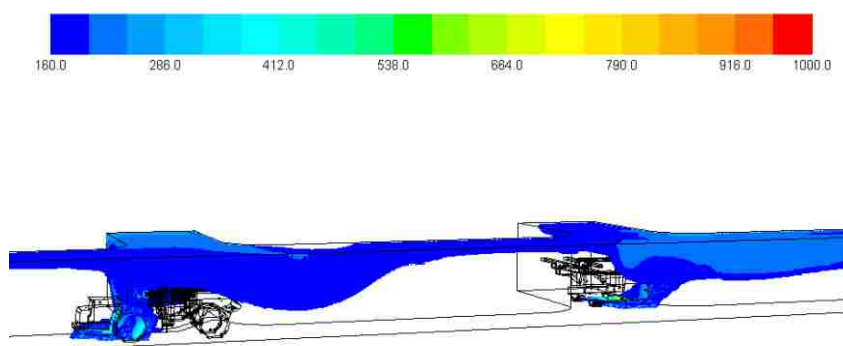
Figure 7.42. DPM Dispersion for Loading + Drilling with DPF

7.5. DPM DISPERSION WITH HIGH VENTILATION AND LOW DPM EMISSION

Section 7.2 reveals that, except for drilling operation, the face area and all of the entry downstream from the diesel engine were out of compliance with the regulation limit. To improve the high DPM working faces, a higher ventilation rate was attained to more effectively dilute DPM. However, by rough calculation, ventilation can only provide improvement that is roughly proportional to airflow increase. That is, if the ventilation doubles, the DPM level will be roughly cut in half. By more accurate CFD simulation, as in Section 7.3, some high DPM regions still existed even though the overall DPM level was lower than regulation limit.

That was because the DPM plume did not readily be mixed with surrounding fresh air. It needed time and space to be diluted below certain levels. To dramatically clear the DPM plume in most of the face areas, DPF was used for simulation in Section

7.4. DPM emission was reduced from 7 ppm to 1.7 ppm for the LHD and from 7 ppm to 2 ppm for the truck and drill jumbo. It can be observed that only limited areas had a high DPM level. If miners in the scenarios above can be made aware of regions with high DPM levels, then different practices like using remote-control devices upstream may be used. The DPM problem will then be greatly reduced.

In this section, high DPM regions were further reduced by high ventilation rates and a low DPM emission rate (after installation of DPF). In such good working conditions, high DPM levels still existed and all miners at the face should be aware of this.

Except for different ventilation and DPM emissions, all of the simulations below were executed using the same operation and location in the face area.

7.5.1. Drilling Operation (Case 1). Using the low DPM emission rate calculated in 7.1.3, DPM production from the tailpipe of the drill was 578 µg/s. When provided with 39 m^3/s (82,600 cfm) of fresh air, the uniform DPM concentration was 14.82 µg/m^3 (578 µg/s / 39 m^3/s), which was much below the current regulation limit of 160 µg/m^3.

Although the uniform DPM level from the single drill was well under regulation limit, it was still observed that, within 3 – 4 m directly downstream of the exhaust outlet, a high DPM plume rose to the breathing level of the miners (Figure 7.43). This definitely affected the miners located in the plume and should be avoided. No other high DPM regions are detected in other places.
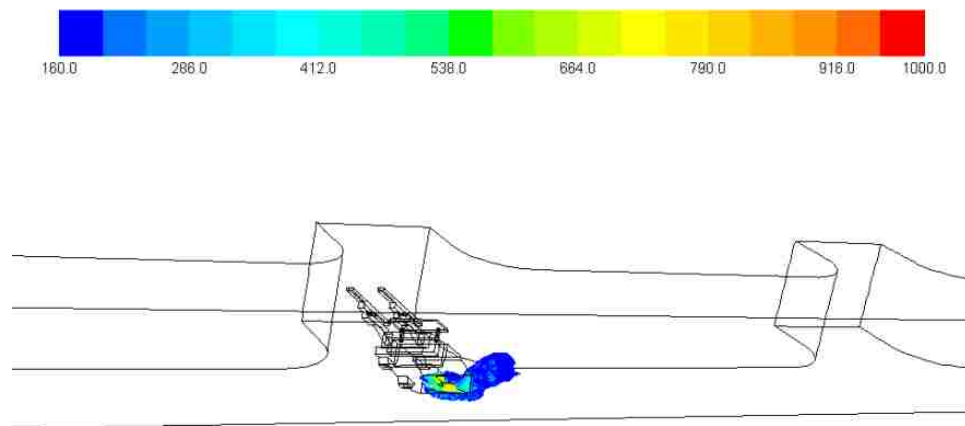
Figure 7.43. DPM Dispersion for Drilling with High Ventilation and DPF

7.5.2. LHD Mucking and Tramming Operations (Cases 2, 3 and 4). Using the low DPM emission rate calculated in 7.1.3, DPM production from the tailpipe of the LHD was 963 µg/s. When provided with 39 m^3/s (82,600 cfm) of fresh air, the uniform DPM concentration was 24.69 µg/m^3 (963 µg/s / 39 m^3/s), which was much below the current regulation limit of 160 µg/m^3.

When the exhaust flows were horizontally perpendicular to the main airflow, as illustrated in Figure 7.44, it can be seen that the high DPM plume affected 3 - 5 m at the back of the LHD and downstream from the tailpipe. When the exhaust flowed in the same direction as the fresh airflow, as shown in Figure 7.45, the high DPM colored regions extended 10 – 12 m downstream from the tailpipe and curved slightly above breathing level at the end of the plume. When the exhaust flowed against the fresh airflow, as revealed in Figure 7.46, the high DPM exhaust flow bent toward the roof and only affected the region that was less than 4 m upstream from the exhaust outlet.

7.5.3. Truck Hauling Operation (Cases 5 and 6). Using the low DPM emission rate calculated in 7.1.3, DPM production from the tailpipe of the truck was 1,210 µg/s. When provided with 39 m^3/s (82,600 cfm) fresh air, the uniform DPM concentration was 31.03 µg/m^3 (1,210 µg/s / 39 m^3/s), which was much below the current regulation limit of 160 µg/m^3.
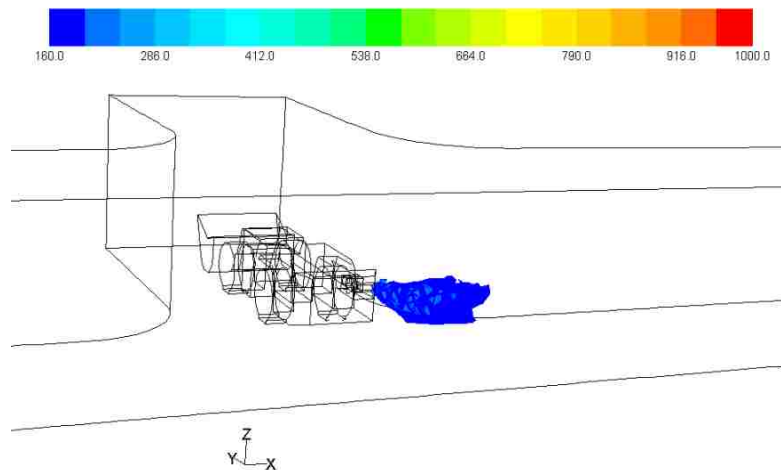
Figure 7.44. DPM Dispersion for LHD Mucking with High Ventilation and DPF
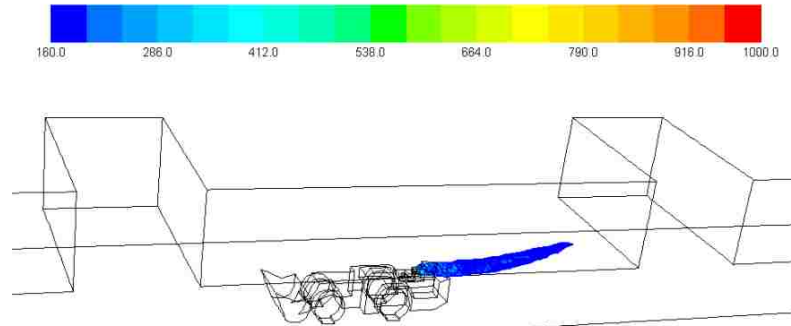
Figure 7.45. DPM Dispersion for LHD Driving against Fresh Air with
High Ventilation and DPF
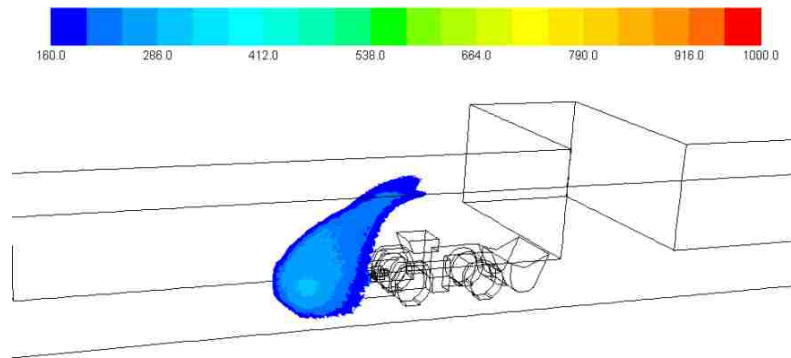
Figure 7.46. DPM Dispersion for LHD Driving in the same Direction as
Fresh Air with High Ventilation and DPF

By comparing the DPM dispersion pattern of the truck at high ventilation and
DPF installation with the cases in Section 7.4, it can be observed that the affected areas
were quite similar, but had a lower DPM concentration level (as shown in Figures 7.47
and 7.48). Because the exhaust first flowed downward and hit the floor, it mixed more
quickly with the surrounding air, as compared to the horizontal flow from an LHD ex-
haust pipe. This phenomenon will be addressed in more detail later.

7.5.4. Loading Operation (Case 7). Using the low emission rate calculated in 7.1.3, DPM production from the tailpipes of the LHD and truck was 963 µg/s and 1,210 µg/s, respectively. When provided with 39 m^3/s (82,600 cfm) of fresh air, the uniform DPM concentration was 55.72 µg/m^3 ((963 + 1,210) µg/s / 39 m^3/s), which was below the current regulation limit of 160 µg/m^3.
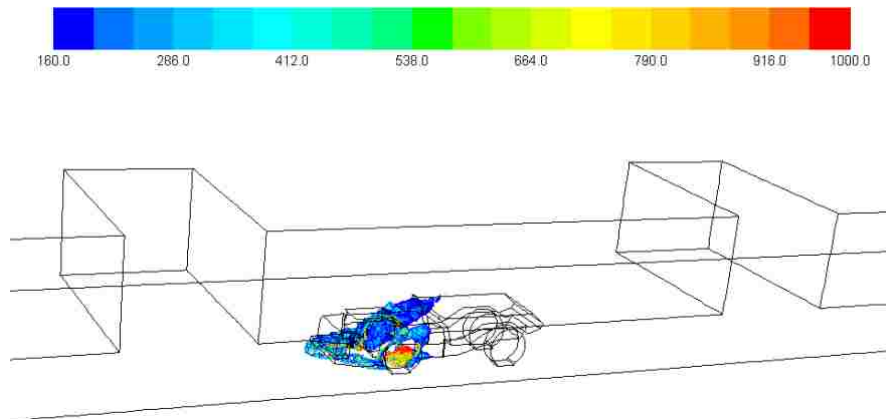
Figure 7.47. DPM Dispersion for Truck Driving in the Same Direction as Fresh Air with High Ventilation and DPF
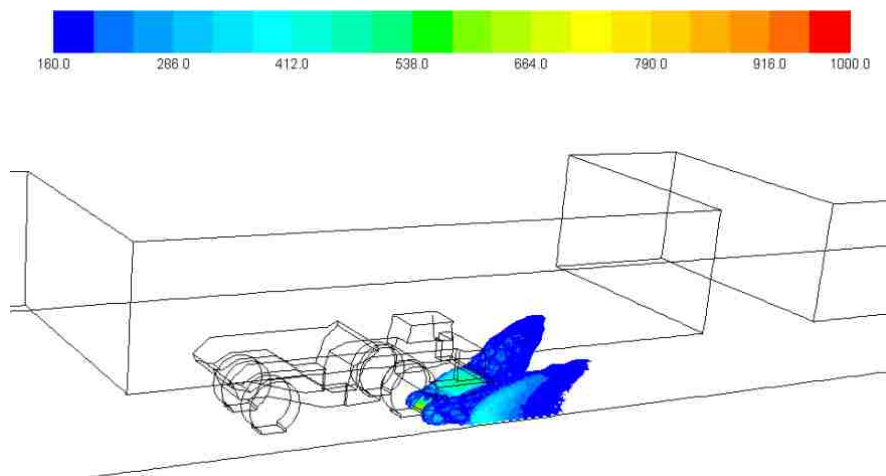
Figure 7.48. DPM Dispersion for Truck Driving against Fresh Air with High Ventilation and DPF

It can be observed in Figure 7.49 that the DPM pattern close to the truck was similar to the DPM dispersion for truck hauling. The truck driver was not affected by the high-DPM plume. The same was also true for the LHD operator. It can be seen from the simulation that DPM from the LHD hit the vertical face and bent upward toward the roof. At the down corner of the roof, the DPM level was relatively high. After that, the DPM migrated outside the loading face at high levels and did not affect the LHD driver when he was located in the cab.

7.5.5. Loading + Drilling Operations (Case 8). Using the low emission rate calculated in 7.1.3, DPM production from the tailpipes of the drill, LHD, and truck was 578 µg/s, 963 µg/s, and 1,210 µg/s, respectively. When provided with 39 m^3/s (82,600 cfm) of fresh air, the uniform DPM concentration was 70.54 µg/m^3 ((578 + 963 + 1,210) µg/s / 39 m^3/s), which was below the current regulation limit of 160 µg/m^3.

The loading face was quite similar to the simulation made above, except some of the DPM plume from truck flowed into the face area (Figure 7.50). It could be that, during the process of building the geometric model, the location of the truck was slightly different from that of the loading case alone.

7.6. THE EFFECT OF ORIENTATION OF TAILPIPE

Two types of tailpipe orientations were considered in this study: for LHD, the tailpipe was horizontal and DPM was discharged toward the back of the vehicle; for the truck and drill jumbo, DPM discharged toward the floor. These tailpipe orientations are widely used by underground engines. Although other tailpipe orientations exist, like the discharge of DPM vertically or inclined toward the roof, they were not considered in the current simulation. In the future, similar comparisons may be made between all of the possible orientations.

To reveal the effect of the orientation of the tailpipe on DPM dispersion, a set of "sweep surfaces" were built in the simulation domain about 20 m upstream from the tailpipe to the outlet of the straight entry, with 2-m intervals between adjacent planes to display the simulation values in each plane (Figure 7.51). The DPM distribution data from the cells of these surfaces were obtained from the simulation results and are compared later in this section.
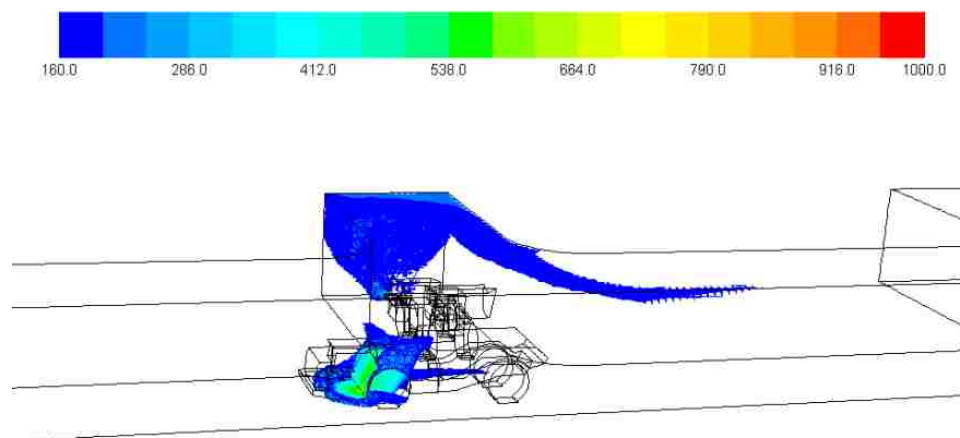
Figure 7.49. DPM Dispersion for Loading with High Ventilation and DPF
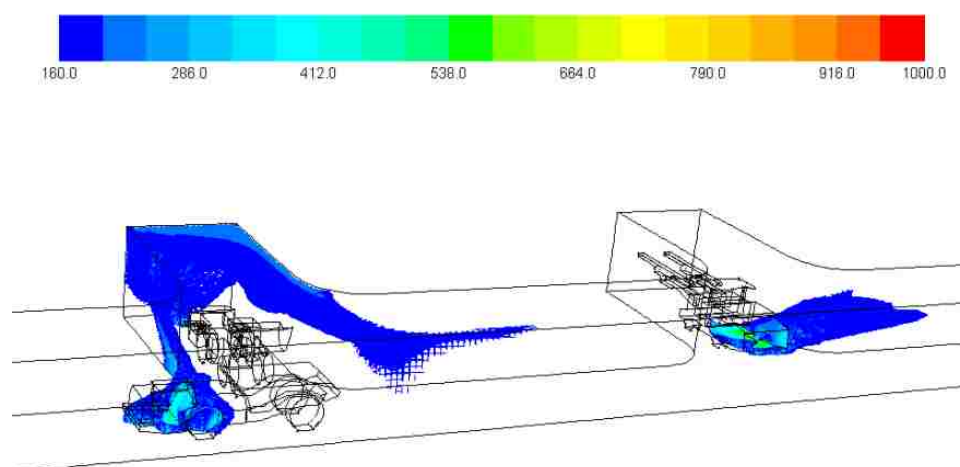
Figure 7.50. DPM Dispersion for Loading + Drilling with High Ventilation and DPF
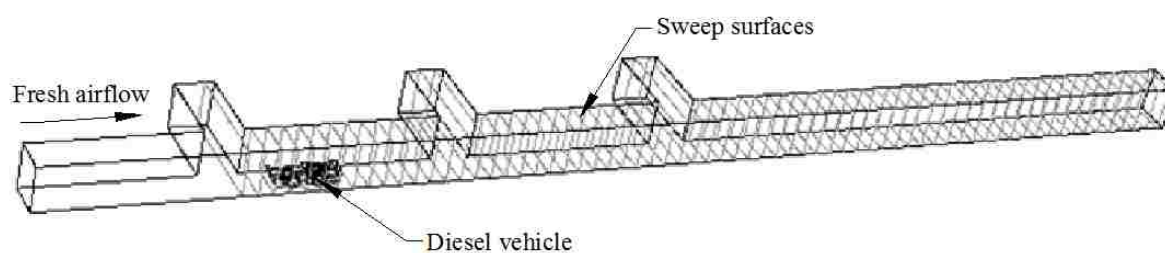
Figure 7.51. Cross Section Planes in the Simulation Domain

7.6.1. Effects of Tailpipe Orientation in Baseline Simulation. Figure 7.52 illustrates DPM dispersion for a truck and LHD in baseline condition when the ventilation was at a low setting and DPM emission was high (7 ppm from both tailpipes). In Figure 7.52(a), the truck was heading downstream. In Figure 7.52(b), the truck was facing the fresh airflow from the left to the right of the entry (fresh air always flows from left to right of the entry of other straight entry cases). In Figure 7.52(c), the LHD was heading downstream with the DPM emitted against the fresh airflow. In Figure 7.52(d), the LHD was facing the fresh airflow with DPM emitted in the same direction as the fresh airflow. The simulation assumed that the vehicle was stationary for 300 seconds. It can be observed from the figure that the high DPM plume affected downstream regions in all four scenarios. Because of high DPM emission from the diesel engine, all miners downstream should wear some personal protection items (like air purifying respirators), or the return air guided directly outside the mine. No miners should work downstream of a high DPM plume. However, when the LHD discharge diesel exhaust went against the fresh airflow, as shown in Figure 7.52 (c), the high DPM plume migrated upstream of the engine because of the high exhaust flow from the tailpipe (24 m/s). The affected region was 45 m upstream when the LHD was stationary for 300 s. Therefore, when the tailpipe was emitting against ventilation airflow, the miners upstream of the engine should also be aware of the possible health problems. When possible, the engine should either shut down or redirect the tailpipe to let exhaust flow downstream.

Figure 7.53 illustrates the maximum DPM level at different sweep surfaces. The vertical axis showed the DPM concentration, while the horizontal axis was the distance between the sweep surfaces and the tailpipe, with 0 being the location of the tailpipe opening. Minus values indicate the analysis planes were upstream from the tailpipe opening and positive values were downstream from the tailpipe.

The lines named LHD_HIHE and Truck_HIHE mean that the LHD and truck were facing the inlet of the entry with high emissions. LHD_HOHE and Truck_HOHE indicate that the LHD and truck were heading downstream from the entry with high emissions.

At a high emission rate (7 ppm) for both vehicles, it can be observed from the figure that, in areas immediately adjacent to the tailpipe, the maximum DPM concentration

readings were as high as approximately 4,000 $\mu g/m^3$. As this front moved, it quickly mixed with the fresh air and maximum concentration readings dropped sharply at 20 m downstream (of the tailpipe), and then gradually dropped and stabilized.
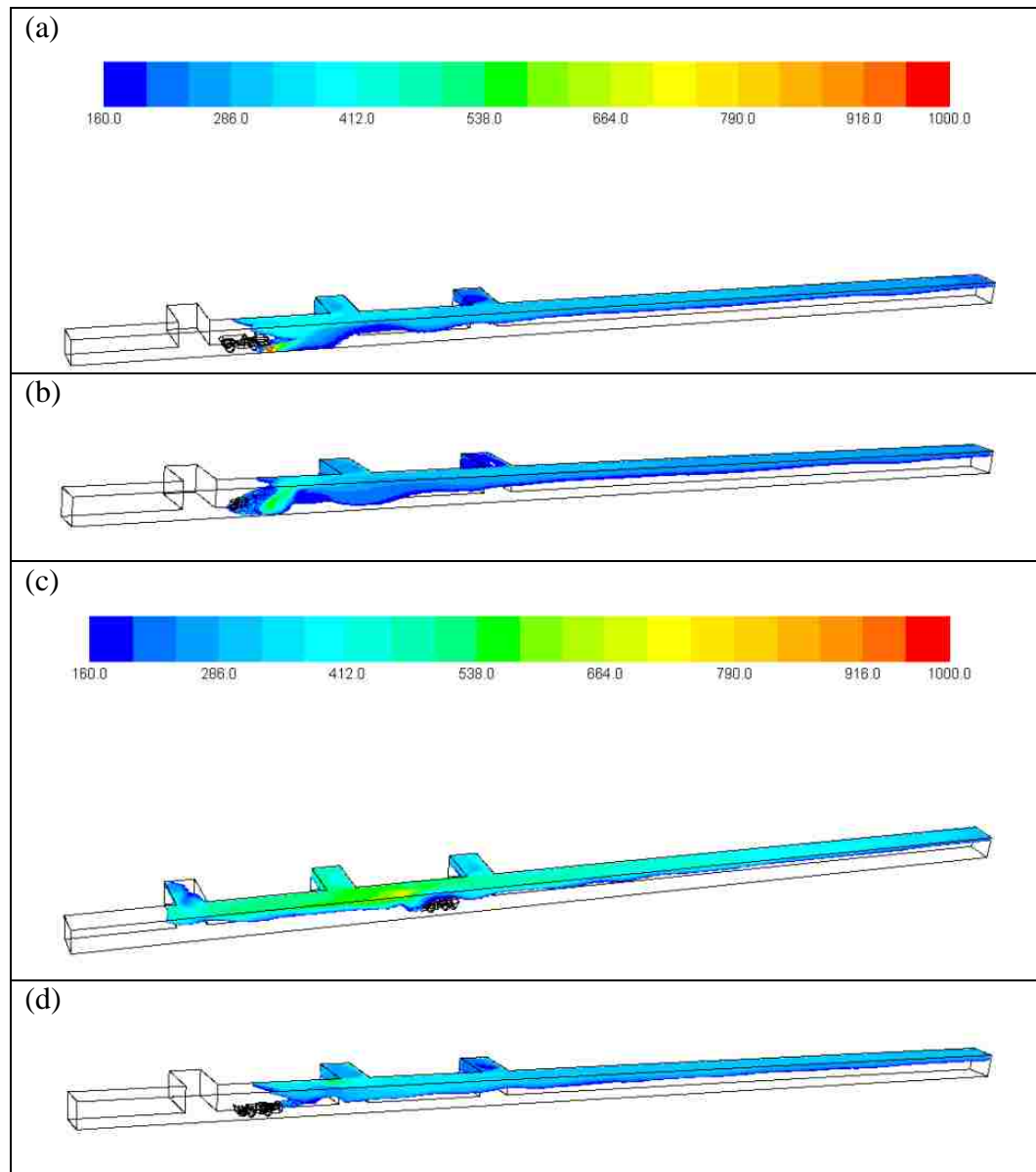
Figure 7.52. Comparison of DPM Dispersion for Truck and LHD in Baseline Condition at 300 s. (a) Truck is Heading toward the Downstream; (b) Truck is Facing the Fresh Air-flow; (c) LHD is Heading toward the Downstream; (d) LHD is Facing the Fresh Airflow

Figure 7.53. DPM Levels at Different Sweep Surfaces for LHD and Truck
in Baseline Simulation

With a high DPM emission and low ventilation, it seemed that the trend of the lines for the LHD and truck were very similar. Still, it can be observed that the LHD with an exhaust flow against the fresh airflow had higher DPM levels than the others. This indicates that, with this emission condition, it was very difficult for DPM to mix with fresh air, as compared with the cases in Figure 7.52 (a) (b) and (d).

7.6.2. Effects of Tailpipe Orientation with High Ventilation and Emission. To improve the working environment, the ventilation was doubled to dilute DPM more effectively with fresh air. At the same time, DPM emission from the engine was set at a high level (7 ppm).

Big differences in high DPM dispersion can be observed under this condition in Figure 7.54 (the scenarios are in the same position as in Figure 7.52). For the truck, it can be seen that high DPM regions only existed in the immediate areas downstream from the tailpipe, while for the LHD, the DPM plume existed far downstream of the exhaust pipe. Based on the previous calculation with high ventilation (39 m^3/s, or 82,600 cfm) and high DPM emission (7 ppm), the uniform DPM level was 101.67 μg/m^3 for the LHD and

109.49 µg/m^3 for the truck. Both DPM levels were under the regulation limit. However, for the LHD with DPM emitted horizontally, it was still difficult for DPM to mix effectively under such ventilation conditions (fresh air flows from left to right at 1.3 m/s).

This phenomenon can also be clearly observed in Figure 7.55, which shows the maximum DPM level at different sweep surfaces. In the figure, the lines named LHD_HI_HVHE and Truck_HI_HVHE mean that the LHD and truck were facing the inlet of the entry with high emissions and high ventilation. LHD_HO_HVHE and Truck_HO_HVHE indicate that the LHD and truck were heading downstream of the entry with high emissions and high ventilation.

At a high emission rate (7 ppm) for both vehicles, it can be observed in the figure that, in areas immediately adjacent to the tailpipe, the maximum DPM concentration readings were nearly 4,000 µg/m^3. As this front moved, it quickly mixed with the fresh air and the maximum concentration reading dropped sharply at 20 m downstream (of the tailpipe). For the truck, the DPM level dropped below the regulation limit, but for the LHD, this dramatic dropping trend stopped before the DPM went below the regulation limit and only gradually dropped afterwards.

7.6.3. Effects of Tailpipe Orientation with Low Ventilation and Emission. The DPM dispersion levels below are based on a low ventilation and a low emission. Ventilation provided fresh air flows from left to right of the entry at 0.65 m/s and emission was set at 1.7 ppm for the LHD and 2.0 ppm for the truck to represent DPM emission after installation of DPF. With a low ventilation (19.5 m^3/s, or 41,300 cfm) and a low DPM emission rate, the uniform DPM level was 49.38 µg/m^3 for the LHD and 62.05 µg/m^3 for the truck.

High DPM dispersion can be observed under this condition in Figure 7.56 (the scenarios are in the same position as in Figure 7.52). For both vehicles, it can be seen that high DPM regions only existed in the immediate areas around the tailpipe. For the truck, most of the high DPM plume was located downstream from the tailpipe. For the LHD, the high DPM region appeared downstream from the tailpipe when the exhaust was emitted downstream, or upstream from the tailpipe, if the exhaust flowed against the fresh airflow. Beyond that, all of the other regions in the entry were below the regulation limit.

Figure 7.54. Comparison of DPM Dispersion for Truck and LHD with High Ventilation and High Emission at 300 s. (a) Truck is Heading toward the Downstream; (b) Truck is Facing the Fresh Airflow; (c) LHD is Heading toward the Downstream; (d) LHD is Facing the Fresh Airflow
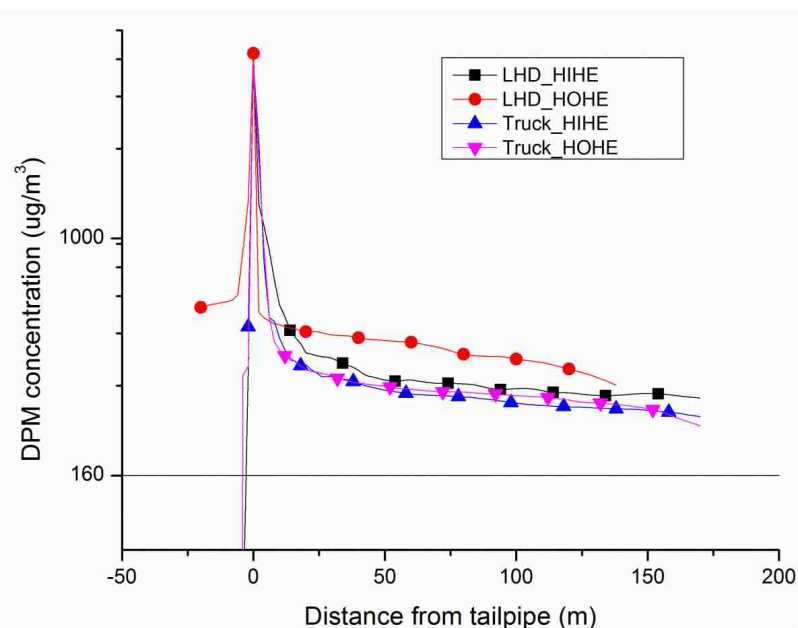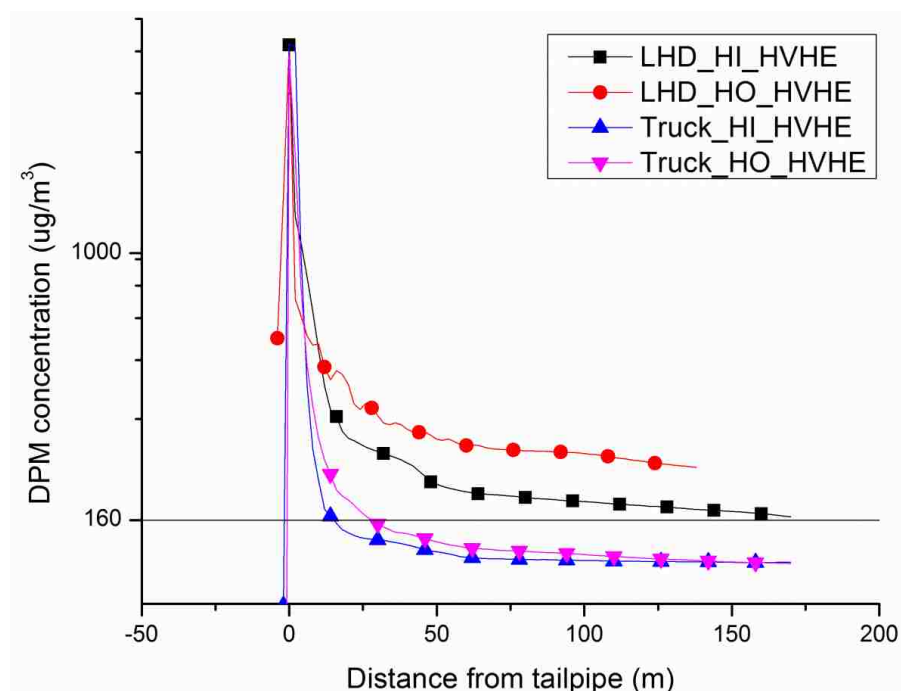
Figure 7.55. DPM Levels at Different Sweep Surfaces for LHD and Truck with
High Ventilation and High Emission

This phenomenon is also shown in Figure 7.57, which shows the maximum DPM level at different sweep surfaces. In the figure, the lines named LHD_HI_DPF and Truck_HI_DPF mean that the LHD and truck were facing the inlet of the entry with low emissions. LHD_HO_DPF and Truck_HO_DPF indicate that the LHD and truck were heading downstream of the entry with low emissions.

At a low emission rate, it can be observed in the figure that, in areas immediately adjacent to the tailpipe, the maximum DPM concentration readings were nearly 1,000 $\mu g/m^3$. As this front moved, it quickly mixed with the fresh air and maximum concentration readings dropped sharply at 20 m downstream (of the tailpipe). For both vehicles, DPM levels dropped below the regulation limit. Downstream of that, it gradually dropped and stabilized.

In summary, when DPM level in the face area was high, as in the baseline conditions, tailpipes emitting toward the floor polluted all of the area downstream of the

engine. Tailpipes discharging horizontally not only polluted the area downstream of the engine, but they also affected the upstream areas when the exhaust flowed against the fresh air. When DPM levels were controlled to 2/3 of the regulation limit (as in high ventilation and high emission conditions), tailpipes emitting toward the floor were more efficient than those shooting horizontally. When DPM levels were lowered further to 1/3 of the regulation limit (as in low ventilation and low emission conditions), there was not much difference in DPM dispersion. However, when the exhaust flowed against the fresh airflow, horizontal DPM discharge affect downstream regions as well as some upstream regions close to the pipe. Overall, in the simulation executed in this study, it seemed that exhaust pipes discharged toward the floor were a better choice than those that discharged horizontally.
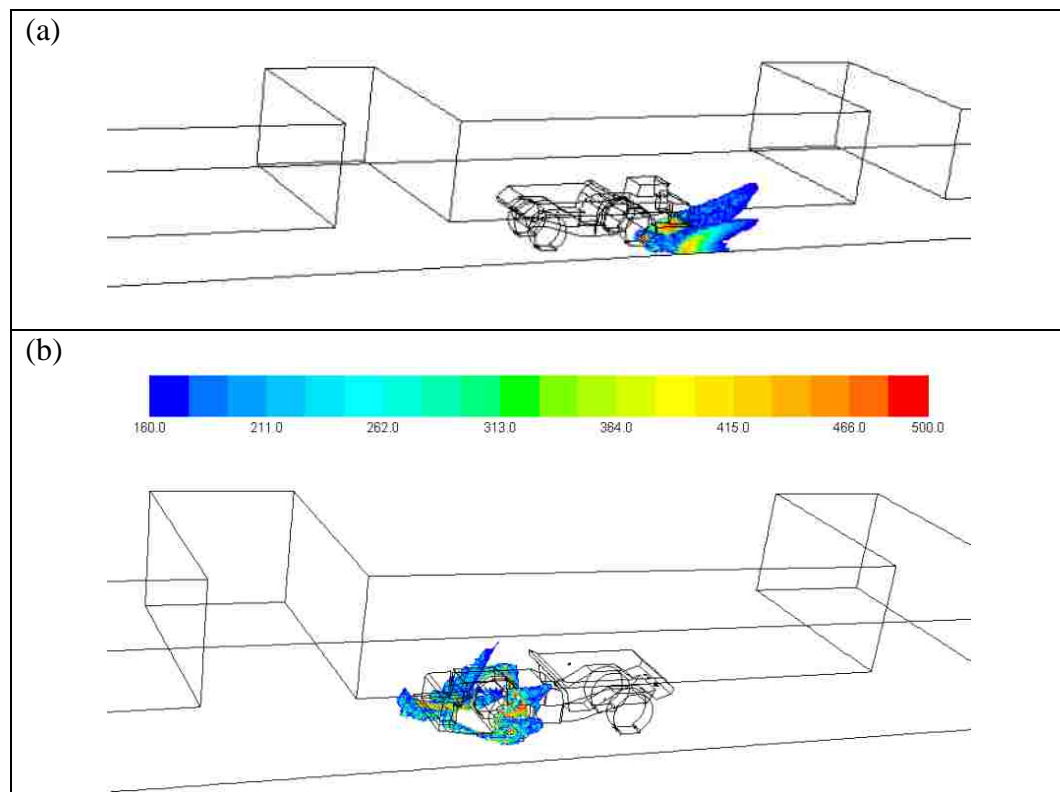
Figure 7.56. Comparison of DPM Dispersion for Truck and LHD with Low Ventilation and Low Emission at 300 s. (a) Truck is Heading toward the Downstream; (b) Truck is Facing the Fresh Airflow; (c) LHD is Heading toward the Downstream; (d) LHD is Facing the Fresh Airflow
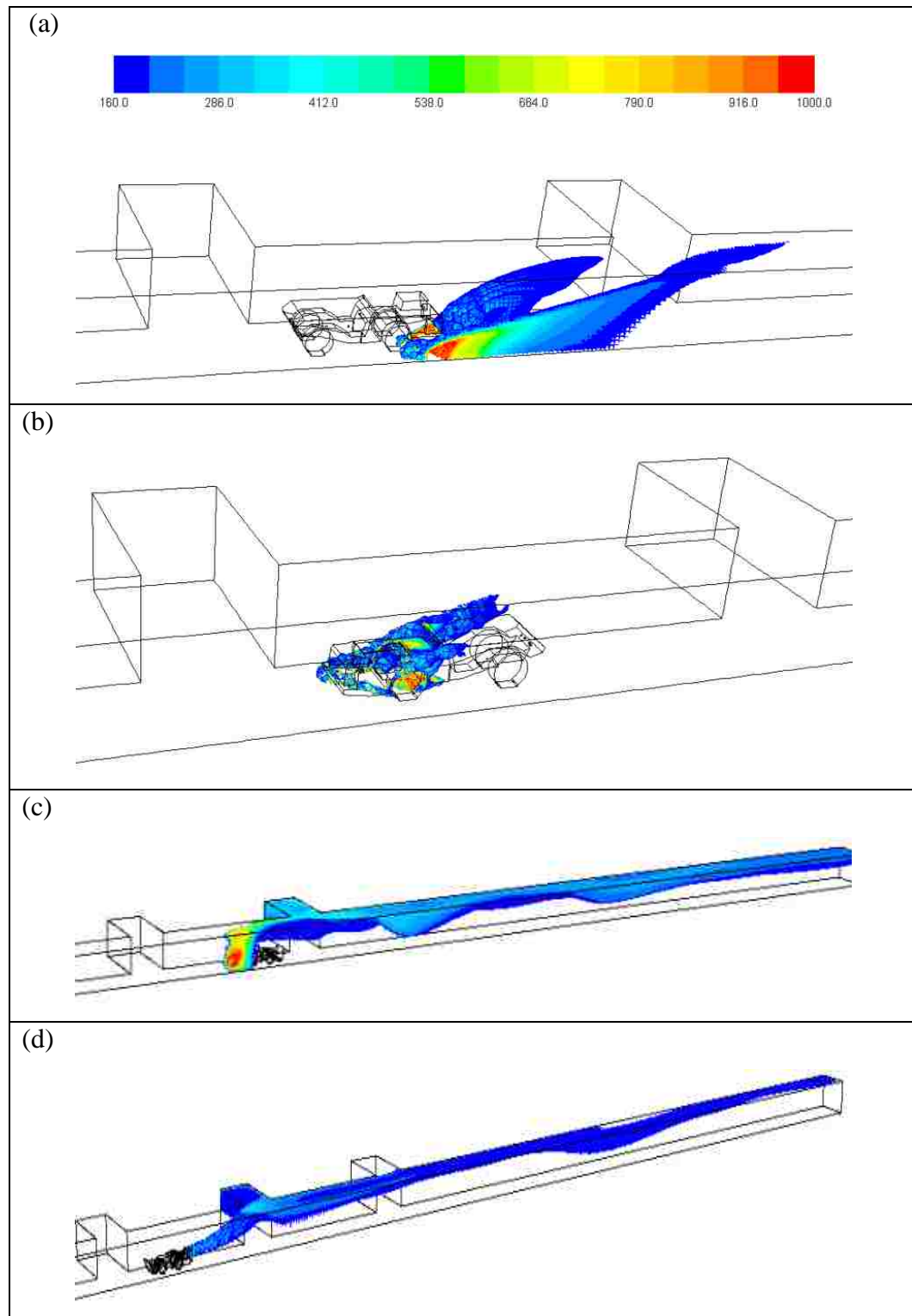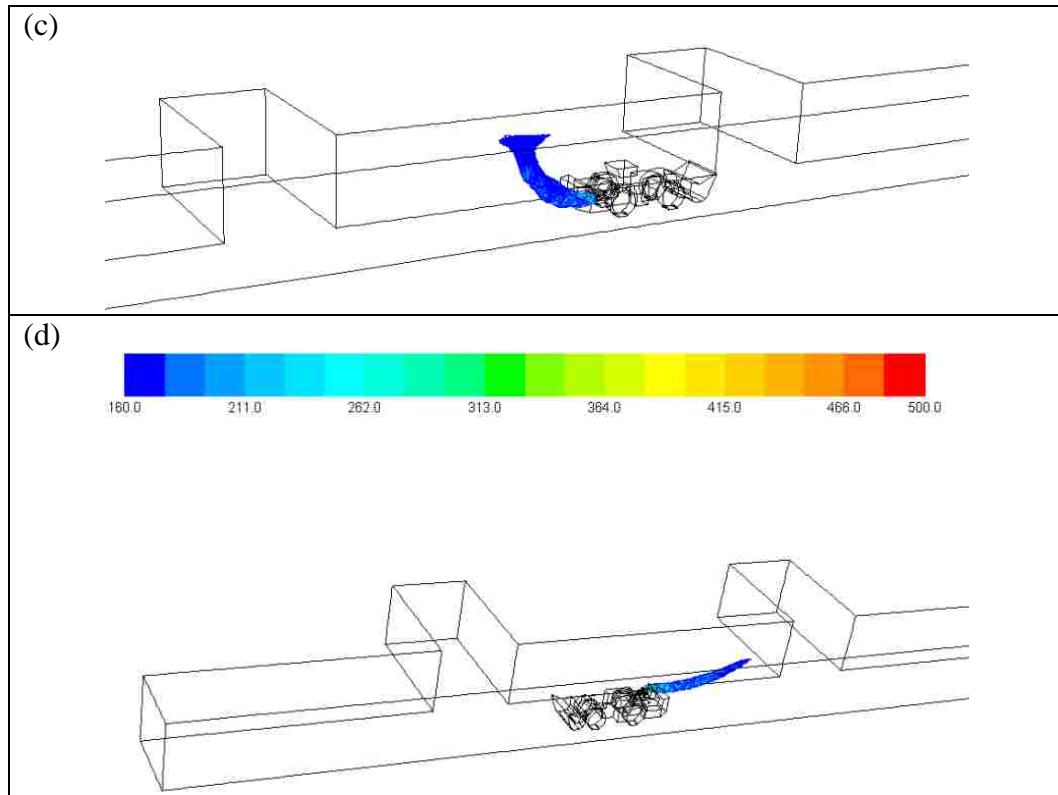
Figure 7.56. Comparison of DPM Dispersion for Truck and LHD with Low Ventilation and Low Emission at 300 s. (a) Truck is Heading toward the Downstream; (b) Truck is Facing the Fresh Airflow; (c) LHD is Heading toward the Downstream; (d) LHD is Facing the Fresh Airflow (cont.)

7.7. COMPARISON OF DIFFERENT VEHICLES' MOTION

Most simulations have assumed that the vehicles were stationary in the mine. However, the vehicles were working and moving around inside the mine, so it was necessary to consider the motion of the vehicles and the effect of that motion on the ventilation and DMP concentration. In this study, the motion of the vehicles was assumed to be at different velocities. Since the mesh in the CFD model was usually fixed (i.e. the mesh was generated from the vehicles surfaces to the whole domain) so that vehicles could not move in such a fixed mesh. Otherwise, the generated mesh would be damaged and broken. In order to avoid this, the motion of vehicles had to be taken into account. A technology called "dynamic mesh simulation" was introduced. This permitted some components in a domain to move, while other components remain stationary.
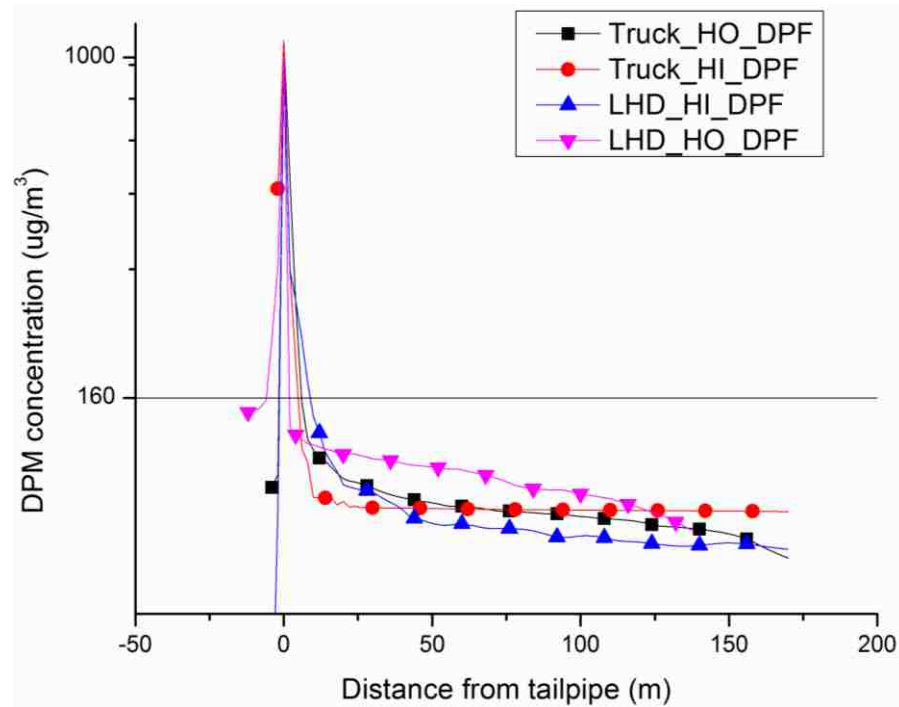
Figure 7.57. DPM Levels at Different Sweep Surfaces for LHD and Truck with Low Ventilation and Low Emission

The dynamic mesh model in FLUENT is capable of being used to model flows where the shape of the domain is changing with time due to motion on the domain boundaries. Usually the dynamic mesh model is used for an unsteady-state solver. The motion can be a prescribed motion, where one can specify the linear and angular velocities about the center of gravity of a solid body with time. On the other hand, it can be a non-prescribed motion where the subsequent motion is determined based on the solution at the current time (e.g., the linear and angular velocities are calculated from the force balance on a solid body). The update of the volume mesh is handled automatically by FLUENT at each time step, based on the new positions of the boundaries.

To use the dynamic mesh model, a starting volume mesh needed to be provided and a description of the motion of any moving zones in the model needed to be specified. FLUENT required that a description of the motion be specified for either the face or cell zones. When the model contained moving and non-moving regions, these regions were identified by being grouped into their respective face or cell zones in the starting volume

mesh that was generated. Furthermore, regions that were deforming, due to motion on their adjacent regions, were also grouped into separate zones in the starting volume mesh. The boundary between the various regions was not conformal, and the sliding interface capability in FLUENT made it possible to adopt the non-conformal mesh that connected the various zones in the final model.

In prismatic (hexahedral and/or wedge) mesh zones, the dynamic layering meshing option were used to add or remove layers of cells adjacent to a moving boundary. The option was either based on the height of the layer adjacent to the moving surface (the dynamic mesh model in FLUENT was allowed to specify an ideal layer height for each moving boundary) or based on the height-ratio between the neighbouring layers. The layer of cells adjacent to the moving boundary was either split or merged with the layer of cells next to it, based on the height selection.

In this study, the moving vehicle was defined as a separate zone from other parts of the domain, and the zone was meshed with tetrahedral mesh. The neighbouring zones were meshed with hexahedral mesh to facilitate the new mesh generation, as shown in Figure 7.58. Whenever the zone moved to a new location, one layer ahead the zone collapsed while one layer was added behind it. In this process, the time step was very critical. When the time step was too big, then the motion of the vehicle might cause greater deformation in the generated mesh that could result in divergence in the simulation.

7.7.1. Moving Effect of LHD in Straight Entry. To study the effect of a vehicle's motion on DPM dispersion, dynamic models of LHD driving against the fresh airflow under different velocities were built. Figures 7.59 and 7.60 illustrate the starting and ending locations of the vehicle. In all of the cases following below, the LHD drove about 90 meters with velocities of 1 m/s, 2 m/s, 3 m/s, 5 m/s, and 10 m/s. Fresh airflow was at 0.65 m/s provided from left to right, as before. The emission from the tailpipe of the LHD was at the high emission rate of 7 ppm.

Figures 7.61-7.66 reveal DPM dispersion patterns of the LHD with different driving velocities. To be consistent in the comparison, all of the illustrated DPM levels were after the vehicle had driven about 60 m from the start point and close to the second face in the straight entry. The colored region below shows the space where DPM was above the regulation limit.
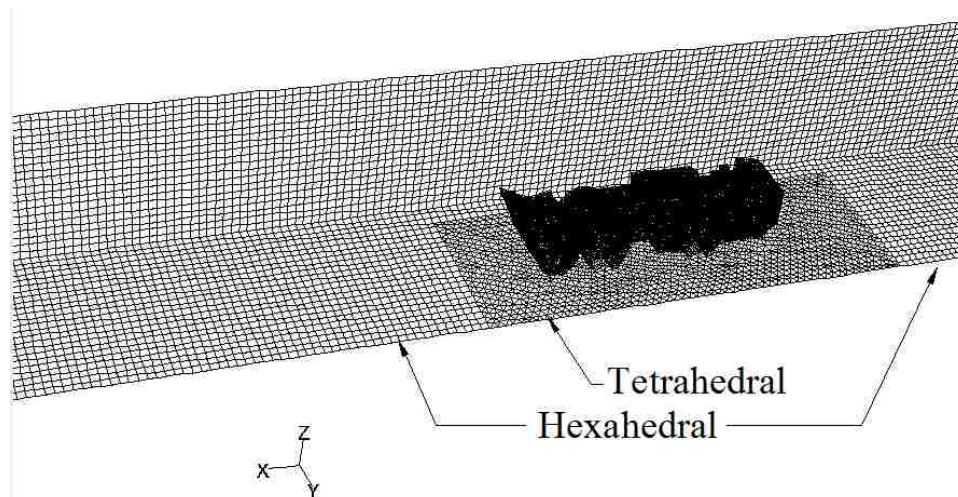
Figure 7.58. Different Mesh Generation for Vehicle's Motion Study
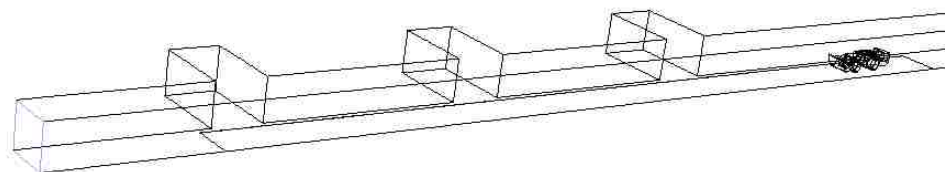
Figure 7.59. Starting Location of LHD Driving against Fresh Airflow
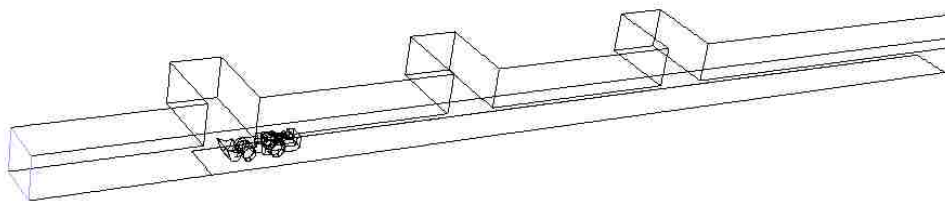
Figure 7.60. Ending Location of LHD Driving against Fresh Airflow

Figure 7.61 illustrates the shape of the DPM plume when the LHD was driven at 1 m/s against fresh airflow. After DPM left the tailpipe, it gradually flowed upward to about 20 m downstream of the exhaust outlet, and touched the roof of the entry. Then it

flowed to the top level of the entry as it mixed with the ventilation flow further downstream. A detailed view in Figure 7.62 reveals that miners at ground level were affected by the DPM plume when they were constantly within 10 m downstream of the tailpipe.

160.0   286.0   412.0   538.0   684.0   790.0   916.0   1000.0
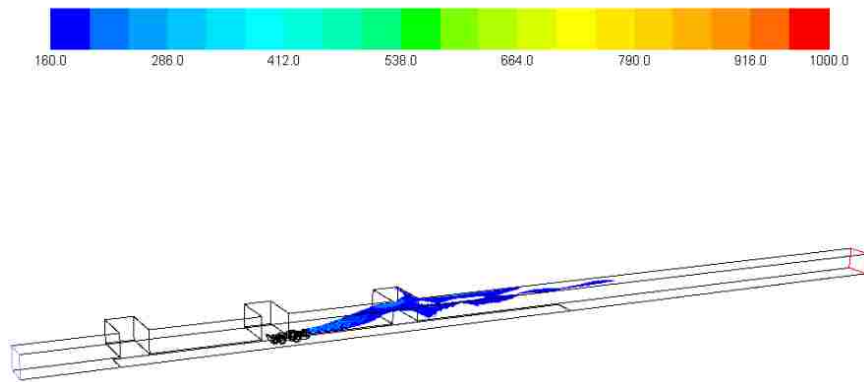
Figure 7.61. Overview of DPM Dispersion for LHD Driving against Fresh Air at 1 m/s

Figure 7.63 shows the DPM pattern if the LHD was driven at 2 m/s against fresh airflow. It can be observed that the DPM plume curved slightly upward downstream of the engine. Before it touched the roof, DPM was diluted below the regulation limit. Compared with that shown in Figure 7.61, the plume was more flattened and affected more regions downstream of the engine at ground level. This time, miners who were constantly within about 16 m downstream of the tailpipe were affected by the DPM plume.

It was observed that the DPM plume became parallel to the ground, as shown in Figure 7.64, when the vehicle drove at 3 m/s, and about 30 meters downstream of the tailpipe, miners at ground level were affected. As the vehicle drove faster, the DPM plume actually curved downward, as shown in Figures 7.65 and 7.66, when the LHD moved upward at 5 m/s and 10 m/s, respectively. At the same time, the length of the DPM plume became shorter. When the LHD drove at 5 m/s, miners within 24 m downstream of the exhaust pipe were affected by the high DPM plume. When driving 10 m/s, miners within 18 m downstream of the vehicle were affected.
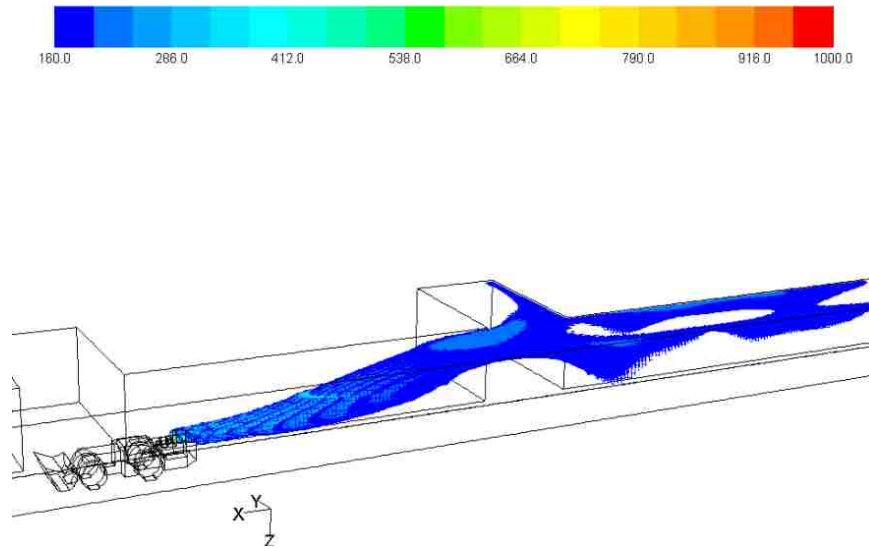
Figure 7.62. Detailed View of DPM Dispersion for LHD Driving against
Fresh Air at 1 m/s
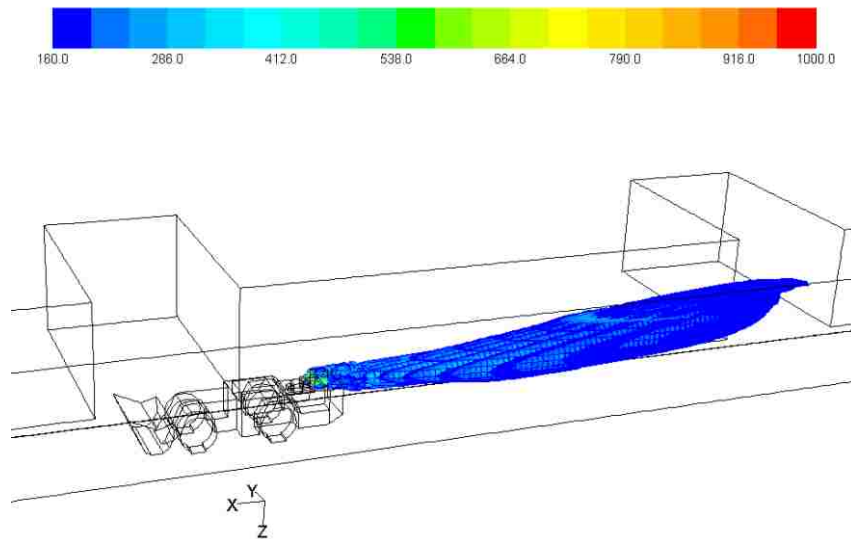
Figure 7.63. DPM Dispersion for LHD Driving against Fresh Air at 2 m/s

It can be observed from the simulation results that, when the vehicle drove faster, the buoyancy effect had less effect on DPM dispersion. Driving above 3 m/s against the fresh airflow, the buoyancy effect of the horizontally emitted exhaust flow was not observed, although it still existed.
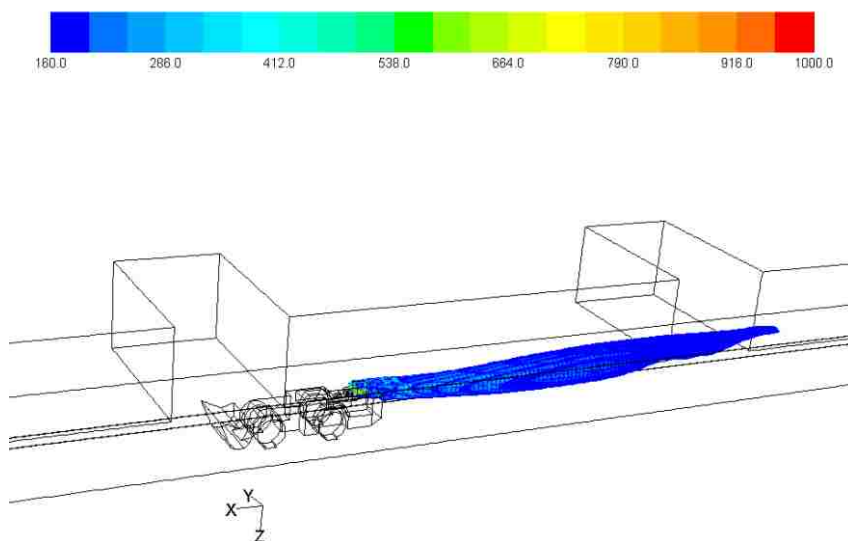
Figure 7.64. DPM Dispersion for LHD Driving against Fresh Air at 3 m/s
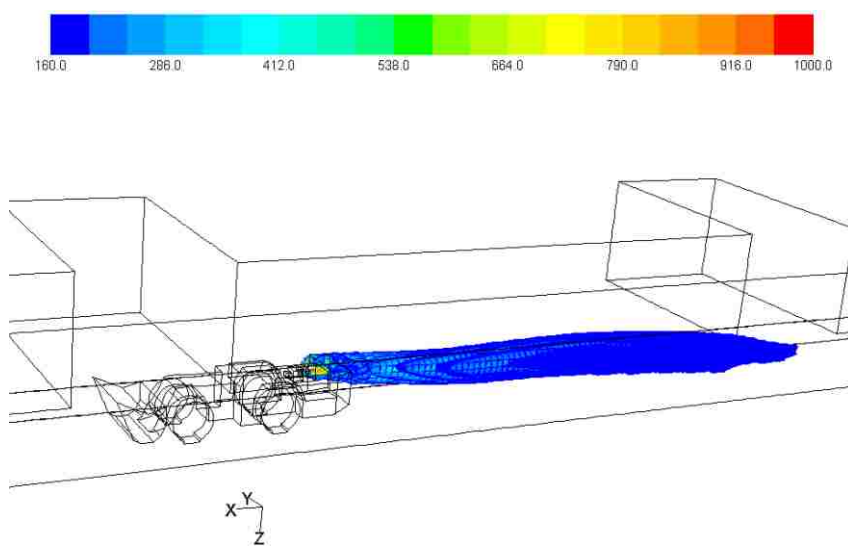
Figure 7.65. DPM Dispersion for LHD Driving against Fresh Air at 5 m/s
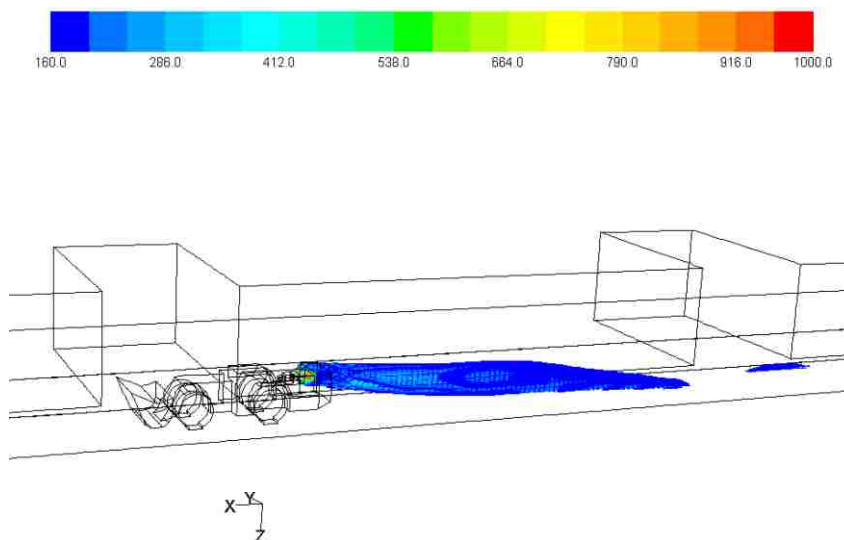
Figure 7.66. DPM Dispersion for LHD Driving against Fresh Air at 10 m/s

Using the calculation in 7.1.3 of a high emission rate (7 ppm) and ventilation that provided 19.5 m^3/s (41,300 cfm) of fresh air, the uniform DPM concentration was 203.33 μg/m^3. This was higher than the current regulation limit of 160 μg/m^3. However, the simulation results seemed to be incorrect. Actually, the simulation here covered only the first several seconds of the exhaust dispersion. When the vehicle continued to work in the face area, this region eventually became polluted above the regulation limit.

In this dynamic study, the LHD was the only source of DPM emission and the fresh airflow almost uniformly flowed from left to right of the straight entry. It was still possible to study the effect of the vehicle's motion by just increasing the fresh airflow speed. For example, to study DPM dispersion at the LHD's speed of 1 m/s, the fresh air-flow speed should be changed to 1.65 m/s. When the LHD drove at 3 m/s, the ventilation airflow velocity should increase to 3.65 m/s. However, when there were multi DPM sources (as in loading operation) or the airflow was not uniformly distributed (as in dead-end entry), dynamic mesh provided a possible solution.

7.7.2. Moving Effect of Loading in Straight Entry. The loading simulation in the straight entry below included two scenarios. Scenario 1 indicated that the truck drove upstream against the fresh airflow after loading (Figures 7.67-7.68). Scenario 2 demon-strated that the truck drove downstream after the loading operation (Figures 7.69-7.70).
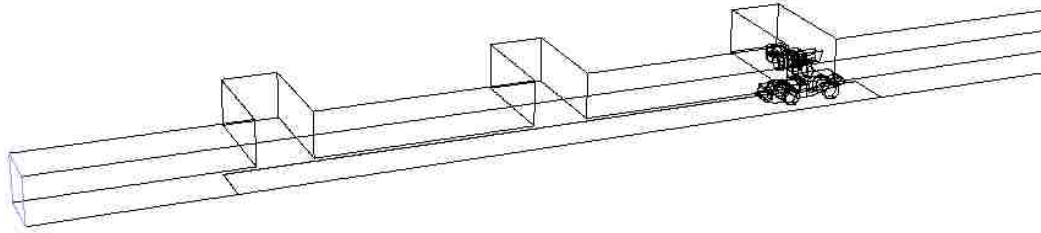
Figure 7.67. Starting Location of Loading Scenario 1
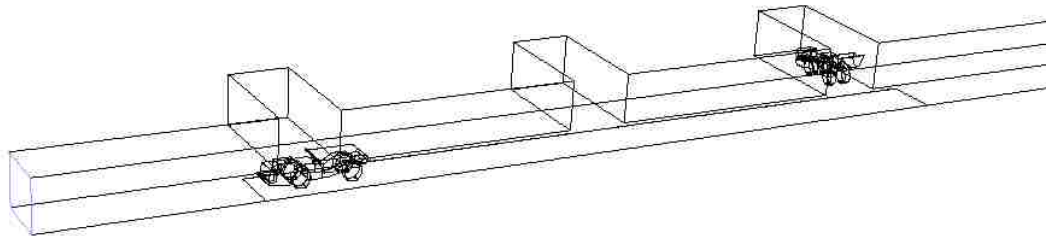
Figure 7.68. Ending Location of Loading Scenario 1
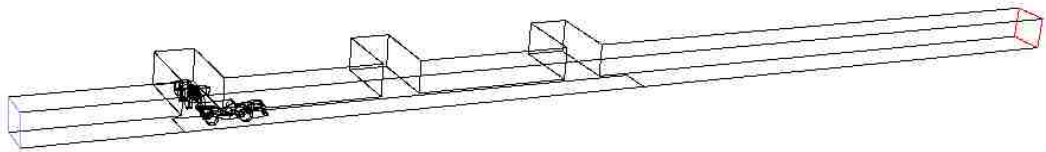
Figure 7.69. Starting Location of Loading Scenario 2
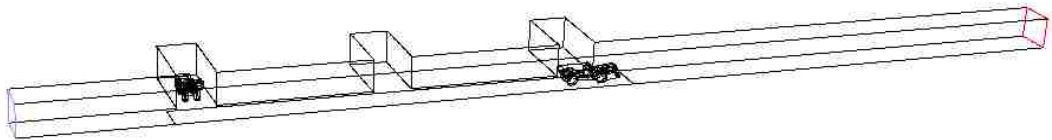
Figure 7.70. Ending Location of Loading Scenario 2

In both cases, the loading operation lasted 180 seconds (3 minutes). After that, the truck moved from the loading face, either upstream or downstream, about 60 m at a driving speed of 1 m/s. The fresh air still flowed at 19.5 m^3/s (41,300 cfm) from left to right of the entry, and DPM emissions from both engines were set high (7 ppm).

For loading scenario 1, the truck was facing the fresh airflow during loading and driving against (into) the fresh airflow after loading. At the end of the loading operation (180 s), it was observed that the loading area and the immediate downstream regions were filled with high DPM levels (Figure 7.71). However, the truck driver was not affected by the high DPM plume. After loading, the truck drove at 1m/s against the fresh air. It can be seen in Figure 7.72 that the DPM plume produced an effect about 30 m downstream from the truck engine, but the truck driver was still outside the high DPM plume. At the same time, the LHD was still operating inside the face area where the DPM level was very high. Other DPM controls were needed to improve the LHD operator's working conditions.

For loading scenario 2, the truck was facing downstream and then was driven into the exhaust flow after loading. At the end of the loading operation (180 s), it was observed that the loading area and the immediate downstream regions were filled with high DPM levels (Figure 7.73). This time, the cab of the truck was merged into the high DPM plume. Both LHD and truck operators, including miners working in the immediate downstream area of the loading face, were affected. After loading, the truck drove at 1m/s downstream. It can be seen from Figure 7.74 that the truck driver was still affected by the high DPM plume produced in the loading operation. Since the truck drove faster than the fresh airflow, it seemed that the truck escaped the low profile DPM plume afterwards (Figure 7.75). Again, in real working conditions, this scenario may not happen. After a long work period, the downstream area was already filled with high DPM fumes at all levels. There was no clear space when the truck drove downstream.

From the simulation results of loading scenario 1 and 2, it was concluded that the truck driving upstream after loading was better than driving downstream. However, at high emission rates and low ventilation quantities, the working conditions for the LHD driver and the miners downstream definitely needed improvement.
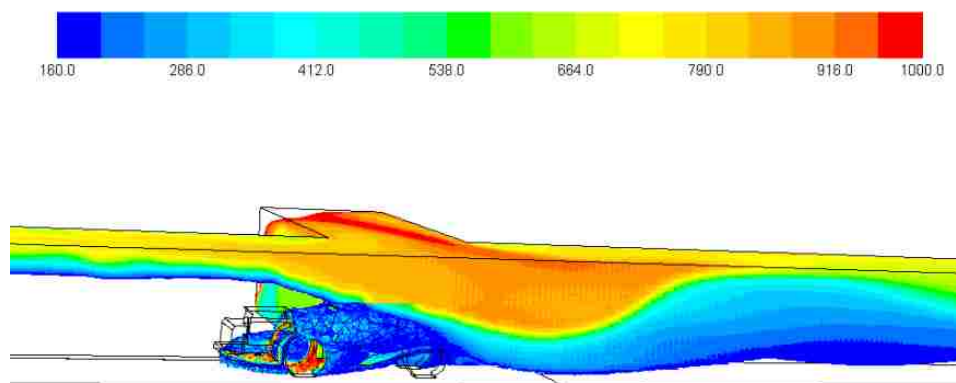
Figure 7.71. DPM Dispersion for Loading Scenario 1 at 180 s
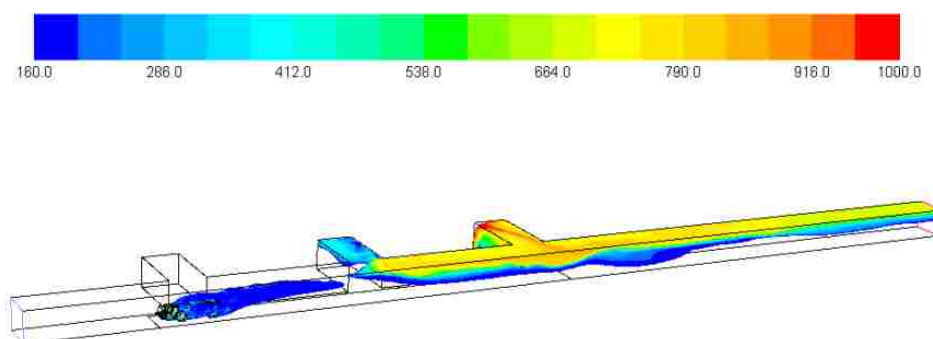
Figure 7.72. DPM Dispersion for Loading Scenario 1 at ~240 s
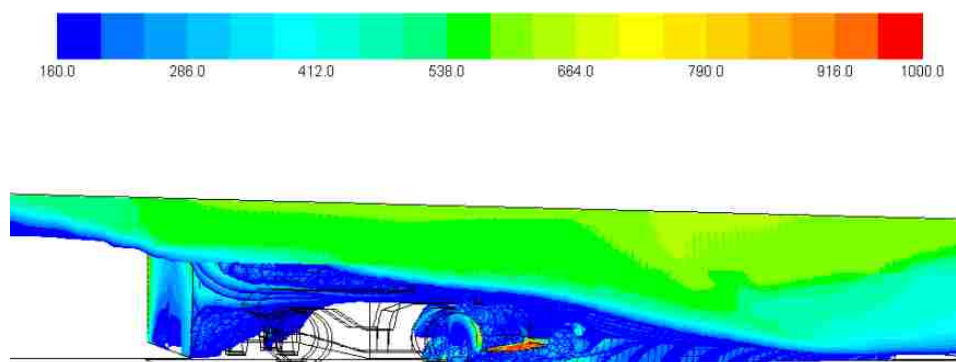
Figure 7.73. DPM Dispersion for Loading Scenario 2 at 180 s
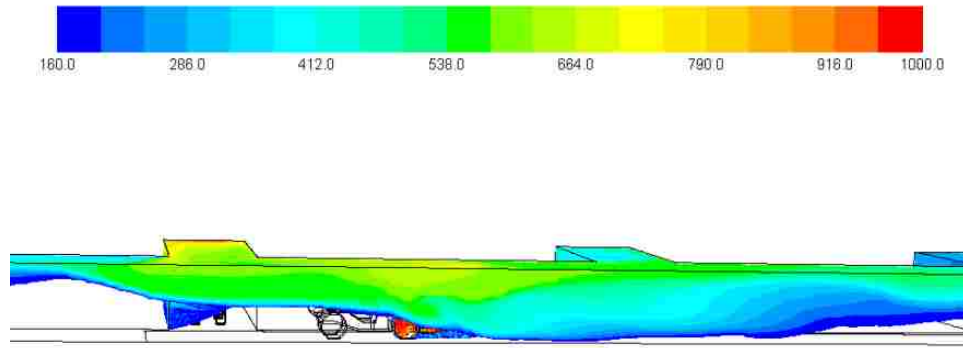
Figure 7.74. DPM Dispersion for Loading Scenario 2 at ~190 s
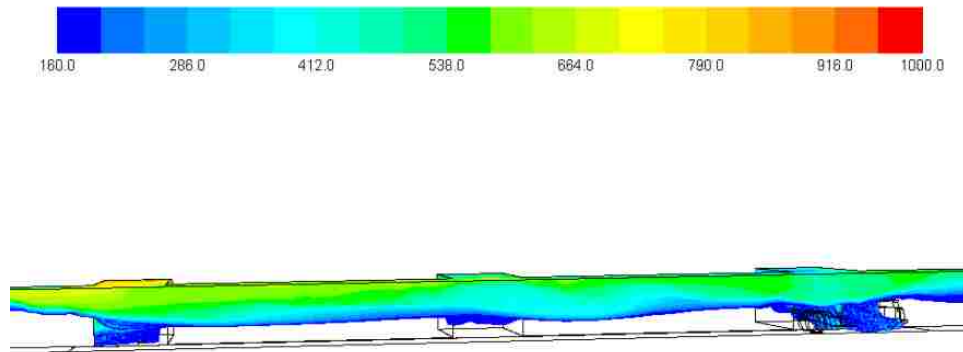
Figure 7.75. DPM Dispersion for Loading Scenario 2 at ~240 s

7.8. COMPARISON OF DIFFERENT CROSS-SECTIONAL AREAS

In the simulation previously revealed, most of the cases of straight entry and dead-end entry were under a cross sectional area that was 6 m in width and 5 m in height. However, these numbers may be different from mine to mine, face to face, or even within one single face. For underground metal mines (gold, silver, platinum, lead-zinc, copper, etc.), the size of the main entry can be around 4 m to 6 m wide by around 4 m to 6 m high. For some high roof mines (stone, lead, salt, etc.), the entry dimensions can be 12 m to 15 m wide to about 6 m to 10 m high. In some stone mines, another 6 m to 10 m of floor may be mined out, resulting in a height up to 20 m. What needs to be pointed out is

that, in the U.S., about half of all underground metal/non-metal mines are stone, which includes limestone, dolomite, marble, sandstone, etc. Therefore, it was critical to study the effects of different entry sizes on DPM simulation results included in previous sections.

To reveal the tendency of DPM dispersion to be at other commonly used entry sizes, the LHD driving against the fresh airflow in straight entry was simulated at 4m w × 4m h; 4m w × 5m h; 4m w × 6m h; 5m w × 4m h; 5m w × 5m h; 5m w × 6m h; 6m w × 4m h; 6m w × 5m h; 6m w × 6m h; 5m w × 12m h; and 12m w × 5m h. In these simulations, fresh air flowed at 0.65 m/s from left to right of the straight entry. The DPM emission from the tailpipe of the LHD was set at a high emission rate (7 ppm). The vehicle was stationary for 300 seconds during the simulation; the results are discussed below.

From the simulation results, it was observed that the DPM dispersion pattern was quite similar for all of the entry dimensions, except for the high-roof case (5m w × 12m h). Figures 7.76 and 7.77 illustrate high DPM levels for entry dimensions of 4m w × 4m h and 12m w × 5m h. It can be seen from the figures that the DPM plumes had a tendency to flow toward the roof and then occupy all of the width of the entry. This was due to the buoyancy effect of the exhaust flow. The difference between Figures 7.76 and 7.77 is the different DPM level at the roof area downstream of the tailpipe. This was due to the quantity of fresh air provided in each case when the fresh airflow speed was 0.65 m/s (from left to right).

For the high roof case (5m w × 12m h), as shown in Figure 7.78, it was observed that the DPM plume touched the roof, but did not spread to all of the roof area. This phenomenon depended on the DPM production from the tailpipe, ventilation flow rate, temperature of the exhaust flow, etc. It showed that the DPM plume tended to flow toward the roof because of its buoyancy effect while DPM levels continuously decreased as the DPM was diluted by the incoming fresh air. When the engine was stationary and the exhaust flow was hot, the roof was the place where the DPM tended to accumulate. Another fact that must be pointed out is that, when DPM plume lost its high temperature far downstream from the diesel engine, the air had a more or less uniform DPM concentration.
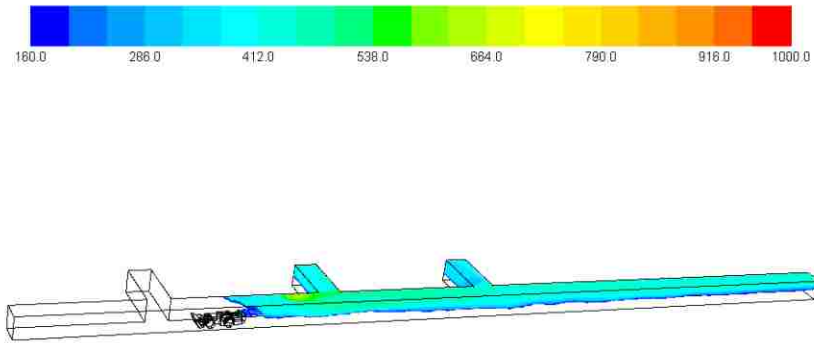
Figure 7.76. DPM Dispersion for LHD Driving against Fresh Air in 4m w × 4m h Entry
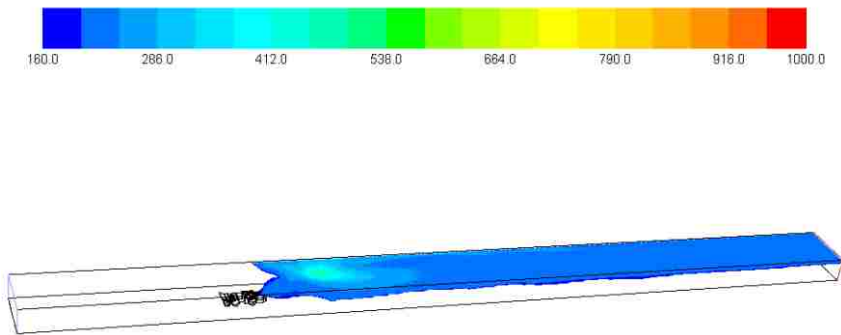
Figure 7.77. DPM Dispersion for LHD Driving against Fresh Air in 12m w × 5m h Entry
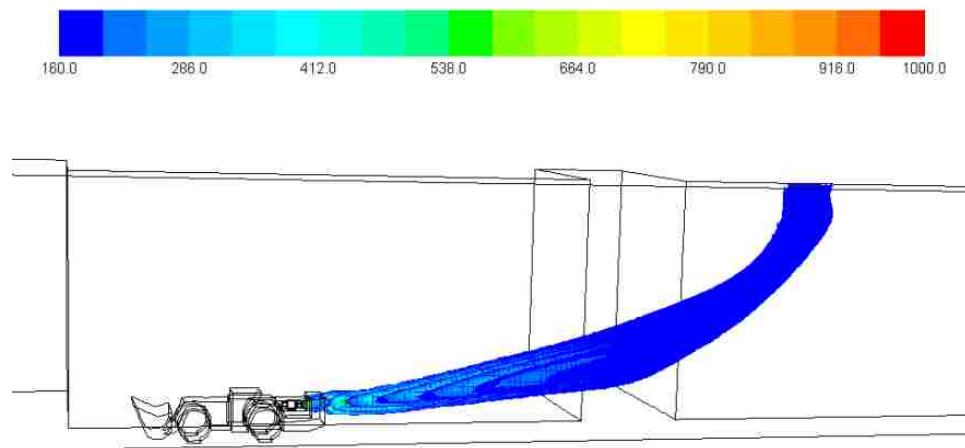
Figure 7.78. DPM Dispersion for LHD Driving against Fresh Air in 5m w × 12m h Entry

The simulation results in this section were executed under the assumption that the diesel engine did not move during the operation. This would be correct for some cases like drilling operations and scaling. However, when the vehicle was constantly moving, DPM dispersion patterns were totally different. As revealed by the study of the vehicle's motion (with the LHD under the same exhaust temperature, exhaust flow, and DPM emission rate) when the vehicle moved faster than 3 m/s against the fresh airflow, the buoyancy effect was not detectable, although it still existed. The high turbulence of the flow mixed DPM with fresh air quicker than it flowed upward. As a result, the high DPM plume was diluted below the regulation limit before it went up. In that condition, the higher DPM region existed at about the level of the exhaust pipe. Once the vehicle slowed down, the buoyancy effect was dominant again and the higher DPM would flow toward the roof.

7.9. SUMMARY OF SIMULATION RESULTS FOR STRAIGHT ENTRY

It can be concluded in this study, that DPM dispersion patterns depend on the following factors: DPM production rate from the diesel engines, exhaust temperature, speed and direction of the exhaust flow, location of the exhaust pipe, shape and sizes of the entry, fresh airflow speed and distribution, time period of operation, etc. It is very difficult to predict the exact pattern for a general conclusion.

If the DPM production rate is higher than the ventilation capacity (as shown by the results in the baseline simulation, except for the drill jumbo alone), then all of the mining areas downstream of the diesel engine would be out of compliance with the DPM regulation. From the simulation results, it can be observed that miners upstream of the engine would not be affected by DPM problems if the profile of the entry is high (5 m in height in the simulation). Otherwise, if the height of entry is low, it is still possible that the DPM from LHD can migrate upstream if it is emitting against fresh airflow. The only possible way to bring the working environment under control is to shut down the diesel engine frequently to dilute DPM.

If the ventilation rate is increased, as shown in the high ventilation and high emission section, it can be observed that all of the working conditions with a single engine cases are improved. With a single engine in the face area, only limited regions close to

the tailpipe will have DPM above the regulation limit. However, if more than one diesel vehicle is present in the face, the ventilation capacity is still not sufficient to dilute DPM down to the limit. The entire airway downstream of the working face will be out of compliance. Since ventilation can only provide improvement roughly proportional to airflow increase, if the ventilation doubles then DPM levels will be roughly cut in half. This is probably not a very effective way to solve the problem.

By installation of DPF, it can be observed that DPM production rate is greatly reduced. With only a low ventilation rate, it is possible to clear most previously high DPM regions. One must be aware that a high DPM plume still exists. The location of the plume depends on the mining machine and direction of the exhaust pipe. It can be observed in Section 7.5 that, with high ventilation and DPF, the high DPM plume will affect fewer working areas.

It has also been revealed in this study that, if the tailpipe is emitting DPM toward the floor of the entry, emissions can be more quickly diluted than if the tailpipes were discharging horizontally. If no other problems (like dust) arise with this tailpipe orientation, it may be a better choice to select diesel engines that discharge DPM toward the floor.

Diesel engines in the face area need to move during the operation. It has been revealed that, if the vehicle moves more than 3 m/s in the simulated entry, the buoyancy effect that was frequently observed in the previous studies will not be detectable. In that case, the DPM plume will not go toward the roof, but the DPM will dissipate according to the direction it is projected.

If the straight entry has other dimension sizes, it can be observed that the buoyancy effect will force DPM plume to migrate toward the roof and spread across the full width of the entry roof when the engine is stationary. Because of the buoyancy effect, high DPM plume will try to occupy the highest level of the entry first provided the engine does not move. However, if the engine is in a constant moving mode, the buoyancy effect will not dominate. Therefore, a high DPM plume will occupy the lower levels of the entry according to the speed of the vehicle.

This section covered DPM dispersion in a straight entry working face; DPM dispersion in a dead-end entry will be discussed in the next section.

8. SIMULATION RESULTS AND ANALYSIS FOR SINGLE DEAD-END ENTRY

8.1. THE EFFECT OF FLOOR INCLINATION

An inclined floor is often encountered in underground mines and the floor can be either an upward or a downward inclination. When a floor has slope, especially in dead-end regions of a mine, it causes problems and difficulties for ventilation, and diesel fumes may accumulate in the area close to the face while diesel vehicles are operating there. Due to the temperature difference between diesel exhaust and fresh ventilation air, which results in a buoyancy force to diesel fume, that fume, including diesel particulate matter (DPM), transports toward the ceiling of the airway. It may accumulate or circulate in the corners of the working face area if local ventilation is poor. In order to control DPM better in an underground mine, it is necessary to understand its diffusion pattern and the influences of some related factors and parameters.

In this study, the focus was on the effect of the floor inclination. The CFD approach was used to simulate DPM distribution as well as to identify areas with high DPM concentration in a dead-end region. The effect of the floor inclination was evaluated by comparing the DPM concentration and the flow temperature, etc. between the two cases.

8.1.1. Problem Description and CFD Modeling. Proper ventilation and compliant DPM levels are always expected during production. As shown in Figure 8.1, the floor slope of a dead-end caused significant differences in local air quality. In this study, the CFD approach was used to simulate flow field, thermal field, and the DPM distribution pattern in two different cases, while the truck and loader were working in the area. The local air quality and DPM levels were examined, and the area with high DPM concentration was identified. By studying the DPM distribution pattern, a proper mine ventilation plan, with auxiliary fan and tubing devices for the face area, was designed. Some recommendations can be given to improve safety in operations such as the appropriate fresh air flow rate through the auxiliary ventilation system and the estimated area of the polluted region.

As shown in Figure 8.2, three-dimensional CFD models of two underground mines were created to study the effect of floor slope on flow and heat transfer. The first model represented a mine with an upward dead-end, and the second one was for the case

of mining downward. The straight duct section that was on the left was the main airway; the other duct, which was perpendicular to the main airway, was the dead-end section. The floor slope of the dead-end was selected as ±8.5° relative to the horizontal plane where the main airway is sitting. In the 3-D view, the flow inlet of the main airway and the ventilation pipe were on the front-most plane of the domain, and the outlet of the airway was on the rearmost plane of the domain.
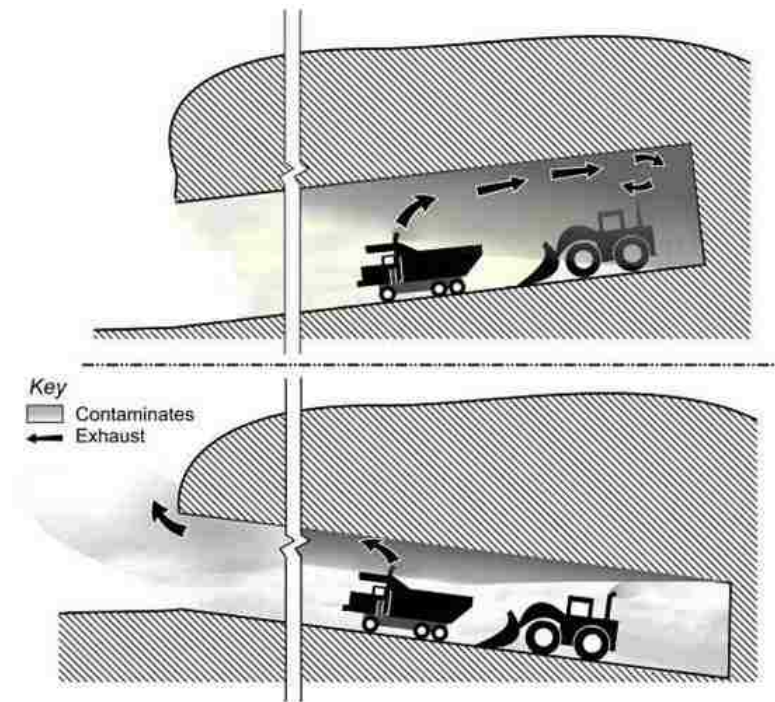
Figure 8.1. Schematic of Mining Upwards and Downwards

The dimensions of the models are described below. The height of the whole mine entry is 6m (~20ft), and the widths of the main airway and dead-end sections were 8m (~26ft) and 5.5m (~18ft), respectively. The length of the dead-end was selected as 50m (~165ft). Two diesel vehicles were considered in the study: one was a truck and the other was a loader. They were working in the face area, i.e., in the very end section of a dead-end region. The pipe in the right upper corner of the mine represented the auxiliary fan and tubing system. The diameter of the pipe was 0.6m (~2ft). In this study, only forcing

pipe was used, i.e., fresh air was forced in to ventilate the dead-end region. The truck was around 15m away from the working face, and the loader was about 5m away from the working face.
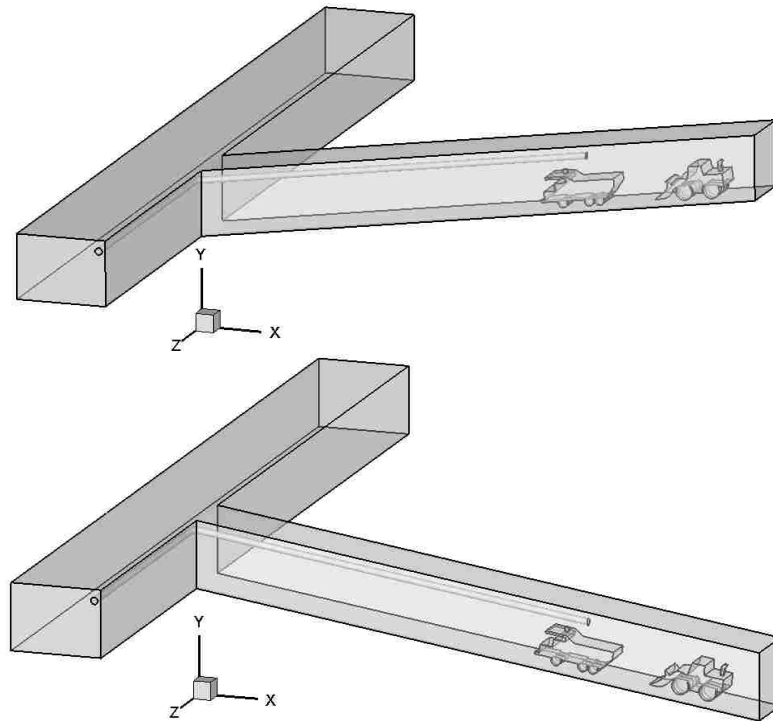
Figure 8.2. CFD Models of Upward Mining and Downward Mining

Fresh air was supplied at the inlet of the main airway with an average velocity of 0.6 m/s and with a temperature of 300 K (27°C), which is equivalent to a volume flow rate of 28.78 m^3/s (61,000 cfm). The auxiliary ventilation tubing conducted fresh air to the face area carrying a volume flow rate of 4.72 m^3/s (10,000 cfm). The diesel exhaust volume flow rates for the vehicles were set at 0.94 m^3/s (2,000 cfm) for the truck and 1.09 m^3/s (2,300 cfm) for the loader. The exhaust temperature was set as 623K (350°C). The exhaust flow was approximated by a mixture of air and DPM. The DPM mass fraction from both of the tailpipes was selected as 2.0ppm.

The DPM was treated as a separate species from the air in the exhaust flow. The species transport model, together with standard k-ε turbulence model from FLUENT, was used for the numerical simulation. Although the DPM is actually composed of particles, it was reasonably approximated as a species in this study by considering the fact that the particles are small in size (diameter in magnitude of one micrometer) and its diffusion readily follows with the flow pattern of a continuous medium. The species transport equation was solved together with N-S equations. DPM concentration distribution in the mine can be solved after exhaust leaves the tailpipes. Due to the temperature difference between the ventilation air flow and tailpipe exhaust flow, the buoyancy effect was taken into account by solving an energy equation and considering gravity in the simulation.

Meshes were generated using Gambit, a pre-processor of FLUENT, and both hexahedral and tetrahedral meshes were used. In order to achieve accuracy in the simulation results, finer meshes were generated for the area close to the ventilation tubing and near the vehicle tailpipes. For each of the models, about 0.9 million computational elements (cells) were generated.

8.1.2. Results and Discussion. The effect of floor slope on DPM distribution and the effect of applying auxiliary ventilation to improve the mining environment are showed and discussed bellow.

8.1.2.1 The effect of floor slope on DPM distribution. Two cut-planes were created to show the contours in the mid-plane of the dead-end section and the mid-plane of the main airway. The DPM distribution and temperature contour are shown in Figure 8.3 and Figure 8.4, respectively. In the upward dead-end, the right upper corner had high DPM concentration which meant that diesel exhaust lingered there and accumulated with time. Although the auxiliary ventilation flow reached the face and swept the face, it was still hard to get the hot fume out of the corner and achieve good air quality. However, the DPM concentration in downward dead-end was much more uniform throughout the whole dead-end. Although the DPM dispersed into the lower portion of the section, a high DPM concentration only existed in a layer close to the ceiling. In that case, the working face was well ventilated.

The DPM concentration regulation specified by MSHA requires the concentration to be less than $160\mu g/m^3$. With existing flow conditions and vehicle operating conditions,

about 1/3 of the dead-end area exceeded the maximum DPM concentration in the upward mining case. In the downward mining case, although a small percentage of the area exceeded the limit, the area was above all of the vehicles beyond the miners' respiratory space.

It is obvious that the mining upward case showed a larger area, with a high temperature, than the mining downward case did because of poorer ventilation. Figure 8.5 shows the plot of the area-averaged DPM concentration and temperature on different cutplanes that are parallel to the working face. The two variables are expressed as functions of the distance away from the working face. It can be observed that the curves for the two variables follow almost the same patterns. All of the peaks appear at the planes where the tailpipes are located. The upward dead-end had a higher DPM concentration, higher temperature, and higher gradient for the two properties. DPM concentration exceeded the allowed limit in the area adjacent to the working face that covered about 1/6 of the length of the dead-end. The mining downward case had a lower DPM concentration, and the average concentration always remained within the limit.
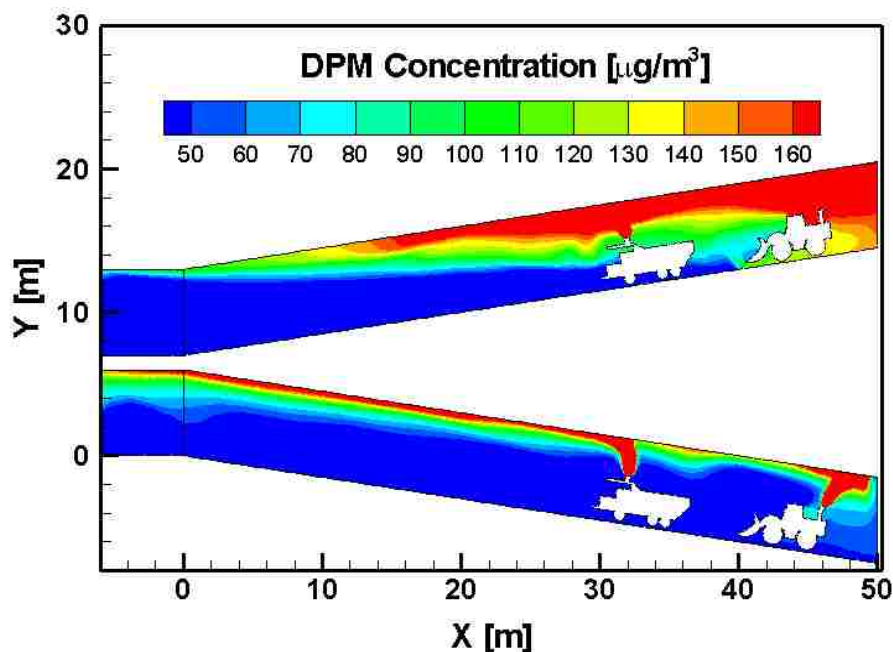
Figure 8.3. Contour of DMP Concentrations in Dead-end Entry
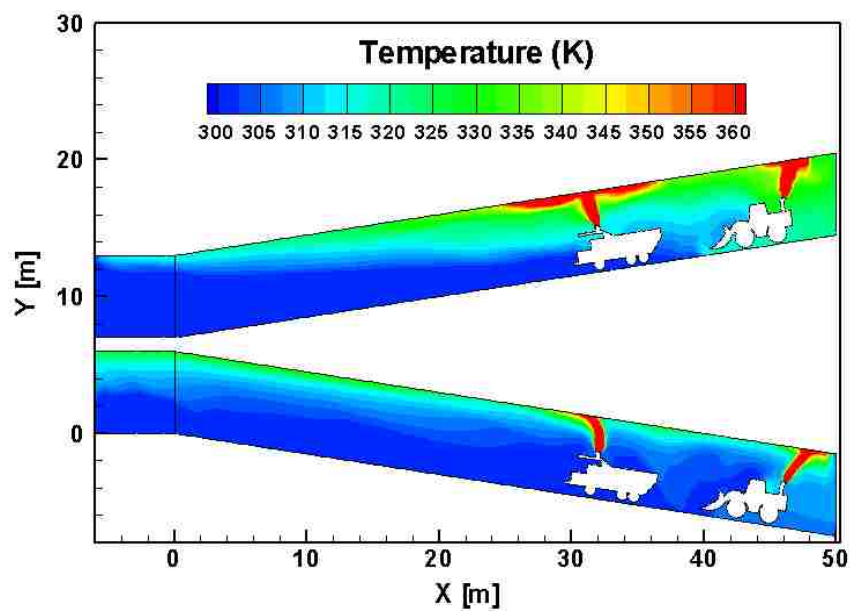
Figure 8.4. Contour of Temperature in Dead-end Entry
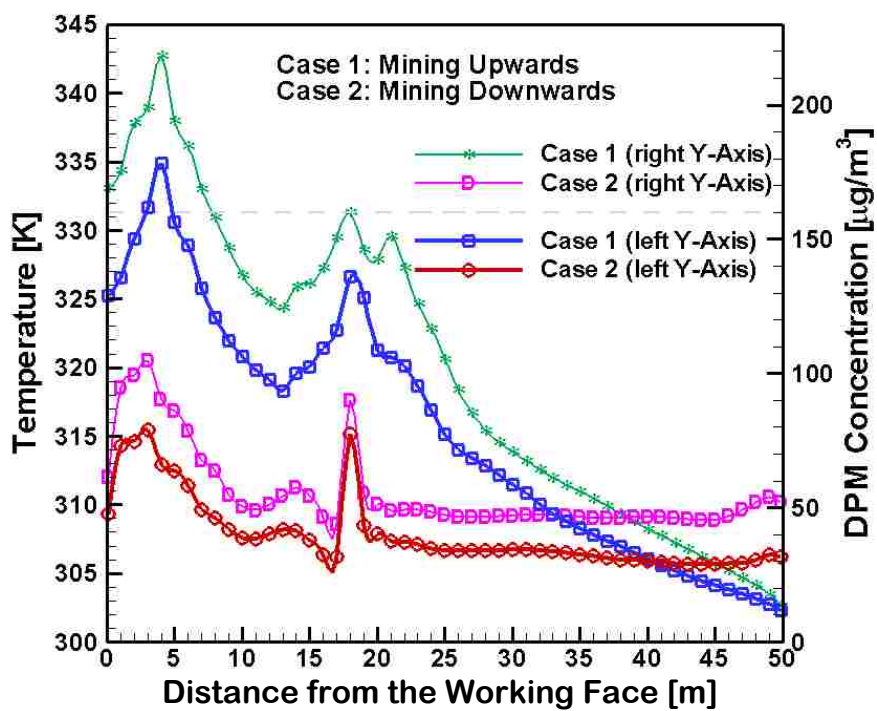
Figure 8.5. Average Temperature and DPM Concentration in Dead-end Entry

8.1.2.2 The effect of auxiliary ventilation flow rate. Since optimum ventilation for the upward dead-end is relatively more difficult to achieve, the effects of the volume rate of the auxiliary ventilation flow for this case were studied to determine the possible improvement. Three volume flow rates were used to evaluate the effect. The results of this study concerning the effect of flow rate on DPM concentration are shown in Figure 8.6.

It can be observed from Figure 8.6 that the average DPM concentration decreased with the increase in the auxiliary ventilation flow rate. It was found that the ventilation flow rate had to be at least three times the tailpipe emission rate in order to achieve DPM concentration levels below the allowed limit. The locations of the maximum DPM concentration did not vary with changes in the ventilation flow rate from the ventilation tubing. Ventilation was effectively improved by increasing the auxiliary ventilation flow rate. However, it needs to be noted that this is not necessarily true, that the more flow rate the better. Beyond a certain flow rate, the change in DPM concentration along with a flow rate change was smaller and smaller.
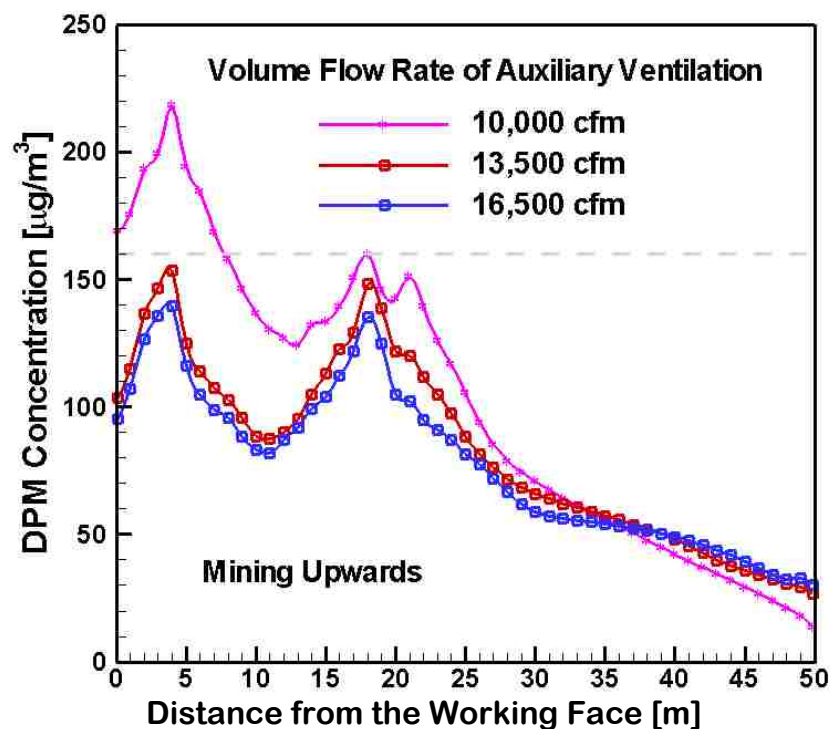
Figure 8.6. Average DMP Concentrations in Dead-end Entry

8.1.3. Summary and Conclusions. The effect of the floor slope in a dead-end section of an underground mine on ventilation and DPM distribution was studied using CFD simulation. It was found that the floor slope made a significant difference in the ventilation. In the upward dead-end, there were high temperature and high DPM concentrations. Ventilation was especially poor in the working face area. When the auxiliary ventilation flow rate was not enough, the upward dead-end contained a larger area with lingering and contaminated air with too high DPM concentrations. However, the downward dead-end section had appropriate DPM levels under the same flow conditions. Due to the buoyancy effect, the hot exhaust flow rose toward the ceiling and experienced different resistance in different dead-ends. Usually, the downward dead-end had a safer working environment since the hot fume flowed out of the region relatively more easily along the ceiling and a majority of the space was within the allowed DPM limit. Ventilation was significantly improved by increasing the auxiliary ventilation rate; however, the increase in flow rate resulted in only a negligible difference beyond a certain flow rate.

8.2. THE EFFECT OF AUXILIARY VENTILATION SYSTEM SELECTION FOR SINGLE DEAD-END ENTRY

In this section, the effect of four different auxiliary ventilation systems on DPM distribution inside a single dead-end entry was studied for a loading operation. The ventilation systems considered in this study were: a blower fan with push tubing, an exhaust fan with pull tubing, a jet fan, and a combination of blower and exhaust fans with both push and pull tubing (push-pull). Both the LHD and the truck in the loading operation were assumed to be fitted with DPF and to have a minimum DPM emission from the tailpipe. The loading operation was assumed to be in the inner most face area of the dead-end.

8.2.1. Problem Description and CFD Modeling. The schematics of a single dead-end entry with four different auxiliary ventilation systems installed are shown in Figure 8.7. The push tubing extended into the dead-end entry for about 70 m and about 3.4 m into the main entry. The pull tubing extended into the dead-end entry for about 81 m, while 22 m remained in the main entry. The diameter of both the push and pull tubings was 0.8 m. The main entry measured 6 m in width, 5 m in height and 131 m in length, while the dead-end measured 6 m in width, 5 m in height, and 90 m in length.

The main entry had of 19.35 m^3/s (41,000 cfm) of fresh air flowing from the left to the right. The blower fan at the inlet of the push tubing was set to provide 8.02 m^3/s (17,000 cfm) of fresh air into the face area. The exhaust fan at the outlet of the pull tubing drew the diesel exhaust mixture at a rate of 9.44 m^3/s (20,000 cfm) from the face area and released it into the main entry.
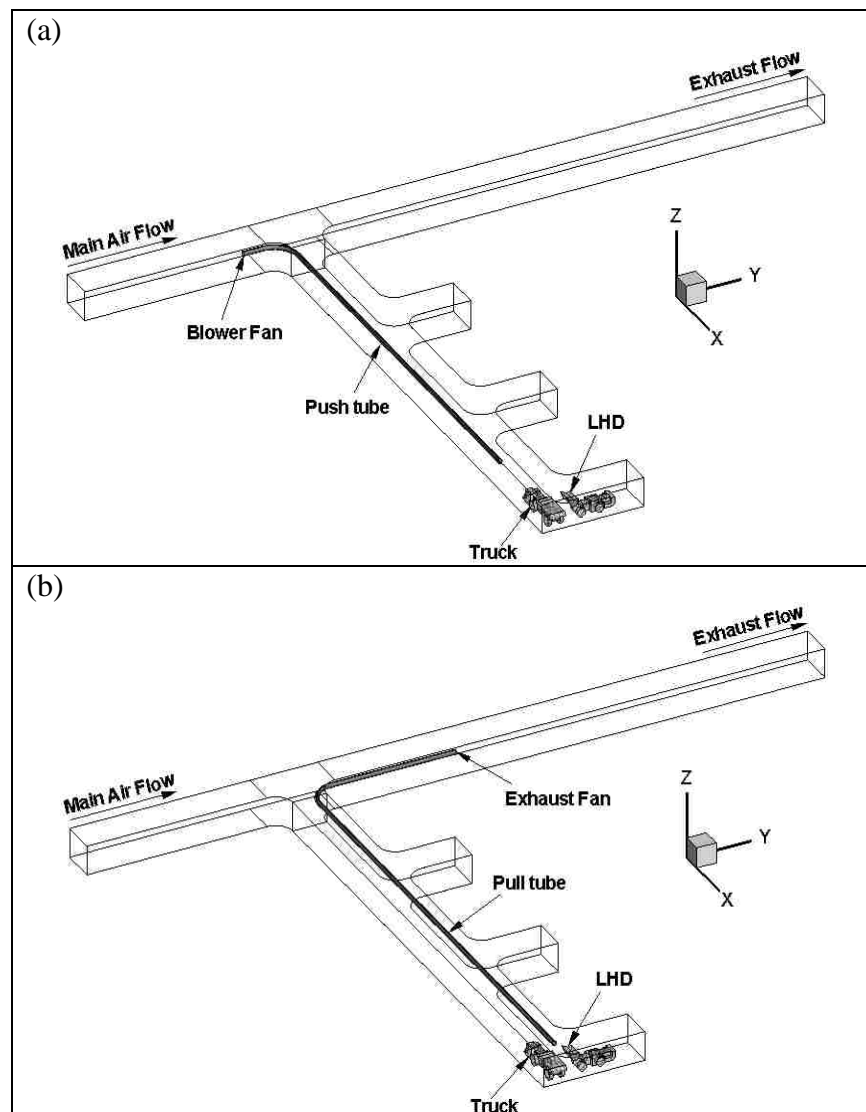
Figure 8.7. Computational Domain for Selection of Auxiliary Ventilation System. (a) Blower fan and tubing; (b) Exhaust fan and tubing; (c) Jet fan; (d) Push-pull system
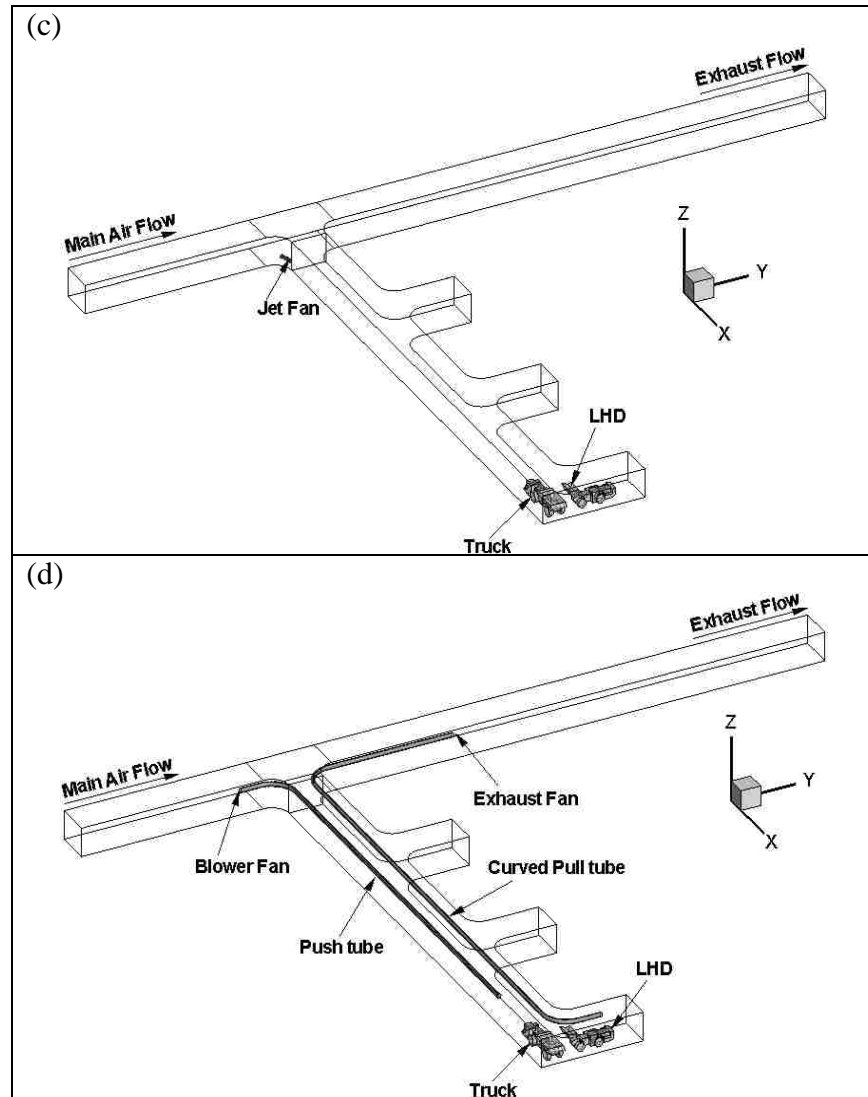
Figure 8.7. Computational Domain for Selection of Auxiliary Ventilation System. (a) Blower fan and tubing; (b) Exhaust fan and tubing; (c) Jet fan; (d) Push-pull system (cont.)

Three-dimensional incompressible unsteady turbulent continuity, momentum, and energy equations, along with standard k-ε turbulent and non-reacting transport equations (2 species, DPM and air) were solved using FLUENT CFD software. The Species transport model, available in FLUENT, was used to determine the DPM distribution pattern.

Due to the multiple cases covered in this section, all of the boundary conditions are summarized in Table 8.1. The detailed meanings of the boundary conditions are presented in other sections and in the FLUENT manual.

Table 8.1. Summary of Boundary Conditions

	Boundary	Detailed settings
Main ventilation	Inlet	0.65 m/s, normal to boundary; DPM: 0 ppm.
	Exit	Outflow or fully developed flow.
Diesel equipments	LHD tailpipe	24.1 m/s, normal to boundary; 594 K; DPM, 1.73 ppm.
	Truck tailpipe	27.5 m/s, normal to boundary; 644 K; DPM, 2.0 ppm.
Walls		No slip, adiabatic walls.
Auxiliary Ventilation	Push-tube	Inlet: fan ($\Delta P = 481$ Pa); outlet: interior.
tion	Pull-tube	Inlet: interior; outlet: fan ($\Delta P = 800$ Pa).
	Jet fan	Inlet: interior; outlet: ($\Delta P = 1200$ Pa).

A numerical solution of the governing equations and boundary conditions was performed by utilizing the commercial computational fluid dynamics (CFD) code FLUENT 6.3. The unsteady flow calculations were made by using time step ($\Delta t = 0.1$ s) for the time period of 200 s (3 minutes and 20 seconds). Calculations were performed on the NIC CLUSTER using 16 processors. The CPU time to obtain 200 s data was approximately 36 hours.

8.2.2. Results and Discussion. Simulations of the flow and heat transfer inside the dead-end entry were carried out and are presented, along with the general flow features that arise in a single dead-end entry, in Figure 8.8 for all four auxiliary ventilation systems. The large recirculation flow region that developed in the face area can be clearly seen in the figure. In Figure 8.8 (a), the blower fan supplied fresh air at a high velocity through the push tubing into the face area, creating a recirculation flow region. The fresh air mixed with the diesel exhaust to form a diluted mixture. However, the lack of a means for quickly removing this diluted mixture from the face area affected the ventilation. When an exhaust fan with pull tubing was used, a local pressure drop occurred in the face area which resulted in a flow of fresh air from the main entry and circulation of fresh air,

as shown in Figure 8.8 (b). The advantage of using pull tubing was that the diesel exhaust mixture was quickly removed from the face area. However the lack of enough fresh air affected the ventilation.
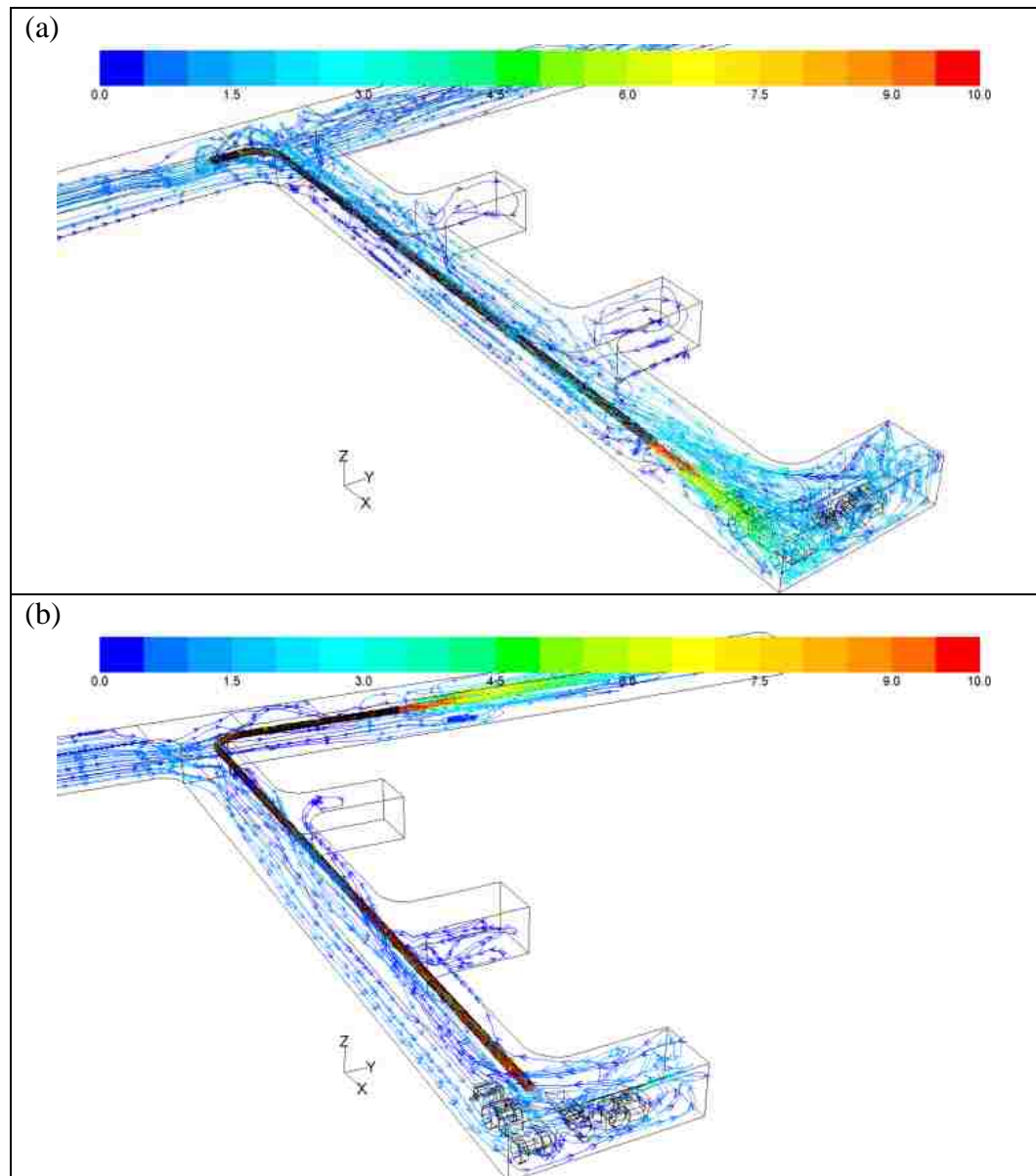
Figure 8.8. Pathlines Colored by Velocity Magnitude Demonstrating General Flow Features. (a) Blower fan and tubing; (b) Exhaust fan and tubing; (c) Jet fan; (d) Push-pull system
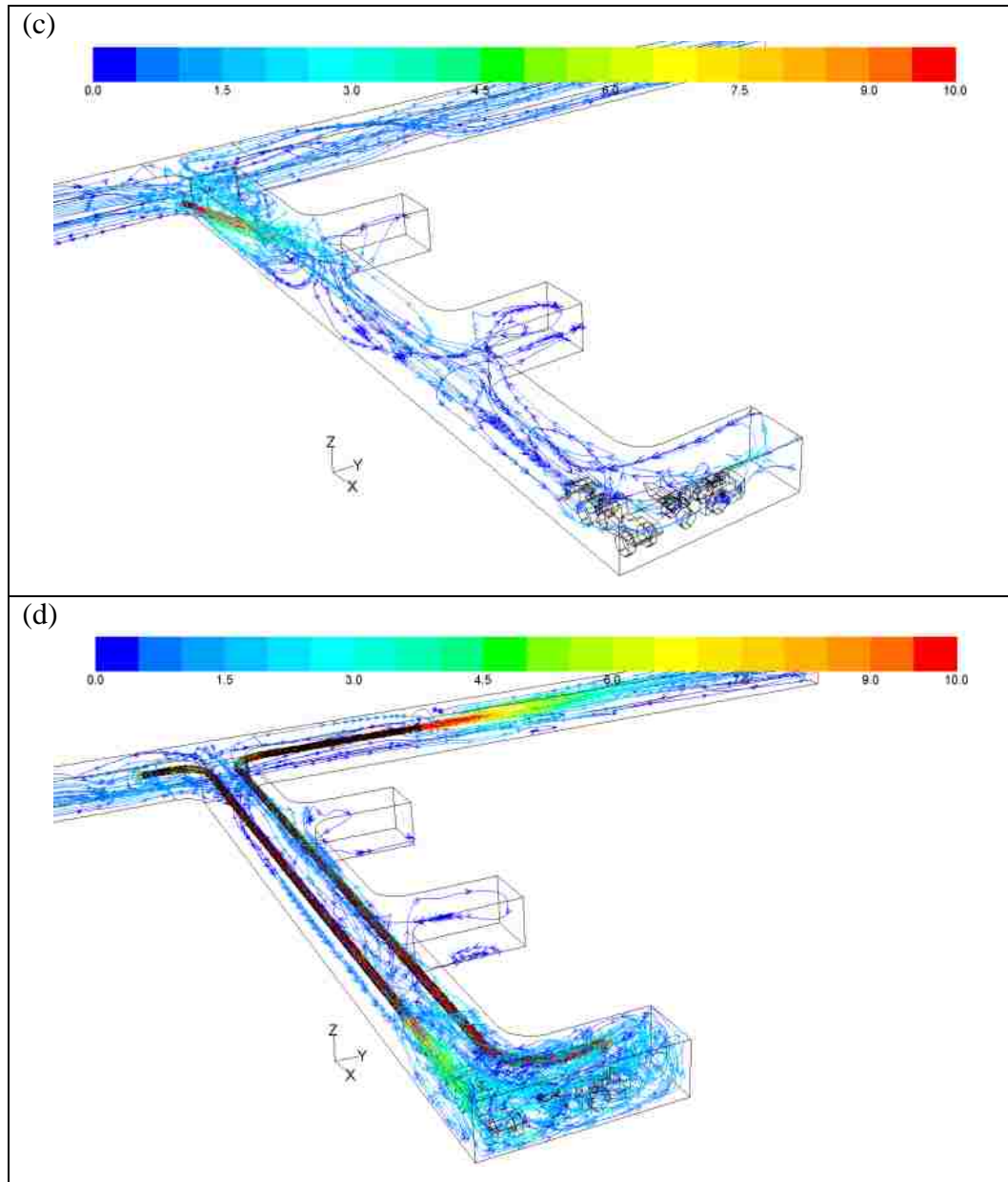
Figure 8.8. Pathlines Colored by Velocity Magnitude Demonstrating General Flow Features. (a) Blower fan and tubing; (b) Exhaust fan and tubing; (c) Jet fan; (d) Push-pull system (cont.)

With a jet fan, as shown in Figure 8.8 (c), very little fresh air reached the interior face area of the dead-end. This resulted in a weak form of recirculation in the region. When both blower and exhaust fans were used for the ventilation, a relatively stronger recirculation occurred in the region, as compared to the push only, pull only, and jet fan

systems shown in Figure 8.8 (d). This three dimensional, complicated flow behaviour that developed in the face area was responsible for the dilution of the DPM emitted from the tailpipes of the LHD and the truck. The effect of four auxiliary ventilation systems on DPM distribution is discussed in detail below.

8.2.2.1 Blower fan with push tubing (Case 1). The DPM distribution inside the dead-end when a blower fan with push tubing was used for ventilation at the dead-end entry, is shown in Figure 8.9. The blower fan provided 8.02 m^3/s (17,000 cfm) of fresh air through the push tube into the face area to dilute the high-temperature diesel exhaust of the LHD and the truck engines. From the colored contours, it can be seen that, except in the regions behind the truck and in front of the LHD, all other regions in the face area and a portion of the roof area in the dead-end were out of compliance with a DPM concentration that was higher than the prescribed regulatory limit of 160µg/m^3. Although fresh air was being supplied continuously, the slow movement of the diluted mixture in the face area and resulting delay in reaching the main entry was responsible for this behavior. In this configuration, both the LHD and the truck driver were required to use enclosed cabs for protection from the harmful effects of DPM during the loading operation.
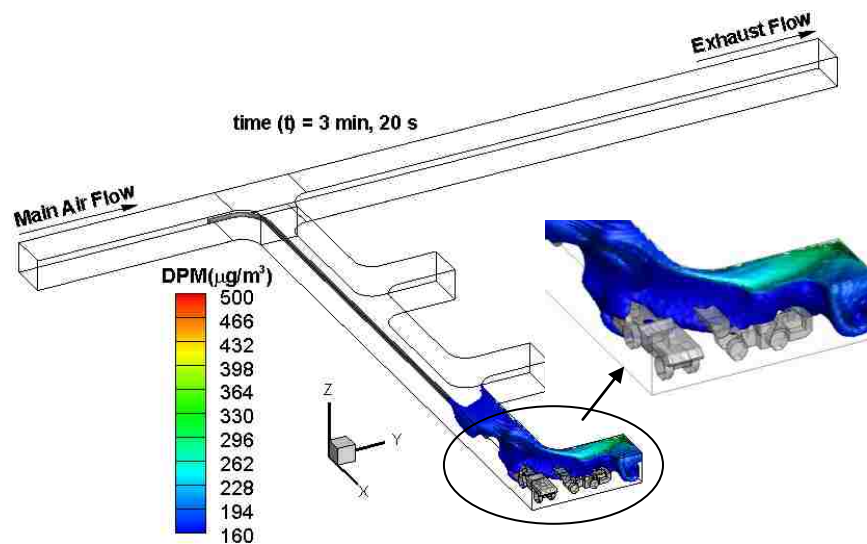
Figure 8.9. DPM Distribution (>160µg/m^3) inside the Single Dead-end
Entry with Push Tubing

8.2.2.2 Exhaust fan with pull tubing (Case 2). The effect of using an exhaust fan and pull tubing to ventilate the dead-end, is shown in Figure 8.10. A portion of the fresh air from the main entry entered into the dead-end and diluted the diesel exhaust of the LHD and the truck engines, forming a DPM air mixture. The exhaust fan drew this mixture through the pull tubing from the face area at a rate of 9.44 m^3/s (20,000 cfm) and released it into the main entry. It can be seen that, when compared with a push tubing ventilation system, the pull tubing ventilation results had far more DPM-covered regions inside the dead-end. Although the flow capacity of the exhaust fan was higher than that of the blower fan and continuously removed the DPM-air mixture, the inability to divert sufficient fresh air from the main entry into the working face area resulted in a high concentration of DPM being built up in the face areas. However, in the face area where miners were working, DPM primarily covered the roof region and did not affect the miners. Therefore, based on the size of the harmful DPM covered area inside the dead-end, the push system performed better than the pull tube system in ventilating the face area during the loading operation.
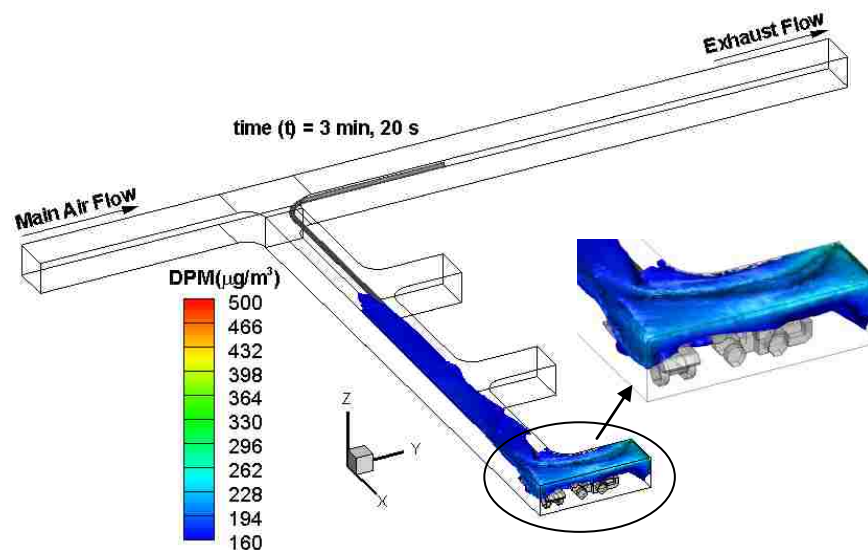
Figure 8.10 DPM Distribution (>160μg/m^3) inside the Single Dead-end Entry with Pull Tubing

8.2.2.3 Jet fan (Case 3). The DPM distribution, when a jet fan was used to venti-
late the face area of the single dead-end entry, is shown in Figure 8.11. The jet fan was
located at the entrance to the dead-end and supplied 8.73 m^3/s (18,500 cfm) of fresh air.
From the colored contours it can be seen that the jet fan underperformed, in comparison
with push only or pull only tubing systems. The DPM level above the critical limit of
160μg/m^3 engulfed the entire face area and most of the roof areas of the dead-end. This
was due to the fact that the jet fan had no tubing to extend inside the dead-end to supply
enough fresh air to dilute the diesel exhaust. The lack of pull tubing to remove the high
concentration of DPM from the face area further compounded the problem. Therefore, a
jet fan was not the right choice to ventilate the loading operation occurring deep inside
the dead-end.
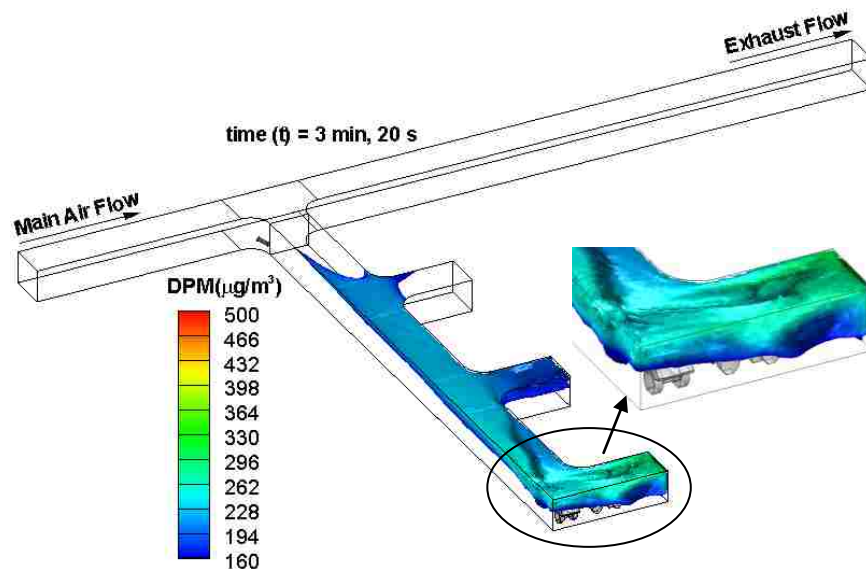
Figure 8.11. DPM Distribution (>160μg/m^3) inside the Single Dead-end
Entry with Jet Fan

8.2.2.4 Push-pull system (Case 4). Figure 8.12 shows the DPM distribution
where both the blower fan with push tubing and the exhaust fan with pull tubing were

used to ventilate the face area. This system used the well-designed push and curved pull tubing for ventilation (refer to Section 8.3 of this study). Compared with the previously used pull only tubing system, the pull tube here curved an additional 12 meters into the working face area. The loading operation was repeated and, from the colored contours, it can be seen that there was a significant reduction in the harmful DPM-occupied regions inside the working face area and at the roof area of the dead-end. Therefore, the operators of both the LHD and the truck did not require enclosed cabs to protect themselves from the harmful effects of DPM in this configuration.
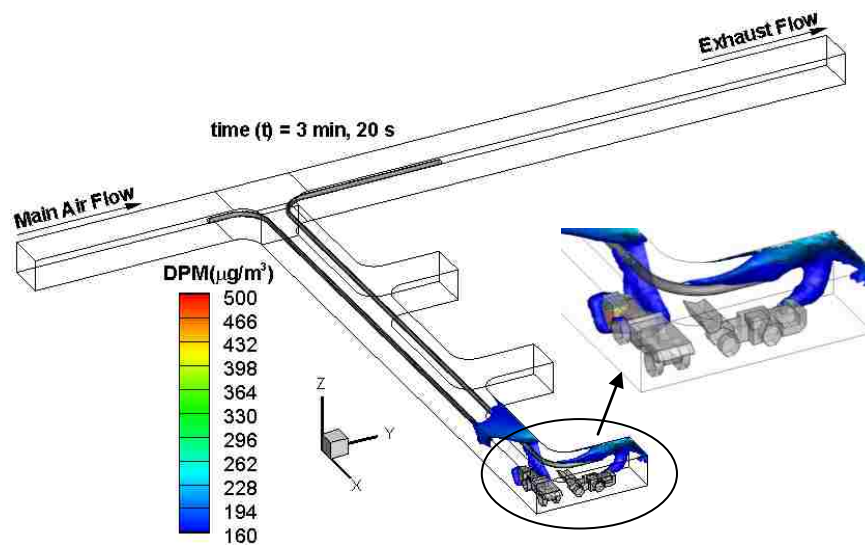
Figure 8.12 DPM Distribution (>160µg/m^3) inside the Single Dead-end with Push-pull

8.2.3. Comparison of Different Auxiliary Ventilation Systems. To further understand the effect of auxiliary ventilation systems on DPM distribution, many two-dimensional cut cross-sectional planes were created inside the dead-end. A sample of the push tubing ventilation system is shown in Figure 8.13. Similar cross-sectional planes were created for other ventilations systems as well, but are not shown here. The performance of these four auxiliary ventilation systems was evaluated by plotting contours and

line curves of DPM distribution at these cross-sectional planes. This is described in the next paragraph.

The contours of DPM that were greater than 160 μg/m^3 at these cross sectional planes are shown in Figure 8.14. When a push only tubing system was used, as shown in Figure 8.14 (a), it can be seen that high concentrations of DPM occupied most of the working face area. With the pull only tubing system, as shown in Figure 8.14 (b), the harmful DPM primarily occupied the roof region of the face area. When compared with the push tubing system, the exhaust fan with pull tubing performed better in ventilating the face area. However, DPM occupied more roof regions in the remaining areas of the dead-end. It can be clearly seen in Figure 8.14 (c) that the jet fan system performed poorly with DPM completely covering the face area and most of the remaining regions of the dead-end. The push and pull tubing system, with minimum DPM occupied regions in the face area, performed the best in ventilating the face when compared with the other three ventilation systems, as shown in Figure 8.14 (d).
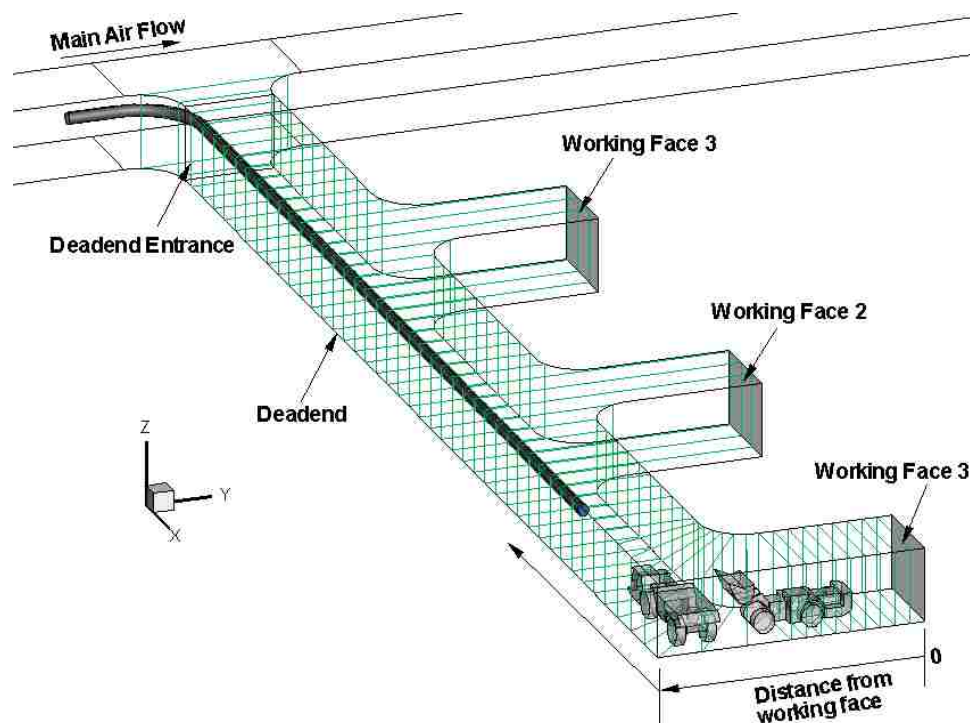
Figure 8.13. Schematic of the Cross-sectional Planes inside the Dead-end
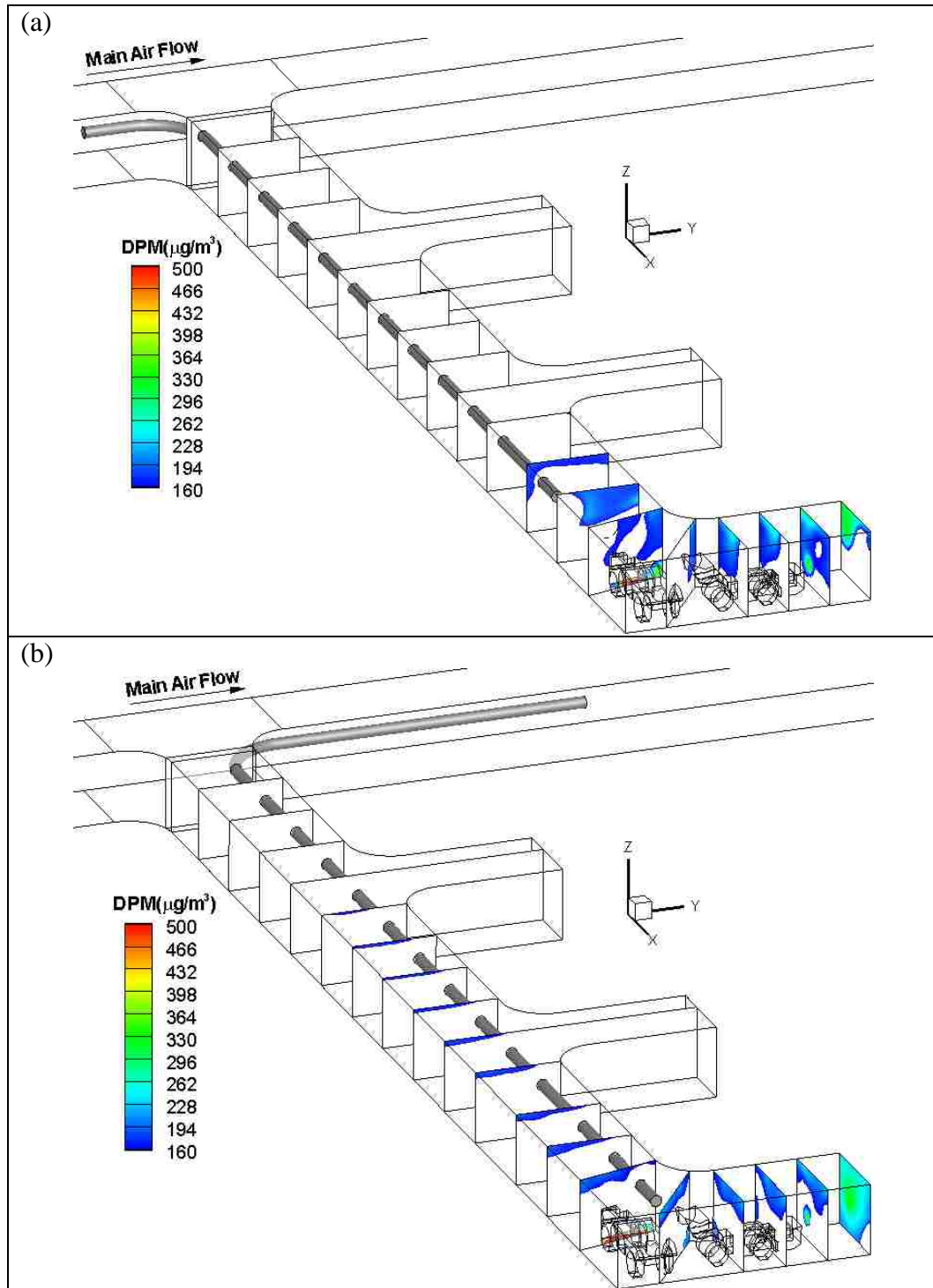
Figure 8.14. DPM Distributions at Cross Sectional Planes for Different Auxiliary Ventilation. (a) Blower fan and tubing; (b) Exhaust fan and tubing; (c) Jet fan; (d) Push-pull system
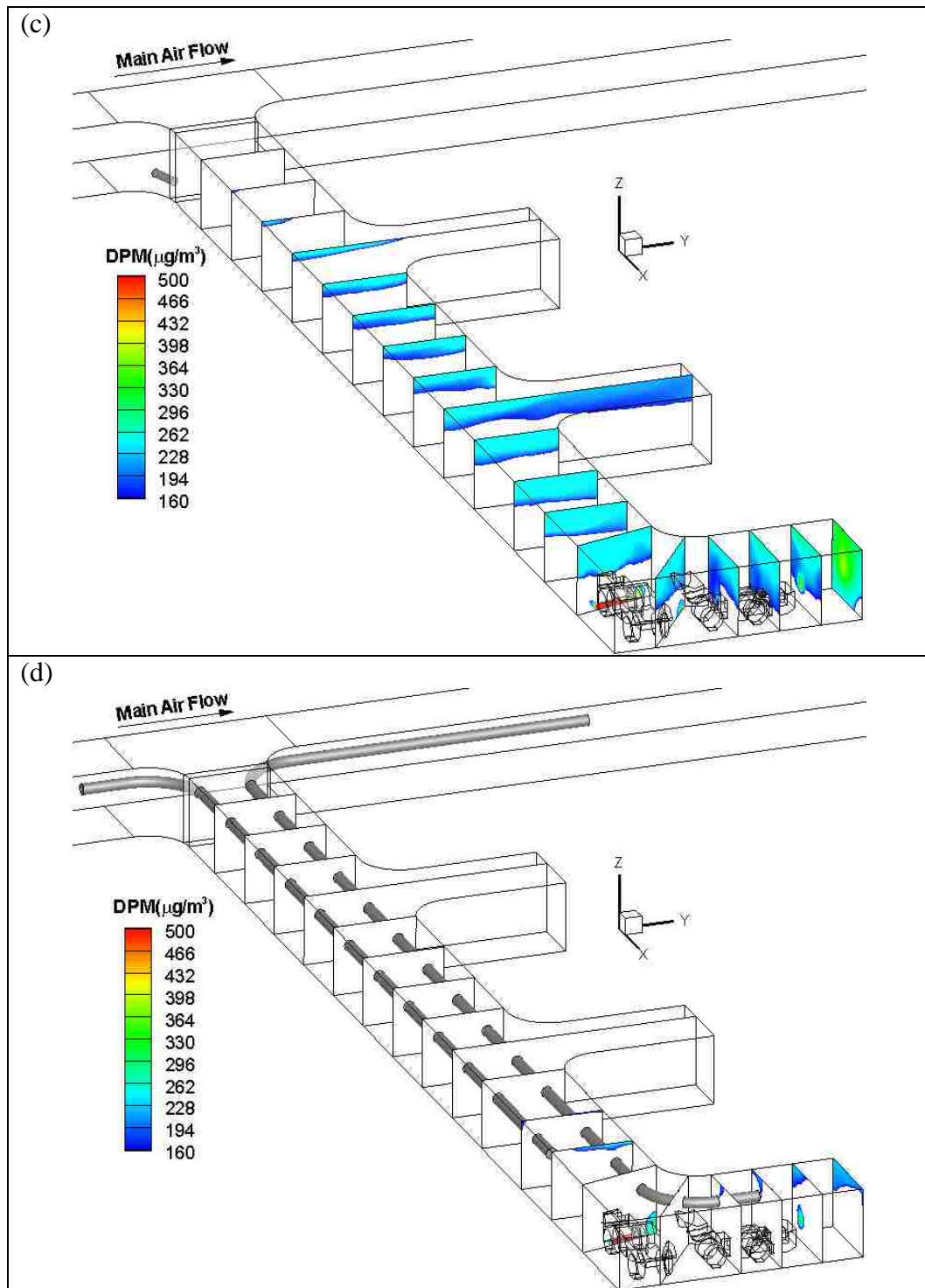
Figure 8.14. DPM Distributions at Cross Sectional Planes for Different Auxiliary Ventilation. (a) Blower fan and tubing; (b) Exhaust fan and tubing; (c) Jet fan; (d) Push-pull system (cont.)

The performance of the ventilation systems was also evaluated by plotting the average, maximum, and minimum values of DPM for each cross-sectional plane against the distance, as shown in Figure 8.15. The distance was calculated from the working face area to each cross sectional plane, as shown in Figure 8.13. It can be clearly seen from Figure 8.15 (a) that the average DPM values were minimum for the push-pull system and maximum for the jet fan system in the working face region of the dead-end. In the remaining areas of the dead-end, the pull tubing and combined push-pull tubing systems out performed the other two ventilation systems, as shown in Figure 8.15 (a).

The plot of the maximum DPM values at each cross-sectional plane is presented in Figure 8.15 (b). It can be seen that all of the ventilation systems produced approximately similar distributions inside the face area. The DPM values reached as high as 1000 $\mu g/m^3$ inside the face area where the truck tailpipe was located and as high as 700 $\mu g/m^3$ where the LHD tailpipe was located. Away from the tailpipe regions, these values fell sharply; however, these maximum values were still higher than the prescribed regulatory limit. The plot of the minimum values of DPM, shown in Figure 8.15 (c), demonstrated that an exhaust fan with pull tubing could dilute the DPM exhaust to a minimum value, as compared to other systems inside the face area.

8.2.4. Conclusions. From the comparison study of these four auxiliary ventilation systems, it was concluded that the combined blower and exhaust fans with push-pull tubing ventilates the face area effectively during the loading operation. When only one fan is required to reduce power requirements in the underground mine, the DPM distribution inside the dead-end suggested that the exhaust fan with pull tubing should be used in preference to a blower fan with a push tubing system. The DPM distribution also dictated that a jet fan system should not be used for ventilating the face area located deep inside the dead-end.

8.3. DESIGN FOR PUSH-PULL VENTILATION SYSTEM

In the previous section, the effect of four types of auxiliary ventilation systems on DPM distribution was discussed in detail. It was stated that the well-designed short push and curved pull tubing system ventilated the face area effectively for the LHD-truck loading operation. In this section, the design of the aforesaid push-pull auxiliary ventilation

system for the LHD-truck loading operation was carried out using CFD simulations. Both the LHD and the truck were fitted with DPF and had a minimum DPM emission from the tailpipe. The loading operation was assumed to take place in a time duration of 200 seconds in the inner most face area of the dead-end.

8.3.1. Problem Statement and CFD Modeling. A schematic of the computational domain for each push-pull ventilation design is shown in Figure 8.16. The four design cases considered in this study were: case (a), long push and short pull tubing (Figure 8.16 (a)); case (b), short push and long pull tubing (Figure 8.16 (b)); case (c), long push and curved pull tubing (Figure 8.16 (c)); and case (d), short push and curved pull tubing (Figure 8.16 (d)). The dimensions of the main entry, the dead-end and the diameter of the push and pull tubing remained the same as before and are described in previous sections. The main entry fresh air flow rate and the auxiliary ventilation flow rates remained the same as before and are also described in the previous sections.
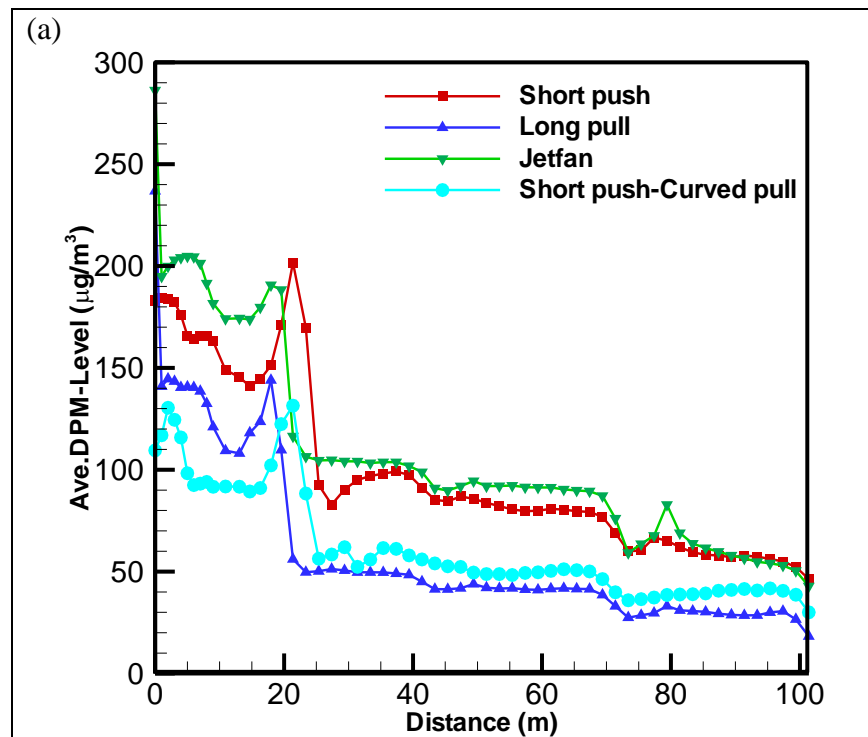
Figure 8.15. Comparison of DPM Values at Different Planes at t = 200 s
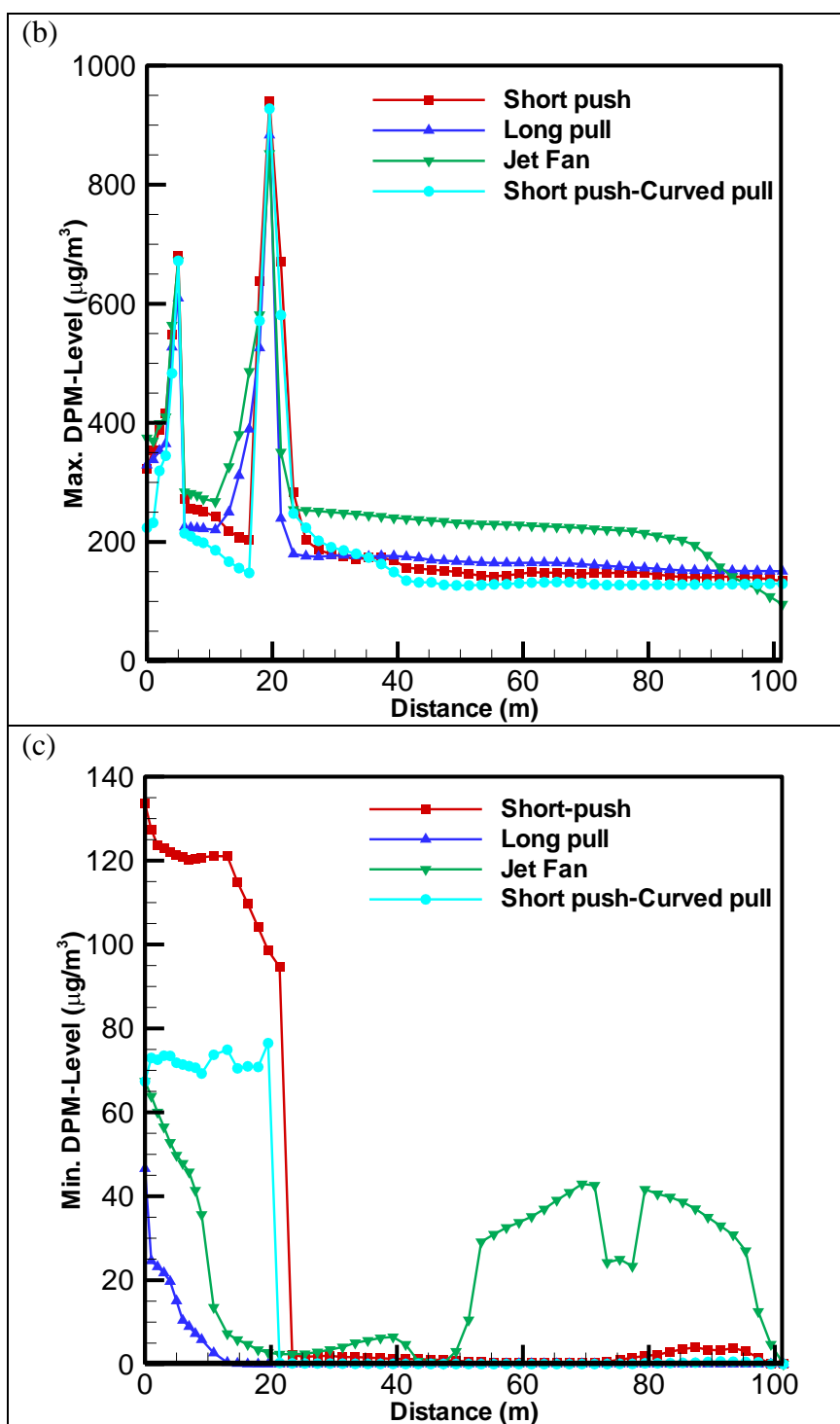
Figure 8.15. Comparison of DPM Values at Different Planes at t = 200 s (cont.)
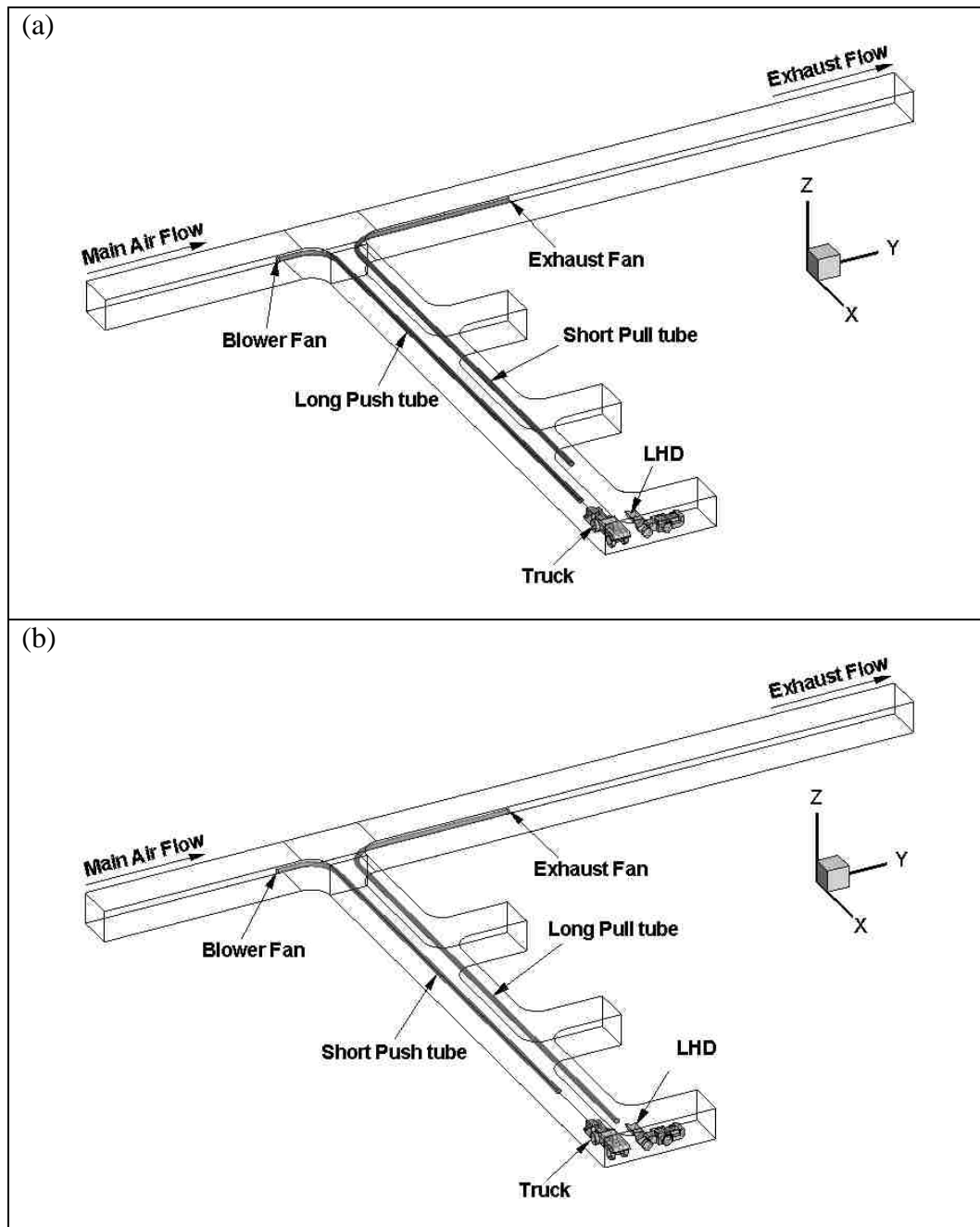
Figure 8.16. Computational Domain with Different Push-pull Design Settings. (a) Long push short pull; (b) Short push long pull; (c) Long push curved pull; (d) Short push curved pull
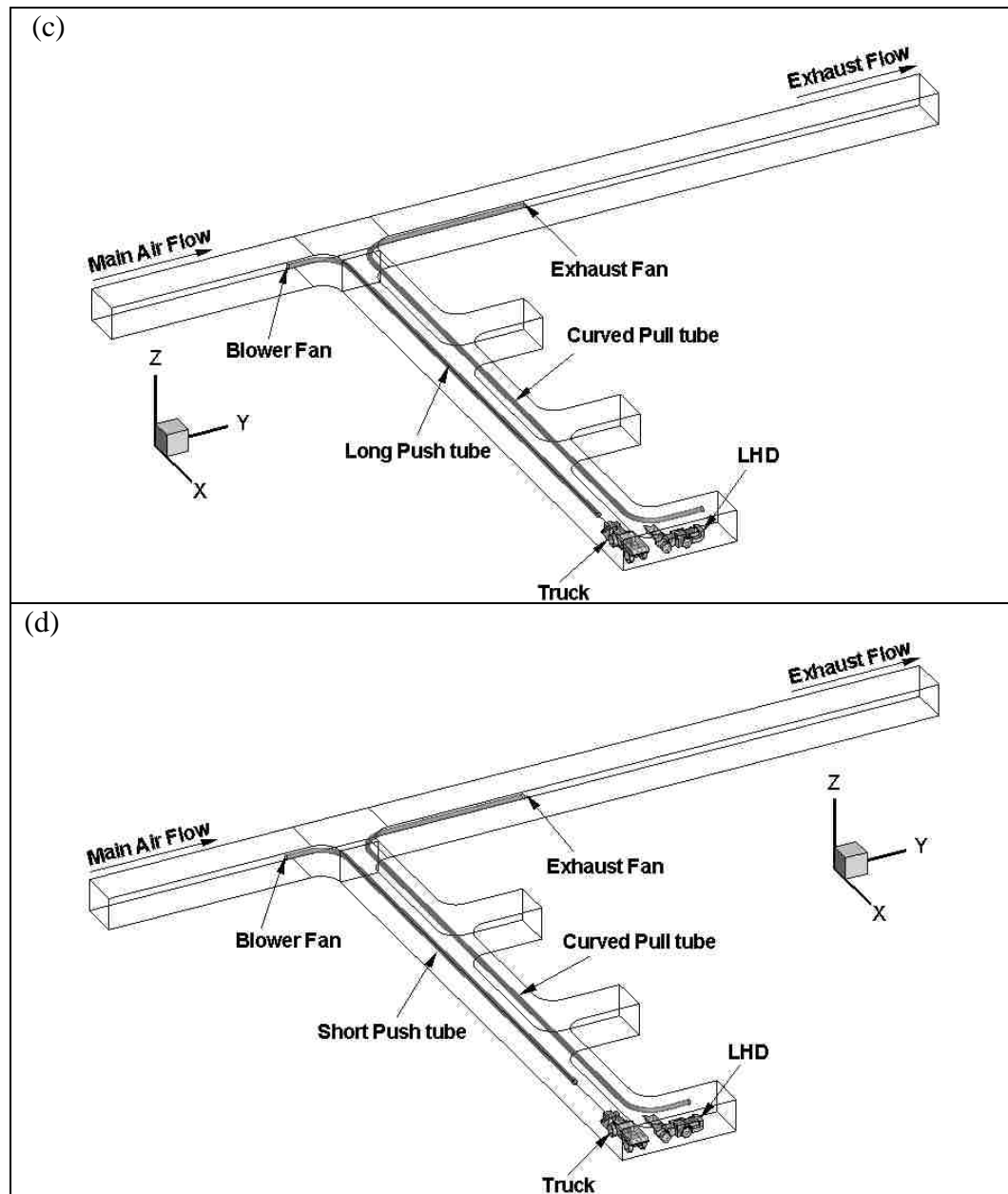
Figure 8.16. Computational Domain with Different Push-pull Design Settings. (a) Long push short pull; (b) Short push long pull; (c) Long push curved pull; (d) Short push curved pull (cont.)

For case (a), the push tubing extends into the dead-end entry for approximately 77 m while the pull tubing extended for approximately 67 m. For case (b), the push tubing extended for 70 m into the dead-end and the pull tube extended for approximately 81 m.

In case (c), the length of the push tubing remained the same as in case (a) but the pull tubing, in addition to extending for 78 m into the dead-end, curved for an additional 12 m into the face area. In case (d), the length of the push tubing remained the same as in case (b) but the pull tubing, in addition to extending for 78 m into the dead-end, curved for an additional 12 m into the face area. Details of the governing equations, boundary conditions, mesh generation, and the solution procedure are included in the previous sections.

8.3.2. Results and Discussion. Simulations were carried out for all of the four designs of the push-pull tube auxiliary ventilation system. The general flow features are presented in Figure 8.17 for each ventilation design. The flow features occurring in the geometry are discussed in detail in the previous section. It can be seen from Figure 8.17 (a) that, when the pull tubing was shorter than the push tubing, the fresh air from the push tubing impinged on the rear wall of the dead-end and made a 90 degree turn to enter the face area. However, only a small portion of that fresh air reached the interior of the face area to ventilate the LHD emission. The remaining portion created a recirculation region in the rear section of the truck and in the frontal portion of the LHD. Also, this recirculation region was not large enough to ventilate the tailpipe emission of the truck. The distant location of the pull tubing also made it difficult to remove the exhaust mixture from the face area in a timely manner.

To avoid this condition, the pull tubing was made longer than the push tubing, as shown in Figure 8.17 (b). With this modified design, the fresh air flow impinging on the rear wall of the dead-end created a strong vortex-like flow in the presence of pull tubing, as shown in the figure. Again, not enough fresh air reached the interior of the face area but a closer location of the pull tubing ventilated, to some extent, the tailpipe emission of the LHD.

Since none of the above two ventilation designs were able to ventilate the interior of the face area effectively, the pull tubing was made to curve into the face area for both long and short push tubing, as shown in Figure 8.17 (c) and (d). It can be seen in Figure 8.17 (c) that two small recirculation regions were created in the face area which, again, prevented enough fresh air from reaching the interior of the face area. However, when compared with Figure 8.17 (a), there was a large improvement in the ventilation of the face area. With short push tubing, as shown in Figure 8.17 (d), there was a single large

recirculation region which effectively ventilated the entire face area. The resultant DPM distributions in the dead-end for each of these ventilation designs is discussed in detail in the next paragraphs.
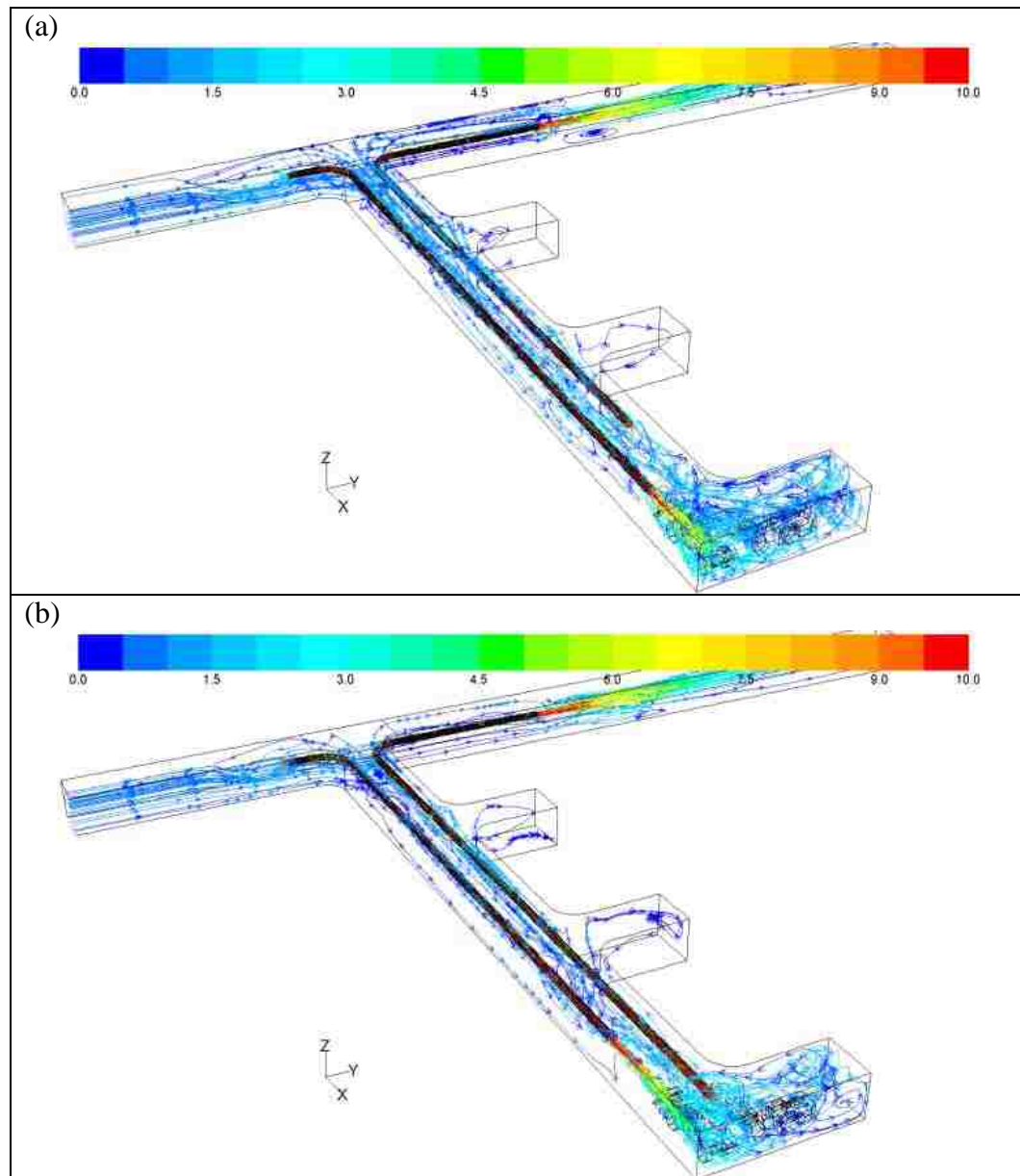
Figure 8.17. Pathlines Colored by Velocity Magnitude Demonstrating General Flow Features. (a) Long push short pull; (b) Short push long pull; (c) Long push curved pull; (d) Short push curved pull
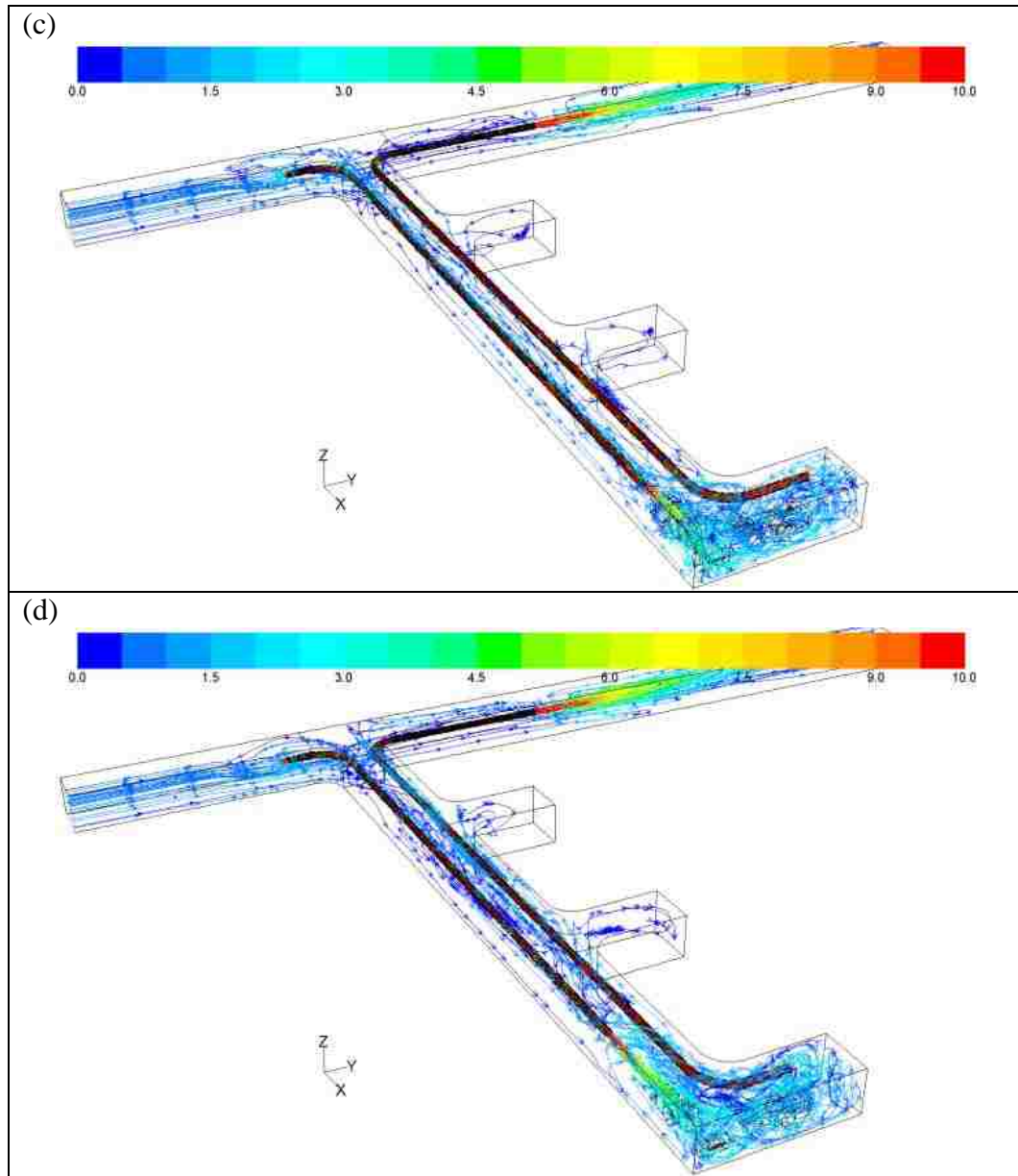
Figure 8.17. Pathlines Colored by Velocity Magnitude Demonstrating General Flow Features. (a) Long push short pull; (b) Short push long pull; (c) Long push curved pull; (d) Short push curved pull (cont.)

**8.3.2.1 Long push and short pull tubing system (Case 1).** The DPM distribution with long push tubing and short pull tubing is shown in Figure 8.18. The push tubing was longer than the pull tubing by 10 m. The colored contours represent the diesel exhaust, with the DPM level above the regulation limit of 160 μg/m^3. The blower fan at the

inlet of the push tubing provided 8.02 m³/s (17,000 cfm) of fresh air to the face area. This low-temperature fresh air mixed and cooled the high-temperature diesel exhausts of the LHD and truck engines and formed a DPM-air mixture. The exhaust fan at the outlet of the pull tubing sucked this exhaust mixture at a rate of 9.44 m³/s (20,000 cfm) and re-leased it into the main entry. The high concentration DPM completely engulfed the active face area in the dead-end, except for small regions behind the truck and in front of the LHD. Most of the remaining areas of the dead-end were also filled with diesel fumes near the roof region by the end of the loading operation due to the buoyancy effect. The opera-tors of the LHD and the truck should use enclosed cabs to protect themselves from the harmful effects of DPM. This design of long push and short pull tubing system failed to ventilate the active face area effectively.
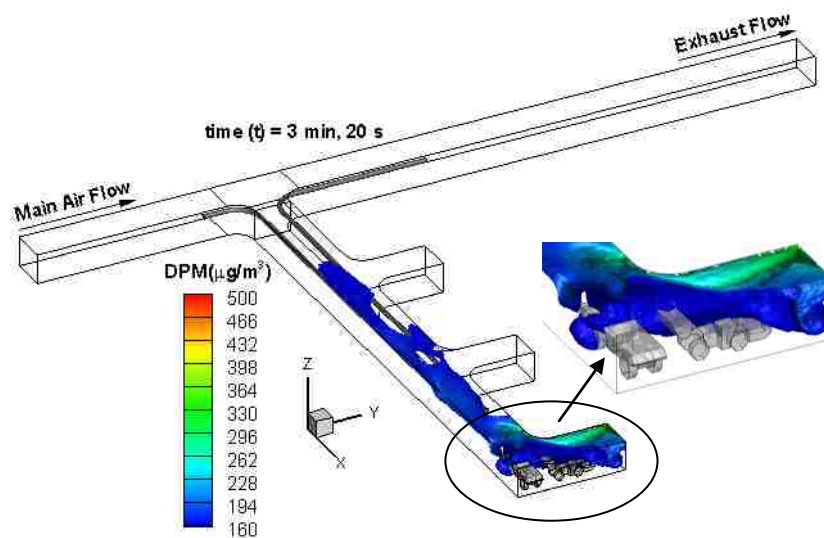
Figure 8.18 DPM Distribution inside the Single Dead-end Entry

8.3.2.2 Short push and long pull tubing system (Case 2). Figure 8.19 shows the DPM distribution in the same dead-end with a short push and long pull tubing system for the LHD-truck loading operation. This modified design of short push and long pull tub-ing system effectively ventilated the face area, when compared with the long push and

short pull tubing ventilation system. The DPM occupied a small region behind the tail-pipe of the LHD, a small region around the tailpipe of the truck and the roof region near the face area due to the buoyancy force, as shown by the colored region. The miners working in this colored region should use personal protection instruments. The remaining areas of the dead-end were free of any DPM above the regulatory limit.
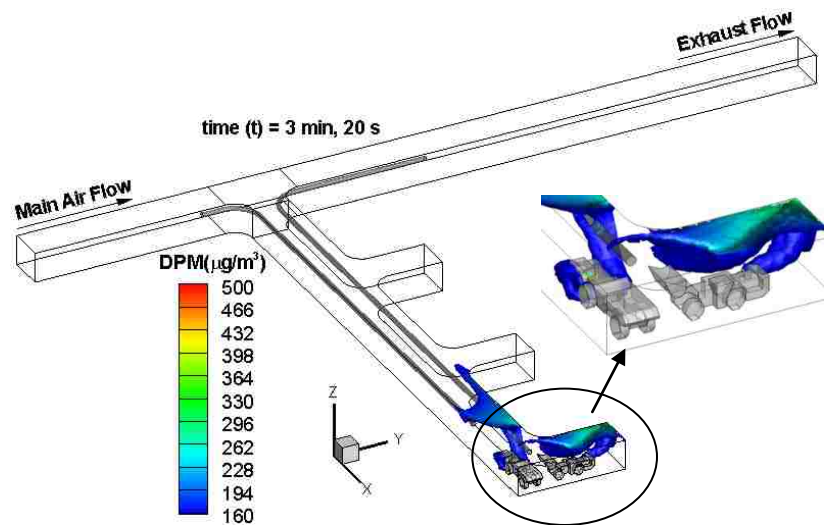
Figure 8.19. DPM Distributions inside the Single Dead-end Entry

8.3.2.3 Long push and curved pull tubing system (Case 3). This system is similar to case 1 except that the pull tubing was extended and made to curve inside the face area. The resultant DPM distribution in the dead-end is shown in Figure 8.20. When compared with case 1, there was a dramatic improvement in the DPM distribution in the dead-end. There was no high concentration DPM accumulation in the dead-end other than in the face area. However, this system did not perform better than the system in case 2 since there was significant DPM accumulation inside the face area where the LHD was located. The miners working in the colored region should use personal protection instruments.
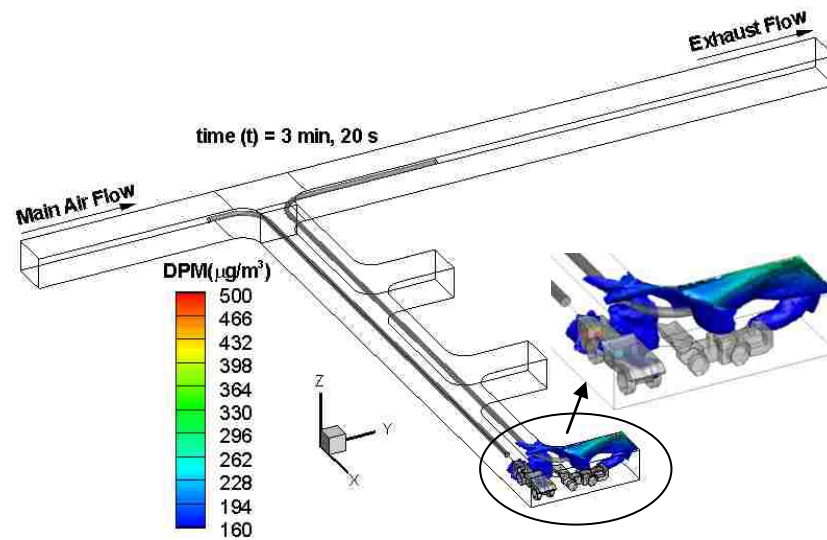
Figure 8.20 DPM Distributions inside the Single Dead-end Entry

8.3.2.4 Short push and curved pull tubing system (Case 4). The DPM distribution, when a short push and long curved pull tubing auxiliary ventilation system was used for the LHD-truck loading operation, is shown in Figure 8.21. This design is similar to case 2 with the short push and long pull tubing design except that the long pull tubing was made to curve for an additional 12 m into the working face area of the dead-end. A comparison of the design of the short push and long curve pull tubing system with short push and long straight pull tubing system showed only a negligible difference for the DPM affected areas near the tailpipe of the LHD and the truck. However, it significantly reduced the DPM accumulation in the roof region of the face area. As before, the miners working in the colored regions should use personal protection instruments.

8.3.3. Comparison of Different Push-Pull Tubing Designs. A comparison of the different designs of the push-pull ventilation systems was made by plotting the two-dimensional DPM contours and area weighted average DPM values at cut cross-sectional planes inside the dead-end. The cross-sectional planes are shown in Figure 8.22 for the long push and short pull tubing ventilation system. Similar cross-sectional planes were created for other ventilations systems and are not shown here due to space limitations. The performance of each push-pull design system was evaluated based on its DPM dilution capability in the face area, as described in the next paragraph.
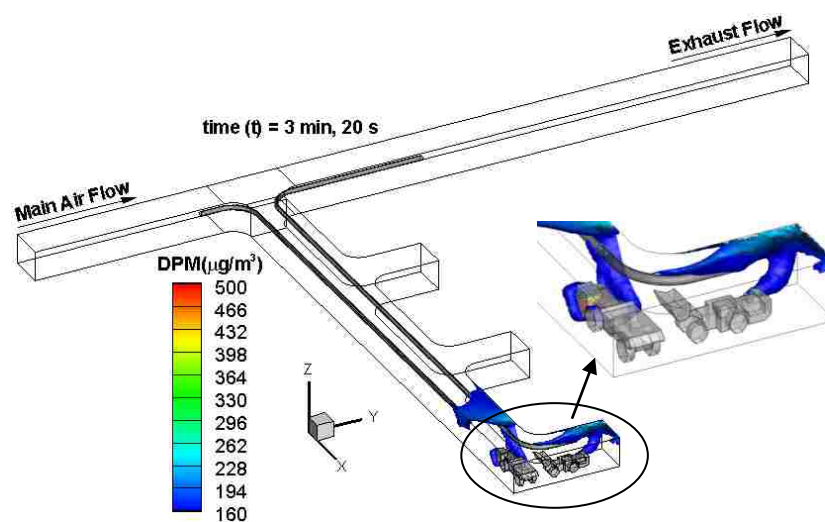
Figure 8.21. DPM Distributions inside the Single Dead-end Entry

.
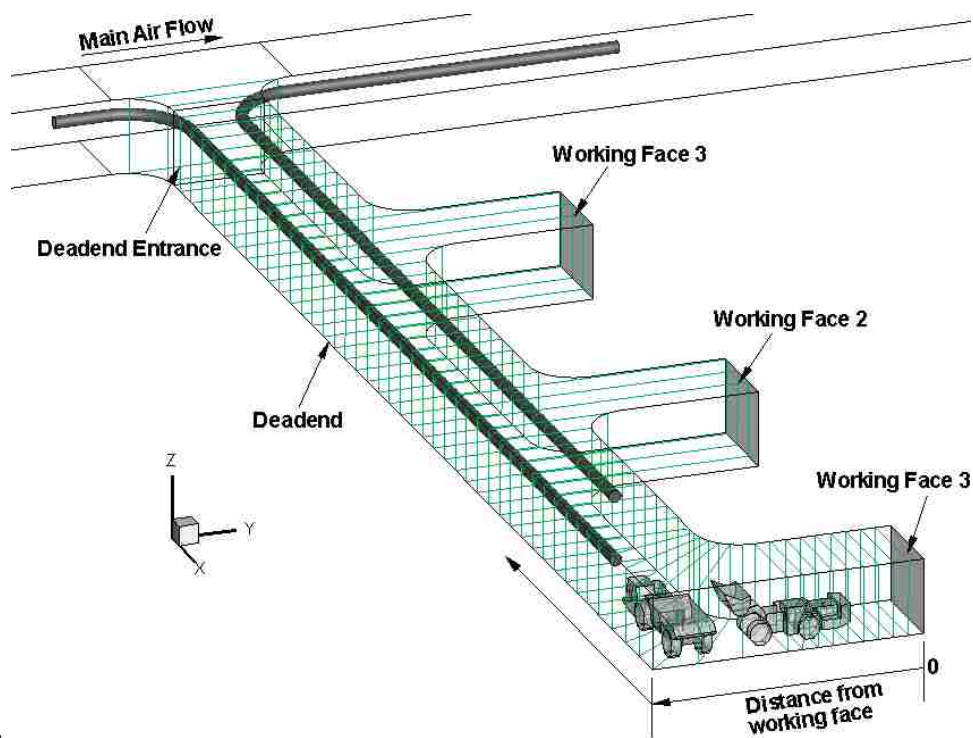
Figure 8.22. Schematic of the Cross-sectional Planes inside the Dead-end

The contours of DPM, greater than 160 μg/m^3 at these cross-sectional planes, are shown in Figure 8.23. It can be seen from Figure 8.23 (a) that when the case 1 long push and short pull tubing system was used, DPM occupied the entire face area and roof areas in the remaining regions of the dead-end. However, when the case 2 short push and long pull tubing system was used, as shown in Figure 8.23 (b), the size of the DPM occupied region in the face area was greatly reduced. The DPM distribution, when pull tubing was curved into the face area, is shown in Figure 8.23 (c) and (d) for the above two configurations. It can be seen that the case 3) long push and curved pull system performed better than the systems in case 1) and case 2) in diluting DPM in the face area, as shown in Figure 8.23 (c). However, in case 4) the short push and curved pull tubing system performed the best, when compared with the other three cases, in effectively ventilating the face area and the other regions of the dead-end, as shown in Figure 8.23 (d).

The overall performance evaluation of the different push-pull designs was made by plotting the area-weighted average, maximum, and minimum values of DPM at these cross-sectional planes against the distance, as shown in Figure 8.24. The distance of the cross-sectional planes from the interior face area was evaluated, as shown in Figure 8.22. It can be seen from Figure 8.24 (a), that case 4), the short push and curved pull tubing system, performed the best with the minimum average DPM value inside the face area, while case 1), the long push and short pull tubing system, performed the worst with the maximum average values inside the face area, when compared with other push-pull deisgns. Although case 3), the long push and curved pull system, resulted in minimum average values in the remaining areas of the dead-end, when compared with other systems, in the important face region where miners were working, case 4), the short push and curved pull tubing design, performed the best.

This fact was further substantiated with the plots of maximum and minimum values of DPM at the cross-sectional planes, as shown in Figures 8.24 (b) and (c). Although the plot of maximum values (Figure 8.24 (b)) showed negligible differences in the distribution, the plot of minimum values (Figure 8.24 (c)) showed that minimum DPM values were obtained in the face area when case 4), the short push and curved pull tubing system, was used.
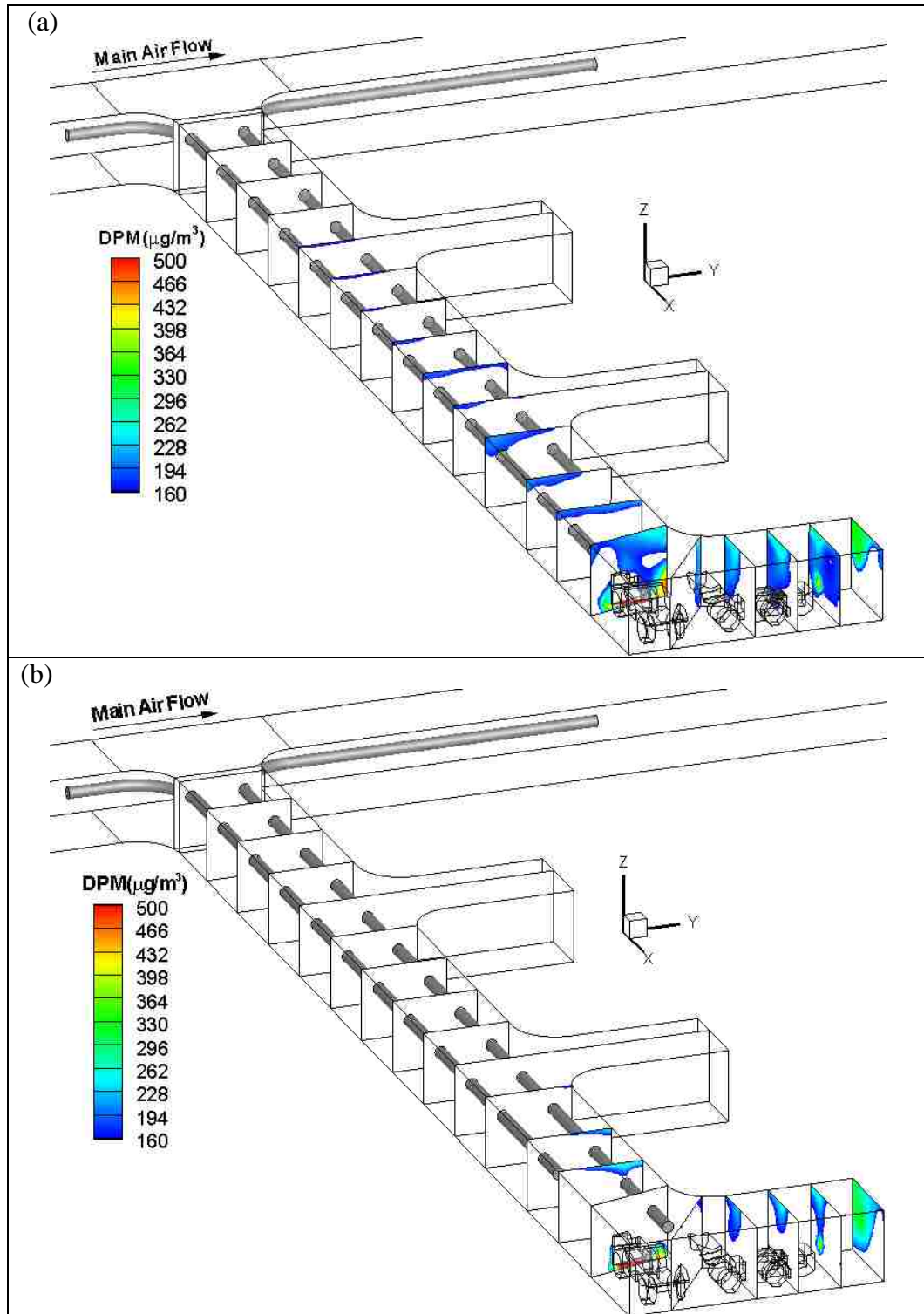
Figure 8.23. DPM Distributions at Different Cross Sectional Planes. (a) Long push short pull; (b) Short push long pull; (c) Long push curved pull; (d) Short push curved pull
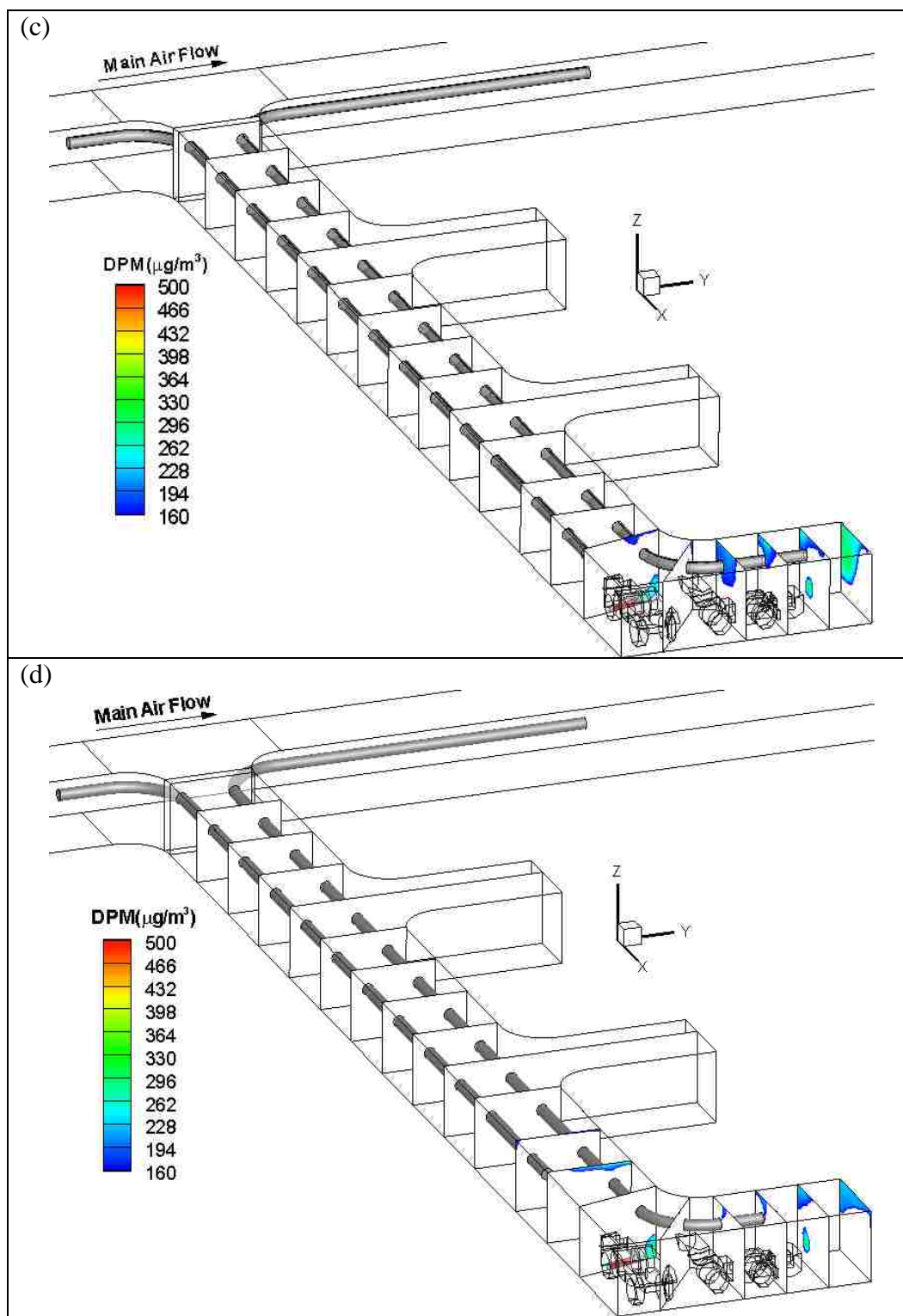
Figure 8.23. DPM Distributions at Different Cross Sectional Planes. (a) Long push short pull; (b) Short push long pull; (c) Long push curved pull; (d) Short push curved pull (cont.)
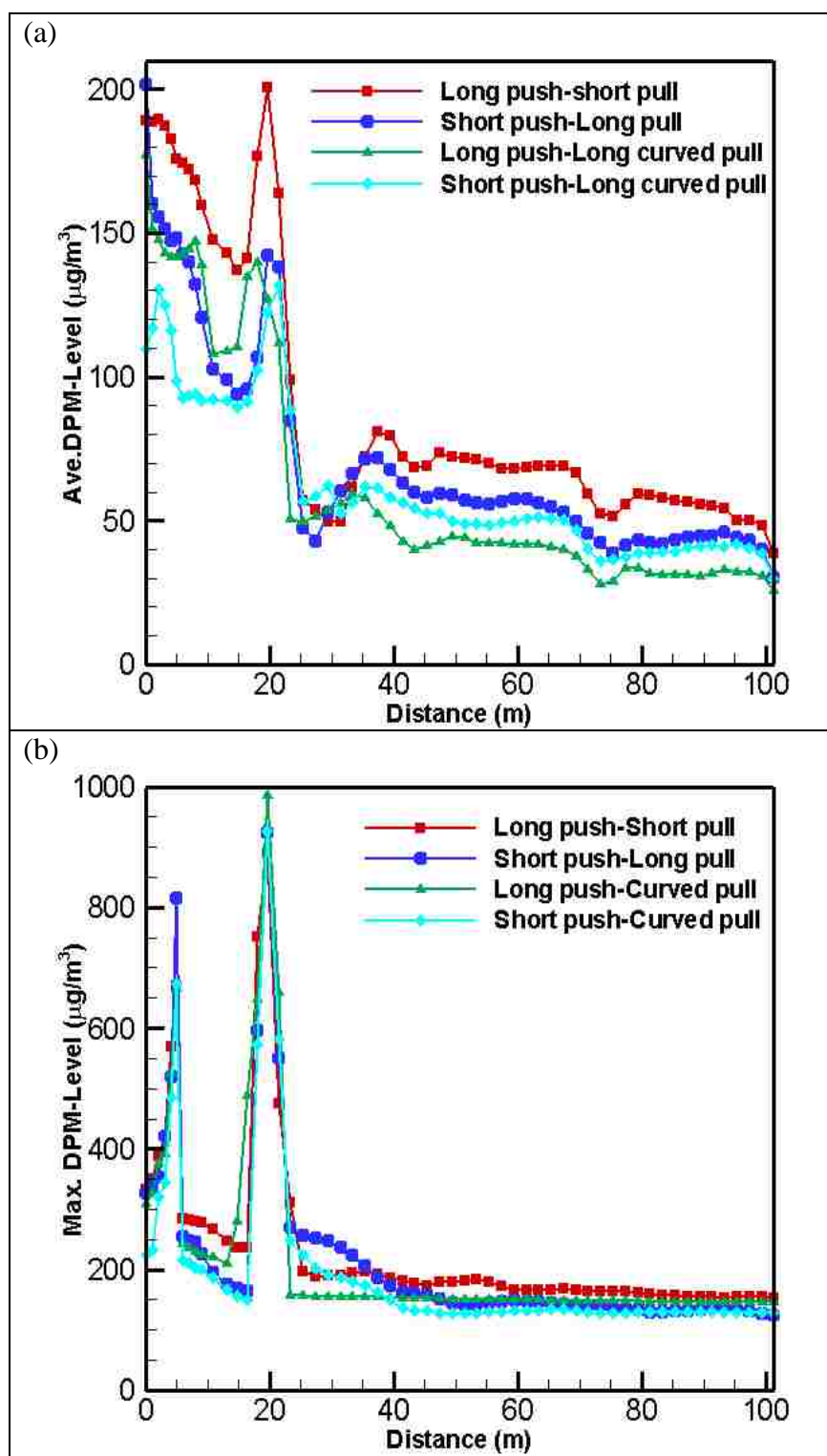
Figure 8.24. Comparison of Average, Maximum and Minimum DPM Values
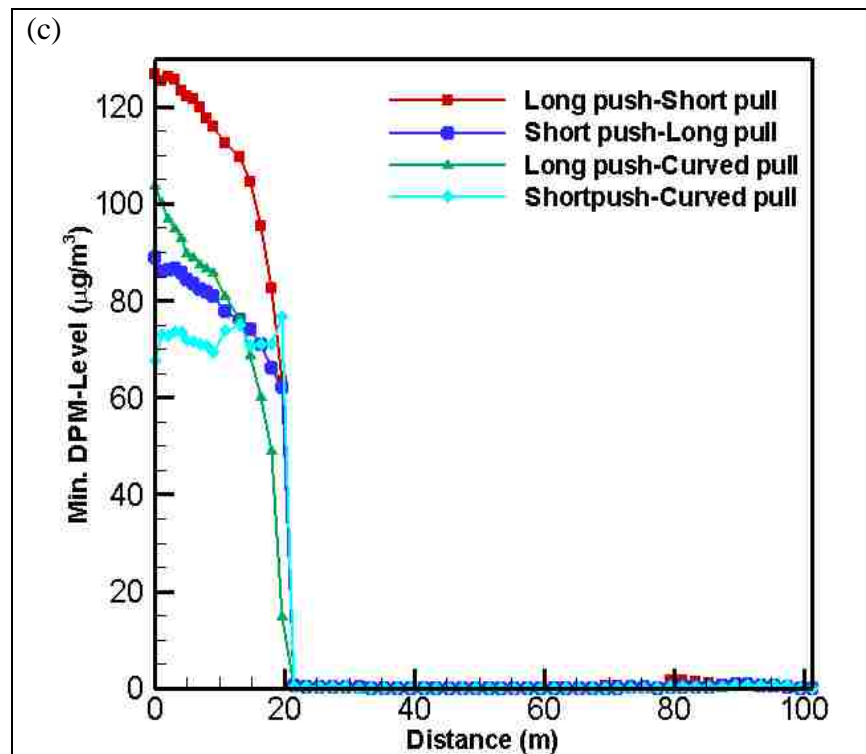
Figure 8.24. Comparison of Average, Maximum and Minimum DPM Values (cont.)

8.3.4. Conclusions. The performance of four different push-pull ventilation designs in effectively ventilating the face area inside the dead-end was studied. Based on this study, it was concluded that the short push and curved pull tubing system was the optimum design of all four designs, and effectively ventilated the face area during the truck loading operation.

8.4. THE EFFECT OF DIFFERENT MINING OPERATIONS ON GIVEN AUXIL-IARY VENTILATION

Several mining operations were taking place inside the face area of the underground metal/non-metal mines. Depending on the mining operation, different types of diesel vehicles were used and each diesel vehicle emitted DPM from the tailpipe at different concentrations. Therefore, it was important to study the DPM distribution in the face area for each, or a combination of, mining operations. In this section, the mining

operations that were considered inside the face areas include 1) LHD working alone doing mucking operation, 2) drilling jumbo working alone doing drilling operation, 3) LHD and truck doing loading operation and 4) LHD and truck doing loading operation in one face area and a drill-jumbo doing drilling operation in another face area. It was assumed that all of the diesel vehicles were fitted with DPF and had minimum DPM emissions from the tailpipe.

From the study of auxiliary ventilation systems and detailed design of push-pull system, it was found that a blower fan with short push tubing and an exhaust fan with long curved pull tubing effectively ventilated the face area during the loading operation. Since different mining operations were taking place in this study, short push and long straight pull tubing were used for ventilating the face area.

The ventilation flow rates of the main fan flow and the auxiliary fan flow were fixed in this study. The distributions of DPM concentration were presented along with area-weighted average DPM values inside the dead-end to study the effect of different mining operations on the DPM distribution pattern.

8.4.1. Problem Statement and CFD Modeling. The schematic of the single dead-end entry with push-pull tube ventilation is shown in Figure 8.25 for different mining operations. The dimensions of the main entry, the dead-end, the diameter of the push and pull tubing, the main entry fresh air flow rate and the auxiliary ventilation flow rates remained the same as before, and are described in Section 8.2. For all mining operations, with the exception of the combined drilling and loading activity, the push tubing extended into the dead-end entry for approximately 70 m while the pull tubing extended for approximately 81 m. The lengths of the push and pull tubing inside the main entry were 3.4 m and 22 m, respectively.

The mining operations of LHD mucking, drilling, and LHD-truck loading were carried out in the inner-most face area of the dead-end. In the case of a combined operation, loading took place in the middle face area and drilling took place in the inner-most face area of the dead-end. All of the mining operations are set to take place for the time duration of 200 seconds. All diesel vehicles were fitted with DPF and had minimum DPM emission from their tailpipes.
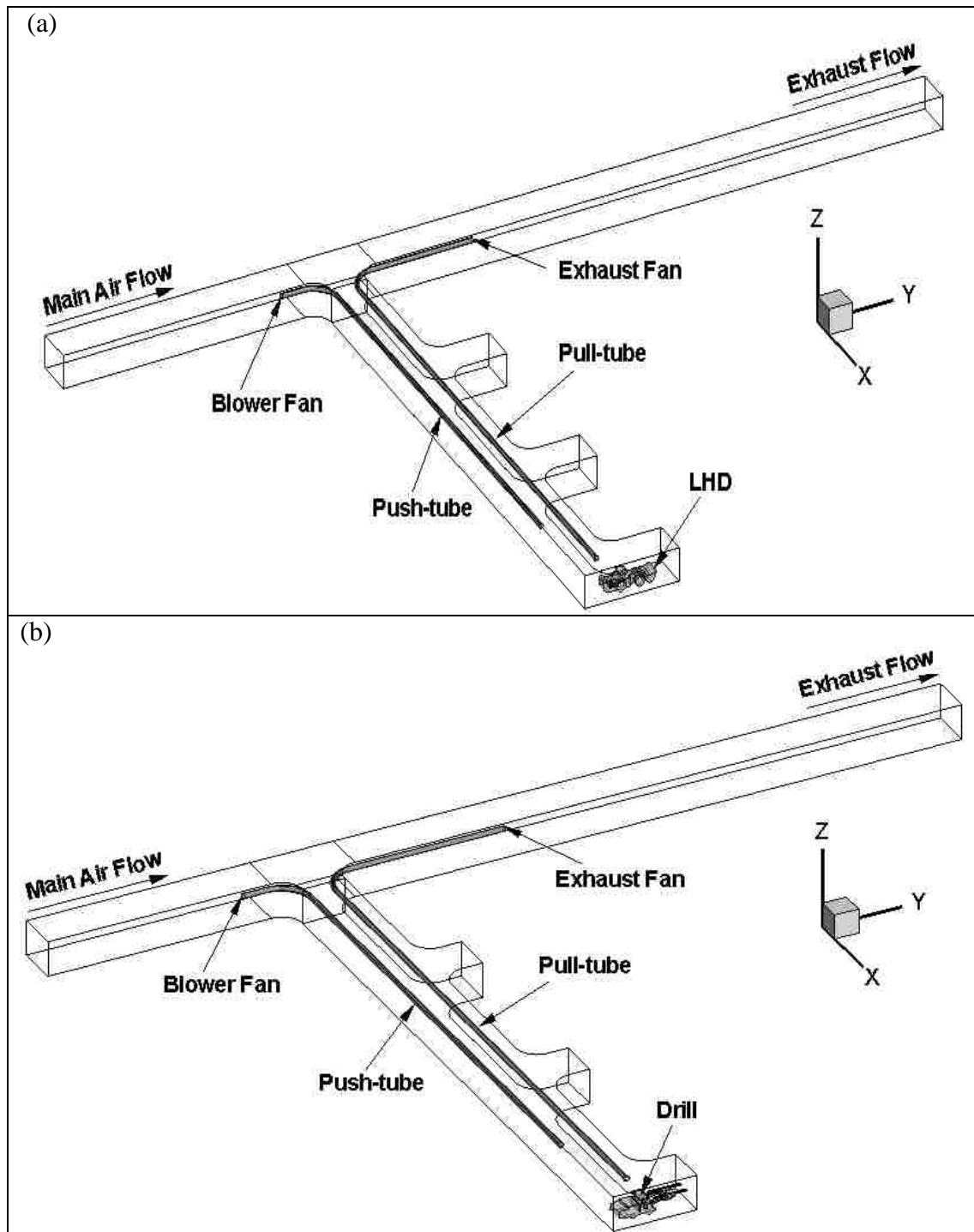
Figure 8.25. Schematic of Mining Operations in Dead-end Entry with Push-pull System. (a) LHD mucking operation; (b) Drill jumbo drilling operation; (c) LHD and truck loading operation; (d) Loading and drilling operation
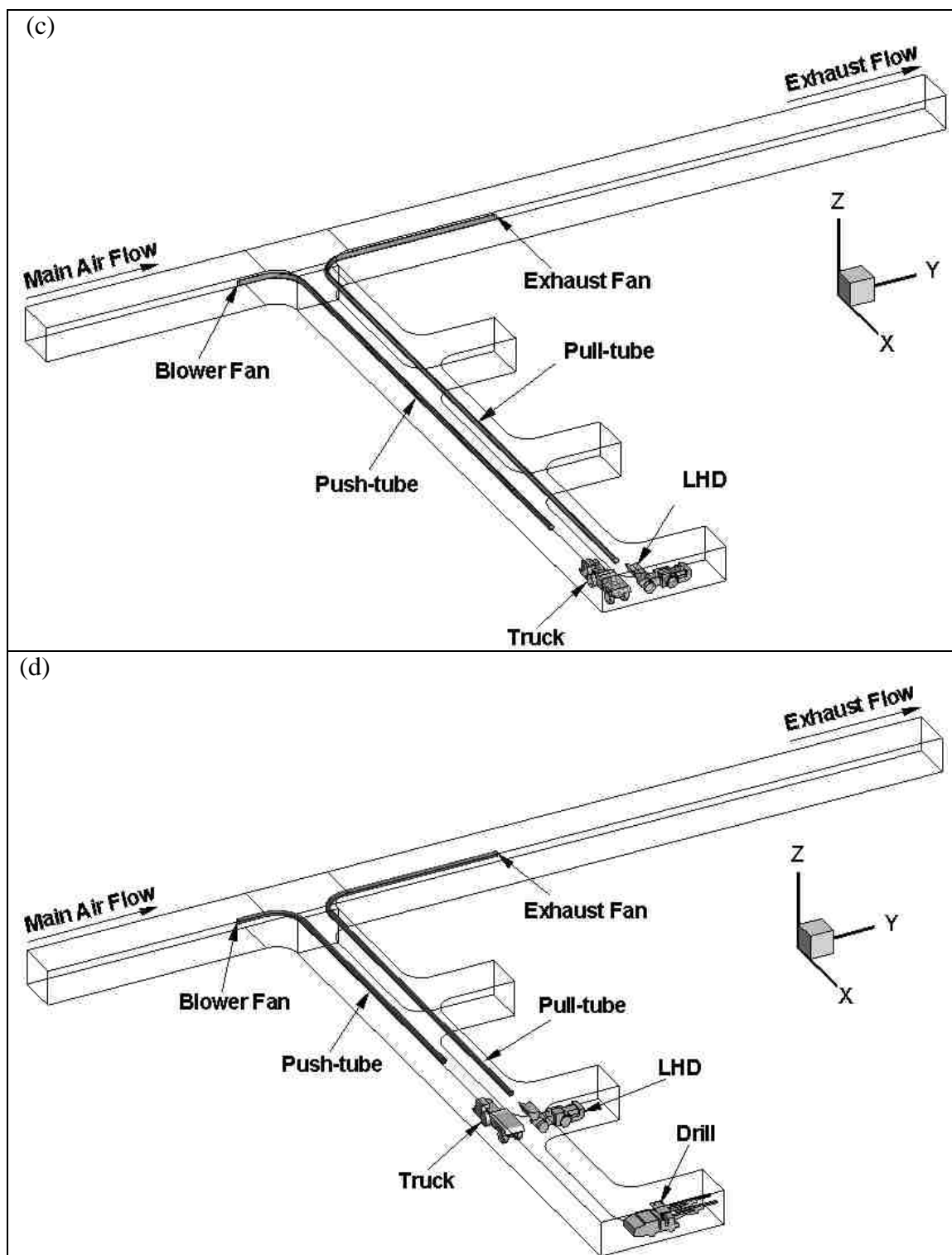
Figure 8.25. Schematic of Mining Operations in Dead-end Entry with Push-pull System. (a) LHD mucking operation; (b) Drill jumbo drilling operation; (c) LHD and truck loading operation; (d) Loading and drilling operation (cont.)

The three-dimensional transient Navier stokes, continuity, and energy, along with species transport and standard k- ε turbulence model equations were solved to determine the transient DPM distribution pattern in the single dead-end entry. The species transport model available in FLUENT was used to determine the DPM distribution pattern. The boundary conditions used in the cases can be referred to in Table 8.1.

8.4.2. Results and Discussion. The three dimensional numerical simulation was carried out for all four mining operation inside the single dead-end entry, i.e., the LHD in the mucking operation, the drilling jumbo in the drilling operation, the LHD-truck in the loading operation and the LHD-truck in the loading operation in one face area, along with the drilling jumbo operation in the other face area.

The general flow feature that arose in the single dead-end entry is shown in Figure 8.26 for all of the mining operations. It shows the fresh air that entered the main entry and split into two parts. The first part flowed directly downstream to the exhaust section and exited the domain. The second part entered into the dead-end while the remaining part was drawn by the blower fan into the push tubing and delivered it to the working face area where the mining operation was taking place. This fresh air inside the dead-end flowed over the diesel vehicles and mixed with the emissions from their tailpipes creating a large recirculation flow region inside the working face area as shown in Figure 8.26. Due to the effect of buoyancy, this diffused mixture flowed upward towards the roof of the mine, reversed direction and started flowing upstream toward the main entry. A majority of this reversed flow was drawn by the exhaust fan through the pull tubing and drained into the main entry at high velocity. The remaining part reached the middle section of the main entry and divided into two parts. One part flowed upstream and reentered the push tubing while the other part flowed downstream and mixed with the exhaust flow from the pull tubing. This complex flow behavior was due to the interaction between the high temperature tail pipe flow and the low temperature fresh air flow. The resulting DPM distributions inside the dead-end for each mining operation are discussed in detail in the next section.

8.4.2.1 LHD-Mucking (Case 1). The DPM distribution inside the dead-end during the LHD mucking operation is shown in Figure 8.27. From the colored DPM contours, it can be seen that, except for a very small region behind the tailpipe of the LHD,

all other places in the single dead-end entry were in compliance with a DPM concentration of less than the prescribed regulatory limit of $160\mu g/m^3$. It can be seen that the DPM distribution inside the dead-end attained a steady state condition within 10 seconds from the start of the operation. This was due to the low emission from the tailpipe of the LHD resulting from the installation of DPF. Similar DPM distribution results were obtained when only a blower fan was operating and the exhaust fan was turned off, or vice versa, to save cost and power. In this configuration, the LHD driver was not required to use enclosed cabs to provide protection from the harmful effects of DPM.

8.4.2.2 Drilling (Case 2). Figure 8.28 shows a drilling jumbo carrying out a drilling operation in the inner-most face area of the dead-end. From the colored contours, it can be clearly seen that, except for the immediate tailpipe regions of the drilling jumbo, all of the remaining areas were in compliance with a DPM concentration of less than 160 micrograms per cubic meter. It can also be seen that the DPM distribution during the drilling operation attained a steady state within 10 seconds from the start of the simulation. Similar to the mucking operation, there was a negligible difference in the DPM occupied areas inside the dead-end when either the blower fan or the exhaust fan was turned off to save power. Only a blower fan with push tubing, or an exhaust fan with pull tubing, was sufficient to obtain effective ventilation in the face area. During drilling, the operators of the drilling jumbo may have to use enclosed cabs to be protected from the harmful effects of DPM.

8.4.2.3 LHD-truck loading (Case 3). The DPM distribution in the same dead-end while the LHD-truck loading operation was occurring in the interior face area is shown in Figure 8.29. For this mining operation, the pull tubing was curved for an additional 12 meters into the face area, as per the requirement from the detailed design study for loading operation in Section 8.3. From the colored contours, it can be seen that DPM above the regulation limit occupied a small region behind the tailpipe of the LHD and a small region in the roof above the LHD. The DPM also covered small regions in front of the truck and in the roof area of the dead-end. From the distribution pattern, it can be seen that both blower and exhaust fans with push and pull tubing were necessary to effectively ventilate the face area. The LHD and the truck drivers may not require enclosed cabs to protect themselves from the harmful effects of DPM in this configuration.

8.4.2.4 Drilling and LHD-truck loading (Case 4). The DPM distribution, while both the loading and drilling operations were taking place inside the dead-end, is shown in Figure 8.30. The design of the push-pull tubing system was altered for this combined operation. Since most of the tail pipe emission was coming from the mid face area of the dead-end, the length of the push and pull tubing was shortened. In this case, the push tube extended for approximately 40 meters while the pull tubing extended for approximately 51 meters into the dead-end. The colored contours show the harmful diesel fumes that gradually filled the drilling and the loading face areas. The pull tubing was intentionally not curved into the middle face area in order to facilitate the absorption of harmful DPM resulting from the drilling operation in the interior face area. From the colored contours, it can be clearly seen that the fan capacities of the push and pull tubing were not high enough to effectively ventilate the face areas. The operators of the LHD, the truck, and the drilling jumbo should use enclosed cabs in order to safeguard themselves against the harmful effects of DPM.

8.4.3. Comparison of Different Mining Operations. A comparison of the distribution of DPM inside the dead-end for different mining operations was made by plotting colored contours and curves for different cross-sectional planes inside the dead-end. The cross-sectional planes of the mucking operation are shown in green color in Figure 8.31. Similar cut planes were also generated for other mining operations. The working face 1 was used when a single mining operation (mucking or drilling or loading) was taking place, but both working face 1 and working face 2 were used when two mining operations (drilling in work face 1 and loading in work face 2) were taking place. No mining operation took place in work place 3.

The DPM contours that were greater than 160 $\mu g/m^3$ for these cross-sectional planes are shown in Figure 8.32. It can be clearly seen from Figures 8.32 (a) and (b) that, except near the tailpipe region, the miners moved freely inside the working face and the remaining areas of the dead-end during the mucking and drilling operations without using any personal protection instruments. However, during the loading operation, as shown in Figure 8.32 (c), the LHD operator was affected by a high-concentration DPM if protective devices were not used. This situation would have been averted if a curved pull tubing had been used instead of straight tubing, as per the design study for the push-pull system

discussed in the previous section. For the combined drilling and loading operation, shown in Figure 8.32 (d), both of the working face areas were covered with a high concentration of DPM. The miners should use enclosed cabs and personal protective instruments during the combined operations. The main flow rate, or the auxiliary ventilation flow rates, had to be increased from their designed values to achieve effective ventilation in the face area.
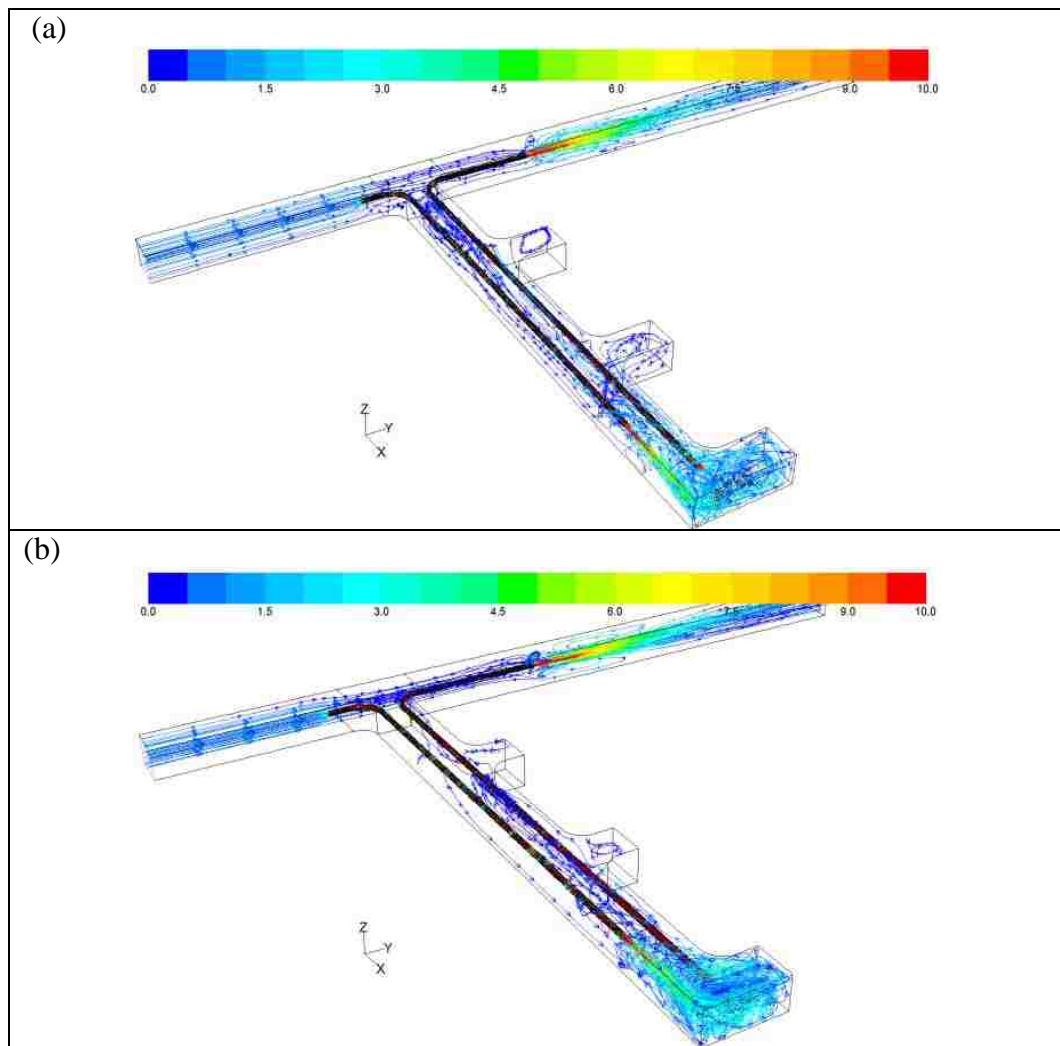
Figure 8.26. Pathlines Colored by Velocity Magnitude Demonstrating General Flow Features. (a) Mucking operation; (b) Drilling operation; (c) Loading operation; (d) Loading and drilling operation
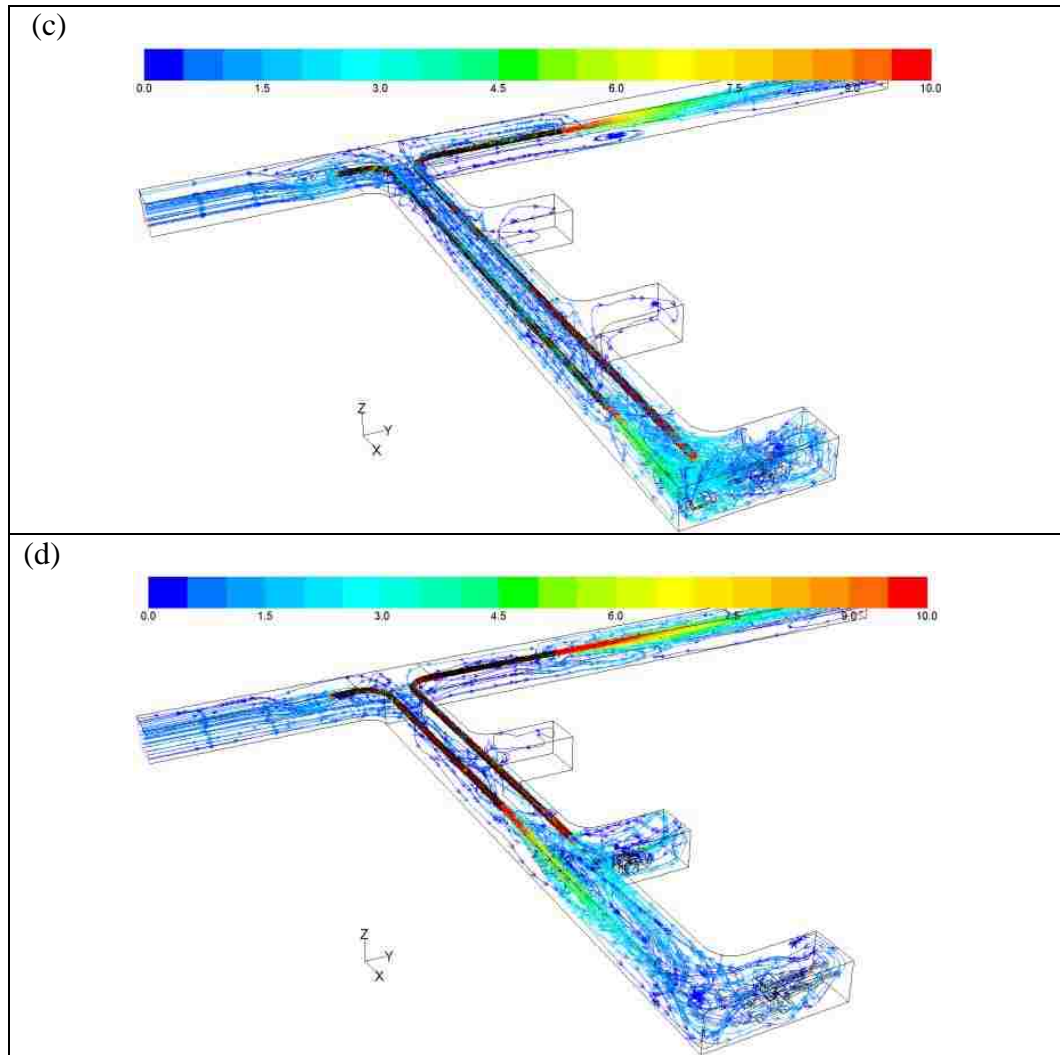
Figure 8.26. Pathlines Colored by Velocity Magnitude Demonstrating General Flow Features. (a) Mucking operation; (b) Drilling operation; (c) Loading operation; (d) Loading and drilling operation (cont.)

The area weighted averaged DPM values at these cross-sectional planes for different mining operations were plotted against the distance and compared, as shown in Fig. 8.33. The distance was measured from the working face 1, as shown in Figure 8.33. It can be clearly seen from the plot that the average DPM concentration was maximum for the combined drilling and loading operations.
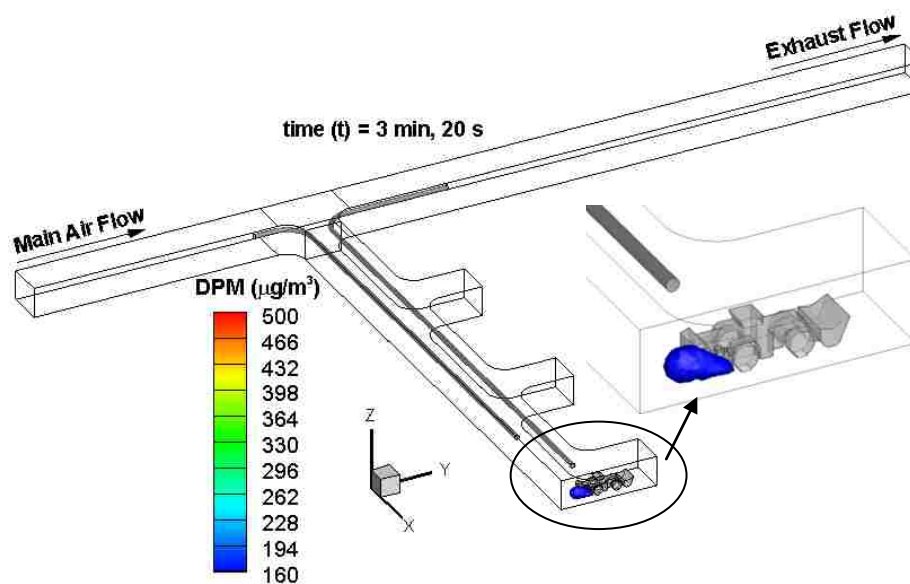
Figure 8.27. DPM Distribution (>160µg/m³) from LHD Mucking
Operation in the Dead-end Entry
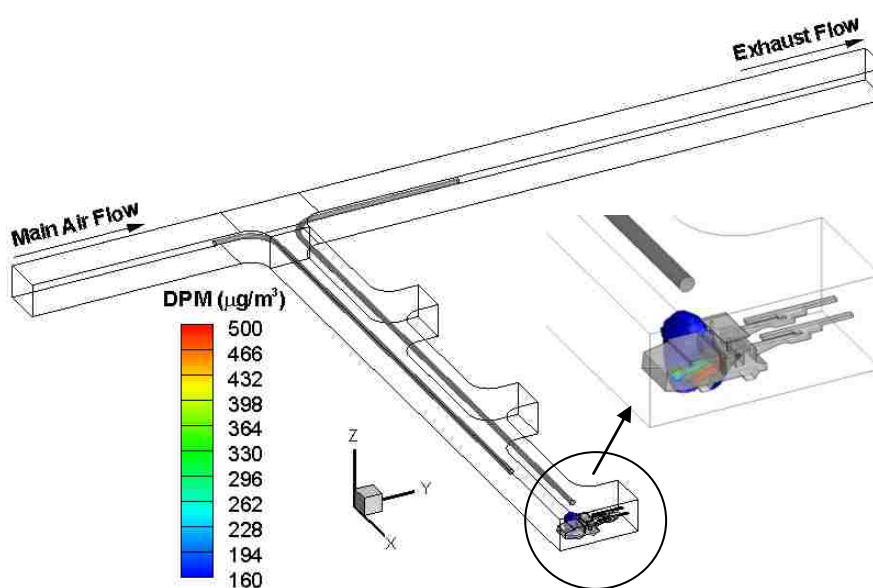
Figure 8.28. DPM Distribution (>160µg/m³) from Drilling Operation in Dead-end Entry
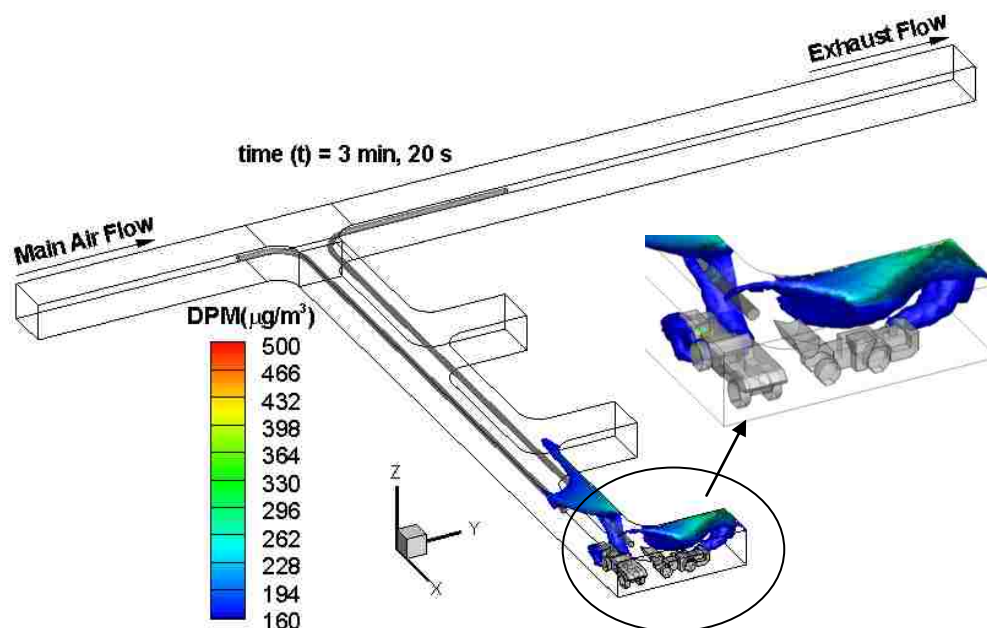
Figure 8.29. DPM Distribution (>160µg/m^3) from Loading Operation in Dead-end Entry
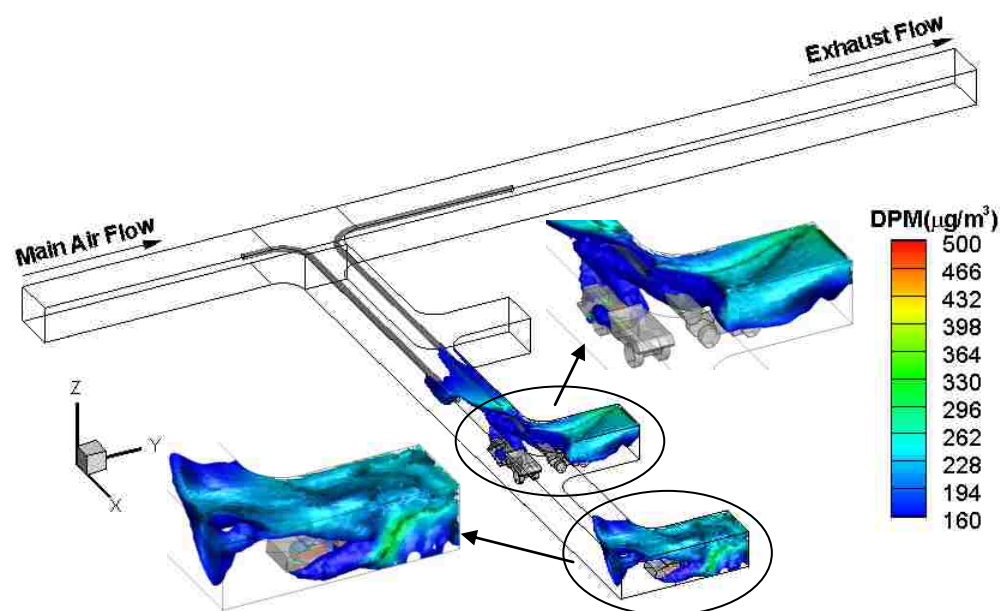
Figure 8.30. DPM Distribution (>160µg/m^3) from Drilling and Loading
Operation in Dead-end Entry
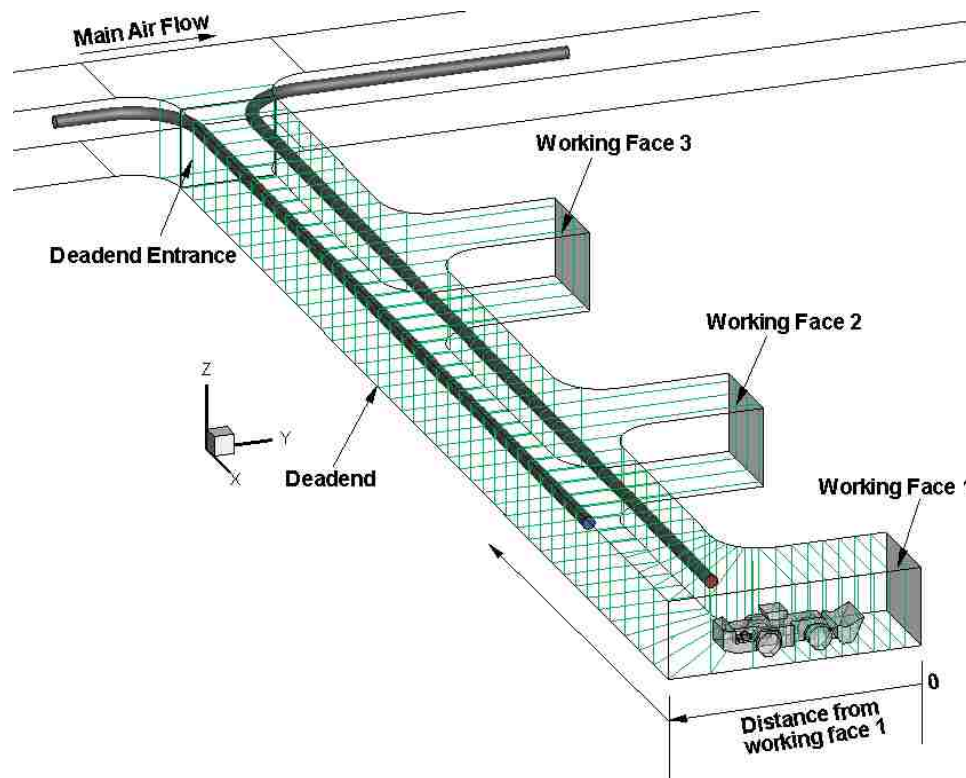
Figure 8.31. Schematic of the Cut Cross-sectional Planes inside the Dead-end

This was expected because of the presence of three diesel vehicles inside the dead-end area of the combined operation. However, the minimum average DPM concentration distribution occurred in the drilling jumbo operation. The DPM mass fraction set at the tailpipe of the drill (2.0 ppm) was higher than the DPM mass fraction set at the tailpipe of the LHD (1.73 ppm). However, the plot shows that the average DPM concentration inside the dead-end of the LHD mucking operation was greater than the drilling operation. This was due to the orientation of the tailpipes of the diesel vehicles. For the drilling jumbo and trucks, the tailpipes were pointing downward toward the floor but, for the LHD vehicles, they pointed backward and faced the rear of the vehicle. The effect of this tailpipe orientation, combined with the buoyancy force arising from the temperature difference, resulted in effective DPM dilution for the drilling jumbo operation, in comparison with the LHD mucking operation of the same auxiliary ventilation system.
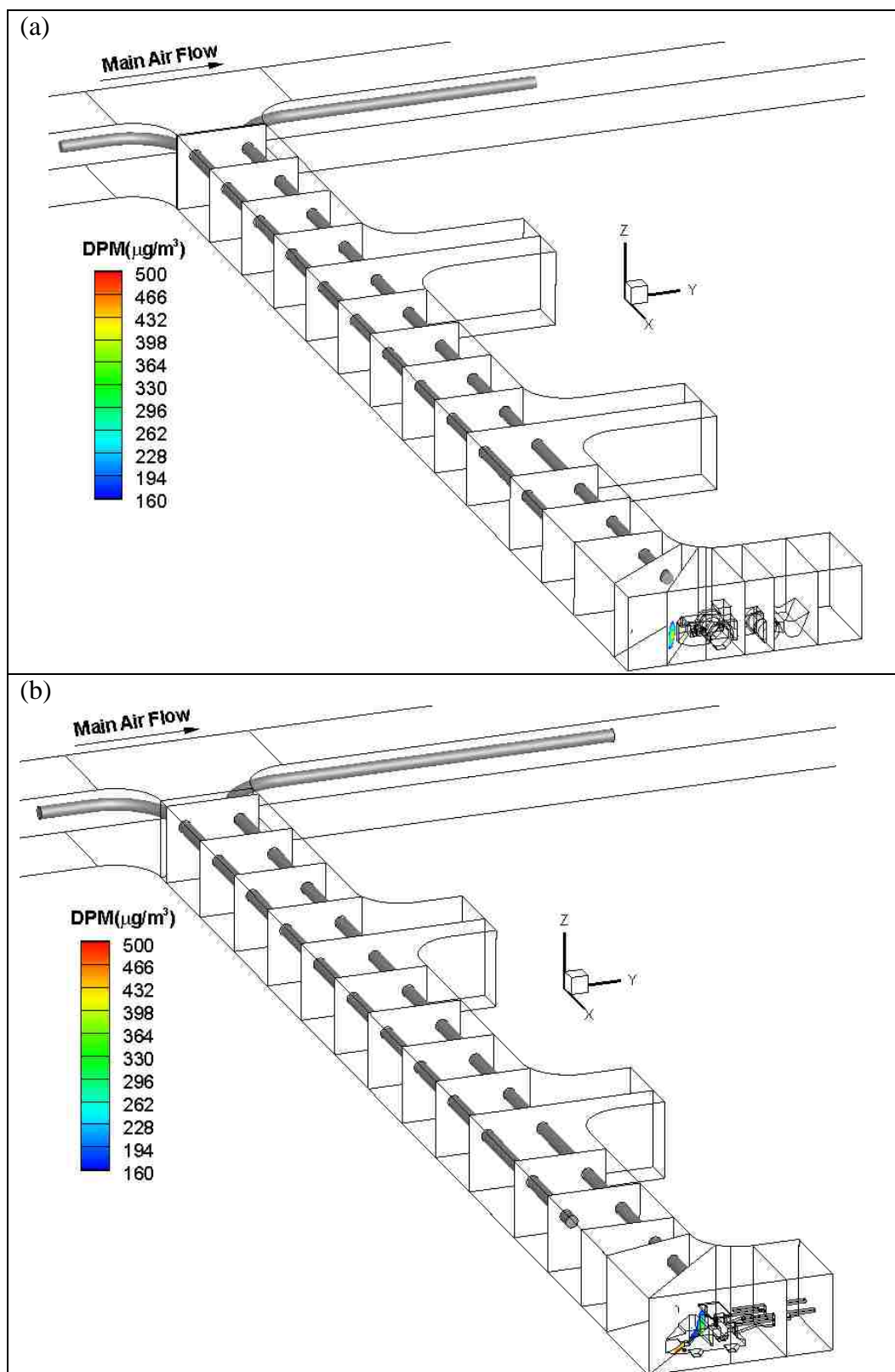
Figure 8.32. DPM Distributions at Different Cross Sectional Planes. (a) Mucking operation; (b) Drilling operation; (c) Loading operation; (d) Loading and drilling operations
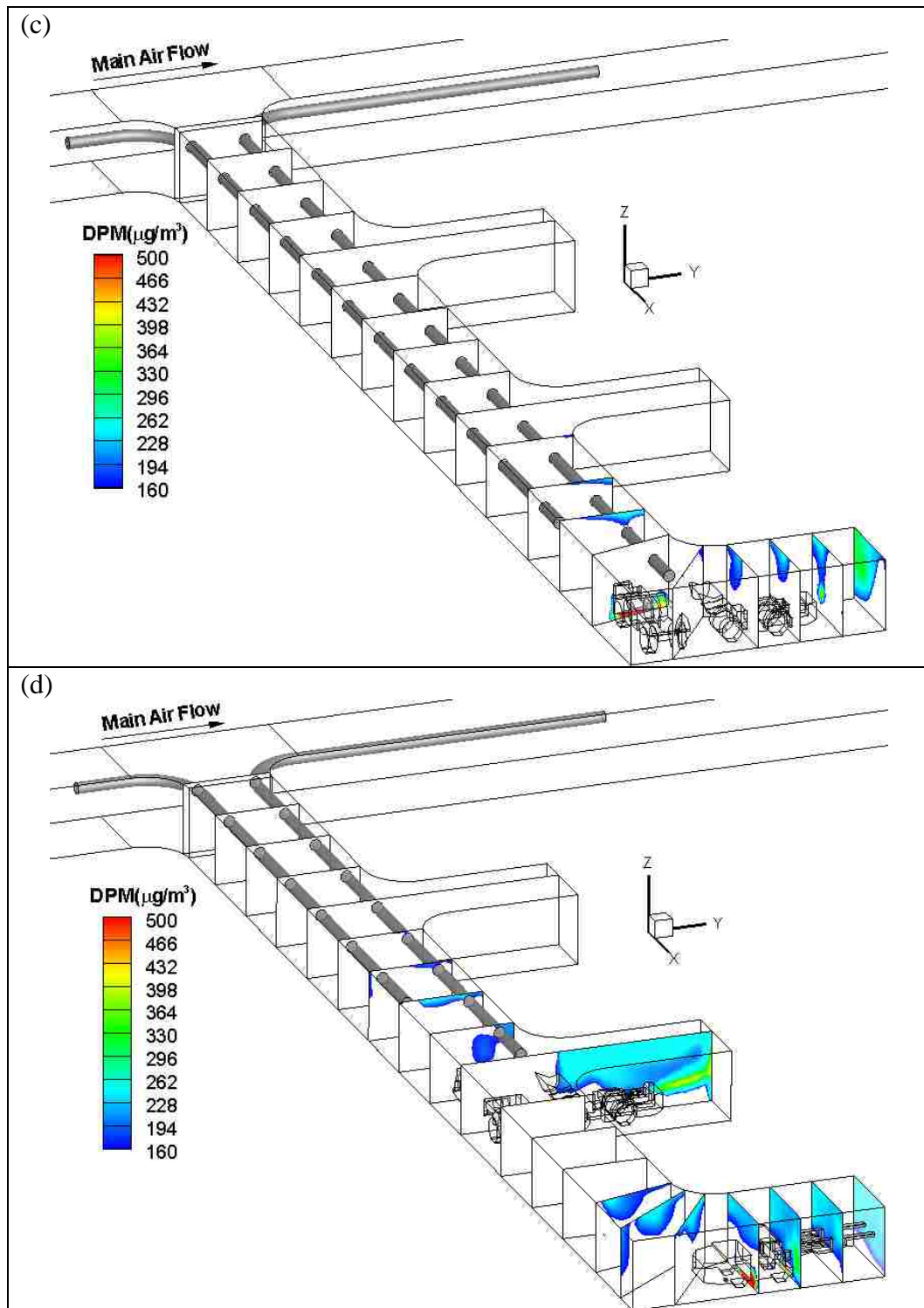
Figure 8.32. DPM Distributions at Different Cross Sectional Planes. (a) Mucking operation; (b) Drilling operation; (c) Loading operation; (d) Loading and drilling operations (cont.)
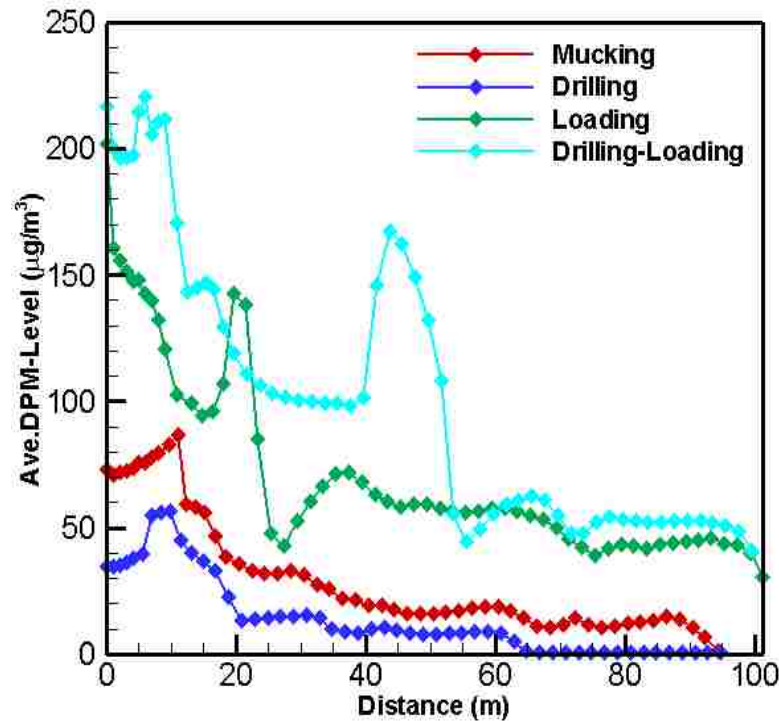
Figure 8.33. Comparison of Averaged DPM Values at Different Cross-sectional
Planes inside the Dead-end

8.4.4. Conclusions. The effect of different mining operations inside the single dead-end entry were studied and are discussed in this section. It can be clearly seen that the combination of two mining operations, or a mining operation that required two diesel vehicles inside the dead-end entry, increased the DPM production. The combined push-pull system was not required for single mining operations like drilling and LHD mucking. A blower fan with push tubing or an exhaust fan with pull tubing was sufficient to achieve effective ventilation in the face area. One of the fans could be shut down to save the amount of power required. During the LHD-truck loading operation, the short push and curved pull tubing systems were used to achieve effective ventilation in the face area. With the loading operation in one working face and the drilling operation in the other working face, the DPM production rate was large and the push-pull tube auxiliary ventilation system was ineffective for achieving the designed fresh air flow rates. The flow capacities of the blower and the exhaust fans were increased from their designed values to achieve effective ventilation in the face area.

# 9. CONCLUSIONS AND RECOMMENDATIONS

9.1. CONCLUSIONS

      This research used a state-of-the-art CFD tool to model the dispersion of DPM by industrial field studies, and by experiments taking place at S&T's Experimental Mine. A commercial CFD software, FLUENT^{TM}, was applied for framing the physical phenomena with the species transport model that included the effects of turbulent mixing, buoyancy, diffusion, temperature variations, and DPM dilution among others (air). The DPM concentration predicted by the CFD model was validated with the experimental data in a real mining environment with acceptable accuracy. Then, the species transport model was used to study commonly used face configurations in underground mines, which included both a straight entry and a dead-end entry. DPM dispersion under different mining operations, main airflow rates, auxiliary ventilation types, with and without DPF, vehicle motion, inclination of the floor, cross sectional areas, and push-pull layouts were compared to better understand the movement of DPM and to select control strategies.

      It was found from the industrial field studies that the exhaust flow from a regularly maintained LHD and truck will contain about 7 - 10 ppm of DPM, while this mass fraction number was decreased to about 2 ppm when a diesel particulate filter (DPF) was installed. When the diesel engine was not properly maintained or was an old model, this mass fraction number was greatly increased. As in the NIOSH field study, the LHD without DPF had as much as 35 ppm of DPM in the exhaust flow. For underground commonly used LHDs, loaders, and trucks, the DPM emission rate from tailpipe was around 4,000 µg/s (based on 7 ppm calculation) without DPF and about 1,000 µg/s when installed with DPF. When a working face had only one diesel engine, for example a LHD, it was calculated that the face needed at least 25 m^3/s (53,000 cfm) of fresh air to assure that the airflow downstream of the face will be below the regulation limit (4,000 (µg/s) / 25 (m^3/s) = 160 µg/ m^3) without DPF. When installed with a DPF, this ventilation requirement was reduced to about 6.25 m^3/s (1,000 (µg/s) / 6.25 (m^3/s) = 160 µg/ m^3). When more than one diesel engine was operating in the face area, the DPM production and thus the ventilation requirement increased accordingly. In the future, new generation of diesel engines will generate less DPM. However, the methods introduced by the

NIOSH and DEEP studies can still be used to sample the DPM and the calculation made in this study be used to determine the DPM production rate. The ventilation requirement for a face area can be estimated based on these numbers.

A validation study was executed using the experiments performed at S&T's Experimental Mine. It was observed from the experiments that DPM concentration fluctuated significantly in a real mining environment. This may have been due to the short sampling time period and other uncontrollable factors. The comparison of DPM concentration between simulation and experiments also showed noticeable differences at some points. However, by considering the distance between the simulated locations and the DPM sampling locations underground, it was found from the second experiment at S&T's Experimental Mine that this distance was within 18.0 cm at the plane 6.78 m downstream of the exhaust pipe. The average distance for the 27 sampling points was 8.2 cm for the three planes 2.80 m, 4.76 m, and 6.78 m, respectively, downstream of the tailpipe. This precision was considered acceptable for study of the DPM in a real working environment. Although a more accurate CFD model could be obtained through ideal lab conditions, it may not be necessary for the DPM dispersion to be exact within centimeters.

Accordingly, CFD simulation was used to study DPM dispersion in the straight and dead-end entries commonly utilized in underground metal and nonmetal mines. In this study, many practical scenarios were simulated with commonly encountered factors being considered. The following is a brief summary of the completed research work and some of the important findings.

When DPM production rate is higher than the ventilation capacity that can dilute it below the regulatory limit, all mining areas downstream of the diesel engine will be out of compliance. The only possible way to control the working environment is to frequently shut down diesel engines to reduce DPM emissions.

Since DPM cannot instantly mix uniformly with incoming fresh air, the areas downstream and those areas adjacent to the tailpipe will be surrounded with a high DPM plume, even when the ventilation rate is high and/or the vehicle is equipped with DPFs. The areas will be affected differently according to the orientation of the tailpipe, DPM emission rate, airflow velocity, airway cross-sectional area, etc. However, since a high

DPM plume normally exists in the immediate region upstream and $10 - 20$ m downstream of the tailpipe, these regions should be aware of by miners.

Since ventilation can only provide dilution that is proportional to the airflow provided, when the ventilation is doubled, the DPM level will be roughly reduced by half. Oftentimes, DPF is needed in working areas with multiple diesel engines.

It was also revealed in this study that, when the tailpipe emitting DPM points toward the floor of the entry, it can be more quickly diluted by this tailpipe arrangement, as compared to the tailpipe that discharges horizontally. When no other problems, such as dust, arise with this tailpipe setting, it may be a better choice for diesel engines to discharge DPM toward the floor.

Due to the buoyancy effect, the DPM plume tends to flow toward the roof of an entry and become diluted during the process. However, when a vehicle moves at a speed greater than 3 m/s, it was observed from the LHD moving cases (DPM discharged horizontally) that the DPM plume will be flattened and will affect more of the lower level of the entry.

For different entry sizes, it was observed that the buoyancy effect will make a DPM plume migrate toward the roof and spread the full width of the entry roof when the engine is stationary. But when the engine is constantly moving, the buoyancy effect will not be dominant. A high DPM plume will first occupy the lower level of an entry according to the speed of the vehicle.

Floor inclination has a significant effect on ventilation and on DPM concentration distribution. When possible, a downward sloping face is preferable to an upward face. If not possible, good ventilation should be provided to the roof of the face area to make sure the DPM will not accumulate in that region.

DPF and a proper auxiliary ventilation facility must be used when operating in a dead-end entry at more than 20 m in depth. In this study, it was found that a jet fan cannot provide enough ventilation to a deep dead-end entry. A blower fan with tubing or an exhaust fan with tubing may offer an airflow rate that is good enough if only one diesel machine is operating inside the dead-end entry. However, a properly used push-pull system will be needed if more than one engine is working together. The optimum push-pull

system is a short push pipe and a long curved pull pipe inside the face area in accordance with the scenario presented in this study.

9.2. RECOMMENDATIONS FOR FUTURE WORK

Based on this study, both in numerical simulation and in field tests, some interesting topics are proposed for future research. With a goal of looking for possible measures to improve ventilation and to better control DPM, continuing effort should be made in these research areas. The following topics are recommended for further investigation:

1. Transient DMP dispersion by considering the transient operation of diesel equipment, such as the working cycle of "full load – idle – full load".
2. The optimal selection of auxiliary ventilation equipment and flow rate based on the depth or length of the dead-end.
3. Thermal analysis of deep underground mines where there is a heat source.
4. Study DPM accumulation and ventilation solutions in multi-entry areas.
5. Optimized ventilation design or improvements based on current mine layout, diesel engine fleet, production, etc.
6. Improve the experimental design and increase the precision of the measurement to enhance the accuracy of the simulation results.

REFERENCES

Ames, R.G., Attfield, M.D., Hankinson, J.L., Hearl, F.J. and Reger, R.B. (1982) ''Acute respiratory effects of exposure to diesel emissions in coal miners,'' American Review of Respiratory Disease, Vol. 125, pp. 39–42.

Aminossadati, S.M. and Hooman, K. (2008) "Numerical simulation of ventilation air flow in underground mine workings," Proceedings of the 12th U.S./North American Mine Ventilation Symposium, Reno, NV, June 9-12, pp. 253-259.

Anon. (1981) "Health effects of exposure to diesel exhaust," The Report of the Health Effects Panel of the Diesel Impacts Study Committee, National Academies Press, Washington, DC, 169 pp.

Anon. (1988) "Carcinogenic effects of exposure to diesel exhaust," National Institute for Occupational Safety and Health (NIOSH), Department of Health and Human Services, Publication (No. 88-116), http://www.cdc.gov/niosh/nas/RDRP/appendices/chapter5/a5-29.pdf, 26pp.

Anon. (1998) "Clean diesel engine – emission control technologies, DieselNet technology guide," DieselNet, http://www.DieselNet.com/tg.html.

Anon. (1999) "Diesel Emission Control Strategies Available to the Underground Mining Industry," ESI International, http://www.deep.org/reports/esi_final_report.pdf, 38 pp.

Anon. (2002) "Health assessment document for diesel exhaust," U.S. Environmental Protection Agency (EPA), Report EPA/600/8-90/057F, May, http://www.epa.gov/ttn/atw/dieselfinal.pdf, 669 pp.

Anon. (2001a) Federal Register Vol. 66, No. 13, MSHA, January 19, p. 5715.

Anon. (2001b) Federal Register Vol. 66, No. 13, MSHA, January 19, p. 5532.

Anon. (2001c) Federal Register Vol. 66, No. 13, MSHA, January 19, p. 5536.

Anon. (2001d) Federal Register Vol. 66, No. 13, MSHA, January 19, p. 5537.

Anon. (2001e) Federal Register Vol. 66, No. 13, MSHA, January 19, p. 5539.

Anon. (2005a) Federal Register Vol. 70, No. 107, MSHA, June 6, pp. 32889-32890.

Anon. (2005b) Federal Register Vol. 70, No. 107, MSHA, June 6, pp. 32891-32892.

Anon. (2006a) Federal Register Vol. 71, No. 96, MSHA, May 18, p. 28928.

Anon. (2006b) "Program structure," Fluent, Inc., Release 6.3.26.

Anon. (2010a) "Coal diesel equipment health and safety," Mine Safety and Health Administration, http://www.msha.gov/S&HINFO/DIESEL.HTM.

Anon. (2010b) "Part 7—testing by applicant or third party," Mine Safety and Health Administration, http://www.msha.gov/30cfr/7.0.htm.

Anon. (2010c) "Atmospheric plume dispersion," ANSYS website: http://www.fluent.com /solutions/environmental/env2.htm.

Anyon, P. (2008) "Managing diesel particle emissions through engine maintenance - an Australian perspective," Proceedings of the 12th U.S./North American Mine Ventilation Symposium, Reno, NV, June 9-12, pp. 521-526.

Bagley, S., and Gratz, L. (1998) "Evaluation of biodiesel fuel and oxidation catalysts in an underground metal mine, part 3 – biological and chemical characterization," DEEP Technical Report. http://www.deep.org/reports/inco_bio_mtu.pdf, 37 pp.

Balczó, M., Faragó, T. and Lajos, T. (2005) "Modelling urban pollution dispersion by using MISKAM," Proceedings der Konferenz microCAD 2005, Miskolc University, Hungary, March 10-11, Supplementary Volume pp. 7-13.

Barna, M.G. and Gimson, N.R. (2002). "Dispersion modelling of a wintertime particulate pollution episode in Christchurch, New Zealand," Atmospheric Environment, Vol. 36 (No. 21), pp. 3531-3544.

Bennett, J.S., Crouch, K.G. and Shulman, S.A. (2003a) "Control of wake-induced exposure using an interrupted oscillating jet," American Industrial Hygiene Association Journal, Vol. 64 (No. 1), pp. 24–29.

Bennett, J.S., Feigley, C.E., Khan, J. and Hosni, M.H. (2003b) "Comparison of emission models with computational fluid dynamic simulation and a proposed improved model," American Industrial Hygiene Association Journal, Vol. 64 (No. 6), pp. 739–754.

Birch, M.E., Dahmann, D. and Fricke, H. (1999) "Comparison of two carbon analysis methods for monitoring diesel particulate levels in mines," Journal of Environmental Monitoring, Vol. 1, pp. 541-544.

Biswas, N. (1966) "The effect of periodic variations in temperature and humidity of air due to seasonal and diurnal changes on climate in underground airways," Mining and Mineral Engineering, Vol. 2 (No. 6), pp. 219-225.

Brunner, D.J., Miclea, P.C., McKinney, D. and Mathur, S. (1995) "Examples of the application of computational fluid dynamics simulation to mine and tunnel ventilation," Proceedings of the Seventh U.S. Mine Ventilation Symposium, Lexington, KY, June 5–7, pp. 479–484.

Bugarski, A.D., Schnakenberg, G.H., Noll, J.D., Mischler, S.E., Patts, L.D., Hummer, J.A., Vanderslice, S., Crum, M. and Anderson, R. (2004a) "The effectiveness of selected technologies in controlling diesel emissions in an underground mine – isolated zone study at Stillwater Mining Company's Nye Mine," Final Report to Metal/Nonmetal Diesel Partnership, http://www.cdc.gov/ niosh/mining/pubs/pdfs/teost.pdf, 86 pp.

Bugarski, A., Mischler, S., Noll, J., Schnakenberg, G.H., Crum, M., and Anderson, R. (2004b) "An evaluation of the effects of diesel particulate filter systems on air quality and personal exposure of miners at Stillwater Mine case study: production zone," National Institute for Occupational Safety and Health, Pittsburgh, PA, April 1, 24 pp.

Czerwinski, J., Kasper, M., Petermann, J.L. and Mosimann, Th. (2003) "Characterization of a coated StobbeDPF diesel particle filter on the Liebherr D914T engine," Report, http://www.ehcteknik.com/userFiles/myFiles/LiqTechReportB140.pdf, 26 pp.

Dahmann, D., Fricke, H.H. and Bauer, H.D. (1996) "Diesel engine emissions in workplace – atmospheres in Germany," Occupational Hygiene, Vol. 3, pp. 255-262.

Dahmann, D. and Bauer, H.D. (1997) "Diesel particulate matter (DPM) in workplaces in Germany," Applied Occupational and Environmental Hygiene, Vol. 12, pp. 1028-1031.

Dean, A, and Voss, D. (1999) "Design and analysis of experiments," Springer Press, Verlag, NY, 740 pp.

Desantes, J.M., Margot, X., Gil, A. and Fuentes, E. (2006) "Computational study on the deposition of ultrafine particles from Diesel exhaust aerosol," Aerosol Science, Vol. 37, pp. 1750-1769.

Edwards, J.C. and Hwang, C.C. (2006) "CFD modeling of fire spread along combustibles in a mine entry," 2006 SME Annual Meeting, March 27-29, St. Louis, MO, Preprint No. 06-027, pp. 1-5.

Falk, L.K., Martin, V.S. and Keen, B. (2010) "The role of computational fluid dynamics to reduce losses and increase airflow at Vale Inco's Coleman Mine," Proceedings of the 13th U.S./North American Mine Ventilation Symposium, Sudbury, Ontario, Canada, June 13-16, pp. 415-423.

Friel, G.F., Yuan, L., Edwards, J.C. and Franks, R.A. (2006) "Fire-generated smoke roll-back through crosscut from return to intake − experimental and CFD study," Proceedings of the 11th U.S./North American Mine Ventilation Symposium, University Park, PA, June 5-7, pp. 483-489.

Gamble, J. and Jones, W. (1983) ''Respiratory effects of diesel exhaust in salt miners,'' American Review of Respiratory Disease, Vol. 128, pp. 369–394.

Gamble, J., Jones, W., Hudak, J. and Merchant, J. (1978) "Acute changes in pulmonary function in salt miners,'' Proceedings of an American Council of Governmental Industrial Hygienist Topical Symposium: Industrial Hygiene for Mining and Tunneling, Denver, CO, November 6-7, pp. 119-128.

Gangal, M., Rubeli, B., Young, D. and Stachulak, J.S. (2006) "Post-field evaluation of diesel particulate filters," Proceedings of the 11th U.S./North American Mine Ventilation Symposium, University Park, PA, June 5-7, pp. 135-142.

Gangal, M., Rubeli, B., Young, D., Paas, N., and Robson, T. (2008) "The effects of bio-diesel fuel and intake air methane on the emissions of a flameproof diesel power package," Proceedings of the 12th U.S./North American Mine Ventilation Symposium, Reno, NV, June 9-12, pp. 469-473.

Gangal, M.K., Rubeli, B., Young, D.A. and Stekar, J. (2010) "Performance evaluation of advanced technology diesel oxidation catalysts," Proceedings of the 13th U.S./North American Mine Ventilation Symposium, Sudbury, Ontario, Canada, June 13-16, pp. 31-37.

Gidhagen, L., Johansson, C., Ström, J., Kristensson, A., Swietlicki, E., Pirjola, L. and Hansson, H.C. (2003). "Model simulation of ultrafine particles inside a road tunnel," Atmospheric Environment, Vol. 37 (No.15), pp. 2023-2036.

Grenier, M., Gangal, M., Lastra, R., Mikhail, S., Turcotte, A.M., Butler, K., Edwardson, E. and Laflamme, G. (1998) "Evaluation of existing diesel particulate matter sampling and analysis methods at a high sulphide ore mine," Diesel Emissions Evaluation Program, http://www.deep.org/reports/canmet_bms.pdf, 59 pp.

Haney, R.A., and Saseen, G.P. (2000) "Estimation of diesel particulate concentration in underground mines," Mining Engineering, Vol. 52 (No. 4), pp. 60–64.

Heerden, J. and Sullivan, P. (1993) "The application of CFD for evaluation of dust suppression and auxiliary ventilating systems used with continuous miners," Proceedings of the Sixth U.S. Mine Ventilation Symposium, Salt Lake City, UT, June 21–23, pp. 293–297.

Heywood, J.B. (1988) "Internal combustion engine fundamentals," McGraw-Hill Book Co., Inc., New York, NY, 930 pp.

Howell, S., Weber, A.J. (1997) "Biodiesel use in underground metal and nonmetal mines, " DieselNet technical reports, http://www.DieselNet.com/papers/9705howell.html.

Howard, J.B. and Kausch, W.J. Jr. (1980) "Soot control by fuel additives - a review," Progress in Energy and Combustion Science, Vol. 6, pp. 263–276.

Huber, A. (2006) "Pollution dispersion in urban landscapes," ANSYS website: http://www.fluent.com/about/news/newsletters/06v15i2/a3.pdf, 5 pp.

Hurtado, J.P., Gutiérrez, O. and Moraga, N.O. (2010) "Numerical simulation of shock losses at the intake and exhaust raises of block caving production level drifts," Proceedings of the 13th U.S./North American Mine Ventilation Symposium, Sudbury, Ontario, Canada, June 13-16, pp. 425-432.

Hwang, C.C. and Edwards, J.C. (2005) "The critical ventilation velocity in tunnel fires - a computer simulation," Fire Safety Journal, Vol. 40, pp. 213-244.

Jade, R.K. and Sastry, B.S. (2008) "An experimental and numerical study of two-way splits and junctions in mine airways," Proceedings of the 12th U.S./North American Mine Ventilation Symposium, Reno, NV, June 9-11, pp. 293-297.

Janisko, S. and Noll, J. (2008) "Near real time monitoring of diesel particulate matter in underground mines," Proceedings of the 12th U.S./North American Mine Ventilation Symposium, Reno, NV, June 9-11, pp. 509-513.

Kahn, G., and Orris, P. (1988) "Acute overexposure to diesel exhaust: report of 13 cases," J. Am. J. Ind. Med., Vol. 13, Issue 3, pp. 405-406.

Karacan, C.Ö., Ren, T.X. and Balusu, R. (2008) "Advances in grid-based numerical modeling techniques for improving gas management in coal mines," Proceedings of the 12th U.S./North American Mine Ventilation Symposium, Reno, NV, June 9-11, pp. 313-320.

Kollipara, V.K. and Chugh, Y.P. (2010) "A numerical analysis of the mine ventilation performance of selected tail-gate entry supports," Proceedings of the 13th U.S./North American Mine Ventilation Symposium, Sudbury, Ontario, Canada, June 13-16, pp. 433-440.

Krog, R.B., Schatzel, S.J., Garcia, F., and Marshall, J.K. (2006) "Predicting methane emissions from longer longwall faces by analysis of emission contributors," Proceedings of the 11th U.S./North American Mine Ventilation Symposium, University Park, PA, June 5-7, pp. 383-392.

Lepperhoff, G., Lüders, H., Barthe, P. and Lemaire, J. (1995) "Quasi-continuous particle trap regeneration by cerium additives," Society of Automotive Engineers (SAE), No. 950369, pp. 689-700.

Manos, E.Z. (2010) "Continuation of DPM control strategy at the Detroit Salt Mine using RYPO HDPF/c filters on diesel equipment," Proceedings of the 13th U.S./North American Mine Ventilation Symposium, Sudbury, Ontario, Canada, June 13-16, pp. 79-82.

Mayer, A., Matter, U., Czerwinski, J. and Heeb, N. (1999) "Effectiveness of particulate traps on construction site engines: VERT final measurements," DieselNet technical report, http:// www.DieselNet.com/papers/9903mayer/index.html.

Mayer, A., Czerwinski, J., Matthews, L. and Mosimann, T. (2005) "Filtration of diesel soot nanoparticles and reliability in Swiss HDV retrofitting," AKPF website: http://www.akpf.org/pub/2005_siat_mayer.pdf, 13 pp.

McGinn, S. (1999) "Maintenance guidelines and best practices for diesel engines," Diesel Emissions Evaluation Program, http://www.deep.org/reports/mtce_guidelines.pdf, 23 pp.

McGinn, S. (2000) "The relationship between diesel engine maintenance and exhaust emissions," Diesel Emissions Evaluation Program, http://www.deep.org/reports/mtce_report.pdf, 93 pp.

McGinn, S., Grenier, M., Gangal, M. Rubeli, B., Bugarski, A. Schnakenberg, G., Johnson, R., Petrie, D., Crowther, G. and Penney, J. (2004) "Noranda Inc. – Brunswick Mine diesel particulate filter field study," DEEP final report of investigation, http://www.deep.org/reports/nordpf_final.pdf , 91 pp.

Mischler, S.E., Bugarski, A.D., Noll, J.D. (2006) "Instrumentation for diesel particulate matter emissions research," Proceedings of the 11th U.S./North American Mine Ventilation Symposium, University Park, PA, June 5-7, pp. 99-104.

Nikitin, V.S., and Bitkolov, N.Z. (1981) "Open-pit ventilation," Coal Mine Industry Press, Beijing, China, 254 pp. [in Chinese].

Noll, J.D., Mischler, S.E., Patts, L.D., Schnakenberg, G.H. Jr., Bugarski, A.D., and Timko, R.J. (2006) "The effects of water emulsified fuel on diesel particulate matter concentrations in underground mines," Proceedings of the 11th U.S./North American Mine Ventilation Symposium, University Park, PA, June 5-7, pp. 159-164.

Noll, J. D., Patts, L. and Grau, R. (2008) "The effects of ventilation controls and environmental cabs on diesel particulate matter concentrations in some limestone mines," Proceedings of the 12th U.S./North American Mine Ventilation Symposium, Reno, NV, June 9-12, pp. 463-468.

Noll, J.D., Mischler, S., Cauda, E., Patts, L., Janisko, S. and Grau, R. (2010) "The effects of passive diesel particulate filters on diesel particulate matter concentrations in two underground metal/non-metal mines," Proceedings of the 13th U.S./North American Mine Ventilation Symposium, Sudbury, Ontario, Canada, June 13-16, pp. 83-89.

Penman, D. (1947) "Rock temperatures and natural ventilation," The Principles and Practice of Mine Ventilation (2nd edition), Charles Griffin & Company, Ltd, London, pp. 75-80.

Pomroy, B. (2002) "Diesel particulate matter sampling," Mine Safety and Health Administration, http://www.msha.gov/01-995/powerpoints/dpmsampling.pdf, 20 pp.

Pomroy, W.H. and Saseen, G.P. (2008) "MSHA's DPM rule for metal and nonmetal mines," Proceedings of the 12th U.S./North American Mine Ventilation Symposium, Reno, NV, June 9-12, pp. 455-462.

Purushotham, T. and Bandopadhyay, S. (2010) "Analyzing shock losses at air-crossings in a mine ventilation network using CFD simulations," Proceedings of the 13th U.S./North American Mine Ventilation Symposium, Sudbury, Ontario, Canada, June 13-16, pp. 463-468.

Ray, R.E., Kang, K. and Gilbey, M. (2004) "CFD analysis of diesel emissions in a railroad tunnel," Proceedings of the 10th U.S./North American Mine Ventilation Symposium, Anchorage, Alaska, May 16-19, pp. 117-126.

Reed, W.R. (2005) "Significant Dust Dispersion Models for Mining Operations," IC 9478, U.S. Department of Health and Human Services, Centers for Disease Control and Prevention, National Institute of Occupational Safety and Health, 29 pp.

Reger, R., Hancock, J., Hankinson, J., Hearl, F. and Merchant, J. (1982) ''Coal miners exposed to diesel exhaust emissions,'' Annals of Occupational Hygiene, Vol. 26 (No. 1-4), pp. 799–815.

Rundell, B., Ledin, M.C., Hammarström, U., Stjernberg, N., Lundbäck, B. and Sandström, T. (1996) "Effects on symptoms and lung function in humans experimentally exposed to diesel exhaust," Occupational and Environmental Medicine, Vol. 53, pp. 658-662.

Schnakenberg, G.H. and Bugarski, A.D. (2002) "Review of technology available to the underground mining industry for control of diesel emissions," IC 9462, U.S. Department of Health and Human Services, Centers for Disease Control and Prevention, National Institute of Occupational Safety and Health, http://www.cdc.gov/niosh/mining/pubs/pdfs/ic9462.pdf, 51 pp.

Schultz, M.J., Tomko, D.M., and Rude, R.L. (2006) "DPM reductions at underground metal and nonmetal mines using alternative fuels," Proceedings of the 11th U.S./North American Mine Ventilation Symposium, University Park, PA, June 5-7, pp. 151-158.

Smith, A.C. and Yuan, L. (2008) "Simulation of spontaneous heating in longwall gob area with a bleederless ventilation system," Mining Engineering, Vol. 60 (No. 8), pp. 61-66.

Smith, A.C. and Yuan, L. (2010) "Modeling the effect of seal leakage on spontaneous heating in a longwall gob area," Proceedings of the 13th U.S./North American Mine Ventilation Symposium, Sudbury, Ontario, Canada, June 13-16, pp. 479-484.

Spears, M.W. (1997) "An emissions-assisted maintenance procedure for diesel-powered equipment," Center for Diesel Research, University of Minnesota, Minneapolis, MN, http://www.cdc.gov/niosh/mining/topics/diesel/eamp/eamp.htm.

Srinivasa, R.B., Baafi, E.Y., Aziz, N.I. and Singh, R.N. (1993) "Three dimensional numerical modelling of air velocities and dust control techniques in a longwall face," Proceedings of the Sixth U.S. Mine Ventilation Symposium, Salt Lake City, UT, June 21–23, pp. 287–292.

Stachulak, J.S. and Hensel, V. (2010) "Successful application of DPF system at Vale Inco's Creighton Mine," Proceedings of the 13th U.S./North American Mine Ventilation Symposium, Sudbury, Ontario, Canada, June 13-16, pp. 123-128.

Stephens, M. and Calizaya, F. (2010) "A study of leakage flow in a laboratory model and using CFD," Proceedings of the 13th U.S./North American Mine Ventilation Symposium, Sudbury, Ontario, Canada, June 13-16, pp. 485-491.

Ström, H. and Andersson, B. (2009) "Simulation of trapping of diesel and gasoline particulate matter in flow-through devices," Topics in Catalysis, Vol. 52 (No. 13-20), pp. 2047-2051.

Takiff, L. and Aiken, G. (2010) "A real-time, wearable elemental carbon monitor for use in underground mines," Proceedings of the 13th U.S./North American Mine Ventilation Symposium, Sudbury, Ontario, Canada, June 13-16, pp. 137-141.

Trevits, M.A., Yuan, L. Teacoach, K. Valoski, M.P. and Urosek, J.E. (2009) "Understanding mine fires by determining the characteristics of deep-seated fires," 2009 SME Annual Meeting, February 22-25, Denver, CO, USA, preprint 09-150, 9 pp.

Uhrner, U., Löwis, S., Vehkamäki, H., Wehner, B., Bräsel, S., Hermann, M., Stratmann, F., Kulmala, M. and Wiedensohler, A. (2007) "Dilution and aerosol dynamics within a diesel car exhaust plume — CFD simulations of on-road measurement conditions," Atmospheric Environment, Vol. 41, pp. 7440-7461.

Wade, J. F. III, and Newman, L. S. (1993) "Diesel asthma: reactive airways disease following overexposure to locomotive exhaust," Journal of Occupational Medicine, Vol. 35, pp. 149-154.

Wala, M.A., Yingling, J.C., Zhang, J. and Ray, R. (1997) "Validation study of computational fluid dynamics as a tool for mine ventilation design," Proceedings of the 6th International Mine Ventilation Congress, Pittsburgh, PA, May 17-22, pp. 519–525.

Wala, M.A., Jacob, Huang, P.G., and Brown, J.T. (2003) "A new approach to evaluate mine face ventilation," Mining Engineering, Vol. 55 (No. 3), pp. 25-30.

Wala, M.A., Vytla, S., Taylor, C.D., and Huang, P.G. (2007) "Mine face ventilation: a comparison of CFD results against benchmark experiments for the CFD code validation," Mine Engineering, Vol. 59 (No. 10), pp. 49-55.

Wala, M.A., Vytla, S., Huang, G. and Taylor, C.D. (2008) "Study on the effects of scrubber operation on the face ventilation," Proceedings of the 12th U.S./North American Mine Ventilation Symposium, Reno, NV, June 9-12, pp. 281-286.

Wang, W.G., Lyons, D.W., Clark, N.N., Gautam, M. and Norton, P.M. (2000) "Emissions from nine heavy trucks fuelled by diesel and biodiesel blend without engine modification," Environmental Science & Technology, Vol. 34 (No.6), pp. 933–939.

Watts, W.F., Cantrell, B.K., Bickel, K.L., Olson, K.S., Rubow, K.L., Baz-Dresch, J.J. (1995) "In-mine evaluation of catalyzed diesel particulate filters at two underground metal mines," Minneapolis, MN: U.S. Department of the Interior, Bureau of Mines, RI 9571, 12 pp.

Watts, W.F., Spears, M., Johnson, J., (1998) "Evaluation of biodiesel fuel and oxidation catalysts in an underground metal mine," DEEP Technical Report, http://www.deep.org/reports/inco_bio.pdf, 51 pp.

Waytulonis, R.W. (1992) "An overview of the effects of diesel engine maintenance on emissions and performance," Bureau of Mines, Pittsburgh, Pennsylvania, IC9324, pp. 113-120.

Wu, H.W. and Gillies, A.D.S. (2008) "Developments in real time personal diesel particulate monitoring in mines," Proceedings of the 12th U.S./North American Mine Ventilation Symposium, Reno, NV, June 9-12, pp. 629-636.

Yuan, L. and Smith, A.C. (2008) "Effects of ventilation and gob characteristics on spontaneous heating in longwall gob areas," Proceedings of the 12th U.S./North American Mine Ventilation Symposium, Reno, NV, June 9-12, pp. 141-147.

Yuan, L. and Smith, A.C. (2009) "CFD modeling of spontaneous heating in a large-scale coal chamber," Journal of Loss Prevention in the Process Industries, Vol. 22 (No. 4), pp. 426-433.

Zheng, Y., and Tien, J.C. (2007) "Analyzing air distribution in open-pit mines using CFD method," SME Annual Meeting, Feb. 25-28, Denver, Colorado, Preprint 07-131, 12 pp.

Zheng, Y., and Tien, J.C. (2008a) "Simulation of DPM dispersion in underground metal/nonmetal mines using computational fluid dynamics (CFD) method," SME Annual Meeting, Feb. 24-27, Salt Lake City, UT, Preprint 08-104, 7 pp.

Zheng, Y., and Tien, J.C. (2008b) "DPM dispersion using CFD for underground metal/nonmetal mines," Proceedings of the 12th U.S./North American Mine Ventilation Symposium, Reno, NV, June 9-12, pp. 487-493.

Zheng, Y., and Tien, J.C. (2009a) "Simulation of methane distribution at longwall face," 2009 SME Annual Meeting, Feb. 22-25, Denver, Colorado, Preprint 09-155, 8 pp.

Zheng, Y., and Tien, J.C. (2009b) "Reconstruction of diesel emissions distribution based on an isolated zone experiment by using CFD method," Proceedings of the 9th International Mine Ventilation Congress, New Delhi, India, Nov. 10-13, pp. 869-878.

Zheng, Y., Thiruvengadam, M., Lan, H., and Tien, J.C. (2010) "Simulation of DPM distribution in a long single entry," Proceedings of the 13th Mine Ventilation Symposium, Sudbury, Ontario, Canada, June 13-16, pp. 149-156.

Zheng, Y., Lan, H., Thiruvengadam, M. and Tien, J.C. (2011) "DPM dissipation at S&T's Experimental Mine and comparison with simulation," Journal of Coal Science & Engineering (China) Vol. 17 No. 3, Sep., pp. 285-289.

VITA

Yi Zheng was born in Handan, Hebei province on June 30, 1974. He received his Bachelor of Science degree in Mechanical Engineering from the Hebei Institute of Architectural Science and Technology in July 1997 and the Master of Science degree in Mechanical Engineering from the China University of Mining and Technology in June 2000. He began his studies at the Missouri S&T in January 2005 and earned the Ph.D. degree in Mining Engineering in December, 2011.

Before entering the Mining Engineering Program at Missouri S&T, he had 4 years of industrial and research experience with the Institute of Electrical Engineering, Chinese Academy of Sciences, in Beijing, China. At Missouri S&T, he taught an undergraduate course on computer-aided mine design. As an Outstanding Graduate Teaching Assistant (2007) of the Department, he also involved in mine ventilation, mine economics, and senior design courses.

He has seven patents in China in magnetohydrodynamic (MHD) related areas and has published 20 conference and journal papers. He has been a member of the Society of Mining, Metallurgy and Exploration (SME) since 2007.